

WOODHEAD PUBLISHING  
IN MECHANICAL ENGINEERING

# Dynamics of tethered satellite systems

Vladimir S. Aslanov and Alexander S. Ledkov



**WP**  
WOODHEAD  
PUBLISHING

# Dynamics of tethered satellite systems

## **Related titles:**

*Welding and joining of aerospace materials*  
(ISBN 978-1-84569-532-3)

Welding and joining techniques play an essential role in both the manufacture and in-service repair of aerospace structures and components, and these techniques become more advanced as new, complex materials are developed. Welding and joining of aerospace materials provides an in-depth review of different techniques for joining metallic and non-metallic aerospace materials. Part one opens with a chapter on recently developed welding techniques for aerospace materials. The next few chapters focus on different types of welding such as inertia friction, laser and hybrid laser-arc welding. The final chapter in part one discusses the important issue of heat affected zone cracking in welded superalloys. Part two covers other joining techniques, including chapters on riveting, composite-to-metal bonding, diffusion bonding and recent improvements in bonding metals. Part two concludes with a chapter focusing on the use of high-temperature brazing in aerospace engineering. Finally, an appendix to the book covers the important issue of linear friction welding.

*Spacecraft thermal control*  
(ISBN 978-1-84569-996-3)

Spacecraft thermal control covers the necessary material required for engineers to perform the design and qualification of a space thermal control system comprehensively. Beginning with the fundamentals of space missions and following with the indispensable background on heat transfer, a full description of current thermal control technologies is presented. The book details the complete process in the design and validation (analysis and tests) of these systems. Finally relevant data on material properties are given.

*Introduction to aerospace materials*  
(ISBN 978-1-85573-946-8)

The structural materials used in airframe and propulsion systems influence the cost, performance and safety of aircraft, and an understanding of the wide range of materials used and the issues surrounding them is essential for the student of aerospace engineering. Introduction to aerospace materials reviews the main structural and engine materials used in aircraft, helicopters and space craft in terms of their properties, performance and applications. The first three chapters of the book introduce the reader to the range of aerospace materials, focusing on recent developments and requirements. Following these introductory chapters, the book moves on to discuss the properties and production of metals for aerospace structures, including chapters covering strengthening of metal alloys, mechanical testing, and casting, processing and machining of aerospace metals. The next group of chapters look in depth at individual metals including aluminium, titanium, magnesium, steel and superalloys, as well as at the properties and processing of polymers, composites and wood. Chapters on performance issues such as fracture, fatigue and corrosion precede a chapter focusing on inspection and structural health monitoring of aerospace materials. Disposal and recycling and materials selection are covered in the final two chapters.

Details of these and other Woodhead Publishing books can be obtained by:

- visiting our web site at [www.woodheadpublishing.com](http://www.woodheadpublishing.com)
- contacting Customer Services (e-mail: [sales@woodheadpublishing.com](mailto:sales@woodheadpublishing.com); fax: +44(0) 1223 832819; tel: +44(0) 1223 499140; address: Woodhead Publishing Limited, 80 High Street, Sawston, Cambridge CB22 3HJ, UK)

If you would like to receive information on forthcoming titles, please send your address details to Customer Services, at the address above. Please confirm which subject areas you are interested in.

# Dynamics of tethered satellite systems

VLADIMIR S. ASLANOV AND ALEXANDER  
S. LEDKOV



Oxford   Cambridge   Philadelphia   New Delhi

Published by Woodhead Publishing Limited, 80 High Street, Sawston,  
Cambridge CB22 3HJ, UK  
[www.woodheadpublishing.com](http://www.woodheadpublishing.com)  
[www.woodheadpublishingonline.com](http://www.woodheadpublishingonline.com)

Woodhead Publishing, 1518 Walnut Street, Suite 1100, Philadelphia, PA 19102-3406, USA

Woodhead Publishing India Private Limited, G-2, Vardaan House, 7/28 Ansari Road,  
Daryaganj, New Delhi – 110002, India  
[www.woodheadpublishingindia.com](http://www.woodheadpublishingindia.com)

First published 2012, Woodhead Publishing Limited  
© V. S. Aslanov and A. S. Ledkov, 2012  
The authors have asserted their moral rights.

This book contains information obtained from authentic and highly regarded sources.  
Reprinted material is quoted with permission, and sources are indicated. Reasonable  
efforts have been made to publish reliable data and information, but the authors and the  
publisher cannot assume responsibility for the validity of all materials. Neither the authors  
nor the publisher, nor anyone else associated with this publication, shall be liable for any  
loss, damage or liability directly or indirectly caused or alleged to be caused by this book.

Neither this book nor any part may be reproduced or transmitted in any form or by  
any means, electronic or mechanical, including photocopying, microfilming and  
recording, or by any information storage or retrieval system, without permission in  
writing from Woodhead Publishing Limited.

The consent of Woodhead Publishing Limited does not extend to copying for general  
distribution, for promotion, for creating new works, or for resale. Specific permission  
must be obtained in writing from Woodhead Publishing Limited for such copying.

Trademark notice: Product or corporate names may be trademarks or registered  
trademarks, and are used only for identification and explanation, without intent to  
infringe.

British Library Cataloguing in Publication Data  
A catalogue record for this book is available from the British Library.

Library of Congress Control Number 2012938316

Woodhead Publishing ISBN: 978-0-85709-156-7 (print)  
ISBN: 978-0-85709-600-5 (online)

Typeset by RefineCatch Limited, Bungay, Suffolk  
Printed in the UK and USA

---

# Contents

<i>List of figures</i>	ix
<i>List of tables</i>	xix
<i>About the authors</i>	xxi
Introduction	1
<b>1 Space tether systems: review of the problem</b>	<b>3</b>
1.1 Application of space tether systems	4
1.2 Chronology of experiments with the use of space tethers	44
1.3 Materials for tether production	61
1.4 Study of space tether dynamics: state of the problem	65
1.5 References	89
<b>2 Mathematical models of space tether systems</b>	<b>103</b>
2.1 Simple models of space tether system consisting of two point masses connected by a massless tether	104
2.2 Simple model of a space tether system consisting of two point masses connected by a heavy tether	114
2.3 Model of a space tether system with a heavy flexible tether	123

2.4	Model of a space tether system consisting of a point mass connected by a heavy tether with a rigid body	126
2.5	Model of a space tether system consisting of two rigid bodies connected by a heavy elastic multipoint tether	146
2.6	References	179
<b>3</b>	<b>Motion of a spacecraft with a tethered payload</b>	<b>183</b>
3.1	Mathematical model of a base spacecraft with a tethered payload	184
3.2	Analytical solution in case of a slow changing of the parameters	192
3.3	The approximate analytical solutions in the variables of the amplitude-phase	198
3.4	Analytical solutions for small oscillations	203
3.5	Estimation of the microaccelerations level on board the spacecraft	207
3.6	Motion of the spacecraft with a propulsion system	213
3.7	Motion of a spacecraft around its centre of mass in a circular orbit with a vertically deployed elastic tether	215
3.8	References	222
<b>4</b>	<b>Delivery of a payload from an orbit by means of a space tether</b>	<b>225</b>
4.1	Tether deployment schemes	226
4.2	Project YES2	229
4.3	Modelling of the YES2 tether deployment	235
4.4	Abnormal situations during tether deployment	242
4.5	References	260

---

<b>5      Use of methods of chaotic dynamics for the analysis of tether system motion</b>	<b>263</b>
5.1    Some elements of chaotic dynamics	265
5.2    The chaotic approach in STS dynamics	278
5.3    References	324
<b>Conclusion</b>	<b>327</b>
<b>Index</b>	<b>329</b>



---

## List of figures

1.1	The creation of artificial gravity	5
1.2	Goman's scheme of two-impulse transfer between circular orbits	7
1.3	Use of a spinning space tethering system for lifting a payload into high-altitude orbit	9
1.4	Comparison of a space tethering system's effectiveness in the cases of small (a) and large (b) differences between the masses of the bearing satellite and the lifting spacecraft	11
1.5	Space escalator	13
1.6	Space elevator	14
1.7	The traffic artery consisting of two space elevators	17
1.8	The traffic artery consisting of an escalator and a lunar elevator	18
1.9	Scheme of operation of the Lunovator	20
1.10	Intersection of a spacecraft orbit and the orbit of its ejected payload	21
1.11	The advanced scheme of placing a spacecraft into an orbit	25
1.12	Changing of a spacecraft's parameters by means of a tethered wing	28

1.13	Studying of the upper atmosphere by means of a tethered probe	29
1.14	Gravity stabilisation of a spacecraft	33
1.15	Current in a conductive tether at its motion in a magnetic field of the Earth	34
1.16	Space ring	39
1.17	Tether as a base for placement of a solar battery	41
1.18	Tether sling shot assist	44
2.1	STS consisting of two point masses connected by a massless tether in Keplerian orbit	106
2.2	STS consisting of two point masses connected by a massless tether	111
2.3	Wind coordinate system	112
2.4	STS consisting of two point masses connected by a heavy tether	115
2.5	STS consisting of two point masses connected by a flexible tether	123
2.6	STS consisting of a point mass connected by a heavy tether with a rigid body	128
2.7	Geometry of the points of a STS	133
2.8	Phase portraits of [2.121] at various values of eccentricity	147
2.9	Phase portraits of [2.121] at various values of tether elastic modulus	148
2.10	A multipoint tether	151
2.11	Effect of increasing the number of particles on the geometry of a tether in a multipoint model	153
2.12	Coordinate systems	154

---

2.13	Velocities of a part of a tether	157
2.14	The relative position of vectors	158
2.15	The forces acting on a part of the tether	161
2.16	STS consisting of two rigid bodies connected by a tether	166
2.17	The relative position of coordinate systems	167
2.18	Coordinate systems	173
3.1	Base spacecraft with a tethered payload	185
3.2	The arm of the tension force	190
3.3	Trajectory of the payload in $D_0\tau n$	209
3.4	Dependence of the tether deflection $\varphi$ on time	210
3.5	The law of tension force	211
3.6	Dependences of $\beta$ and $\xi$ on time	211
3.7	Dependences of $\alpha$ and $\varphi$ on time	212
3.8	Dependence of additional acceleration on time	213
3.9	Deflection of the tether $\varphi$ and the spacecraft $\alpha$ , $\alpha_{ps}$ from the local vertical	214
3.10	Dependence of $\alpha$ on time at $E = 5$ GPa	217
3.11	Dependence of $\alpha$ on time at $E = 50$ GPa	218
3.12	Dependence of $\alpha$ on time at $E = 100$ GPa	218
3.13	Dependences of $T_0$ , $T_t$ on the tether elastic modulus at $l_0 = 30$ km, $m_2 = 100$ kg	219
3.14	Dependences of $T_0$ , $T_t$ on mass of the payload at $l_0 = 30$ km, $E = 50$ GPa	220
3.15	Dependences of $T_0$ , $T_t$ on the tether length at $m_2 = 100$ kg, $E = 50$ GPa	220
3.16	Spacecraft with a vertical tether	221
3.17	Dependence of $\alpha$ on time	222

3.18	Phase portrait	222
4.1	Tether deployment schemes	226
4.2	Comparison of the length of tethers required for payload descent at static and dynamic deployment	228
4.3	Construction of the Young Engineers Satellite 2	230
4.4	The scheme of YES2	231
4.5	Brake gear	233
4.6	Calculated tether length used in control law [4.1]	234
4.7	Calculated tether outlet velocity used in control law [4.1]	234
4.8	Calculated tension force used in control law [4.1]	235
4.9	Motion of MASS/Fotino in a barycentric coordinate system connected with the base spacecraft	237
4.10	Motion of MASS/Fotino in a barycentric coordinate system connected with the base spacecraft	237
4.11	Dependences of a spacecraft and MASS/Fotino velocities on time	238
4.12	Dependences of a spacecraft and MASS/Fotino altitude on time	238
4.13	Dependence of the angle of tether deflection from a spacecraft's local vertical on time	239
4.14	Dependence of the distance between tether points and the line connecting a spacecraft with MASS/Fotino, on a number of rejected points	239

4.15 Comparison of the model tether length (dashed curve) with the design value (solid curve)	240
4.16 Comparison of the model tether outlet velocity (dashed curve) with the design value (solid curve)	240
4.17 Comparison of the model tension force (dashed curve) with design the value (solid curve)	241
4.18 Abnormal situations at tether deployment	243
4.19 Direction of the initial velocity of a payload	244
4.20 Calculated velocities of the tether outlet for control law [4.1]	245
4.21 Scheme of payload descent	245
4.22 Safe and danger regions in space of the initial parameters for case 1	246
4.23 Safe and danger regions in space of the initial parameters for case 2	246
4.24 Safe separation region for first method of deployment	247
4.25 Payload trajectories at various angles $\phi$ ( $\beta = 0$ ) for first method of deployment	248
4.26 Payload trajectories at various angles $\beta$ ( $\phi = \pi/3$ ) for first method of deployment	249
4.27 Tether jamming at 10 s	250
4.28 Tether jamming at 20 s	251
4.29 Tether jamming at 50 s	251
4.30 Comparison of the results of jamming modelling	252

4.31	Dependences of $\beta$ and $\xi$ on time at breakage of a spacecraft's attitude control system	253
4.32	Additional acceleration at breakage of a spacecraft's attitude control system	253
4.33	Wind coordinate system	255
4.34	Dependence of a payload's velocity on time	257
4.35	Dependence of a payload's trajectory slope angle on time	257
4.36	Dependences of a payload's and a spacecraft's altitude on time	258
4.37	Trajectory of a payload in a barycentric coordinate system connected with the base spacecraft	258
4.38	Dependence of the time of payload descent in the atmosphere on time of the tether breakage	259
4.39	Dependence of altitude of the payload on time	260
5.1	Potential energy and phase portrait of some mechanical systems	267
5.2	Homoclinic and heteroclinic trajectories	267
5.3	Intersection of the manifolds of an unperturbed system	268
5.4	Intersection of the manifolds of a perturbed system	272
5.5	The Melnikov distance in a point $P$	272
5.6	Cross-sections of the manifolds	275
5.7	Poincaré section of an unperturbed system	277
5.8	Poincaré section of a perturbed system	278

5.9	Potential energy and a phase portrait of [5.9]	281
5.10	Poincaré section of an unperturbed system [5.9]	282
5.11	Poincaré section of a perturbed system [5.8] at $e = 0.001$	283
5.12	Poincaré section of a perturbed system [5.8] at $e = 0.01$	283
5.13	Poincaré section of a perturbed system [5.8] at $e = 0.1$	284
5.14	Oscillation of a STS at $\varphi_0 = \pi/2 - 0.001$ , $e = 0.01$	285
5.15	Oscillation of a STS at $\varphi_0 = \pi/2 - 0.002$ , $e = 0.01$	285
5.16	Phase portrait at $\varphi_0 = \pi/2 - 0.001$ , $e = 0.01$	285
5.17	Phase portrait at $\varphi_0 = \pi/2 - 0.002$ , $e = 0.01$	286
5.18	The Melnikov function for a perturbed system at $e = 0.01$	287
5.19	Bifurcation diagram	290
5.20	Potential energy and a phase portrait of [5.18] for $\gamma > 1$	291
5.21	Potential energy and a phase portrait of [5.18] for $ \gamma  \leq 1$	294
5.22	Potential energy and a phase portrait of [5.18] for $\gamma < -1$	295
5.23	Dependences of $\Delta_i$ and $\alpha_*$ on $a$ for $b = -1$ and $\omega = 1$	300
5.24	Dependences of $\Delta_i$ on frequency $\omega$	301
5.25	Poincaré section for $\varepsilon = 0$ , $\delta = 0$	333
5.26	Poincaré section in the case of $c_1 = 0$ , $c_2 = 0$ , $c_3 = 1$ for $\varepsilon = 0.01$ $\delta = 0$	304

5.27 Poincaré section in the case of for $c_1 = 0$ , $c_2 = 0$ , $c_3 = 1$ for $\varepsilon = 0.02$ , $\delta = 0$	304
5.28 Poincaré section in the case of $c_1 = 1$ , $c_2 = -1$ , $c_3 = 0$ for $\varepsilon = 0.01$ , $\delta = 0$	305
5.29 Poincaré section in the case of $c_1 = 1$ , $c_2 = -1$ , $c_3 = 0$ for $\varepsilon = 0.02$ , $\delta = 0$	305
5.30 Poincaré section in the case of $c_1 = 0$ , $c_2 = 0$ , $c_3 = 1$ for $\varepsilon = 0.02$ , $\delta = 0.0001$	306
5.31 Poincaré section in the case of $c_1 = 1$ , $c_2 = -1$ , $c_3 = 0$ for $\varepsilon = 0.02$ , $\delta = 0.0001$	306
5.32 Phase trajectory for $a = 1$ , $b = -1$ , $\varepsilon = 0.02$ , $\Omega = 1$ and two different values of $\delta$ close to the critical value $\delta_0 = 0.01823$	308
5.33 Phase trajectory for $a = 1$ , $b = -1$ , $\varepsilon = 0.02$ , $\Omega = 1$ and two different values of $\delta$ close to the critical value $\delta_1 = 0.00906$	309
5.34 Dependence of the principal moment of inertia on the manner of tether fastening	311
5.35 Poincaré section of an unperturbed system	312
5.36 Poincaré section at $V_0 = 0.001$	312
5.37 Poincaré section at $V_0 = 0.002$	313
5.38 Poincaré section at $V_0 = 2$	313
5.39 Dependence of integrals [5.70]–[5.73] on the dimensionless frequency	315
5.40 Dependence of the dimensionless frequency $\Omega_3$ on the elastic modulus of the tether	316
5.41 Dependence of the dimensionless frequency $\Omega_3$ on the payload mass	317
5.42 Dependence of the dimensionless frequency $\Omega_3$ on the tether length	317

---

5.43 The Melnikov function	321
5.44 Phase trajectory for $\alpha_0 = 3.11$ , $\dot{\alpha}_0 = 0\text{s}^{-1}$	321
5.45 The Melnikov function at various values of $\delta$	322
5.46 Dependences of $\tilde{\Delta}$ and $\Delta_4$ on $\delta$	322
5.47 Phase trajectory for $\alpha_0 = 3.141$ , $\dot{\alpha}_0 = 0\text{s}^{-1}$	323



---

## List of tables

1.1	Experiments with space tethers	45
1.2	Properties of materials	64
5.1	Homoclinic and heteroclinic trajectories	319



## About the authors

**Professor Vladimir Stepanovich Aslanov** graduated from the Kuibyshev Aviation Institute, Kuibyshev, USSR (KuAI) in 1972 as a speciality Aircraft Engineer. In 1974 he entered postgraduate school of the Kuibyshev Aviation Institute and in 1977 received his PhD. In the period 1978–1982 Aslanov worked as an assistant professor in the KuAI. In 1990 he defended his doctoral dissertation at the Moscow Aviation Institute, Moscow/USSR, on the motion of a rigid body in the atmosphere. Since 1989 Professor Aslanov is the head of the Department of Theoretical Mechanics of Samara State Aerospace University, Samara, Russia.

Professor Aslanov takes an active part in Russian scientific community life. He is a member of the Mathematics and Mechanics Education Methodology Council of Russian Universities (Moscow/Russia), the Scientific Advisory Board for Awarding Doctoral Degrees in Mechanics and Ballistics, (Samara/Russia), and an expert of the Russian Foundation for Basic Research, Moscow/Russia and the Federal Agency of Education at the Ministry of Education and Science of the Russian Federation.

Professor Aslanov's scientific interests are classical mechanics, nonlinear oscillations and chaotic dynamics, mechanics of space flight, dynamics of gyrostats, dynamics of tethered satellite systems and spacecraft stability. For a long time the focus of his research was the nonlinear dynamics of the uncontrolled motion of a rigid body in the

atmosphere. This problem has great practical significance, since the scientific results can be used for describing the uncontrolled descent of the spacecraft into the atmosphere of planets. The main scientific results were included in the monograph ‘The spatial movement of the body during the descent in the atmosphere’, which was published in Russia in 2004.

Another area of Professor Aslanov’s research is the dynamics of a gyrostat. The problem of free gyrostat motion can be treated as an extension of a classical Euler’s case of rigid body motion around a fixed point when one degree of freedom – relative rotation of bodies – is added. Professor Aslanov obtained analytical solutions for describing the dynamics of a free gyrostat, found adiabatic invariants for gyrostats of variable structure, and studied the chaotic regimes of asymmetric gyrostats.

In 2006 Professor Aslanov headed the scientific group which is engaged in research of dynamics of space tether systems, which covered mathematical modelling of tether deployment, prediction and analysis of consequences of possible abnormal situations, study of influence of a tether on the spatial motion of connected space vehicles and the study of chaotic modes of space tether systems’ motion. The Aslanov group, on request of TSSKB-PROGRESS, has also executed an independent expert estimation of safety (the experiment YES2) for the space vehicle Foton-M3.

Professor Aslanov has published approximately 140 articles in international and national journals and for conference proceedings. The list of his most significant papers can be found on the website <http://aslanov.ssau.ru>.

Besides his scientific activity Professor Aslanov is actively engaged in educational work. He conducts lecture courses ‘Analytical mechanics’, ‘Modern problems of mechanics’ and ‘Dynamics of the space vehicle in atmosphere’. Under

the guidance of Professor Aslanov nine of his students received a PhD degree. The high level of teaching has been confirmed by awards: the Academician S.P. Korolev Medal ‘For services to state cosmonautics’ (Federation of Cosmonautics of Russia, Moscow, 2007), the award of the governor of the Samara region (Samara, 2002), and the Mayoral award of Samara (Samara, 1997).

**Dr. Alexander Sergeevich Ledkov** began doing research under the guidance of Professor Aslanov while still at school. In 2000 he was awarded a first degree at the Russian National Conference of Schoolchildren ‘Space 2000’ for research devoted to exploring the possibility of saving the first stage of the rocket Soyuz. In 2006 Dr Ledkov obtained an MS in Mechanical Engineering (Russia – Mechanical Engineer) from the Samara State Aerospace University, Russia. He researched the uncontrolled motion of spacecraft in rarefied atmosphere. This theme was developed in his PhD dissertation, which he defended in 2009. Dr Ledkov investigated the resonances and chaotic modes of motion arising during the descent of spacecraft in the atmosphere and ways of their elimination.

After earning a PhD Ledkov began working as an associate professor at the Department of Theoretical Mechanics in Samara State Aerospace University. He conducts lecture courses such as ‘Dynamics of space tether systems’, ‘Technologies and programming languages’, ‘Integrated mathematical packages’ and ‘Dynamics of nonlinear processes and phenomena’. In 2007 Dr Ledkov was nominated ‘The Best Young Specialist, Samara region’, and in 2009 won the competition for young teachers at Samara State Aerospace University.

Dr Ledkov was engaged in research on the dynamics of space tether systems in 2006 when together with Professor

Aslanov he started working on the project YES2. The main focus of his work was the development of a multipoint model of space tether systems and the analysis of potential abnormal situations. In collaboration with Professor Aslanov the software package named TetherCalc was developed. It allowed simulating the motion of the space tether system with a heavy flexible tether of variable length. Now space tether systems are the basic area of Dr Ledkov's research.

Dr Ledkov has published approximately 20 articles in international and national journals and for conference proceedings. The list of his most significant papers can be found on the website <http://ledkov.com>.

The authors may be contacted at:

Professor Vladimir Stepanovich Aslanov  
Head of Theoretical Mechanics Department  
Samara State Aerospace University  
34 Moskovskoye Shosse, Samara, 443086, Russia  
Tel.: +7 846 267 4597 (office), +7 927 688 9791(mobile)  
E-mail: aslanov\_vs@mail.ru  
Websites: <http://www.termech.ru>, <http://aslanov.ssau.ru>

Dr. Alexander Sergeevich Ledkov  
Associate professor of Theoretical Mechanics Department  
Samara State Aerospace University  
34 Moskovskoye Shosse, Samara, 443086, Russia  
Tel.: +7 046 267 4599 (office), +7 909 342 8886 (mobile)  
E-mail: ledkov@inbox.ru  
Websites: <http://www.termech.ru>, <http://ledkov.com>

# Introduction

During the past few decades, space tether systems have attracted the attention of researchers from around the world. The range of problems, and where they find application, is extremely wide. Various transport operations, electricity generation, exploration of deep space, and many other tasks can be resolved with the help of space tether systems. The main differences of the tether systems from conventional spacecraft are their great length, variable configuration, and their ability to interact with the Earth's magnetic field. These features give a variety of possible ways for using tethers in space.

Space tether systems have long ceased to be just theory. The first experiments with using them were conducted in the mid 1960s, and currently more than ten programs have been realised. The problems of returning payloads from orbit and of atmospheric sounding have a wide practical implementation. These tasks require the creation of a space tether system based on multipurpose spacecraft or space stations. Using a tether system should not preclude any other planned experiments and operations using a base spacecraft. In this connection, the task of developing mathematical models describing the dynamics of space tether systems while taking into account the motion of the base spacecraft relative to its centre of mass is very important. The problem of predicting abnormal situations that may arise during tether deployment is also significant. In addition, the study of a spacecraft's chaotic motion caused by oscillations while

tethered is of great scientific interest. These questions are considered in detail in this book.

In Chapter 1, we provide an introductory review of the concept of space tether systems and describes their applications. The reader is acquainted with the chronology of various experiments and with the major scientific works on the dynamics of space tether systems.

Chapter 2 is devoted to mathematical models used for the study of space tether system dynamics, and particular attention is paid to the multipoint model of tether systems which is very convenient for practical usage.

In Chapter 3 we examine the motion of the base spacecraft relative to its centre of mass under the influence of tether tension. The original approximate analytical solutions for the case of planar motion of the system are presented, and an estimation of microaccelerations on board the spacecraft is made.

We devote Chapter 4 to the delivery of a payload from the orbit. With the help of a multipoint model, which was obtained in Chapter 2, the experiment YES2 is simulated. Also, there is an extensive analysis of various abnormal situations.

Chapter 5 explores chaotic motions of the space tether system, whereby both the Melnikov and Poincaré methods are briefly described. The chaotic motion of the space tether system in an elliptical orbit and of a spacecraft with a vertical elastic tether are investigated. For some special cases, the analytical criterion of existing chaos is obtained.

Some of the results presented in this book were obtained with the support of the Russian Foundation for Basic Research (Project Nos. 06-01-00355-a and 09-01-00384-a).

# Space tether systems: review of the problem

**Abstract:** In this first chapter, the reader is acquainted with the concept of space tether systems and the respective areas of their application. In chronological order, we review experiments in which space tethers were used. The chapter provides an overview of existing materials used for tether construction, and there is an extensive review of the literature devoted to the problem. Types of mathematical models, the various modes of space tether systems motion, questions of stability and control, the task of spin-up of the system, and some poorly investigated topics revealed as a result of the scientific literature analysis are considered.

**Key words:** space tether systems; space elevator; chronology of space tether experiments; state of the art.

Space tether systems (STS) are understood as mechanical systems consisting of rigid bodies moving in different orbits, and the tethers that connect these bodies. The lengths of the tethers exceed the size of the connected bodies many times over. In the simplest form, STS represent two spacecrafts connected by a tether with a length of tens, or even hundreds, of kilometres. Space tether systems are distinguished from conventional space vehicles by three main features: their large extent; their flexible configuration which manifests in the tether's ability to change length by deploying and retracting to connected spacecraft; and the ability for active

interaction of an electrodynamic tether with its environment. Depending on what features prevail at the given STS, and what property is used, tether systems can be divided into two types:

- (a) ‘Static’ systems, in which the quantity and lengths of tethers, the quantity and weights of objects, and their relative position and orientation remain constant during activity.
- (b) ‘Dynamic’ systems, which can significantly change configuration and structure.

This latter STS is known as ‘electrodynamic’ if it includes conductive tethers and actively interacts with Earth’s magnetic field and ionosphere, no matter whether the STS is ‘static’ or ‘dynamic’.

## **1.1 Application of space tether systems**

For more than a century involving the existence of the concept of STS, researchers have found plenty of ways for their application. The range of problems which may be solved by space tethers is very wide, and we focus on the most interesting of them below.

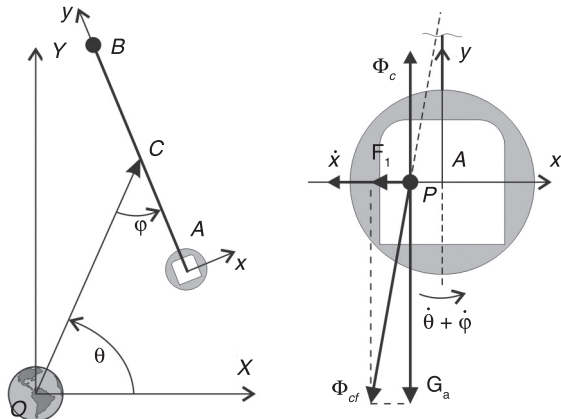
### ***1.1.1 Creation of an artificial gravity on board a space station***

It was exactly for this task that the use of a space tether was first proposed. The idea of using the centrifugal force of inertia for the creation of artificial gravity was suggested by Tsiolkovsky, who proposed to connect two spacecraft by a

chain and to rotate this grouping. The magnitude of this force is proportional to the length of the chain and the square of angular velocity of the mechanical system's rotation. The angular velocity of STS is the sum of the angular velocity of the orbital movement of its centre of mass  $\dot{\theta}$ , and the angular velocity of rotation concerning the centre of mass  $\dot{\varphi}$  (see Figure 1.1), therefore rotating the STS in a direction corresponding to the orbital motion of the system more effectively from the point of view of the creation of gravity.

It is necessary to notice that forces of inertia besides artificial gravitation  $G_a$ , also create other interesting effects. Let us consider mass point  $P$ , which is located on board one of the spacecrafts connected by the tether (see Figure 1.1). Rotation occurs with constant angular velocity, and the rotary force of inertia is absent. Displacement of the point mass from the line connecting the centres of mass of the spacecrafts causes a force  $F_1$ , tending to increase the distance between the point and the axis. Actually, this force represents a projection of the centrifugal force of inertia  $\Phi_{cf}$  to the axis

**Figure 1.1** The creation of artificial gravity



Ax. The Coriolis force,  $\Phi_C$ , also has a crucial impact on the system's movement. This force is proportional to the angular velocity of the STS and to the relative speed of motion of the mass point in the coordinate system connected with the spacecraft; therefore, at slow rotation the Coriolis force can have an influence on the system greater than the centrifugal force – that is, proportional to a square of angular velocity. Thus, artificial gravity can be accompanied by effects which would be unexpected at first sight.

The effect of artificial gravity appears even in the absence of an STS's rotation concerning a local vertical ( $\varphi = 0$ ). That is, being in a condition of gravitational stabilisation the system ( $\varphi = 0$ ) is subject to the specified effects. In this case, the tether always remains parallel to the local vertical. Let us call such a state of STS a radial orientation. In this case, the angular velocity of the system's rotation concerning the centre of mass is equal to the orbital motion's angular velocity of the centre of mass, and has an order of  $10^{-3} \text{ s}^{-1}$ . The 10 km tether will allow the creation of an additional acceleration of  $10^{-2} \text{ m/s}^2$ . A tether with a length of about  $10^7 \text{ m}$  is necessary to provide terrestrial gravity, and is comparable to the size of the Earth.

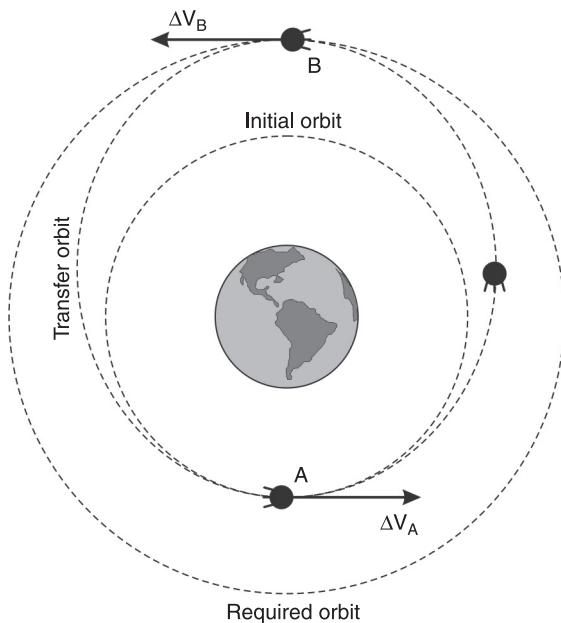
The first experiments on the creation of artificial gravity were carried out by NASA in 1966 during the Gemini-11 mission. The spacecraft, Gemini-11, was connected with the target satellite, Agena GATV-11, by a tether of 30 m in length. After that, the ‘spacecraft–satellite’ bundle was spun around the general centre of mass with an angular velocity of  $1.6 \cdot 10^{-2} \text{ s}^{-1}$ . As a result, on board Gemini an artificial gravity of  $10^{-4} \text{ g}$  was created. Of course, such a low value does not allow people to exist comfortably, but in some cases even such weak gravitation can be useful. For example, microgravity can be useful for transmission of fuel from one spacecraft to another (Lang and Nolting, 1967).

### 1.1.2 Lifting of spacecraft to higher orbit by means of a rotating space tether system

In astronautics, a spacecraft's flight between various orbits is a very common problem. Let us consider the elementary problem of flight between circular orbits and the applied ways of its decision (see Figure 1.2). Now such manoeuvres are carried out by means of jet engines. Let us assume that the initial and required orbits are in one plane. The spacecraft's trajectory can be divided into the active part – when jet engines work – and passive – when they do not work.

The scheme of optimum two-impulse transfer was put forward by Goman. It supposes two activations of engines. The duration of the active parts of the trajectory is negligibly

**Figure 1.2** Goman's scheme of two-impulse transfer between circular orbits

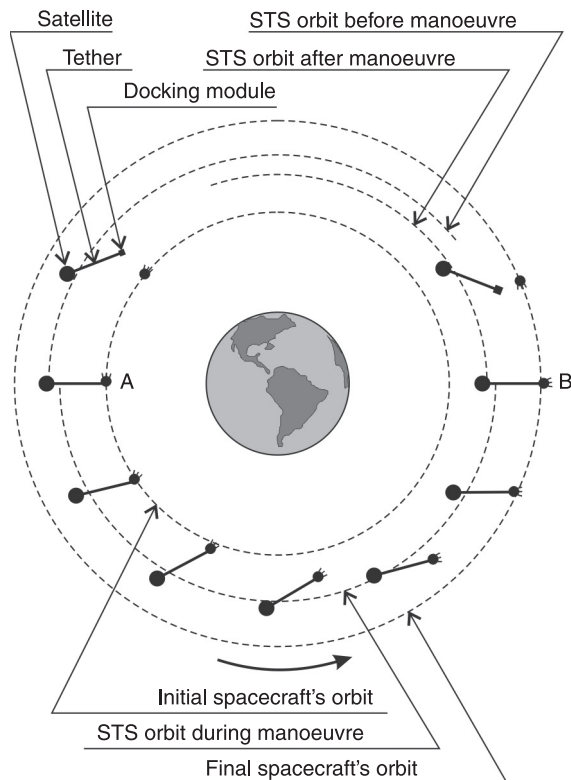


small in comparison with the duration of its passive parts; therefore it is possible to represent them in the form of momentums. It is considered that, at the moment of the instantaneous change of velocity, the coordinates of the spacecraft remain unchanged. Calculation of an impulse manoeuvre is reduced to the number of momentums of velocity, their orientation, and the application points. As two orbits with different radii do not have intersection points, for overfly between them it is necessary to apply two or more impulses. By means of the first momentum  $\Delta V_A$ , the spacecraft is put into an elliptical transfer orbit which contacts the required circular orbit in the apocenter (point B in Figure 1.2). The point of application of the first momentum (point A in Figure 1.2) corresponds to the pericentre of the transfer orbit, and the momentum is directed along the tangent to the initial orbit. At the moment the spacecraft reaches the apocenter, the second momentum of velocity directed along the tangent to the transfer orbit is applied. It forces the spacecraft into the required circular orbit. If the propulsion system parameters and the total increment velocity of a manoeuvre are known, it is possible to calculate the necessary fuel margin easily (Roy, 2005). The manoeuvre discussed above is simple and reliable. Its main shortcoming is the necessity to use jet fuel. The application of the STS allows the transfer between orbits without additional use of fuel.

The principle of delivery of a payload on a higher-altitude orbit by means of STS is simple enough. In an orbit there is a rotating bundle of two bodies, and the mass of one of them (the bearing satellite) exceeds many times over the mass of another (the docking module). The bundle's centre of mass is close to the bearing satellite, and the docking module is circumscribed as a circle around the centre of mass, with the radius close to the tether's length. At the moment when the STS is orientated along a local vertical, and the docking

module is below, docking with the spacecraft in low-altitude orbit occurs (point A at Figure 1.3). After that, the mechanical system consisting of the bearing satellite, the tether, the docking module and the spacecraft moves as a single whole. The centre of mass of this new STS is on a lower altitude than the centre of mass of the initial bundle. Disconnection of the spacecraft happens after the system makes a half turn and its tip with the docking module appears in the upper point B. After separation, the centre of mass of the STS again displaces more closely to the bearing satellite; that is, it will

**Figure 1.3** Use of a spinning space tethering system for lifting a payload into high-altitude orbit



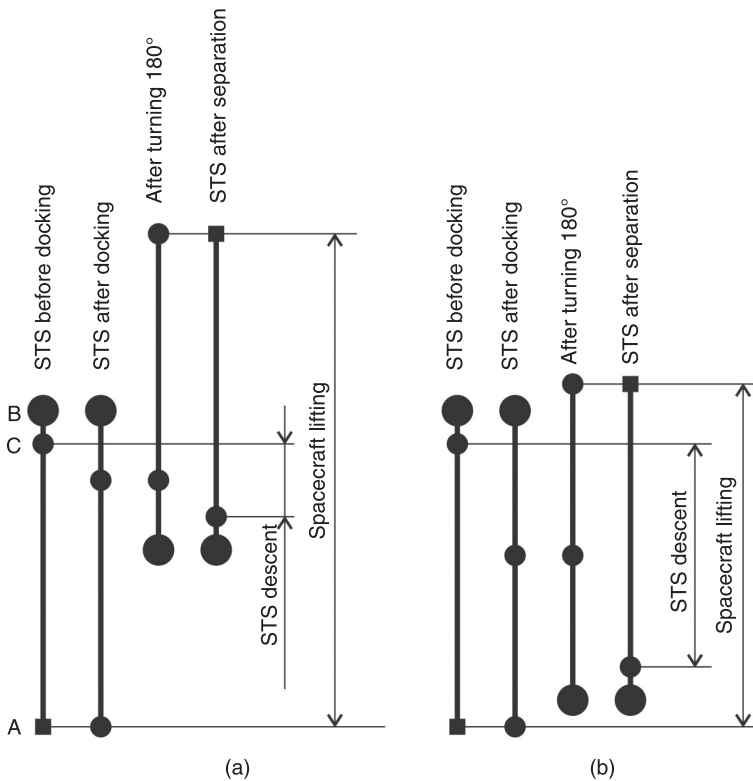
be lowered. Thus, the space vehicle will be transferred to a higher-altitude orbit, but at the expense of the downturn of the STS orbit. The most effective scheme works at the coincidence of direction of the spacecraft's motion, the STS centre of mass and the docking module, and at the moment of docking.

Alert readers will notice that the fuel saved on the raising of a spacecraft's orbit also needs to be spent for the restoration of the orbital altitude of the STS. This is certainly so but, on the one hand, orbital altitude restoration often is not required; for example, in a case when the bearing satellite appears to finish its mission as a multipurpose spacecraft, or the re-entry vehicle descends from an orbit. On the other hand, it is possible to raise the altitude of orbit of a STS without use of jet fuel; for example, solving an inverse problem of a spacecraft's transfer to a low-altitude orbit, or at the expense of interaction of a conductive tether with the electromagnetic field of Earth, as will be discussed below.

Let us note one more obvious fact. The greater the difference between the mass of the bearing satellite and the mass of the lifted spacecraft, the higher the altitude orbit can be achieved through the manoeuvre, and the less the lowering of the system's orbit. In Figure 1.4, the examples for when the mass of the bearing satellite greatly exceeds the spacecraft mass (a), and when these masses are comparable (b), are shown. As a result of this manoeuvre, the centre of masses (point C) in the second case will be lowered much more than in the first, and the raising of the orbital altitude of spacecraft will be less.

The efficiency of spacecraft lifting can be refined, using not merely one but some other tether systems disposed in different orbits within the multiple periods. This way allows for a tripling on the mass put into orbit (Lorenzini et al., 1999).

**Figure 1.4** Comparison of a space tethering system's effectiveness in the cases of small (a) and large (b) differences between the masses of the bearing satellite and the lifting spacecraft



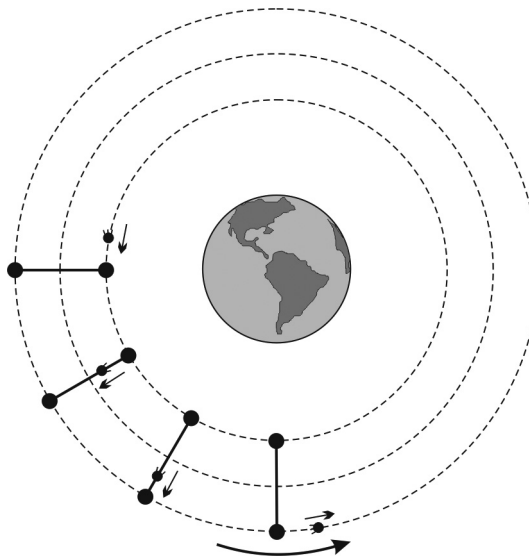
It is possible to accelerate a STS after the spacecraft has joined by increasing the angular velocity of rotation concerning the centre of the masses. In this case, after spacecraft separation, it will be injected onto a higher orbit. Space tethering system speed-up can be executed in many ways. The elementary solution is by the use of jet engines, but it is also possible to use the influence of the Earth's magnetic field for carrying out a tether with a current. It is possible to

boost the system by means of the tether length control, using the principle of swing. Such control allows for considerable dilation of the capabilities of a STS (Troger et al., 2010).

The solution to the problem of carrying the spacecraft into high orbit requires the soft docking of the spacecraft using STS. One way to provide this soft docking is to use loops of a tether which allows for smoothing of errors in the spacecraft's control. The idea consists of the following: the harpoon which clings to a loop is installed on the spacecraft; and this makes the system indifferent to large longitudinal, moderate lateral and small out-of-plane errors (Lorenzini, 2004). Williams, Blanksbya, Trivailoa and Fujii (2005) suggest using the alternative docking gear. They suggest using the original 'basket' that attaches to the tip of a tether and aids the catching of the spacecraft.

### **1.1.3 Space escalator**

The problems of raising a spacecraft to a higher-altitude orbit, and descending from an orbit, can be solved by means of the so-called space escalator. The escalator represents a radially-orientated STS existing in an orbit for the long term. As in the previous case, the spacecraft docks to the lower tip of the tether and by means of the special gear moves upward along the tether. After the spacecraft reaches the upper tip, it disconnects from the escalator and continues in free motion (see Figure 1.5). The mass of the end-bodies of the escalator should exceed the mass of the raising spacecraft significantly. Otherwise the manoeuvre will appear not to lift the spacecraft by the escalator into a higher orbit, but as if the STS is dragged into a lower orbit by the spacecraft. An important point in the design of the space escalator is the question of a lifting speed's selection. As it rises, the Coriolis force moves

**Figure 1.5** Space escalator

along the tether spacecraft. This force is proportional to the lifting speed, and it aims to deflect the spacecraft from the line connecting the escalator's end-bodies' centres of mass. The qualitative analysis of a load motion along a tether is carried out in an article by Rodnikov (2004).

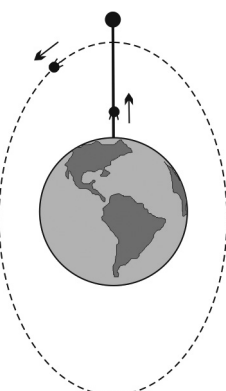
If there are several escalators in different orbits, it is possible to put a spacecraft into a high-altitude orbit sequentially. The problem of inventing a strong material for the manufacture of a very long cable is solved, because instead of one stretched system with a very strong cable, smaller systems with less strong cables are used.

### **1.1.4 Space elevator**

Another interesting way to put a spacecraft into orbit is by using a space elevator. The concept of the space elevator first appeared in 1960 and was suggested by the Russian engineer

Artsutanov (1960). Unaware of this suggestion, Isaacs, Vine, Bradner and Bachus (1966), and Pearson (1975), came to the same conclusion. Its essence consists of using a tether to join the surface of Earth and the station which is in a geostationary orbit, and to put a cargo into orbit on the lift, without expending a propellant. At any moment the cargo can be separated from the tether and sent into free flight. The space elevator allows the load to be carried into orbit with various parameters. For this purpose, in the separation moment it is necessary to give the cargo a directional momentum of velocity in an appropriate manner. By use of engineering, it can be executed by means of a special tube or a chute canted at an angle to the elevator. A variety of accessible orbits can be increased by using jet engines erected on the capsule with the cargo after separation. Depending on altitude and momentum at undocking, the cargo starts to move on a parabolic, elliptical or hyperbolic orbit (see Figure 1.6). The space elevator allows the cargo to be put into orbit with smaller energy expenditure, in comparison with rockets, as fuel is spent only for minor updating of the orbit parameters. In addition, these expenditures can be made by engines of

**Figure 1.6** Space elevator



different types, and with low power usage of the different forms of energy. There is reason to believe that in solving the cargo deorbiting problem the space elevator provides more flight safety, because it is not necessary to enter with space velocities into the atmospheres of planets (Polyakov, 1999).

A considerable quantity of scientific work is devoted to the study of the space elevator. For example, Beletskii, Ivanov and Ovtstavnov (2005) on the basis of the elementary model, illustrate the mechanical principles underlying the concept of the space elevator. The authors also studied the stability of the steady-state regimes of the system's motion. Polyakov (1999) gives a solution to the equilibrium problem for the non-equatorial space elevator. He investigated the dynamics of load lifting and equatorial oscillations of the elevator. Great interest is also shown in the NASA Institute for Advanced Concepts report published in 2003 (Edwards, 2003). The authors investigated the problems of manufacturing, deployment and operation of the space elevator. They tried to rely upon accessible technologies; for example, system deployment is said to be solved by means of conventional rockets.

The space elevator is a very ambitious project. On the one hand the creation of such a system allows for considerable reduction in the price of lifting a load into an orbit; and on the other it demands huge efforts, costs and the solving of many manufacturing problems.

The lunar elevator looks much more of a reality than the space elevator, and its concept was introduced by Moravec (1977) and advanced by Forward (1991). For the lunar elevator a much less strong cable is required, because the gravitational field of the Moon is much weaker than Earth's gravitational field. The lunar elevator represents a typical radial bundle of two bodies, and its uniqueness is that one of the bodies is the natural satellite. If the elevator is disposed on the underside of the Moon with the connected satellite on

the other end of the tether, it will not demand any control as its stabilisation has a passive characteristic (Pearson, 1979).

### **1.1.5 *Interplanetary transfers***

Interest in this theme arose in connection with the renewal of activities over the Martian program at the beginning of the 21st century. The spacecraft is required to be put into a hyperbolic orbit, and this problem can be solved by means of rotating STS or escalators. Sorensen (2003) suggests executing this manoeuvre by an electrodynamic rotating STS. According to Nordley (2001), by means of modern accessible cables it is possible to supply loads to Mars which are comparable in mass injected in an earth orbit. Interesting research was published by Rauwolf, Pelaccio, Patel and Sorensen (2001), when they compared the perspective technologies which enabled the boosting of space vehicles for the flight to Mars. Such competing theories of propulsion as chemical, bimodal nuclear thermal rocket, high-power nuclear electric, momentum tether-chemical hybrid, solar, solar-chemical, and variable specific impulse magnetoplasma rocket were considered. As a result, the authors reached the conclusion that scenarios based on tethers look more realistic, but two points – immaturity of the technology and complexity of operation – made its application impossible for the Mars 2018 project.

### **1.1.6 *Creation of a traffic artery linking Earth and the Moon***

The use of space elevators and escalators allows the creation of an effective space transport system between the surfaces of Earth and the Moon. For example, Levin (2007) examines

a transport system based on two elevators (see Figure 1.7). The essence of the idea consists of the following: a spacecraft with a payload from Earth is lifted into an orbit by means of the space elevator, then it disconnects and moves into a transfer orbit. On reaching the lunar elevator, the spacecraft connects to it and descends onto the Moon's surface. According to Levin's estimates, the perigee and apogee of the transfer orbit should be 50 000 km and 262 000 km, and the length of the lunar elevator should be approximately 120 000 km. The report written by Pearson, Levoin, Oldson and Wykes (2005) is devoted to the problem of a lunar elevator creation. The solutions to some of the engineering and scientific problems are given in it, and it is shown that the lunar elevator can be created now.

The scheme viewed above cannot be realised yet, as there is no material allowing for the creation of Earth space elevator. However, it is possible to use the alternative scheme where, instead of Earth elevator, the escalator rotating round Earth is used (see Figure 1.8).

One more scheme, allowing for the supply of a cyclical delivery of a payload from Earth to the Moon and inversely, is offered by Forward (1991). At the basis of its transport

**Figure 1.7** The traffic artery consisting of two space elevators

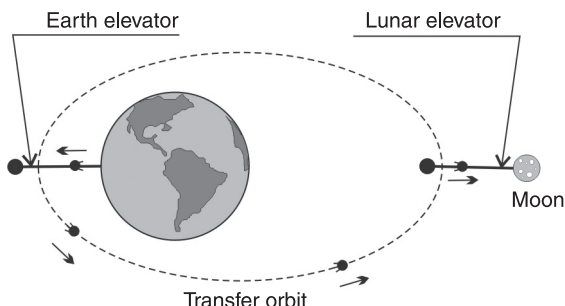
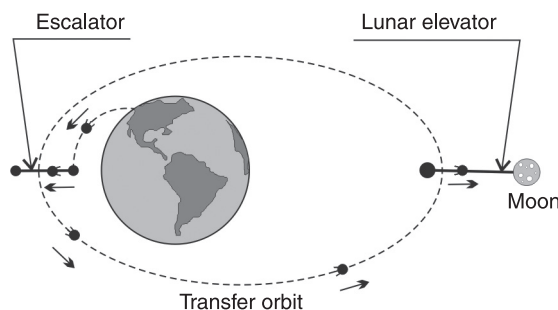


**Figure 1.8** The traffic artery consisting of an escalator and a lunar elevator

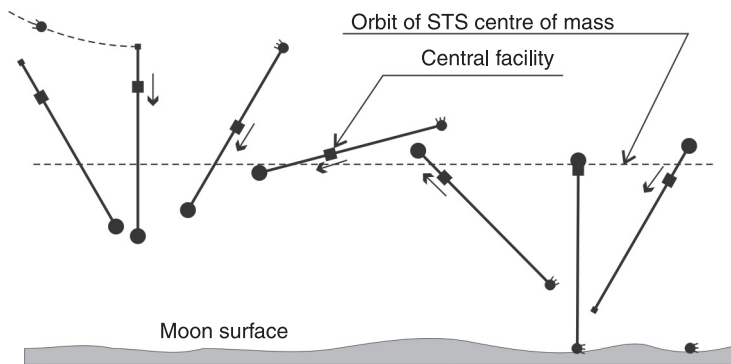


system lie the ideas stated by Maravec (1977) and Carroll (1991). Theoretical examinations and experiments showed that the system should consist of three tether systems. Two of them should be disposed on earth orbits – one low circular and highly elliptical, and the other on an orbit about the Moon. Exchange loads which execute overfly from one tether system to another are included in the offered group besides the orbital tether systems. These overflies of loads tie separate STS into the complete transport artery. In the course of overfly, objects exchange not only masses but also energy. At the lifting of loads into higher-altitude orbit by means of STS, its energy is increased and the energy of tether system is decreased according to the energy conservation law. As a result, the STS orbit is lowered. For restoration of orbit parameters, it is necessary to execute an inverse descent operation with an equivalent mass exchange load. On an earth orbit, there is not enough material for implementation of this process; however it is possible to use lunar soil.

In many respects, a similar transport system was offered by Hoyt and Uphoff (1999). The project was entitled ‘Cislunar Tether Transport System’. Unlike their colleagues, they use only two rotating tether systems: one of which is

disposed in a low equatorial elliptical orbit of Earth, and the other in a low polar circular lunar orbit. According to the authors, such a layout allows the mass of the whole system to be minimised, and achieves the greatest frequency of transport operations. Lengths of the tethers are 80 km and 200 km. According to the design, being on a low Earth orbit, the rotating STS picks up the payload and tosses it in the direction of the Moon. Thus a minimal energy lunar transfer orbit use is intended. After payload disconnection, the STS altitude decreases. For its restoration, it interacts with the magnetic field of Earth as an electrodynamic tether. As the payload approaches the Moon, an updating of its orbit parameters, which can be executed by a jet engine, is required. The necessary value of a momentum of velocity  $\Delta V$  depends on many parameters. For a mass of 2500 kg, it is approximately 25 m/sec. The payload orbiting the Moon is picked up by the lunar tether system, termed Lunavator<sup>TM</sup>, and supplied to the surface of the Moon.

Maravec's (1977) idea is the basis of the Lunavator. He suggested creating a lunar orbit STS (Skyhook) whose rotation requires a Moon with zero velocity on its surface. It is reached because the relative rotation speed of the extremity of the STS around its centre of mass is equal to an absolute velocity of the centre of mass around the centre of the Moon. The rotating tether can be imagined as a spoke of a large wheel which trundles without a sliding on the surface of the Moon. Such a wheel has an instantaneous centre of zero velocity at its tangency point. Skyhook appeared unsuitable for the Cislunar Tether Transport System. At first, its length appeared very large; and second, the velocity of the tether end at the moment of docking considerably exceeded the velocity of the payload on the transfer orbit. Therefore, the authors offered an alternative STS called Lunavator. Its tether system was composed of a tether, a counterbalance mass at one end,

**Figure 1.9** Scheme of operation of the Lunovator

and a central facility with the the capability to climb up or down the tether (see Figure 1.9). On expectation of the approach of the payload, the facility is located near the centre of the tether and Lunovator rotates with a small angular velocity. After acquisition of the payload, the facility starts to move along the tether to the counterbalance. The centres of mass of the system move in the same direction. As the centres of mass remain at one altitude, the distance between the centre of mass and the connected payload increases. The rotation rate of the STS concerning its centres of mass increases also. It allows for a zero relative velocity of payload at the moment of contact with a surface.

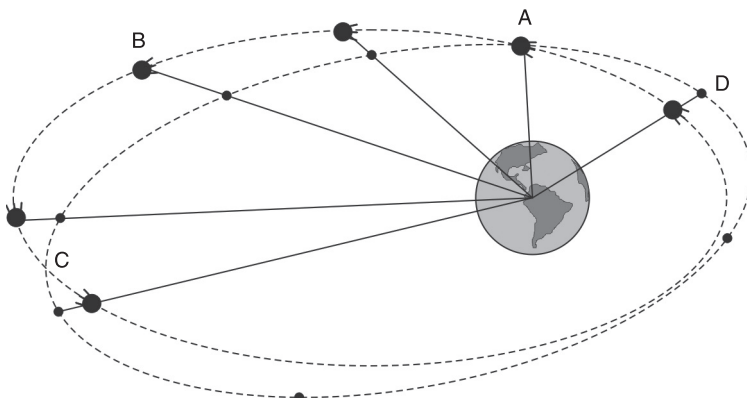
### **1.1.7 Lifting and descent of a payload into an orbit**

By means of space tethers, it is possible to carry out economically, in respect of jet fuel consumption, the lifting and descent of a payload into an orbit. In the case of lifting, the payload is put into a low-altitude orbit by means of the rocket, where it connects to the lower end of the tether

deployed from the spacecraft. After docking, the tether with its payload retracts into the spacecraft. In the case of descent, the payload is lowered into a low-altitude orbit by the tether. At this altitude, which is necessary for motion on a circular orbit, the velocity appears more than the velocity of the payload. Therefore, after detaching from a tether, the payload descends onto the planet surface on a ballistic trajectory (Zimmermann et al., 2005).

Often, the nonspecialist is surprised by the fact that for descent of a payload from an orbit, it is necessary to use a propellant. It is unclear why a jet engine or a tether is needed if it is possible to throw a capsule with its payload downwards, and it will land under the action of a gravity force. Let us assume, for clarity, that the spacecraft moves in an elliptical orbit (see Figure 1.10). At point A, the capsule with its payload is ejected from the spacecraft in the direction of Earth by means of a spring or any other gear. Let us consider that the mass of a capsule is many times less than the mass of the spacecraft, and that the change of the spacecraft's altitude can be ignored. The spacecraft's velocity on an elliptical orbit

**Figure 1.10** Intersection of a spacecraft orbit and the orbit of its ejected payload



equals approximately 8 km/s, and the relative velocity of the capsule ejection can be some tens of metres per second. As a result, after separation the payload orbit will simply be a little inclined in relation to the spacecraft orbit, and the absolute velocity of the payload will be increased in comparison with its initial velocity (more correct would be to eject the payload – not in the direction of Earth, but in the opposite direction to the spacecraft's motion). In point B, an observer on the spacecraft would see how the capsule moves away from him in the direction of Earth. However, after a while the capsule and the spacecraft start to approach again. Their orbits will intersect at point C, and after that the payload will be above the spacecraft. In point D, the amazed observer sees that his payload falls down on him from above.

To solve the problem of descent, it is necessary to return to the task of overfly between orbits. For delivery of a payload to Earth, it is necessary to give an impulse to the capsule which translates it into an orbit intersecting Earth's atmosphere. Aerodynamic resistances reduce the absolute velocity of the payload, and it cannot remain in an orbit. Thus, fuel is spent in giving a braking impulse to the capsule which is sufficient for atmospheric entry.

At tether use, we do not try to reduce the velocity of a payload. Instead, we translocate it into a point where its great speed is insufficient for a motion on an orbit. For example, suppose that a spacecraft initially moves on a circular orbit. By means of the tether's tension force control during its deployment, it is possible to achieve a stationary mode of the STS motion when the tether is oriented along a local vertical at all times, and the bodies connected by it move on circular orbits with an identical orbital angular velocity. The spacecraft disposed above the tether system's centre of mass will have greater speed than its corresponding circular velocity for height, and the speed of the lowered payload will be less than

the circular velocity for its height. If, at any moment of time, we divide the objects connected by the tether, their subsequent free motion will occur on elliptic orbits. The standing of the upper object at the moment of partitioning will correspond to a perigee of its new orbit, and the height of the spacecraft's flight will be incremented. The standing of the lower object at the moment of partitioning will correspond to the apogee of its new orbit. If the perigee radius appears small enough, the payload will enter the atmosphere and will transfer to a descent trajectory (Ivanov and Sitarskiy, 1986).

From a practical point of view, the problem of the definition of motion parameters and STS specifications which provide the required parameters of a payload's entry into the atmosphere is important. Such parameters are: entry velocity; the angle between the vector of velocity and the horizon line in an entry point; and the flight range to an entry point. Ivanov and Sitarskiy (1986) consider a question of the optimum tether length selection at which, for the given height of a spacecraft's orbit and the heights of entry point, the peak angle of entry will be reached. Use of a tether oscillating about a local vertical allows for a considerable increase in the angle of entry. The authors note that at small angles of entry the landing payload can have a considerable longitudinal deviation that impedes selection of a safe landing region and the search for the payload after touchdown.

There are two essentially different approaches to tether deployment as the solution for payload descending problems. The first, termed 'static deployment', means the slow release of a tether which at all times is in a neighbourhood of a local vertical. The second is 'dynamic deployment'. This means that the tether swings at the expense of the Coriolis force acting upon it and use of oscillations to additionally decrease the payload velocity (Zimmermann et al., 2005). These approaches will be viewed in more detail in Chapter 4.

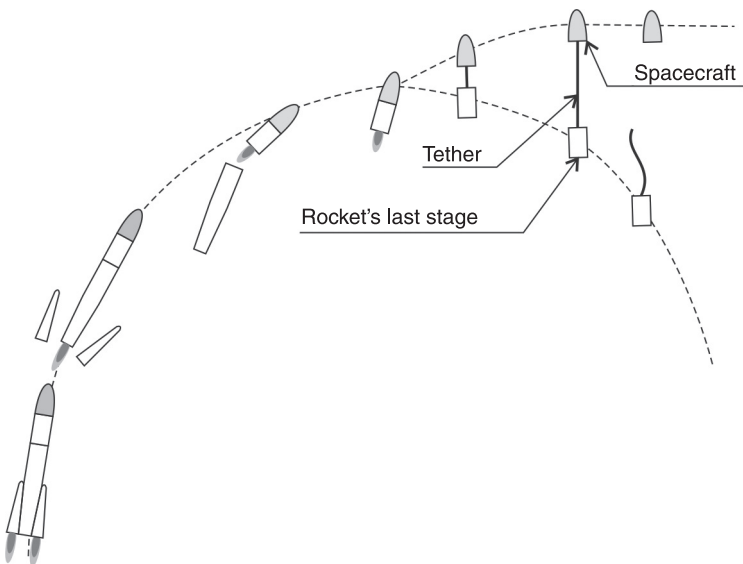
It is important to note that the task delivery of a payload from an orbit is closer to practical realization than all other space tether tasks. Some successful experiments of payload delivery by means of a tether have been executed recently – in a 1993 experiment SEDS-1, and in a 2007 experiment YES2. In first one, a static deployment was used, and in second a dynamic deployment.

The problem of retrieval of a tether is somewhat opposite to the deployment problem. It is much more difficult to embody because of the instability of the tether motion. The problem of retraction of a payload from low-altitude orbit on a large spacecraft, such as a space station, was considered by Djebli et al. (2002). The basic attention was given to the laws of tether control, which are offered for parting on ‘simple’ (the linear or exponential dependence) and ‘fast’ (with different acceleration profiles). They have shown that the damping of transverse oscillations occurs in some cases where there has been ‘fast’ tether retrieval.

### ***1.1.8 Placing a spacecraft into orbit***

One side effect of descent of a payload from an orbit is the upraising of a spacecraft’s orbit. This effect can be used, for example, for developing more effectively in comparison with the traditional approach of putting a spacecraft into orbit. In the latest astronautics for solving this problem, multi-stage carrier rockets are used. In the process of the fuel burning out, the worked-out stages separate, and thus rocket fuel is not spent for the acceleration of empty tanks. The idea of this alternative approach is simple; the last stage of the rocket is connected by a tether to a lifted spacecraft and, after burning-out of the fuel, the parting impulse begins the process of tether deploying. During deployment, the system’s centre of mass stays at the fixed height, the spacecraft

**Figure 1.11** The advanced scheme of placing a spacecraft into an orbit



rises upwards, and the stage lowers. As with the problem of delivery of a payload after separation, the stage descends into the atmosphere, and the spacecraft appears to go higher in comparison with the initial orbit (see Figure 1.11). As with payload descent, various ways of tether deploying can be used for this problem (Shcherbakov, 2010).

Ivanov et al. (2005) estimate the energy gain of using tether systems for placing a spacecraft into an orbit. Cases of moving out from the intermediate circular orbit by means of rotating STS, translated into rotating mode by means of gravitational twist (Komarov, 1974) and with use of stationary radial deployment when the system at all times is oriented along a local vertical, are considered. At first sight, the use of a rotating STS allows it to gain an additional increase of velocity at the expense of the relative rotation STS around its centre of mass; however,

after careful examination, it is not so obvious. The use of a rotating STS means the use of a heavier mechanism. First, centrifugal force creates an additional loading, therefore for a rotating STS a stronger and heavier tether is required. Second, gravitational twist requires the installation of a difficult mechanism of tether deployment control. Static deployment allows for the use of a light tether and deployment system. It is not dependent on the chosen way of deployment that fuel is saved when a large mass is put into orbit.

### ***1.1.9 Lifting of a space station's height of orbit***

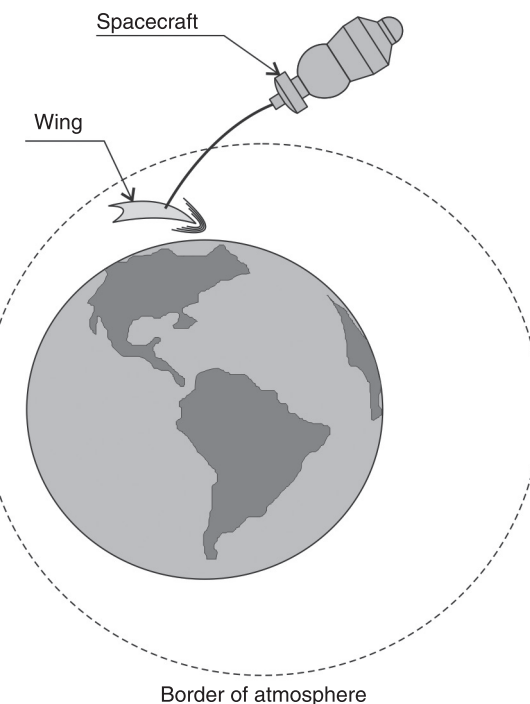
The idea of an orbiting station maintenance of height at the expense of the descent of the cargo spaceships which have executed their primary goal is, in many respects, similar to the idea of putting a spacecraft into a high orbit. It has been taken as a basis for the Russian mission ‘Tros-1’, which was developed by RSC Energia at the end of the twentieth century. In the program ‘Tros-1’, in orbit it was supposed to create the tether system – consisting of space station MIR, the cargo spaceship Progress-M, and the connecting synthetic tether with a 20 km length. It was planned that, within a week, the system would make an orbital flight, the spaceship would be lowered by the tether, then be divided. Such a manoeuvre allowed for saving about 150 kg of fuel. The experiment ‘Tros-1A’ is similar to ‘Tros-1’, and differed from it by the tether’s length being 50 km. Such a STS would allow for descent of the cargo spaceship and its subsequent submersion in the Pacific Ocean without fuel expenditure. Thus, the orbiting station would increment the height of the orbit by almost 10 km, and the fuel saving would be about 400 kg (Shcherbakov, 2010).

### **1.1.10 Orbital manoeuvres without fuel expenditure**

Numerous researches show that it is possible to provide various modes of STS motion, by means of corresponding choices of a tether system's performances and the initial conditions of its motion. Moreover, the selection of the law of a tether's length regulation allows it to carry out a wider spectrum of manoeuvres. Interorbital manoeuvres can be carried out by the continuous action of a constraint force upon a system's elements, and at the expense of constraint provided by a tether (Ivanov and Sitarskiy, 1986).

The force acting on one of the bodies connected by a tether influences that on the second body. This idea is used in the project of lowering of a spacecraft's orbit by a balloon sunk with the help of a tether into the atmosphere. As the density of the atmosphere at the balloon's height is higher than that at a spacecraft's altitude, the considerable aerodynamic drag will reduce the STS velocity and act upon the balloon. In turn, this will lead to a reduction of the spacecraft's orbit height. This problem is viewed by Longuski et al. (1999) in detail. By the use of a special wing instead of a balloon (see Figure 1.12), its deflection from an orbital plane in a resonance with an orbital motion allows it to change not only height but also other parameters of the orbit of the joined spacecraft (Pearson, 1984). It is possible to carry this out by a system of various interorbital and local manoeuvres as a result of tether length control under the specific laws (Lang and Nolting, 1967). By changing the relative location of connected bodies, it is possible to influence an orbital motion of all STS. Use of the cross influence of an orbital and the relative motion of the system underlies a gravity flyer (Beletsky, 2001).

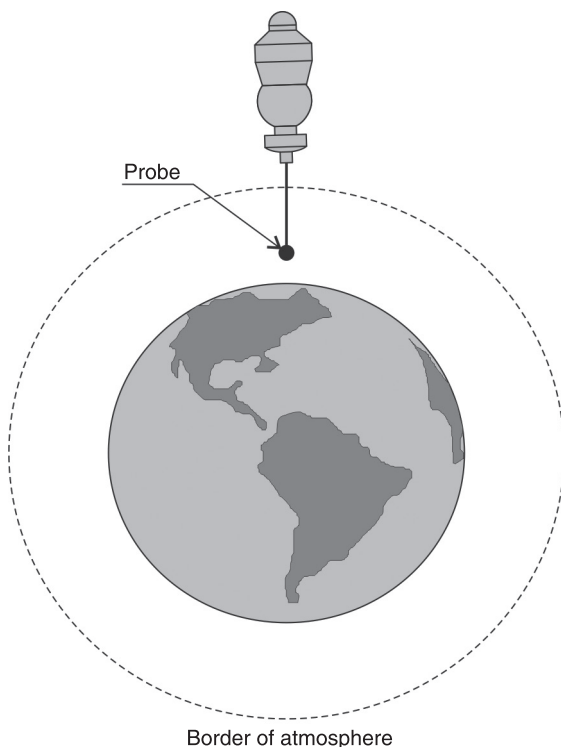
**Figure 1.12** Changing of a spacecraft's parameters by means of a tethered wing



### 1.1.11 *Studying of an upper atmosphere*

The concept of a system for solving the problem of studying an upper atmosphere is, in many respects, similar to the concept of an aerodynamic brake. Study of the atmosphere at altitudes of 100–150 km is impeded, as neither satellites nor airplanes can work at these heights. Descent of a tethered probe from a base spacecraft (see Figure 1.13) at a height of more than 200 km can provide the solution (Beletsky and Levin, 1993). The time of existence of such a system, in comparison with satellites, increases substantially. In particular, for the satellite with a ballistic coefficient in the

**Figure 1.13** Studying of the upper atmosphere by means of a tethered probe



region of  $10^{-4}$  m<sup>2</sup>/kg existence time at heights of 110–120 km is only 1.4 hours. The numerical calculations executed by Ivanov and Sitarskiy (1986) have shown that the body with a ballistic coefficient  $10^{-4}$  m<sup>2</sup>/kg submerged in the atmosphere from the spacecraft in a circular orbit with an altitude of 200 km will descend from a height of 125 km to 100 km in 120 hours. A correcting propulsion system with the power resources supported by quantity of characteristic velocity of 1000 km/s would be required for maintenance of such a duration for a conventional satellite. During the sounding, the STS centre of mass will be lowered at the expense of the aerodynamic drag action on the probe and

the tether. This loss of height can be compensated for by a propulsion system on the base spacecraft. Ivanov and SitarSKIY give an estimate of thrust of the propulsion system required for stationary motion of the bundle, at which the base spacecraft and tethered probe move in circular orbits.

Lowered from the spacecraft in a circular orbit, the probe will move with a velocity smaller than that of a similar sounding satellite moving in a circular orbit at the same height. As the aerodynamic drag is proportional to a squared velocity, the probe pulled down on a tether will feel less resistance from the atmosphere. For a 100 km tether, the aerodynamic drag reduction is 3%, which enables reduction of the heat-resistant coating of the probe. Beletsky and Levin (1981), estimating atmosphere influence on the temperature of the probe and the tether, come to the conclusion that the long-term sounding of the atmosphere on temperature requirements is possible only at heights greater than 90 km.

There is one more scheme of sounding, which estimates the use of a spinning STS. It requires that the rotation happens in the opposite direction to the STS orbital motion. As a result, the probe's atmospheric speed is reduced in comparison with a similar velocity for a nonturning system. Thus, it is possible to provide conditions at which the probe rotating around the STS centre of mass will go out from the atmosphere and will be cooling. This is essential for providing favourable conditions for on board equipment. In addition, a tethered probe can scan different atmospheric layers during rotation (Troger et al., 2010).

### **1.1.12 Gravity stabilisation of an orbital spacecraft**

Often, a spacecraft's orientation in the Earth's direction for a long time is required at the realisation of its mission. The

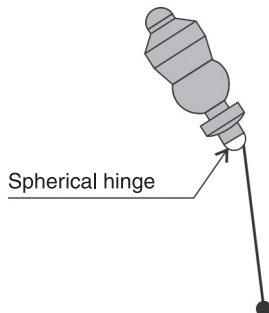
systems of active stabilisation, founded on the use of jet engines with small thrust and gyros, are widely applied to solve this problem. Their obvious deficiency is the requirement for expenditure of a propellant. Since the middle of the last century, a parallel approach, using passive stabilisation systems has developed. The greatest distribution among them was achieved by gravity-gradient stabilisation systems. From the mechanics of space flight, it is known that an orbital prolate rigid body under the action of the gravitational moment occupies a stable position in which the greatest axis of an inertia ellipsoid is orientated along its radius vector. This effect underlies gravity stabilisation systems. The more the inertia ellipsoid is prolated, the better the gravitational moment stabilises the orbital rigid body. If we speak about a spacecraft, an elongation of its inertia ellipsoid is possible through the attachment of a special rigid bar. One of the basic disadvantages of such constructions is their rather small length. With the use of long bars, there are inevitable diversions from the design values of a system's mass-inertial performances, which lead to considerable reduction in stabilisation accuracy. One more deficiency of systems with rigid bars is the presence of bending vibrations, which are transmitted to the spacecraft, and also reduce the accuracy of stabilisation. In connection with these problems, use of a long flexible tether with the load instead a rigid bar has better prospects.

The idea of using a tether in the scheme of a satellite's gravity-gradient stabilisation also was considered in the 1960s by Chobotov (1967) and Robe (1968). The tether allows for an increased distance between the spacecraft and the stabilising load of several kilometres. It causes an increase of the recovering moment of gravity-gradient which is proportional to this distance in its first approximation. The analysis of the perfection capability of a satellite's gravity

stabilisation system by including a tether with a stabilising load in a mechanical system was carried out by Andrienko and Chadaev (1998).

Among its merits, the gravity stabilization system constructed on a tether base also has a number of demerits. They are related to the flexibility of a tether and the impossibility of transfer through it of the damping force's moments. As shown by Beletsky and Levin (1993), the interior friction in a tether quickly enough quenches its elastic oscillations, but practically does not influence the angular oscillations of the system. For the quenching of these oscillations, it is possible to use a longitudinal damping device which has been adjusted to a resonance between the longitudinal and angular oscillations of the system. However, the frequencies of angular oscillations of a system are various and they alter the amplitude of angular oscillations, thus it is impossible to create the passive damper that ensures resonance tuning of frequencies. Andrienko and Chadaev (1998) suggested using the quenching of angular oscillations instead of the damper to use the tether's tension regulator that provides resonance tuning of the oscillation frequencies.

Internal and gravitational forces do not change the total moment of momentum of an STS, therefore a problem of gravity stabilisation by means of internal forces estimates redistribution of a moment of momentum of the relative motion in a moment of orbital motion. The elementary embodying of this idea is executed in 'jo-jo' devices used on the American satellites in the early 1960s (Beletsky and Levin, 1993). Dissipative torque, quenching in-plane and out-of-plane oscillations, can be created by placing a spherical hinge on the spacecraft (see Figure 1.14). The tether fastens to the spherical hinge, and at deflection of the tether from an axis of the spacecraft, a tension force creates the moment that turns the hinge. When the spherical hinge on

**Figure 1.14** Gravity stabilisation of a spacecraft

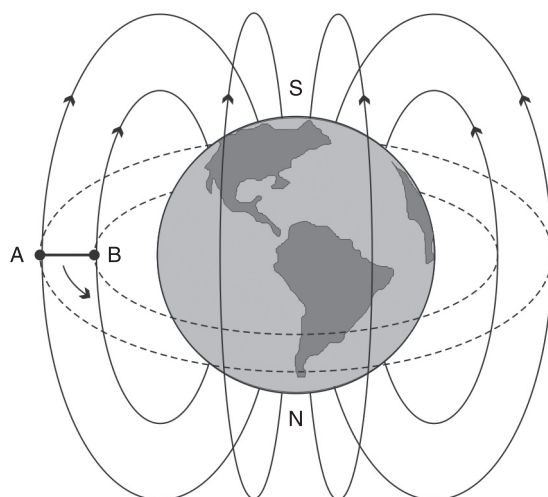
the spacecraft moves, friction is created, which diffuses system mechanical energy. The analysis of such a scheme of damping for vertical orientated spacecraft is discussed by Alpatov et al. (2007).

### **1.1.13 Generation of electrical energy by means of conductive tether**

Problems based on a conductive tether's interaction with the Earth's electromagnetic field are distinct from those solved by tethers. By means of a tether, it is possible to generate electrical energy on board a spacecraft. Let us view in general the physics of the process (Cosmo and Lorenzini, 1997). It is possible to represent a magnetic field of the Earth, as the field created by a dipole directed along the rotation axis of the Earth. Magnetic lines go out from its northern magnetic pole (coinciding with the southern geographical) and enter in a southern magnetic pole on arcs, diving through ionosphere strata. The ionosphere is a part of the upper atmosphere and represents a rarefied weakly-ionised plasma. The difference is that the altitude layers of the ionosphere have very low conductance between its layers in natural conditions. Let us presume that a radially orientated STS moves in a

circular orbit in a plane of the magnetic equator. On the tether's ends, special devices are mounted providing a contact to the plasma. There may be various collectors, electronic guns or hollow cathodes (Parks and Katz, 1987; Wilbur and Laupa, 1988). A conductive tether is covered by the insulation which prevents a direct contact with the plasma. Electromagnetic processes in such a system flow as if connected by the tether, and end-bodies A and B slide on two conducting rings which correspond to the ionosphere layers at the altitude of the bodies (see Figure 1.15). Let us assume that in the tether the electric current flows, and the electrons move from point A to point B. When the electrons appear in point B, they fall in ionospheric plasma through contact devices and move to the poles on spiral trajectories along the magnetic lines, SBN. Missing electrons come from the poles and are captured by the contact device on the upper end, A. There is a layer of high conductance at an altitude of 110 km. The electrons which have left end B of the tether after a

**Figure 1.15** Current in a conductive tether at its motion in a magnetic field of the Earth



while reach this layer and transfer to lines SAN, then the electrons return to the upper end of the STS along these lines. Thus, the closed circuit is organised (Beletsky and Levin, 1993).

Under electromagnetism laws, moving a conductor in a magnetic field causes a voltage induction. Its value is proportional to the speed of the conductor, the inductance of the magnetic field, and the conductor length. This fact can be used to generate electrical energy by means of a STS. The power of a voltage source based on a space tether can reach values of the order of 100 kW. On moving to a magnetic field of a conducting tether, the electrodynamic braking force leads to a descent of the STS altitude. It is possible to indemnify the given braking action by activation of a propulsion system. Thus, by means of an electrodynamic cable, it is possible to convert the mechanical energy of a system into an electrical form (Ivanov and Sitarskiy, 1986). For the first time, similar experiment were implemented in 1996 when, within the TSS-1R program, the electric power was generated by means of a conductive tether.

### ***1.1.14 Use of electrical energy for modification of a STS orbit parameters***

A conductive tether allows the resolution of the opposite problem to the generation of electrical energy. The electricity received by means of solar batteries can be used to modify a STS orbit parameters. When there is a current in a tether, an electrical force will act upon it. In 2001, Sorensen offered the concept of the orbital manoeuvre based on the electrodynamic properties of a tether and its momentum. The project did not assume the use of jet thrust, and was called Momentum eXchange Electrodynamic Reboost (MXER). In essence, it consists of the following: a spinning STS with 100 km

tether moves on an elliptic orbit; lifting into high orbit, a spacecraft locates on a low Earth orbit; at a given time, it docks with the lower end of a rotating STS and starts to move towards it. After the tether system turns over and the spacecraft appears in its highest point, it disconnects from the tether and prolongs the free motion on a high-altitude orbit. As a result of this manoeuvre, the orbital altitude and rotation speed of the system will decrease. For reboost of the STS and the lift of its orbit use Ampere force created by passing of a current in the tether. Thus, the spacecraft lifting into high-altitude orbit happens, in essence, without energy expenditure. Published in 2003, the final report shows that the main problem of embodying the MXER design is the problem of tether reliability and the coordination of its motion with other objects on an Earth orbit (Sorensen, 2003). According to the information given by Bonometti et al. (2006), works on MXER are prolonged within the In-Space Propulsion Technology (ISPT) NASA program. Interaction of a conductive tether with the magnetic field of the Earth and its use as the drive was also considered by McCoy (1984).

### ***1.1.15 Use of electrodynamic tethers for orbital altitude maintenance***

Electrodynamic tethers can be applied to the maintenance of a spacecraft's orbital altitude. Today jet engines are used for these purposes. Levin (2007) investigated in detail the possibility of solving the problems by means of electrodynamic tethers. Using an example of the Soviet space station Mir, flooded in 2001, he showed that the tether system was a simple and effective way of maintaining a station in an orbit. At the same time, Levin notes that use of an electrodynamic tether for orbit maintenance is not a trivial thing. Detailed study of the stability problem is required. The difficulty is

that, acting on the tether with a current, the Ampere force influences a destabilising effect on the system. Also, in the STS there can be resonances of various natures. If the system is in a resonance area, it can be stabilised by means of the gyro-damper and the attitude controlled with thrusters. It is also suggested that the tether's oscillations may be controlled by means of a variation of the current intensity. As described in Levin's book, the project 'Mir Electrodynamic Tether System' could prolong the life of the Mir space station but, unfortunately, it has not been finished and implemented for political reasons. As given in Levin's work, scientific results can appear especially topical for the International Space Station (ISS) in the light of recent trends of cuts in funding of the American space programs. The theme of tether use at the ISS was considered by Vas et al. (2000). They came to the conclusion that the tether would allow a saving in the order of a billion dollars over 10 years.

### ***1.1.16 Use of electrodynamic tethers for spacecrafts and space debris descending***

In near space, there are some thousand failed satellites and a large quantity of smaller objects, such as spent upper portions of rockets with fuel remnants, various fragments of spacecrafts, caps of lenses of satellite photographic cameras, fairings and so on. In the scientific literature all of this is termed as space debris. More strongly than others, it pollutes the near-Earth orbit. Though on low-altitude orbits objects cannot exist for a long time (on average, five years), constantly putting new space objects into orbit plus the upper stages of rockets indemnify this natural utilisation. During past decades, the space debris became a serious problem and various ways of solving it are actively investigated. In 1996,

Joseph P. Loftus from NASA Johnson Space Center put forward the possibility of using electrodynamic tethers for the descent of objects from an orbit. This idea has been advanced by Forward (1991), and the system created on this basis was given the title of Terminator Tether (Forward and Hoyt, 2000). Terminator Tether represents a thin wire, 5 km in length, with a small load at its end. The tether is initially maintained in ‘ready’ mode, reeled on the coil on board the spacecraft. When the decision is made to end the operation of the spacecraft, the command to commence coil unwinding is sent to Terminator Tether. The deployed tether, under the influence of gravitational forces, takes on a stable vertical state. The spacecraft with the tether moves with orbital velocity in the Earth’s magnetic field, and as a result voltage is induced along the tether, and in the conducting cable there is a current. Force of Ampere created by a current pulls the spacecraft with the tether downwards, and diffuses the energy of their orbital motion. As a result, the spacecraft enters into dense beds of the atmosphere and either burns down, or lands on the Earth’s surface. Such a simple and inexpensive method allows for the essentially accelerated departure of a spacecraft from an orbit. If the spacecraft at an altitude of 950 km descends to Earth within 100 years, Terminator Tether reduces this procedure to 18 days. In 1994, Hoyt and Forward founded TUI company for developing Terminator Tether.

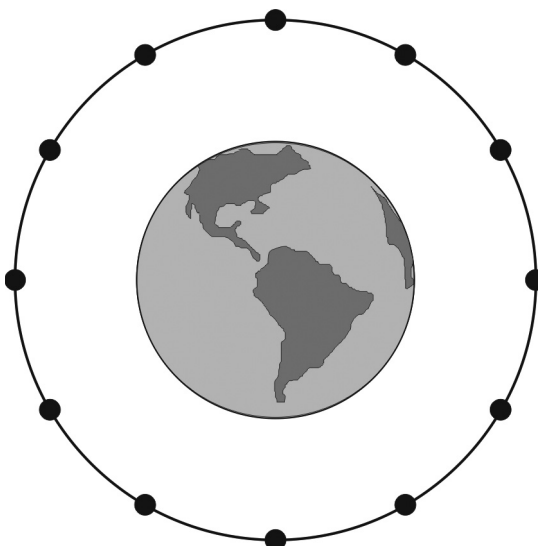
The same idea has been used in a project of the re-entry capsule, EDOARD (Electrodynamic De-Orbiting And Re-entry Device). The system consists of a short tether of 4–5 km in length and a passive collector of electrons of 10 m diameter. The capsule is intended for the descent of a spacecraft with a mass of 4000 kg from an orbit in altitude up to 2000 km and an inclination up to  $65^\circ$  (Bruno et al., 2001).

Prospects for the use of electrodynamic tethers to solve the problem of de-orbiting are considered by many authors. For example, Pardini et al. (2007, 2009) indicate that tethers have great potential, but also discuss a number of unresolved problems which do not yet allow this technology to be widely implemented. The basic problem is fragility of the tethers and the vulnerability to collisions with micrometeorites and space debris.

### 1.1.17 Space rings

The space elevator is not the only grandiose project based on the use of long tethers. Another immense project is called the space ring. The space ring is a large group of spacecrafsts located on a single altitude and connected together by tethers. It looks like beads rotating around the Earth (see Figure 1.16). The main virtue of the space ring is the ability

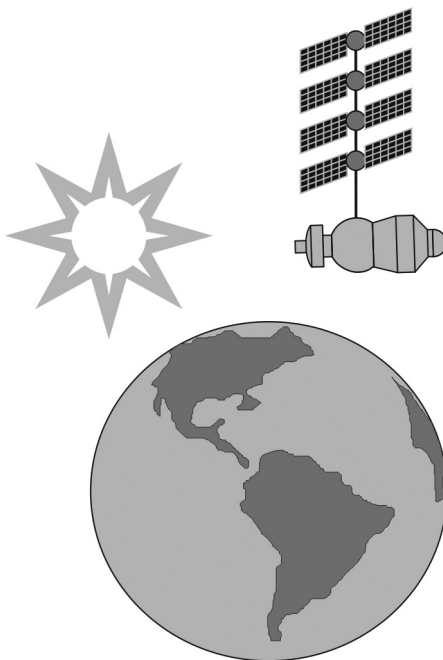
**Figure 1.16** Space ring



to cross coordinate the spacecrafts' motion. Thus, it is possible to create an orbit of a group with very large density, without fear of cross collisions of the elements. Tethers also can be used as transport canals between spacecrafts. The dynamics of space ring motion is considered by Polyakov (1999). He also studied the rings consisting of radially oriented STS. Such a system allows for reduction of stress on the tethers and can be used, for example, as a planetary-ring power station. The voltage is induced in the ring owing to the spinning of the magnetic field of the planet. In other words, the electric power is generated at the expense of a kinetic energy of rotation of the planet.

### ***1.1.18 Use of a tether as an auxiliary structural member***

In the problems viewed above, the singularities of a tether related to the capability of momentum exchange, to an interaction with a magnetic field of Earth, to a convertibility of a configuration were used. Meanwhile, there are a variety of problems where the tether is present exclusively as an auxiliary structural member. For example, tethers can be considered as a base for installation of additional solar batteries (see Figure 1.17). On the basis of a static STS, it is possible to construct interferometers with very large bases for far-space study. One such project is the design of the NASA 'Terrestrial Planet Finder' (Beichman et al., 1999). Space tether systems can be used for creation of a system of global space radio communication; in this case – a tether with a special device on its end to act as an antenna for the low-frequency transmitter. The generated radio-frequency radiation is spread on ionospheric channels across most of the Earth. It is interesting to view the behaviour of a cable as

**Figure 1.17** Tether as a base for placing of a solar battery

units of structure of a solar sail. The study of complicated tether systems led to the shaping of the concept of a space network where sets of cables create a complicated net-like structure (Beletsky and Levin, 1993).

Polyakov (1999) considered a tether system as the base for mounting of space mirrors that can be used for the irradiating of megacities and climate correction on Earth. In 1993, the Russian corporation RSC ‘Energia’ carried out an experiment with a mirror on an orbit. The mission ‘Znamya 2’ envisioned the creation of a sunlight spot with a diameter of 5 km and with luminosity comparable to a 50-w light bulb by means of a 20-metre solar sail with a mirror surface. Polyakov offers various schemes of space mirrors systems, in which the basic ring linking by tethers of a considerable quantity of

various orbital objects lies: satellites with mirrors, bundles of ‘mirror-stations’, a radial STS with a set of mirrors. In addition, Polyakov suggests the possibility of placing separate bundles of ‘mirror-stations’ in regions of five points of the Lagrange Earth–Moon system.

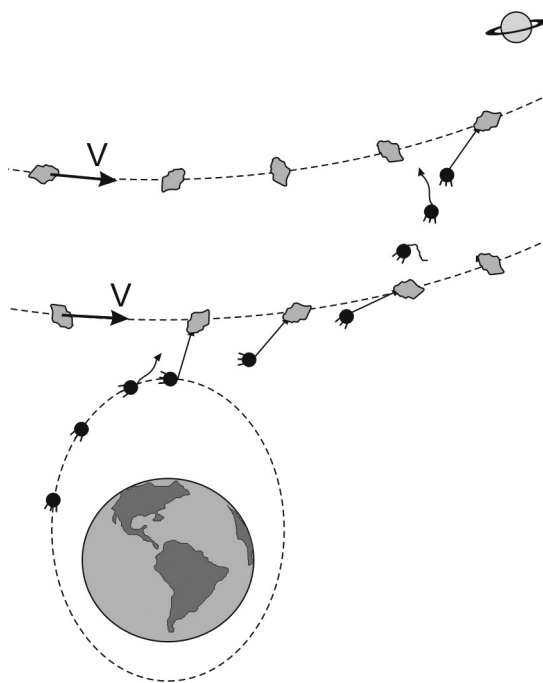
### **1.1.19 Space harpoon**

Tether systems can be applied effectively to collect samples from comets and asteroids. The conventional scheme for solving this problem estimates a spacecraft’s touchdown on their surface. It is a very complicated engineering problem which demands great accuracy. Gravitation of the investigated object is very small, therefore it is necessary to take additional measures for fastening the research module to it. The alternative approach implies the use of a 50–100 m tether (Cosmo and Lorenzini, 1997). After approaching the investigated object, the spacecraft shoots a capsule with the equipment necessary for taking a sample. The capsule is attached to the spacecraft by a tether and, after taking a sample, it is simple enough to retract into the spacecraft. This method has some advantages over classical approaches. First, the construction of a tether system is much easier than a touchdown system. Second, with its help it is possible to take samples from different regions of a meteorite, instead of a limited field around a touchdown point. The dynamics of the featured scheme are particularly considered in Levin’s book (2007). Such a tether system was called a space harpoon.

The idea of using a space harpoon for sample return missions has been advanced by Lanoix and Misra (2000). They suggested using the space harpoon not only for sample gathering, but also for speeding up of a spacecraft enabling it to visit some asteroids without large expenditures of fuel.

The principle underlying the project has been put forward by Penzo and Mayer (1986). Usually, for implementation of interplanetary flights, use of the gravitational fields of planets and their natural satellites is supposed. At the corresponding selection of a trajectory, interplanetary spacecraft can receive essential additional incremental velocity when passing near large celestial bodies. For example, the Cassini spacecraft on its flight to Saturn used the gravitational fields of Venus and Jupiter. It enabled a considerable saving of fuel in comparison with Goman's overfly. Although such manoeuvres are rather effective, they require a certain positioning of planets, therefore they are unable to be implemented often enough. On the other hand, in the solar system there are a considerable quantity of smaller bodies which can also be used. In the immediate proximity of Earth, there are trajectories of several thousand asteroids with diameters of more than a kilometre. Certainly, their feeble gravitational field is not capable of influencing spacecraft to any great degree; however, an asteroid can tow a spacecraft by means of a tether. After the spacecraft and the asteroid are connected by a tether, there will be a redistribution moment of momentum between them. The bundle will start to rotate around the common centre of mass. When the velocity vector of the spacecraft reaches the desired value, the tether is disconnected from an anchor which remains on the asteroid and is retrieved on board. Thereafter, the spacecraft flies to the next asteroid (see Figure 1.18). Lanoix and Misra term such a manoeuvre as a tether sling-shot assist. In his article Lanoix (1996) estimates the quantity of saved fuel on a flight to Jupiter at the expense of using this manoeuvre.

In the above review, the majority of problems which may be solved by means of space tethers are covered; however it is not an exhaustive review. New ideas and ways of using tethers in space are constantly emerging.

**Figure 1.18** Tether sling shot assist

## 1.2 Chronology of experiments with the use of space tethers

The review of a modern level of STS shows that this technology is on the verge of wide practical application (Troger et al., 2010). A variety of orbital experiments using a STS have already been carried out (see Table 1.1).

In the second half of the twentieth century, space exploration has gone rapidly. The catalyst of this process was the uncompromising competition between the USA and the Soviet Union. The 1950s and 1960s marked the triumph of Soviet astronautics. On 4 October 1957, from the cosmodrome Baikonur, the first artificial satellite was put

**Table 1.1** Experiments with space tethers

Mission	Orbit	Year of implementation	Full tether length	Deployed tether length
GEMINI-11	LEO	1966	36 m	36 m
GEMINI-12	LEO	1966	36 m	36 m
TPE-1	Suborbital	1980	400 m	38 m
TPE-2	Suborbital	1981	400 m	103 m
CHARGE-1 (TPE-3)	Suborbital	1983	418 m	418 m
CHARGE-2 (TPE-4)	Suborbital	1984	426 m	426 m
OEDIPUS-A	Suborbital	1989	958 m	958 m
CHARGE-2B	Suborbital	1992	426 m	426 m
TSS-1	LEO	1992	20 km	268 m
SEDS-1	LEO	1993	20 km	20 km
PMG	LEO	1993	500 m	500 m
SEDS-2	LEO	1994	20 km	20 km
OEDIPUS-C	Suborbital	1995	1174 m	1174 m
TSS-1R	LEO	1996	19.7 km	19.7 km
TiPS	LEO	1996	4 km	4 km
YES	GTO	1997	35 km	–
ATEx	LEO	1998	6.05 km	22 m
PICOSAT 1.0	LEO	2000	30 m	30 m
PICOSAT 1.1	LEO	2000	30 m	30 m
YES2	LEO	2007	31.7 km	29 km
T-REX	Suborbital	2010	300 m	300 m

into an orbit of the Earth. On 4 October 1959, the interplanetary station was launched to fly around the Moon and transfer the first photos of its underside to Earth. On 12 April 1961, the first piloted spaceship ‘Vostok-1’ with Yuri

Gagarin on board was launched. On 18 March 1965, from the spaceship ‘Voshod-2’, the Soviet cosmonaut A.A. Leonov carried out the first extravehicular activity. For safety, Leonov was joined to the spaceship by a tether. This was in fact the first application of a tether in space. The American astronauts in the ‘Gemini’ program used a similar safety device.

### ***1.2.1 Gemini missions***

The American government made considerable efforts to change the situation and to take over leadership in the space race. In May 1961, after Yuri Gagarin’s flight, President Kennedy proclaimed the landing of a man on the Moon as a priority for the American nation. In the 1960s, Americans systematically and tirelessly worked on the program of disembarkation of a man to the Moon. In 1965, NASA began the ‘Gemini’ mission with the purpose of developing the technologies and equipment necessary for space travel. Within this project, the experiments of a longer stay of man in space, extravehicular activities, and rendezvous and docking manoeuvres were fulfilled. The Gemini spacecraft was a small two-seater capsule in weight about 3800 kg, placed into a circumterrestrial orbit by a Titan II GLV rocket. In total, within the ‘Gemini’ project, 12 flights have been carried out including 10 with astronauts. Experiments with the use of tethers were carried out in the last two spacecraft missions. In both cases carried out in an orbit, the STS had an identical design: the Gemini spacecraft was connected by a tether with a pilotless 3175 kg Agena spacecraft. The tether was made of a Dacron fibre, and its length was 36 m. The objectives of these experiments with tethers were the testing of STS passive stabilisation under the influence of a gravitational gradient, and the creation of artificial gravitation by means of a spinning tether system.

On 12 September 1966, the launch of Gemini-11 was carried out. One feature distinguishes Gemini missions from a number of subsequent experiments with tethers: Gemini tether experiments were executed on the basis of piloted spacecraft with crew on board; moreover, before the experiment one of the crewmen left the spacecraft and manually connected the Agena and Gemini. Such an unusual scheme has been caused by that experiment with a tether was an accessory. The main objective of the programs was the practising of rendezvous manoeuvres and the docking of Gemini and Agena which were put into orbit by different carrier rockets. After connection by the tether, the undocking was carried out, and Gemini was led away from Agena vertically upwards to a distance which created a tension in the tether. Because of problems during tether deployment, the STS was not used in a gravitational stabilisation mode. Experimentation on creating artificial gravitation passed successfully. Spinning of the system was carried out by means of Gemini's jet engine. During the experiment, an angular velocity of  $0.016 \text{ s}^{-1}$  was reached, and additional acceleration on board the spacecraft created  $10^{-4} \text{ g}$ . According to the astronauts, they felt nothing, but when they placed the camera near the control panel, it started to move slowly in a direction away from the centre of mass of the STS. After finishing the experiment, the docking bar to which the tether was attached was ejected by means of an explosive charge and Gemini entered the atmosphere (Lang and Nolting, 1967).

On 11 November 1966, Gemini-12 was launched and the experiment on gravitational stabilisation was repeated. This time deployment passed smoothly, but the tether was strained more poorly than planned. It did not prevent the success of the experiment. The system was in a mode of gravitational stabilisation for nearly four-and-a-half hours. Gemini

experiments have shown that the dynamics of a tether is much more difficult than researchers supposed. The Apollo project, which finished with the landing of a man on the Moon, was carried out without the use of space cables (Hacker and Grimwood, 1977).

### ***1.2.2 Tethered Payload Experiment (TPE, CHARGE-1, CHARGE-2)***

After the Gemini missions, experiments with tethers were stopped for more than ten years until 1980, when the application of a small tether for an ionosphere study was required. Within the American–Japanese experiments, which were called Tethered Payload Experiment (TPE), light sounding rockets were used. These rockets were not intended for putting a payload into an orbit, but can deliver it to a high altitude for a short time, and then the payload drops to the ground. The essence of the experiment consisted of the following. The rocket was separated into two parts: from the top part in the ionosphere the flow of electrons which interacted with the charged gas of the ionosphere was released, creating around itself a perturbed cloud with 100 m radius; the lower part carried the measuring equipment, which was slowly lowered downwards by the tether, registering the parameters of this charged cloud.

The first attempt at TPE execution was undertaken on 16 January 1980. In the experiment, the Japanese rocket Kappa 9M was used. On reaching an altitude of 150 km, the system started to release electrons and the process of tether deployment began with an initial velocity of 0.5 m/s. The experiment was not fully successful, as the failed batteries did not enable all of the measuring to be carried out; the cable was unreeled at 38 m instead of the planned 400 m. Nevertheless, the passive sensors collected a lot of useful

information, and the rocket reached altitudes of 328 km (Kawashima et al., 1988).

On 29 January 1981, one more attempt at TPE execution was undertaken. This time the sounding rocket S-502 was used as a launcher for the scientific experiment. At an altitude of 200 km, the beam was activated and at 20 km the rocket separated into two parts. This time the tether was deployed at 103 m, but the batteries failed again. The on board camera showed that during deployment the tether was not tensioned all the time and therefore collected in rings.

The third experiment of the TPE series was executed on 8 August 1983. The mission had the alternative title Cooperative High Altitude Rocket Gun Experiment (CHARGE-1). This time the equipment had been substantially improved. The frictional force in the deployment gear had been reduced and, in addition, jet engines were mounted on the lower tethered part of the rocket. They were activated every 40 s and thus gave a new momentum for the tether deployment. For this experiment, the American rocket Black Brant V was used. At an altitude of 142 km, the beam started to release electrons. Then, at an altitude of 169 km deployment of the tether began. The initial velocity of separation was 1.5 m/s. This time the tether was deployed to its full length (418 m). As a result of the emission of electrons by the beam disposed on the upper part of the rocket, it was positively charged in comparison with the lower tethered part. In the experiment, a conducting tether was used. In it there was a current caused by the potential difference of the upper and lower parts. The system also worked as a large antenna for passing electric current through the tether. After separation of the rocket, the battery once again failed, and electrons ceased to be released. The experiment was repeated on 14 December 1985 and was called CHARGE-2. This time

everything went well. The tether was deployed to a length of 426 m, the batteries did not break, and at last the plasma parameters were measured (Pelt, 2009).

### ***1.2.3 Observations of Electric-field Distribution in the Ionospheric Plasma – a Unique Strategy (OEDIPUS-A, OEDIPUS-C)***

On 30 January 1989, the American–Canadian experiment Observations of Electric-field Distribution in the Ionospheric Plasma – a Unique Strategy (OEDIPUS-A) was carried out. It aimed to study conducting tether dynamics, and the Earth's magnetic and ionospheric plasma. The space tethering system consisted of two bodies connected by a tether made of a copper wire covered with tin with a Teflon isolation. During the experiment, the tether was deployed to an overall length of 958 m. For deployment initiation, the spring and cold gas thruster system was used. The experiment did not just estimate the electronic beam; all measuring was conducted in a passive mode. The space tethering system was lifted to an altitude of 512 km by means of a three-stage Black Brant X rocket. On 7 November 1995, a similar experiment (OEDIPUS-C) was made. In contrast to OEDIPUS-A, the 1174 m tether and Black Brant XII rocket were used. The experiment was carried out at an altitude of 843 km (Jablonski, 1996).

### ***1.2.4 Cooperative High Altitude Rocket Gun Experiment – 2B (CHARGE-2B)***

On 29 March 1992, the CHARGE-2B experiment was carried out, and equipment similar to CHARGE-2 was used. The purpose of the experiment was the generation of

radio waves of very low frequency. As with the previous experiments of the TPE series, the electric current was created at the expense of a potential difference of the connected tether rocket's parts. The tether carried out the functions of the large antenna. By changing the beam intensity of the released electrons, it is possible to change the potential difference, thereby generating a current of the necessary frequency. The experiment was successful (Cosmo and Lorenzini, 1997).

### **1.2.5 Tether Satellite System (TSS-1)**

In July 1992, the American–Italian experiment Tether Satellite System (TSS-1) was carried out. The concept had been put forward already in the 1970s by Mario Grossi and Giuseppe Colombo. During the mission, it was planned to carry out a number of the studies into tether dynamics, the physics of space plasma, and the generation of electrical energy based on the Faraday effect. As the base for the experiment, the Space Shuttle Atlantis (STS-46) was used. The subsatellite connected to it carried the various scientific equipment and was spherical in shape. Its diameter was 1.6 m, and it had a mass of 521 kg. The 2.54 mm diameter conducting tether had a complicated construction: a central core of Nomex, a served group of ten #34 AWG copper strands, extruded fluorinated ethylene propylene insulation, Kevlar braid, and an outer Nomex braid. On board the subsatellite, engines were mounted for attitude and rate control which correlated with the initial stage of deployment of the tether. The subsatellite was deployed along a local vertical upwards from Earth. It was originally planned to release 20 km of the tether; however, after 268 m there was a malfunction and the deployment was stopped.

The data obtained during this experiment showed that the short tether deployed from the actively controlled Space Shuttle appeared much more stable than supposed. Program TSS-1 is described in more detail by Cosmo and Lorenzini (1997).

### ***1.2.6 Small Expandable Deployer System (SEDS-1)***

In March 1993, the Small Expandable Deployer System (SEDS-1) experiment was executed. The purpose of the experiment was to demonstrate a capability to lower a payload from an orbit by means of a tether without use of jet fuel, and the study of the dynamics of a payload after its detachment from a tether. SEDS equipment and payload was placed on the second stage of a Delta II rocket that was used for placing GPS satellites into orbit. In the experiment, a 20 km tether made of Spectra-1000 and a 26 kg payload with overall dimensions  $40.6 \times 30.5 \times 20.3$  cm were used. Inside the payload capsule, the autonomous equipment was installed, which allowed for the tracing of the payload dynamics. After separation of the third stage, from the second stage of Delta II in the direction of the Earth, the payload was ejected with an initial velocity of 1.6 m/s. The stage moved on an elliptical orbit with a perigee altitude of 190 km, an apogee altitude of 720 km, and an inclination of  $34^\circ$ . The gear of deployment did not envision feedback. In it the premeditated control law was used. The tether was successfully deployed, but slightly faster than planned. As a result, the relative velocity of the payload at the end of the deployment was about 7 m/s, and it caused a series of rebounds. After deployment, the tether with the payload oscillated in a neighbourhood of a local vertical. At the estimated time, the tether was cut, and the payload descended

on a ballistic trajectory into the atmosphere, and a splash down near to the coast of Mexico. During the experiment, the raising of an orbit of the second stage of Delta II was fixed (Smith, 1995).

### **1.2.7 Plasma Motor Generator (PMG)**

In 1993, besides SEDS-1, the Plasma Motor Generator (PMG) experiment was carried out. In the PMG, a 500 m conductive tether was used. The experiment was made on the basis of the upper stage of Delta II rocket, as in the SEDS-1 case. The objectives of the PMG experiment were to: examine the capability of a hollow cathode assembly to supply a current between a spacecraft and an ionosphere; and demonstrate the capability of an electrodynamic STS to work as an orbit-boosting motor and as a generator translating an orbital motion energy into an electrical one. Tether deployment began after separation of the third stage. The second stage moved in an elliptical orbit with a perigee altitude of 193 km, an apogee altitude of 869 km, and an inclination of 25.7°. The initial velocity of separation was approximately 3 m/s, and the deployment was implemented in a direction upwards from Earth. In the experiment, the deployment gear resembled the SEDS design, but had been adapted for deployment with a massive tether. The tether was made from #18 AWG copper wire with a Teflon insulation blanket. During the experiment, the capability of orbit ascent of the spacecraft by the current feed in the tether, and the generation of electrical energy accompanied by the descent of the spacecraft's orbit were demonstrated. The electric current received was 100–300 mA on the day side of Earth and 10–50 mA on the night side. Induction in the tether electromotive force changed from +150 V to -90 V (McCoy et al., 1999).

### **1.2.8 Small Expandable Deployer System-2 (SEDS-2)**

In 1994, the SEDS-2 experiment was carried out. The system had a configuration similar to the SEDS-1, and pursued two aims. Researchers wanted to check the efficiency of the deployment control mechanism with feedback, which implied a motion of tip payload on an advanced calculated trajectory, and to investigate the long-term evolution of STS. Stage Delta II, from which deployment was implemented, moved on a circular orbit at an altitude of 350 km. The main difference with the SEDS-1 experiment consisted of the feedback use in the deployer, which increased and reduced the tether deployment velocity for the guarantee of a tip payload motion on the preliminarily calculated trajectory with a smooth completion at the end of deployment. Vertical deployment of a tether was realised. Thus the relative velocity of a cable at the end of the deployment did not exceed 0.02m/s, which was a magnificent result in comparison with the 7 m/s in the SEDS-1 experiment. The oscillation amplitude of the tether at the end of the deployment did not exceed 4 degrees. During the experiment, the reliability of the STS was assessed. It was supposed that the STS would be in orbit for 12 days; however, on the fourth day the tether was broken as a result of a collision with a micrometeorite. A 7.2 km part of the tether remained attached to the Delta II stage. The tether occupied a stable position along a local vertical, despite insignificant force with a tension of 0.4 N (Smith, 1995).

### **1.2.9 Tether Satellite System-1R (TSS-1R)**

In 1996, the TSS-1R experiment was carried out. This was actually a repeat of the unsuccessful TSS-1 program of 1992, but this time the equipment was installed on the Space Shuttle

Columbia (STS-75). The electrodynamic tether was unreeled at 19.7 km, and a voltage of 3500 V was received. Because of an isolation disruption, there was an electrical arc which led to a break in the tether. Nevertheless, the experiment showed a great potential for the use of the tether in electrical power generation. The received power exceeded the expected value many times over (Lanoix, 1999).

### **1.2.10 Tether Physics and Survivability (TiPS)**

As well as TSS-1R, the Tether Physics and Survivability (TiPS) mission began in 1996. The study of the reliability of space tethers and their long-term use was the main objective of the experiment. The STS consisted of two spacecraft and a nonconducting tether with a length of 4 km and a diameter of 2 mm. The tether was made of Spectra-1000. On one spacecraft, the SEDS gear for tether deployment was mounted. The other one contained spring thrusters that initiated the division process. At the end of the deployment, the tethered system oscillated in relation to a local vertical with an amplitude of 47 degrees, and after three months the amplitude decreased to 12 degrees. It was planned that the STS would be in orbit for three years; however, the system successfully functioned until 2006. As opposed to all previous orbital experiments where the STS consisted of bodies with different mass and shape, in TiPS two identical spacecrafts were used (Purdy et al., 1997).

### **1.2.11 Advanced Tether Experiment (ATEx)**

In 1998, in many respects thanks to the success of TiPS, the equipment for the realisation of the Advanced Tether

Experiment (ATEx) was put into orbit. Unlike the previous experiments in ATEx, a flat tether was used. It was made of low-density polyethylene with three consolidating wires along it. The STS consisted of two spacecraft connected by a 6.05 km tether. The experiment had three overall objectives. First, researchers wanted to carry out experiments on the control of a tether's oscillations by means of sixteen thrusters mounted on one of the spacecrafts. Second, they wanted to demonstrate a capability for attitude control of a tethered spacecraft with the help of Satellite Laser Ranging. And third, they wanted to show that a multicore flat strip used as a tether can raise the reliability of the tether system (Lanoix, 1999). Unfortunately, a short time after the beginning of the experiment, the onboard computer STEx issued a command for tether cutting. As a result, instead of the scheduled 6.5 km the tether was deployed at 22 m and, up to now there has been no accurate explanation of the causes of this incident. According to one version, the problem of tether deployment led to large amplitude oscillations. It was expected that during deployment the libration angle would decrease through gravitational gradient activity. On the lower spacecraft, the sensor measuring the location of the tether showed a cessation of deployment that led to activation of the separation system. The actual cause of cessation has not been established because of the limited telemetry. According to Gates et al. (2001), the thermal dilatation of the tether was most probably a reason for the failure. Another possible cause is static electricity which was imposed on the telemetry and created a spurious cutting signal.

### **1.2.12 DAPRA Picosat**

An interesting experiment was carried out in 2000 when DAPRA Picosat picosatellites, developed by Aerospace Corporation, were put into space by means of a satellite

Orbiting Picosat Automatic Launcher in an elliptical orbit with a perigee altitude of 750 km, an apogee altitude of 800 km and an inclination of 100.22°. Each picosatellite had a mass of 0.4 kg, and they were joined by 30 m tethers. The objective of the mission was the validation of microelectromechanical systems radio frequency switches. On the picosatellites low-power radio transmitters of a small radius were placed. The tether was necessary to retain them at a small distance from each other. In addition, thin gold thread was interwoven in the cable. It considerably simplified detection of the picosatellites by the tracking system, and the experiment passed successfully (Barnhart et al., 2009).

### **1.2.13 Young Engineers Satellite 2 (YES2)**

In 2007, the Russian–European experiment Young Engineers Satellite 2 (YES2) was carried out, whose purpose was to examine the possibility of using the dynamic scheme of deployment for delivery of a payload from an orbit. The nonconducting Dynema tether with a diameter of 0.5 mm and length of 31.7 km was used in the experiment. The equipment was placed on the Russian scientific satellite, Foton-M3, which was put into orbit by the Soyuz carrier rocket. During the experiment, the spherical capsule with 12 kg cargo was lowered on the tether from the Foton-M3 located at an altitude of 230 km. Tether deployment was carried out at various phases. In the first phase, the tether was slowly deployed to a length of 1.5 km, and during this time the capsule was in the neighbourhood of a local vertical. Then tether deployment stopped, and the STS oscillated with a small amplitude concerning a local vertical. The following phase of experiment included fast deployment. Under the action of a Coriolis force, the tether deflected from a local vertical on a large angle in the direction of the orbital flight, and then made an inverse

oscillation. This return motion executed a role of braking impulse and reduced the absolute velocity of the capsule. In the neighbourhood of a local vertical, the capsule was disconnected from the tether and entered the atmosphere. Because of malfunctions in the deployment gear, the last phase flowed faster than was planned. Nevertheless, according to the data of the on board equipment, the tether was unreeled at 29 km, and the capsule with the cargo successfully descended from orbit. Unfortunately, it was not found on the Earth. Tracking stations confirmed that the capsule did not remain in orbit, and the altitude of Foton-M3 was lifted to 1.3 km (Kruijff and van der Heide, 2009; Williams et al., 2009).

### **1.2.14 Space Tether Experiment (T-REX)**

On 31 August 2010, the Japanese–American Space Tether Experiment (T-REX) was successfully executed. This experiment was developed under the direction of Professor Hironori Fujii, and T-REX for the first time demonstrated the collection of electrons by a nonisolated electrodynamic tether in space. Validation of the orbital motion limited theory, which predicts the efficiency of electrons collecting from ambient plasma in a case when STS sizes are rather small, was the main aim of the experiment.

During the experiment, a 300 m reinforced aluminium tape tether, with a width was 25 mm and thickness 0.05 mm, was deployed from the Japanese sounding rocket S520. In T-REX the new gear of the deployment, which was distinct from all previous ones, was used. The tether was accordion-folded and placed in a box, and its upper end was passed through a slot in the upper face of the box and joined to the end body. The last few metres of the tether had a special cover with slot edges, thereby increasing the frictional force at contact. This enabled quenching of the relative velocity as

the final stage of deployment was reached. Spring thrusters began a separation of the top part of the rocket from the lower part with an initial velocity of 4 m/s at an altitude of 120 km, and the tether deployment took about two minutes.

After deployment, several experiments were carried out. At first, the positive terminal of a power supply was connected to an inflatable conductive boom, and the negative terminal to the tether. The electrons were collected by the boom through the power supply which flowed into a tether at which point some of them were released directly into the ionosphere, and the remainder were leaked as a consequence of ion impacts. During the experiment, the voltage of the power supply was changed cyclically from 500 V to 1000 V. At the second stage, the polarity was switched – the negative terminal was connected to the hollow cathode, and the positive to the tether. The electrons collected by the tether, under the influence of the voltage created by the power supply, flowed to the hollow cathode where they were released into the ionosphere. During this phase, the voltage of the power supply was changed from 100 V to 1500 V. It is necessary to note that the cathode design differed from that applied earlier, because conventional cathodes require a considerable time for pre-warming that is unacceptable for a short sub-orbital flight. Engineers have found a way to allow cold start for the cathode by giving particular attention to its storage environment.

During this experiment, the rocket reached an altitude of 309 km in 283 sec and then fell into the ocean. All scheduled tests were carried out successfully (Johnson et al., 2010).

### ***1.2.15 Unfinished experiments YES1 and ProSEDS***

It is necessary to include YES1 and ProSEDS programs when reviewing experiments with space tethers. Unfortunately,

they were cancelled at their final stages for a variety of reasons.

On 30 October 1997, after numerous delays and postponements, the carrier rocket Ariane 5 was launched. Besides other payloads, it injected into an elliptical orbit the Young Engineers Satellite (YES), developed by students. It was originally planned that the subsatellite would be translated on a descent trajectory by means of a tether. However, as the launch was carried out in the morning instead of in the second half of the day due to ballistic requirements (and also because of the potential danger of a tether collision with other spacecraft during its existence), the deployment of a tether was cancelled. Instead YES was injected in a completely autonomous flight. Nevertheless, it carried out some scheduled experiments, including checking of the capabilities of navigation by means of GPS over orbits of its satellites (Lisov, 1997).

The Experiment Propulsive Small Expendable Deployer System (ProSEDS) is another sorry tale. Its purpose was to demonstrate the possibility of electrodynamic tethers being used for space propulsion. The SEDS deployer was planned for use in the experiment, and it was supposed to deploy a 15 km tether from the upper stage of the Delta II carrier rocket. The tether had a nonuniform structure; the first 10 km was made of a nonconducting material, and the subsequent 5 km was conductive and without isolation. The deployed tether would seize charged particles from the ionosphere, and an electric current of some amperes should be created as a result. The Earth's magnetic field acts on the tether with a current, and the force created by this field would lower a stage orbit by at least 5 km per day. By means of this tether system, the Delta II stage could descend from a 400 km orbit in 17 days instead of 6 months (Johnson and Sanmartin, 2000). Originally, the start was scheduled for autumn of

2000 but was postponed many times. The final officially sanctioned launch date was 29 March 2003; however, because of the accident involving Space Shuttle Columbia, this opportunity was not taken up. In the summer of 2003, the project management carried on negotiations with the International Space Station office, but the cancellation of the experiment ensued because of the danger of collision with the ISS.

### 1.3 Materials for tether production

One of the main problems stopping the wide implementation of STS is the absence of light and strong materials for manufacturing the tethers. Existing materials and production techniques allow for the creation of tether systems with an expansion of about 100 kilometres. Such tether systems can be used to resolve a considerable number of the problems viewed in the first section of this chapter. For example, it is possible to create STS for the sounding of Earth's surface, for providing artificial gravitation on board spacecraft, or for the descent of a payload from orbit. However, for creating systems of a large expansion, such as long escalators or space elevators, these materials are not strong enough. According to estimates by Edwards (2003), for a space elevator's tether a material with tensile strength of 130 GPa must be used. For comparison, the latest, strongest materials have a tensile strength of 3–5 GPa. Scientists have set their hopes on making new materials using carbon nanotube.

Carbon nanotube was first made in 1952 by the Soviet scientists Radushkevich and Lukjanovich; however, their research remained unknown in the West. In 1991, the Japanese physicist Samio Iijima, while experimenting with fullerene

synthesis, discovered tubular structures whose diameter did not exceed several nanometres and the length several microns. The tubes consisted of several strata representing a hexagonal net of carbon atoms (Iijima, 1991). In 1993, Samio and Betjun (independently from each other) reported obtaining carbon nanotube with one-sheet walls. These events caused an eruption of scientific investigations in the field of nanotubes. Besides the experimental evidence, a multitude of theoretical studies predicting the existence of this carbon form have been published. For example, Kornilov in 1985 predicted the existence of one-sheeted carbon nanotube.

For a long time, a carbon nanotube seemed the ideal material for a space elevator's tether; however, the study by Italian scientist Nicola Pugno (2006) indicated that a carbon nanotube tether would not be strong enough for use in the design of the space elevator. Flaws at atomic level will reduce the strength of such a large tether, at least by 70%. Laboratory tests showed that a tensile strength of one nanotube is approximately 100 GPa. But, as indicated by Pugno, if one tube loses at least one atom of carbon, its strength decreases by 30%. According to Pugno, a tensile strength limit of a tether made from nanotube would be way above 30 GPa.

Many adherents of the idea of the space elevator do not share Pugno's pessimism, indicating that in his mathematical model the frictional force between nearby nanotubes is ignored. The friction between nanotubes in a fibril should considerably increase its strength. Besides, the frictional force can be increased at the expense of affixion of buckyball hemispheres to the ends of interwoven nanotubes (Pelt, 2009).

Anyhow, mankind has not yet developed an engineering process allowing for the creation of long tethers with a tensile strength of some hundreds of GPa. In the latest space projects, the following materials are considered for tethers: copper, aluminium, Kevlar-49, Spectra-2000, Zylon and Dyneema.

*Kevlar* – a high-strength aramide fibre. The technology for its manufacture was mastered by Du Pont in 1971. Depending on the technological conditions for extraction during its manufacture, there are two basic versions of Kevlar fibre. The first one is a material with a larger elastic modulus and smaller unit elongation. The second one is a material with smaller elastic modulus and larger unit elongation. These materials have been given the trade marks Kevlar-29 and Kevlar-49.

*Spectra 2000* – a high-strength fibre that is produced from polyethylene. The production technology was developed by Honeywell in the 1980s, and its basis lies in a patented gel-spinning process.

*Zylon* – polyparaphenylene benzobisoxazole (PBO) fibre. Manufacture was started by Toyobo Co. in 1998. There are two kinds of fibre produced today: Zylon AS (as spun) and Zylon HM (high modulus) – Zylon HM is the more elastic and moisture resistant fibre.

*Dyneema* – a high-strength fibre that is produced from polyethylene. The structure of Dyneema fibre was devised in the 1960s by Doctor Pennings in co-operation with a Dutch company, DSM.

In Table 1.2, the basic physical characteristics of these and some other materials are shown ( $\rho_M$  – density,  $\sigma_*$  – tensile strength,  $E$  – elastic modulus). The data is taken from Beletsky and Levin (1993) and also from web-sites of some of the manufacturers.

Modern technology allows for the creation of very thin and light tethers. The decreasing mass and diameter of a tether allows it to reduce its influence on the dynamics of a mechanical system, and maintenance of its main function – the transfer of effort from one body to another. However, the use of thin tethers introduces new problems related to the reduction of life-span. Thin cables are defenceless against

**Table 1.2** Properties of materials

Material	Density $\rho_M$ , g/cm <sup>3</sup>	Tensile strength $\sigma_*$ , GPa	Elastic modulus $E$ , GPa
Aluminum	2.7	0.6	70
Diamond	3.5	54	1050
Dyneema	0.99	3	172
Graphite	2.2	20	690
Kevlar-29	1.44	3.6	83
Kevlar-49	1.44	3.6	124
Silica	2.19	6	74
Spectra-2000	0.97	3.34	124
Stainless steel	7.9	2	200
Tungsten	19.3	4	410
Zylon AS	1.54	5.8	180
Zylon HM	1.56	5.8	270

the threat of collision with micrometeorites and small particles of space debris. For example, a study by Pardini et al. (2009) intimated that an aluminium tether can be broken off by a particle three times smaller than its diameter. The direct solution for this problem, i.e. increasing tether thickness, considerably increases the mass of the whole system and generates new operational problems.

The use of multicore cables can provide a way out from the current situation. In the project EDOARD, it was suggested to use a double tether. Two threads are related together through equal distances. Thus the formed loops considerably raise the reliability of the tether. Even if, as a result of collision, one of the loop edges appears broken off, the STS can prolong its activity thanks to the second untouched edge. The probability that different particles will break off sequentially from both edges of one loop is small

enough; besides, this probability decreases when increasing the number of loops (Bruno et al., 2001). A tether of an even more complicated structure, capable of surviving multiple collisions with space debris, is being developed by TUI. The tether, which is called Hoytether, consists of several threads with numerous interweavings (Forward and Hoyt, 1995).

## 1.4 Study of space tether dynamics: state of the problem

The history of STS study covers more than 100 years, since its bases were laid by Tsiolkovsky in 1895. He suggested connecting a space station by a long circuit to a load and spinning the system to create an artificial gravitation. Many scientists were engaged in study of STS. The first serious scientific works in this field appeared in the 1960s, since when a large quantity of the scientific works devoted to the study of various aspects of STS have been created by scientists throughout the whole world. All studies can be separated into two large groups. In the first one, STS with a nonconducting tether are considered; and in the second, STS with a conductive tether which can interact with the Earth's electromagnetic field. Examinations of the second group appeared recently, at the end of the 1980s, and it is in this area that the greatest attention of researchers now is paid.

### 1.4.1 Reviews and monographs

The largest contribution to the development of the theory of STS was made by Beletsky and Levin (1993). In a monograph, they systematized and summarized the cumulative world experience of STS dynamics study up to 1990. They gave a

review of the problems where these systems can be used. Levin's monograph (2007) can be considered as a prolongation of this work, and an effective approach to the analysis of STS dynamics is given in his book. The focus is on electrodynamic tethers, as the most promising direction of STS theory. Each chapter of the book is related to a real project in which Levin took an active part.

In 1997, a book written by Cosmo and Lorenzini was published, which contained a detailed review of completed experiments, and prospective ways of using STS. In the book, the physical phenomena which determine the dynamics of stretched systems in space are considered, and it can be used as an introduction to STS dynamics. For an acquaintance with the elemental dynamics of STS, the article by Misra and Modi (1986) is also recommended.

In 1999, Johnson, Gilchrist, Estes and Lorenzini published an interesting article containing the information about scheduled NASA programs using electrodynamic tethers. Possible means of developing the European space tether programs are considered in the article by Eiden and Cartmell (2003). They suppose that, in the near future, STS will be used for the delivery of a cargo from an orbit to Earth. The transport systems consisting of platforms related by tethers, for transfer of payload from one orbit into another, and also systems for artificial gravitation creation are more difficult. Such STS will be realised more slowly and, last but not least, STS for interplanetary transfers will be created even later.

It is also necessary to note reviews by Kumar (2006), Cartmell and McKenzie (2008), and Sanmartin (2010) – these authors have carried out a substantial amount of work. They studied and systematised a considerable quantity of the scientific literature concerning STS dynamics. In the first review, the focus is on problems of control and modelling nonconducting STS of motion. Kumar separately considers

the dynamics and control of two point masses connected by a cable, two rigid bodies, and also multibody systems. He reviews existing mathematical models and possible methods of application for nonconducting tethers. Cartmell and McKenzie deal with a wider range of questions, and they divide the work into two large parts. In the first part, problems related to a nonconducting tether are considered, and the second part is devoted to electrodynamic tethers. The authors pay attention both to the theoretical aspects and the various projects and missions of space tether use. The article written by Sanmartin (2010) contains a review of studies devoted to electrodynamic tethers. Asymptotic analysis, numerical simulations, ground and space tests, and past and planned missions are briefly reviewed in it.

In his monograph published in 2009, Michel van Pelt discusses what are tether systems, where and for what can they be applied, and what physical phenomena underlie their dynamics. The book is written simply, and is clear to the non-expert. A large part of the book is devoted to a space elevator: the question of its stage-by-stage building is mentioned, and also a short review of the challenges which impede creation of this grandiose construction is given. Among other books devoted to the space elevator, one more interesting work is by Edwards and Westling (2003).

The book by Troger et al. (2010) has great scientific value, and the authors address very current actual questions and give the results of their studies concerning various aspects of the control and dynamics of STS deployment, the problems of a chaotisation and synchronisation of its motion, the influence of non-linear oscillations of bodies connected by tethers on the interior degrees of freedom on the dynamics of systems, and the uses of resonances for the solution of control problems. The review of mathematical models given in the book is very interesting.

### **1.4.2 Mathematical models of space tether systems and their validation**

In the scientific literature, great attention is given to mathematical models of STS. All existing models can be divided into three groups depending on the definition of a tether. In the first group, there are the models with distributed parameters in which the tether is modelled as a heavy flexible thread by means of partial differential equation (Misra et al., 1995; Liu and Bainum, 1989). In the second group, there are discrete or multipoint models in which the tether is exchanged by a set of concentrated point masses connected by weightless elastic bars (Crist and Eisley, 1970; Aslanov et al., 2007). In the third group, there are models with massless, elastic and thin tethers (Beletsky and Levin, 1993).

Models of the first type give the most exact result, but their use is associated with great difficulties as the creation of a steady difference scheme of the numerical solution of the equations represents a challenge (Alpatov et al., 1997). The majority of results for STS dynamics with a continuous tether are received for stationary or quasi-stationary motion modes, when oscillations are linear. Calculation of STS dynamics as continuous systems is an extremely complicated and labour-intensive process for a number of reasons. For example, boundary conditions for continuous tethers are determined by the dynamics of the end bodies and the way in which the tether is fixed, the effects of exterior forces depend on the motion of the tether and the connected bodies, and the dynamic characteristics of tethers are still investigated for linear motion mode only (Angrilli et al., 1988). The necessity to account for a tether's torsional stiffness, its elasticity of flexure, its plastic deformation after reeling and unrolling provide a problem of mathematical modelling which is difficult to realise at present. Nevertheless,

new studies are devoted to tether modelling as continuous systems constantly appear (Misra et al., 1995; Angrilli et al., 1995).

Continuous models of STS adequately describe the dynamics of a tether. However, their integration is generally possible only with the help of numerical methods and usually demands considerable temporary expenditures (Alpatov et al., 1997). The bulkiness of these models does not allow their use for revealing the common regularities of non-linear STS dynamics. Continuous models can be used for the exact control of computation for the validation of results received by means of more simple models (Troger et al., 2010).

Models of the second group have a more mechanical sense. A calculation executed with their help will conform with the results of a non-linear continuous model. Multipoint models give good results even in the case of a weak strained tether.

Models of the third group can be considered as extreme cases of multipoint models. They are widely used both in theory and in practice and allow speedy access to approximate solutions without large computing expenditures in compliance with the basic regularities of STS motion. Such models were used in the first scientific studies devoted to STS dynamics, for example in Paul (1963).

Another way in which tether simulation mathematical models differ is the method of representation of the connected bodies. Often, in simple models of STS the end bodies are represented in the form of mass points. It is justified in cases when a rough calculation is needed, or if the tether's length considerably exceeds the size of the body's, and their motion with respect to the centre of mass is not important for the mission or experiment. Otherwise, it is necessary to consider the motion of tethered bodies around their centres of mass.

The existence of a great number of STS models is thanks not only to the use of various representations of tethers and connected bodies, but also by accounting for the different sets of external and internal forces. The comparative estimate of perturbing forces acting on a tether was made by Beletsky and Levin (1993). They note that gravitational forces have the greatest impact on STS. If the STS moves in a low-altitude orbit, it is necessary to take into account the influence of aerodynamic forces. If a conductive tether is used in STS, considerable influence on the system will be provided by electromagnetic forces. Research by Lanoix (1999) can serve as an example of scientific work in which the mathematical model with regard to the considerable quantity of the various perturbing factors was constructed. Lanoix considers aerodynamic forces, the perturbations caused by the non-sphericalness of the Earth, solar and ground radiation, electromagnetic forces, the gravity of the Moon and the damping properties of a tether.

Currently, there is a question of the experimental checkout of the theoretical results obtained by means of various mathematical models of STS. The mathematical model of a physical process is always easier than the process. By working on models, researchers reject incidental factors, leaving only the important aspects of the investigated phenomenon. Such abstraction allows us to achieve the tool which is best for analysis; however, the results achieved with its help are not always correct. Quite possibly, the assumptions made during creation of the model may exclude a critical aspect, which in certain cases has considerable impact on the behaviour of the system. Therefore the results obtained by means of the mathematical model should be compared with the results of the physical experiments. If major differences are observed, an improvement of the mathematical model by taking into account the experimental data is required.

Unfortunately, the current level of astronautics does not allow for the implementation of experiments with space tethers to be carried out promptly and cheaply. The numerical experiment is based on a complicated mathematical model, which considered the greatest possible quantity of physical aspects of the investigated phenomenon, and can be the solution for this problem. The bulkiness and complexity of such models does not allow them to be immediately used for analysis, but the numerical results obtained with its help can be applied instead of the experimental data to establish the adequacy of the more simple mathematical model results. It should be understood that such validation cannot take the place of a physical experiment, but in the absence of the latter, it can be quite useful as a first approach.

The process of validation of a simple model with the help of a more difficult one was described in detail by Ellis (2010). Ellis developed a validation procedure which uses the top-level computer model from which results are used instead of the experimental data, and he describes the process of obtaining the top-level continuous model. For its integration he suggests the use of the finite element method.

The impossibility of carrying out the necessary experiments in space has led to some researchers trying to use the results of experiments executed on Earth for validation of the models. For example, laboratory trials were used for the analysis of space tether dynamics by Vigneron et al. (1997). Mankala and Agrawal (2005) considered a process of deployment and retrieval of a tether by means of three models: the constant length tether moving in the parallel gravity field; the variable length tether moving in the parallel gravity field; and the tether being unreeled from a drum mounted on the orbital satellite. By comparing these models, Mankala and Agrawal attempted to extrapolate the results of the experiments on the Earth to the orbital flight of the tether system.

### **1.4.3 Motion modes of space tether systems**

Space tethering systems belong to a class of complicated mechanical systems. Study of such systems is possible only at separation of particular modes of motions. This problem is explicitly addressed by Troger et al. (2010). The concentration of attention on a separate mode allows significant simplification of a mathematical model and better interpretation of the results. The procedure of separation of the motion modes is part of the initial analysis of a system's dynamics. It is based on common representations about the possible ways of motion of mechanical systems, and representations about the dynamics of a particular system. The authors suggest reviewing four modes of STS motion: libration, rotational, resonant and chaotic. The first two modes are tightly interconnected and well investigated by Beletsky and Levin (1993) for the circular orbit.

Libratory motion of a bundle of two bodies in the neighbourhood of a radial equilibrium position is the most intensely studied of all modes. In the estimation of the small size of displacements and velocities, the task has linear characteristics and is reduced to defining the stability of equilibrium positions when taking into account the various factors (Beleicky and Giverc, 1968). The application of methods of the theory of stationary movements allows for good effects to be achieved (Alekseev, 1970; Merkin, 1980). With their help, the task of studying STS dynamics can be reduced to the analysis of the ordinary linear differential equations describing the relative equilibrium of a tether, instead of considering the partial differential equation featuring its common dynamics.

The article written by Takeichi et al. (2004) is a vivid example of libratory motion study. They considered STS as

the stretched rigid body in an elliptical orbit. With the help of the Lindstedt perturbation method, they achieved an approximate analytical solution for STS oscillations. The full mechanical energy of a system is at its lowest when the libratory and orbital motions coincide with the periodic solution. From the mechanical point of view, its solution plays the same role as an equilibrium on circular orbit. The evolution of the libration motion under the influence of an interior friction in a tether was considered by Levin (2002). The received analytical results were compared with data of the TiPS experiment.

At large enough angular velocity, the rotation motion of two bodies connected by a tether provides the essential tension of the tether. Therefore, for this motion mode the transverse vibrations will be small, and their influence on the common motion of the system will be negligible. These oscillations can be disregarded, particularly during the early stages of research. The tether for this mode can be considered as an elastic massless constraint between points of a leash of the end bodies. The main practical problems of the STS rotation motion are related to the study of the evolution of the rotational parameters of the system under the influence of various factors. This motion can be reduced to the study of the change of the parameters of motion of a stretched elastic system.

The earliest scientific studies related to space tethers were devoted to the rotation motion of STS. In 1965, Tai and Loh investigated a plane motion of the space station connected by a tether with a counter-balance. Bainum and Evans (1975) carried out a more complicated study, when they considered the spatial motion of a STS that consisted of two rigid bodies connected by a massless, extendable tether and showed that the deviates of a spinning STS from its orbital plane is small. Transverse vibrations of rotating STS were investigated by Breakwell and Janssens (1992). They considered an

inextensible tether. A STS rotated in orbital plane with an angular velocity equal to the velocity of orbital motion and, as a result, it has been shown that, at a certain ratio of the masses of connected bodies, transverse vibrations can be unsteady. The authors offered a method for selecting STS parameters that excluded the possibility of the occurrence of labile movements. A similar effect was achieved by Beletsky and Levin (1993) for a circular orbit. Studies into the libration and rotational motions are very important from the practical point of view, as tether systems solve the problems entrusted to them in these modes.

In the theory of nonlinear systems, the most complicated and little-studied are the problems related to resonance appearance. Parametric resonances arise in the vibrating systems characterised by several frequencies. For STS, the resonance modes can arise at a commensurability of the medium frequencies of the following movements: orbital motion of STS centre of mass, rotation and libration of STS concerning the centre of mass, longitudinal tether oscillations, and oscillation of the end bodies concerning a tether's leash points. Obviously, the resonance commensurability of frequencies can take place for any pair of movements, and for all degrees of freedom. Besides parametric resonances in the nonlinear dynamics, forced resonances arising in the presence of a periodic perturbing influence are also considered. For example, such resonances can arise as a result of the action of atmospheric forces on a system moving in the elliptical orbits and orbits with inclination.

Currently, the field of resonance movements is still poorly investigated; nevertheless, it is possible to note some interesting studies devoted to resonances in tether systems. Bainum and Evans (1976) linearised the nonlinear system of equations near a stationary rotation. It allowed for finding possible resonances and for giving the results of the numerical

calculations illustrating resonance motions of rigid bodies connected by a tether. Troger et al. (2010), by means of a model problem, studied the possibility of using resonance for controlling STS motion. Levin (2007), in the example of the TiPS experiment, views a resonance between in-plane and out-of-plane oscillations of STS. The loss of stability of STS oscillations owing to a parametric resonance is considered in a paper written by Matteis and Socio (1990). The forced resonance induced by the change of atmospheric density at different points of an orbit was studied by Kokubun (1999). The numerical calculations executed by Kokubun showed that the libration mode can be broken if the angular velocity of the STS is equal to the angular velocity of its orbital motion.

The resonance mode represents a wide and important field of possible STS movements. Resonances are accompanied by a considerable energy of motion redistribution between its various mechanical forms: on the one hand, it can be a reason for motion mode breaking, and on the other hand, it can assure both efficient control and stable forms of motion of the system.

The chaotic motion of the deterministic systems is the new (poorly studied) direction of nonlinear dynamics. In the scientific literature, the chaotic phenomenon has started to be considered widely only in recent decades. The deterministic chaos is not related to random exterior disturbances or uncertainty of a system's characteristics. It is a property defined by the nature of nonlinear systems. The chaotic behaviour can be observed even at the elementary double-frequency systems. Separation of this motion mode is necessary as the classical methods give incorrect results for chaotic systems.

Chaotic motion of STS is investigated in a cycle of articles (Pirozhenko, 2001a, 2001b, 2001c), where, as a modelling

problem, the orbital pendulum with periodically changing length of a bar is considered. The analysis of equations of motion and the attempt to obtain their approximate solution allowed authors to make a conclusion-assumption about the impossibility of an explanation for a chaotic motion by conventional mechanical methods. Many authors try to create a qualitative analysis of a system and to construct a mechanical image of the origin and essence of a chaotic mode. The suggested research technique is based on measuring the performances of separate trajectories and their flocks. It is proposed that experimental research is carried out in which a computer, rather than a laboratory, is used. Also many authors explore the influence of small dissipative forces on the behaviour of a system.

The problem of chaotic oscillations of a tethered system in an elliptical orbit is considered in various studies (Wisdom, 1987; Alpatov et al., 2007; Aslanov et al., 2009). It is noted that the main qualitative effect of STS motion in an elliptical orbit is a capability of a chaotisation of its motion. The major contribution to the onset of chaos is also brought by atmosphere. It especially strongly affects the beginning of a chaotisation process because of the exponential changing of its density in an elliptical orbit. Even rather small eccentricities allow for strong chaotisation.

#### **1.4.4 Stability of space tether systems**

One of the major problems of STS dynamics is the study of motion stability. Great attention is given to this problem in various pieces of literature (Bainum and Evans, 1975; Liberzon, 1998; Pelaez and Andres, 2005). Stationary motions in which tether configuration remains invariable and moves as rigid bodies are most suitable for operation in many applications of space tethers. The process of searching for

stationary movements, along with a fairly detailed investigation of their stability is given by Beletsky and Levin (1993).

Various ways of using tether systems can lead to various formulations of the stability problem. For example, a typical problem for an electrodynamic cord system is that of defining stability areas depending on the current in a tether. In the case of sounding tether systems, it is always necessary to solve the problem of stabilisation depending on the altitude of a tethered subsatellite and its tether lengths. In addition, the problem of STS motion stabilisation for a so-called ‘running’ tether, when it releases from one body and takes in another with the same velocity, is interesting.

Beletsky and Levin (1993) investigated the stability of stationary motions of an electrodynamic tether with a constant current. They showed that, for a circular equatorial orbit, the attitude motion of a STS and its elastic vibration are always unstable. Pelaez and Andres (2005) came to the same conclusion but for a wider class of orbits. Instability is caused by an energy inflow into the pendulous motion from the Earth’s electromagnetic field at the expense of action of a nonconservative force. Instability of the pendulous motion is transmitted to the elastic oscillations of a tether as they are interconnected. Therefore, the application of an electrodynamic STS requires a much higher level of control than that of a STS with a nonconducting tether.

Stability in the Earth’s gravitational field in the absence of other perturbing forces is considered in the majority of studies. In this aspect, the article by Inampudi and Schaub (2011) is interesting, as it considers the STS dynamics in the gravitational field of two large bodies. Behaviour of a STS in the libration points of the Earth–Moon system is investigated.

The stability analysis is carried out within the limits of accepted mathematical models of tether systems. The equations

of small oscillations, or the equation in diversions, are usually worked out, and the stability analysis is carried out by means of the methods used by Rause-Gurvitz, Lyapunov, and other conventional methods. If the mathematical model represents a system of ordinary differential equations with the incomplete information of perturbations, the problem of absolute stability arises: an asymptotic stability of equilibrium at any selection of perturbations from the given class of functions. The problem of the absolute stability of dynamic systems can be solved by various methods (Liberzon, 2006). One effective research technique into the absolute stability of tether systems is another method given by Liberzon (1989). Ivanov et al. (2005) also suggest using a simple analytical indication for the analysis of the absolute stability of tethered systems.

#### **1.4.5 Control of space tether systems**

Any tether system in space requires a high level of control. Thrusters installed on connected bodies and the deployment gear regulating the length and tension of the tether can be used as control devices. In the literature, a number of schemes and scenarios of tether control are considered. Thus the greatest number of papers is devoted to the problems of tether deployment and the control of its retrieval.

Deployment and retrieval of a tether can be executed by means of both the propulsive force of thrusters, and gravitational and inertial forces. The tension of a tether, which is a consequence of a difference between gravitational and inertial forces acting on the tethered bodies, is used as a controlling force in the latter case. The second method is now considered more acceptable because deployment of a tether at the expense of jet force demands considerable fuel expenditure, and essentially complicates the construction of all systems.

Analysis of planned and executed experiments and programs with space tethers shows that the deployment process can be conditionally divided into three phases: initial, basic and final. At the initial phase, the impulsing separation of the bodies connected by the tether occurs. At the basic phase of deployment, the main problem of removing the connected bodies to the necessary distance in the given angular sector is solved. At this stage, control of the deployment is exercised by regulating the tether's length or its tension force. At the final phase, the required terminal conditions are supplied. Here, the problems of initial spinning of the STS, or damping of the angular oscillations and radial velocity, can be solved. In certain cases, the terminal conditions of deployment can be achieved at the end of the basic phase, and the need for a final phase disappears. Tether retrieval consists of the same phases, but with the inverse sequence.

Kumar (2006) indicates the presence of several approaches to STS control, the simplest of which is open loop control. It does not necessitate obtaining the information about tether oscillations, so the deployment gear has a very simple construction. The deployer simply changes the tether's length in conformity with rules given in advance. The linear, exponential and uniform laws are widely investigated by researchers. It is noted that one deployment law, consisting of two or three phases replacing each other (for example, exponential–uniform–exponential), is more effective from the point of view of obtaining low speed at the end of deployment, than in the case of one phase applying. A two-phase uniform–exponential deployment was studied by Pelaez (1995a, 1995b). Zhu et al. (1993) investigated the application of an exponential (accelerate)–exponential–(decelerate) control law for the problem of a spacecraft descending from an orbit.

Deficiencies of control without feedback can be attributed to the fact that deployment remains stable until the velocity of a tether's emission does not exceed some critical value dependent on the tether's length and angular rate of STS orbital motion (Zhu et al., 1994). The use of control laws without feedback can lead to strong oscillations of the tether. Using the exponential or linear law, the velocity of a tether's run-out reaches maximum value at the end of deployment, which leads to a yank and a sharp increase in the tension force. The application of passive dampers or various brake devices in tether deployment can ensure small oscillations at the end of deployment through a process in which the tether can strongly deflect from the local vertical. For example, Estes and Lang (1995) suggest using a skip-rope damper for quenching of a tether's oscillations.

The second method viewed by Kumar is the approach based on feedback use. This approach suggests placing the additional measuring equipment and the active gears of deployment to allow a flexible change of the length of a tether and the tension force on the connected bodies. Many researchers approached the problem of control law selection similarly to an optimisation problem, applying the rich mathematical apparatus of the theory of optimisation. Let us note one more singularity of the second approach: on the one hand, feedback control allows for a more predictable and thus more secure system behaviour to be achieved; on the other hand, gear complication increases the probability of its failure. Therefore, the designers developing space experiments with the use of tethers are forced to search for a compromise between simplicity and functionality of a control system.

The greatest attention to the creation of control laws with feedback is given in the scientific literature. For example, Rupp (1975) suggests controlling a tether's tension force by

taking into account the information about the current and rated length of a tether and its runout velocity. As a result, throughout the whole of its deployment the STS remains in the neighbourhood of a local vertical.

Troger et al. (2010) discusses an approach to creating the control algorithms based on the assignment of certain limitations for a deployment trajectory in a phase space. It allows for construction of the algorithms which provide the required parameters of motion at the end of deployment. Troger and colleagues consider the controls necessary to ensure zero end velocity for a tethered body. Thus, the approach to the end point happens monotonically, without changing deploying velocity.

In their paper, Pascal et al. (1999) investigated the laws of deployment and retrieval by means of a three-dimensional dumbbell model for cases of a circular and elliptical orbit. Some control laws were put forward by the authors and an analytical solution for certain special cases of STS motion was given. It is shown that a tension force can be presented as a function of the instantaneous length of a tether and its corresponding axial acceleration. The authors also considered the various laws for a ‘sliding’ configuration in which a load moves on ahead of the deployed tether.

In their article, Zimmermann et al. (2005) viewed two schemes of tether deployment: static (estimating motion along a local vertical), and dynamic (admitting large-angle deflections). For the dynamic scheme of deployment described in Chapter 4, optimisation of all phases of deployment is conducted and a new concept of control is applied. Selection of the deployment strategy is based on numerical optimisation which, previously, was applied only by a few authors. Optimisation affects some motion parameters and tether length. Zimmermann and colleagues considered a phase of free motion of the descending payload after separation from

the tether as the integral part of the program that influenced the optimised parameters. Ideas relating to this concept have been advanced in a paper by Glabell et al. (2004), where the original control system of tether deployment on the basis of an adaptive neural network was offered.

Stability of STS is studied in He et al. (2011), whereby the basis of the theoretical analysis of the control algorithm of tether deployment is offered. Numerical calculations show that the algorithm can be used for stabilisation of STS oscillations during deployment and retrieval.

In Kumar et al.'s article (1992), the influence of the deploying velocity on the oscillations of a payload rising into an orbit is studied. The authors had obtained a result contradicting their intuitive representation: an increase of the deploying velocity does not necessarily lead to an increase of the orbit altitude on which the payload can be placed. In their article, the common ratio between an apogee altitude and the velocity of the deploying tether is obtained, and the algorithm of an optimal velocity from the point of view of increasing an orbital altitude is offered.

The retrieval of a tether poses the opposite problem to deployment, though it is more complicated in realisation because the tether retraction can lead to large amplitude oscillations. Both approaches can be applied to the solution of this problem. Pascal et al. (1999) showed that application of the sinusoidal law without feedback can provide a stable retrieval with zero final velocity. The problem of retraction of a subsatellite from a space station was considered by Djebli et al. (2002). They suggested dividing control laws into 'simple' (linear or exponential) and 'fast' (with certain acceleration profiles). They showed that, in certain cases, 'fast' retraction allows for damping the transverse vibrations of a tether. Beletsky and Levin (1993) considered a control law with feedback and noted that for

successful docking at the final stage of retrieval the application of a docking boom or jet engines is required.

The above approaches imply control of a tether's tension force as defined by a gravity gradient which depends on the length of the deployed tether; therefore at short lengths such control is ineffective. It causes major problems at the initial stage of tether deployment and at the final stage of its retrieval when the nonlinear effects related to the dynamic singularities of the tether and the deployer play an essential role. In their book, Troger et al. (2010) note that many questions related to initiating deployment and the final retrieval require experimental validation. The installation of small jet engines on tethered bodies can provide a solution for this difficult situation. Thrusters are also effective for damping out-of-plane oscillations. Their application for solving a control problem is discussed in articles by Misra and Modi (1986), and Matteis and Socio (1991).

Electrodynamic cables give additional capabilities for control. From the Earth's magnetic field, an Ampere force acts on the conductive tether with an electric current. It is more than possible to regulate this force by changing the value and direction of the current. Corsi and Iess (2001) showed that it is possible to dampen STS oscillations by a simple on-off switching of the electric current in the tether. A more difficult challenge was solved by Williams (2006) who modulated a current in the motion provided by the tether in the desired periodic trajectory. The control law offered for a current was based on comparison of the Hamiltonian of the calculated and actual motion. Ampere force can be used as an additional factor. The combined scheme, which assumes use of a long tether control and control of the force of the current, was applied by Zhou et al. (2006) for the solution of an STS stabilisation problem in the neighbourhood of a local vertical. Watanabe et al. (2004) showed that it is possible to

dampen elastic vibration of the tether by means of current control.

### **1.4.6 Spinup of space tether systems**

In the first section of this chapter it was shown that a spinning STS can have wide practical applications. Tether systems are placed in orbit in the packaged state, demanding not only deployments, but also spinups. There are two essentially different ways of spinning a STS: the active spinup (Komarov, 1972), and gravitational spinup (Komarov, 1974). The active spinup involves two activations of jet-engines mounted on one of the tethered bodies. The first engine switching allows the bodies to move away to a distance equal to the length of the tether. The thrust vector is directed along the straight line joining the centres of masses of the tethered bodies. The value of this vector is chosen so that the relative velocity of the bodies becomes equal to zero at the end of tether deployment, and it ensures lack of yank. The second jet-engine activation serves for spinup of the STS. The thrust vector is directed along a normal to a line connected to the bodies' centres of mass. The thrust is turned off when the angular velocity of the STS with respect to the centre of mass reaches the necessary value. It should be noted that this method of spinup demands considerable expenditure of fuel.

The second method, gravitational spinup, assumes the presence on one of the tethered bodies of the active control gear for tether deployment. The twist of the STS consists of three stages: separation, oscillation and approaching. At the stage of separation, the connected bodies move away from each other in an orbital plane. This separation can happen by means of thrusters or, in a ‘passive’ mode, at the expense of control of the tether tension (Ivanov and Sitarskiy, 1986).

The connected bodies move away from each other to a distance greater than necessary for the STS operation in a spinning mode. That is, the tether length should be more than the rotating STS length. At the stage of oscillation, the tether length remains constant. The oscillation occurs at the maximum admissible amplitude at which the tether still remains under tension. The approaching stage begins at the moment when the tether passes through a vertical position during its oscillations. The control mechanism starts to take up the tether fast and, as a result, the STS moment of inertia is decreased. That, according to the conservation theorem of a moment of momentum, leads to an increase in the angular velocity of the system. Gravitational spinup in comparison with the active spinup allows jet fuel to be saved, but use of the complicated deployment gear and a much longer tether are required. For example, at the approach of connected bodies from 100 km to 50 km, it is possible to execute a twist that creates artificial gravitation of 0.85 g (Ivanov, 1984).

Mazzoleni and Hoffman (2003) explicitly considered spinup of a STS and showed that an initial angle of deflection of the rotation plane from the orbital plane and the location of the tether fixing points on the connected bodies considerably affect the tether system's dynamics. The authors concluded that for successful implementation of STS spinup it is necessary to control the orientation of the tethered bodies. Viewing as an example the Advanced Safety Tether Operation and Reliability (ASTOR) mission, Mazzoleni and Hoffman (2001) suggested carrying out spinup by means of the thrusters mounted on the connected bodies. The singularities of orbital mechanics create some complexities at space spinup; however, using thrusters is a very promising means of transmitting energy to the system.

### 1.4.7 Survivability of space tether systems

At present, the survivability of STS is a daunting problem. Many STS projects require the long-term existence in orbit of a rather long and fragile tether. If there were no other objects apart from the STS in space, the survivability problem would not be so acute. However, in near space the number of objects of various sizes continues to grow. For example, according to the NASA EVOLVE model, there are more than 58 000 objects and 24 satellites solely at the altitude of 350 km or below. The problem of collision of tethers with space debris is not exaggerated. According to some experts, such collisions were the causes of failures of the SEDS-2 (1994) and TSS-1R (1996) experiments.

In their article, Gittins et al.'s (2004) original Tether Risk Assessment Program is considered. Its basic idea is that collision between a tether and a space object with a diameter about half that of the tether can lead to a break. In the article, single-thread and double-thread tethers are considered. It is ascertained that the hazard of a break for a double-thread tether is two orders less than that for a single-thread. Another algorithm of the definition of probability of STS survival in orbit is offered in the paper presented by Aslanov et al. (2010). The algorithm gives uprated estimates of the probability of STS survival; nevertheless, it allows for a choice of tether design characteristics according to the problems solved by it. Another study devoted to the problem of reliability of a tether was made by Chobotov and Mains (1999). In one example in their experiment, TSS-1R, the authors investigated the probability of tether collision with orbital objects after a tethered subsatellite separation from its base spacecraft. The study showed that a deployed tether will collide with several particles sized from 0.1 mm and above. The probability of collision with objects of size greater than 10 mm is 0.001 per month.

### ***1.4.8 Challenges and poorly investigated questions***

Although the theory of STS is now quite advanced in age and a considerable quantity of scientific studies have been carried out in this field, the analysis of the literature allows us to reveal several poorly investigated problems and directions.

In the majority of existing studies, the bodies connected by a tether are considered as mass points. The influence of the tethered body motion about its centre of mass on the dynamics of the whole system is not considered. Meanwhile, at a commensurability of frequencies of the end bodies' oscillation with frequencies of longitudinal, transversal or out-of-plane oscillations of the tether, or with the frequency of the orbital motion of a STS centre of mass, resonances can occur. These resonances are accompanied by energy redistribution between interior degrees of freedom of the system and lead to the changing of the motion character of STS elements. The resonance motion of STS remains poorly investigated until now.

Besides resonance investigations, a study of the motion of tethered bodies concerning their centres of mass while taking into account their interaction can have independent practical value (Aslanov, 2008). For example, for the problem of photographing the Earth's surface from the lowered tether subsatellite it is very important to understand the scales and singularities of the influence of the tether and base spacecraft on the subsatellite attitude at early stages of the program development. The few works in which the motion of connected bodies concerning their centres of mass is taken into account, do not enhance the single numerical calculations for validation of the results received by means of more simple models.

The research problem of STS motion with a weakly tensioned tether is rarely studied because of its complexity. Upon departure of a tether from constraint, various

perturbing exterior factors, and also interior nonlinear effects, for example residual strain in the tether after reel-out from the spool, start to significantly influence the tether. The motion of a weakly tensioned tether is much more complicated than existing models suppose. In particular, the results from supervising a tether during experiments in space testify to this. Upon departure from constraint, the tether can be twisted into a spiral and form itself into loops. The problem of the return of the tether to constraint, which can be accompanied by the rebounds leading to new departures from constraint, is also difficult.

The study of the dynamics of a weakly tensioned tether in connection with the increasing interest in small orbital spacecraft is also topical. Groups of light spacecraft can be used to solve a wide range of scientific and economic problems. When linked by a tether, the gravitational forces operating on small spacecraft cannot provide appreciable tether tension. One way of stabilising such a system is dynamic stabilisation by a fast rotation of the system. The activity of a small STS requires high-precision control, therefore an important practical problem is the development of an exact, easy and reliable control system.

Apart from a considerable number of studies relating to the breakage of a tether by particles of space debris, various worst-case situations caused by the use of a tether have not been explored. Probably this sort of study will appear with the practical implementation of programs using space tethers. For example, Aslanov and colleagues explored a wide spectrum of worst-case situations during the preparation of the YES2 experiment (2007).

The investigation of the dynamics of multibody STS is a poorly studied field although, possibly, this direction will be actively advanced after space tethers have become a more widely applicable technology.

Speaking of mathematical models of STS, it should be noted that their complexity depends on the completeness of accounting for additional exterior and interior perturbing factors. The majority of existing models do not include deployment systems. In studies of STS, the motion of the part of a tether from the point of its exit from a deployer is considered. Perturbations introduced to the system by deployment mechanism should be considered in more accurate models. In the case of a weakly stretched tether or at the tether retrieval they can exert a strong influence on the dynamics of the system.

The problems relating to the chaotic motion of STS are poorly investigated. Elastic periodic oscillations of a tether, and periodic gravitational and aerodynamic forces of STS motion in an elliptical orbit create prerequisites for chaos motions. The occurrence of this motion mode can lead to unpleasant consequences; for example, the chaotization of one of a tethered body's oscillations can be caused by the winding of the tether onto the body. Therefore, the detection of a chaos occurrence capability and the search for ways of eliminating it is a topical problem.

## 1.5 References

- Alekseev N I (1970) *Statics and Steady Motion of a Flexible String*. Moscow: Legkaja industrija (in Russian).
- Alpatov A P, Dranovskii V I, Zakrzhevskii A E and Pirozhenko A V (1997) 'STSs. The Problem Review' (in Russian), *Cosmic Science and Technology*, 3, 5/6, 21–9.
- Alpatov A P, Beletsky V V, Dranovskii V I, Zakrzhevskii A E, Pirozhenko A V, et al. (2007) *Dynamics of Space Systems Joined by Tethers and Hinges*. Moscow-Izhevsk: Research Center in 'Regular and Chaotic Dynamics' (in Russian).

- Andrienko A Ya and Chadaev A I (1998) ‘An Analysis of Capabilities of the Gravitational Stability Augmentation for Low Orbit Satellites’, *Cosmic Research*, 36, 4, 366–73.
- Angrilli F, Bianchini G, Da Lio M and Fanti G (1988) ‘Modelling the Mechanical Properties and Dynamics of the Tethers for the TSS-1 and TSS-2 Missions’, *ESA Journal*, 12, 354–68.
- Artsutanov Yu N (1960) ‘Space by a Locomotive’ (in Russian), *Komsomolskaya Pravda*, July 31.
- Aslanov V S (2008) ‘The Oscillations of a Spacecraft under the Action of the Tether Tension Moment and the Gravitational Moment’, *American Institute of Physics (AIP) Conference Proceedings 1048*, ICNAAM, Melville, New York, 56–9.
- Aslanov V S, Ledkov A S and Stratilatov N R (2007) ‘Spatial Motion of Space Rope Cargo Transport System’ (in Russian), *Polyot* (‘Flight’), ISSN 1684–1301, 2, 28–33.
- Aslanov V S, Pirozhenko A V, Ivanov B V and Ledkov A S (2009) ‘Chaotic Motion of the Elastic Tether System’ (in Russian), *Vestnik SSAU*, 4(20), 9–15.
- Aslanov V S, Pirozhenko A V, Voloshenjuk O L, Kislov A V and Yaschuk A V (2010) ‘Definition of Survival Time of Space Chord System’ (in Russian), *Izvestiya Samarskogo nauchnogo tsentra RAN*, 4, 138–43.
- Bainum P M and Evans K S (1975) ‘Three-Dimensional Motion and Stability of Two Rotating Cable-Connected Bodies’, *Journal of Spacecraft and Rockets*, 12, 4, 242–50.
- Bainum P M and Evans K S (1976) ‘Gravity-gradient effect on the motion of two rotating cable-connected bodies’, *AIAA Journal*, 14, 1, 26–32.

- Barnhart D J, Vladimirova T, Baker A M and Sweeting M N (2009) ‘A Low-Cost Femtosatellite to Enable Distributed Space Missions’, *Acta Astronautica*, 64, 1123–43.
- Beichman C A, Woolf N J and Lindensmith C A (1999) ‘The Terrestrial Planet Finder’, in *A NASA Origins Program to Search for Habitable Planets*. Pasadena, CA: JPL Publication, 99–3.
- Belecky V V and Giverc M E (1968) ‘About Motion of Pulsing System in a Gravitational Field’, *Cosmic Research*, 6, 2, 304–6.
- Beletskii V V, Ivanov M B and Otstavnov E I (2005) ‘Model Problem of a Space Elevator’, *Cosmic Research*, 43, 152–6.
- Beletsky V V (2001) *Essays on the Motion of Celestial Bodies*. Basel: Birkhauser.
- Beletsky V V and Levin E M (1981) ‘Orbital Tether Systems’ (preprint, in Russian), *M.V. Keldish Institute of Applied Mathematics Academy of Sciences of the USSR*, 13, 1–32.
- Beletsky V V and Levin E M (1993) *Dynamics of STSs*. San Diego, CA: American Astronautical Society.
- Bonometti J A, Sorensen K F, Dankanich J W and Frame K L (2006) ‘2006 Status of the MXER Tether Development’, *Proceedings of the 42nd AIAA/ASME/SAE/ASEE Joint Propulsion Conference and Exhibit*, AIAA, AIAA 2006–4521.
- Breakwell J V and Janssens F L (1992) ‘On the Transverse Vibrations of a Revolving Tether’, *Celestial Mechanics and Dynamical Astronomy*, 54, 312–41.
- Bruno C, Bussolino L, Iess L, Licata R and Schirone L (2001) ‘EDOARD: A Tethered Device for Efficient Electrodynamic De-Orbiting of LEO Spacecraft’, *Space Technology and Applications International Forum – 2001*. AIP Conference Proceedings, 552, 433–44.

- Carroll J A (1991) ‘Preliminary Design of a 1 km/sec Tether Transport Facility’, March 1991, *Final Report on NASA Contract NASW-4461*, San Diego, CA.
- Cartmell M P and McKenzie D J (2008) ‘A Review of Space Tether Research’, *Progress in Aerospace Sciences*, 22, 1–21.
- Chobotov V A (1967) ‘Gravitational Excitation of an Extensible Dumbbell Satellite’, *Journal of Spacecraft and Rockets*, 4, 10, 1295–300.
- Chobotov V A and Mains D L (1999) ‘Tether Satellite System Collision Study’, *Acta Astronautica*, 44, 7–12, 543–51.
- Corsi J and Iess L (2001) ‘Stability and Control of Electrodynamic Tethers for De-orbiting Applications’, *Acta Astronautica*, 48, 5, 491–501.
- Cosmo M L and Lorenzini E C (1997) *Tethers in Space Handbook* (3rd edn). Cambridge, MA: Smithsonian Astrophysical Observatory.
- Crist S A and Eisley J G (1970) ‘Cable Motion of a Spinning Spring-Mass System’, *Journal of Spacecraft and Rockets*, 7, 11, 1352–7.
- Djebli A, El-Bakkali L and Pascal M (2002) ‘On Fast Retrieval Laws for Tethered Satellite Systems’, *Acta Astronautica*, 50, 8, 461–70.
- Edwards B C (2003) *Space Elevator NIAC Phase II Final Report*, available from: [www.niac.usra.edu/files/studies/final\\_report/521Edwards.pdf](http://www.niac.usra.edu/files/studies/final_report/521Edwards.pdf)
- Edwards B C and Westling E A (2003) *The Space Elevator: A Revolutionary Earth-to-Space Transportation System*. Published by B C Edwards (author).
- Eiden M and Cartmell M P (2003) ‘Overcoming the Challenges: Tether Systems Roadmap for Space Transportation Applications’, *Proceedings of the AIAA/ICAS International Air and Space Symposium and Exposition*, Dayton, 14–17 July 2003 [AIAA 2003–2840].

- Ellis J R (2010) *Modeling, Dynamics, and Control of Tethered Satellite Systems*, Dissertation of Doctor of Philosophy in Aerospace Engineering, Blacksburg, Virginia.
- Estes J N and Lang D D (1995) ‘Simulation of TSS Passive Skip-Rope Damper’, *Proceedings of the Fourth International Conference on Tethers in Space*, Science and Technology Corp., Hampton, VA, 409–18.
- Forward R L (1991) ‘Tether Transport from LEO to the Lunar Surface’, *Proceedings of the 27th AIAA/ASME/SAE/ASEE Joint Propulsion Conference and Exhibit*, AIAA, 91, 2322.
- Forward R L and Hoyt R P (1995) ‘Failsafe Multiline Hoytether Lifetimes’, AIAA Paper 5-28903, in: *Proceedings of the First AIAA/SAE/ASME/ASEE Joint Propulsion Conference*, San Diego, CA, July 1995.
- Forward R L and Hoyt R P (2000) ‘Terminator Tether<sup>TM</sup>: A Spacecraft Deorbit Device’, *Journal of Spacecraft and Rockets*, 37, 187–96.
- Gates S S, Koss S M and Zedd M F (2001) ‘Advanced Tether Experiment Deployment Failure’, *Journal of Spacecraft and Rockets*, 38, 1, 60–8.
- Gittins G L, Swinerd G G, Lewis H G and Williams D N (2004) ‘A Study of Debris Impact Collision Probabilities to Space Tethers’, *Advances in Space Research*, 34, 1080–4.
- Glabel H, Zimmermann F, Bruckner S, Schottle U M and Rudolph S (2004) ‘Adaptive Neural Control of the Deployment Procedure for Tether-Assisted Re-entry’, *Aerospace Science and Technology*, 8, 73–81.
- Hacker B C and Grimwood J M (1977) *On the Shoulders of Titan: A History of Project Gemini*. NASA Special Publication-4203 in the NASA History Series.
- He Y, Liang B and Xu W (2011) ‘Study on the Stability of Tethered Satellite System’, *Acta Astronautica*, 68, 1964–72.

- Hoyt R and Uphoff C (1999) ‘Cislunar Tether Transport System’, *35th AIAA/ASME/SAE/ASEE Joint Propulsion Conference & Exhibit*, 20–24 June 1999, Los Angeles, CA.
- Iijima S (1991) ‘Helical Microtubules of Graphitic Carbon’, *Nature*, 354, 56–8.
- Inampudi R and Schaub H (2011) ‘Orbit-Radial Control of a Two-Craft Coulomb Formation about Circular Orbits and Libration Points’, *4th International Conference on Spacecraft Formation Flying Missions & Technologies*, St-Hubert, Quebec, May 18–20, 2011.
- Isaacs J D, Vine A C, Bradner H and Bachus G E (1966) ‘Satellite Elongation into a True “Skyhook”’, *Science*, 151, 682–3.
- Ivanov V A (1984) ‘Tether Systems in Space’ (in Russian), *Aviation and Cosmonautics*, 5, 43–4.
- Ivanov V A and Sitarskiy Yu S (1986) *Dynamics of Flight of Flexibly Linked Space Objects Syste I*. Moscow: Mashinostroenie (in Russian).
- Ivanov V A, Kupreev S A and Liberzon M R (2005) *Space Tethering System*. Moscow: Russian Engineering Academy.
- Jablonski A M, Vigneron F R, Tyc G, Han R P S, Mirsa A K, Modi V J and Chandrashaker R (1996) ‘OEDIPUS-C Tether Dynamics Experiment’, *9th CASI Conference on Astronautics*, Ottawa, ON, November, 13–15.
- Johnson L and Sanmartin J (2000) ‘Propulsive Small Expendable Deployer System Experiment’, *Journal of Spacecraft and Rockets*, 37, 173–6.
- Johnson L, Fujii H A and Sanmartin J R (2010) ‘Electrodynamic Propulsion System Tether Experiment (T-Rex)’, *57th JANNAF Joint Propulsion Meeting*; 3–10 May 2010; Colorado Springs, CO; United States.
- Johnson L, Gilchrist B E, Estes R D and Lorenzini E C (1999) ‘Overview of Future NASA Tether Applications’, *Advanced Space Researches*, 24, 4, 1055–63.

- Kawashima N, Sasaki S, Oyama K I, Hirao K, Obayashi T, Raitt W J, White A B, Williamson P R, Banks P M and Sharp W F (1988) ‘Results from a Tethered Rocket Experiment (Charge-2)’, *Advances in Space Research*, 8, 197–201.
- Kokubun K (1999) ‘Resonated Libration of Tethered Subsatellite by Atmospheric Density Variation’, *Journal of Guidance, Control, and Dynamics*, 22, 6, 910–11.
- Komarov V I (1972) ‘Study of Dynamics of Spinup Scheme for Two-Sectional Spacecraft’, *Cosmic Research*, 11, 1, 14–20.
- Komarov V I (1974) ‘About Gravitational Twist of a Two-Section Satellite’ (in Russia), *Cosmic Research*, 12, 6, 856–62.
- Kornilov M Yu (1985) ‘Tubular Carbon is Needed’ (in Russian), *Chemistry and Life*, 8, 55–9.
- Kruijff M and van der Heide E J (2009) ‘Qualification and In-Flight Demonstration of a European Tether Deployment System on YES2’, *Acta Astronautica*, 64, 9–10, 882–905.
- Kumar K D (2006) ‘Review of Dynamics and Control of Nonelectrodynamic Tethered Satellite Systems’, *Journal of Spacecraft and Rockets*, 43, 4, 705–20.
- Kumar K, Kumar R and Misra A K (1992) ‘Effects of Deployment Rates and Librations on Tethered Payload Raising’, *Journal of Guidance, Control, and Dynamics*, 15, 5, 1230–5.
- Lang D D and Nolting R R (1967) ‘Operations with Tethered Space Vehicles’, *Gemini Summary Conference*, February 1–2, 1967, Houston, Texas, NASA SP, 138, 55–66.
- Lanoix E LM (1996) ‘Tether Sling Shot Assists: A Novel Approach to Travelling in the Solar System’, *Proceedings of the 9th Canadian Aeronautics and Space Institute Conference on Astronautics*, Canadian Aeronautics and Space Inst., Ottawa, ON, Canada, 1996, 62–71.

- Lanoix E LM (1999) *A Mathematical Model of the Long-Term Dynamics of Tethered Spacecraft*, Montreal, Department of Mechanical Engineering. Montreal, Quebec: McGill University.
- Lanoix E LM and Misra A K (2000) ‘Near-Earth Asteroid Missions Using Tether Sling Shot Assist’, *Journal of Spacecraft and Rockets*, 37, 475–80.
- Levin E M (2002) ‘TIPS Dynamics Analysis’, *Acta Astronautica*, 50, 9, 527–34.
- Levin E M (2007), *Dynamic Analysis of Space Tether Missions*. San Diego, CA: Univelt.
- Liberzon M R (1989) ‘Inner Indication of Absolute Stability of Nonstationary Systems’ (in Russian). *Avtomatika i Telemehanika*, 5, 40–6.
- Liberzon M R (1998) ‘Inners and Absolute Stability of Time-Lag Systems’, *Proceedings of the International Congress of Mathematicians*, August 18–27, Berlin, Germany.
- Liberzon M R (2006) ‘Essays on the Absolute Stability Theory’, *Automation and Remote Control*, 67, 10, 1610–44.
- Lisov I (1997) ‘ESA. The Second Start of ‘Ariane 5’: Incomplete Success’ (in Russian), *New Journal of Cosmonautics*, 22.
- Liu L and Bainum P M (1989) ‘Effect of Tether Flexibility on Tethered Shuttle Subsatellite Stability and Control’, *Journal of Guidance, Control, and Dynamics*, 12, 6, 866–73.
- Longuski J M, Tragesser S G and Puig-Suari J (1999) ‘Characterisation of the Optimal Mass Problem for Aerobraking Tethers’, *Acta Astronaut*, 44, 5, 227–41.
- Lorenzini E C (2004) ‘Error-Tolerant Technique for Catching a Spacecraft with a Spinning Tether’, *Journal of Vibration and Control*, 10, 1473–91.
- Lorenzini E C, Cosmo M L, Kaiser M, Bangham M E, Vonderwell D J and Johnson L (1999) *Mission Analysis of*

- Spinning Systems for Transfer from Low Orbits to Geostationary.* Cambridge, MA: Harvard-Smithsonian Center for Astrophysics.
- Mankala K K and Agrawal S K (2005) ‘Dynamic Modeling and Simulation of Space Tethered Systems’, *Journal of Vibration and Acoustics*, 127, 2, 144–57.
- Maravec H (1977) ‘A Non-Synchronous Orbital Skyhook’, *Journal of the Astronautical Sciences*, 25, 4, 307–22.
- Matteis G and Socio L M (1990) ‘Equilibrium of a Tether-Subsatellite System’, *European Journal of Mechanics*, 9, 2, 207–24.
- Matteis G and Socio L M (1991) ‘Stabilization of a Tethered Satellite System by Thrusters in Station-Keeping’, *Advances in the Astronautical Sciences*, 75, 2, 1007–28.
- Mazzoleni A P and Hoffman J H (2001) ‘Nonplanar Spin-Up Dynamics of the ASTOR Tethered Satellite System’, *Proceedings of the AAS/AIAA Space Flight Mechanics Meeting*, AAS [AAS 01–193].
- Mazzoleni A P and Hoffman J H (2003) ‘End-Body Dynamics of Artificial Gravity Generating Tethered Satellite System During Non-Planar Spinup with Elastic Effects Included’, *Proceedings of the AAS/AIAA Astrodynamics Specialists Conference*, AAS, 03–537.
- McCoy J E (1984) ‘Electrodynamic Tethers’, *35th International Astronautical Congress*, Lausanne, Switzerland, October 7–13, 84–440.
- McCoy J E, Grossi M D and Dobrowolny M (1999) ‘Plasma Motor Generator (PMG) Flight Experiment Results’, *Proceedings of the Fourth International Conference on Tethers in Space*, Smithsonian Institution, Washington, DC, 57–82.
- Merkin D R (1980) *Introduction to a Mechanics of a Flexible String*. Moscow: Nauka (in Russian).

- Misra A K and Modi V J (1986) ‘A Survey on the Dynamics and Control of Tethered Satellite Systems’, *Advances in the Astronautical Sciences*, 62, 667–719.
- Misra A K, Modi V J, Tyc G, Vegneron F and Jablonski A (1995) ‘Dynamics of Low-Tension Spinning Tethers’, *Fourth International Conference of Tethers in Space*, Washington, 10–14 April.
- Moravec H (1977) ‘A Nonsynchronous Orbital Skyhook’, *Journal of the Astronautical Sciences*, 25, 4, 307–22.
- Nordley G (2001) ‘Tether-Tossed Mars Mission Examples’, *Proceedings of the 37th AIAA/ASME/SAE/ASEE Joint Propulsion Conference and Exhibit* [AIAA 2001–3375].
- Pardini C, Hanada T, Krisko P H, Anselmoa L and Hirayama H (2007) ‘Are De-orbiting Missions Possible Using Electrodynamic Tethers? Task Review from the Space Debris Perspective’, *Acta Astronautica*, 60, 916–29.
- Pardini C, Hanada T and Krisko P H (2009) ‘Benefits and Risks of Using Electrodynamic Tethers to De-orbit Spacecraft’, *Acta Astronautica*, 64, 571–88.
- Parks D E and Katz I (1987) ‘Theory of Plasma Contactors for Electrodynamic Tethered Satellite System’, *Journal of Spacecraft and Rockets*, 24, 3, 245–9.
- Pascal M, Djebli A and Bakkali L El (1999) ‘Laws of Deployment/Retrieval in Tether Connected Satellite Systems’, *Acta Astronautica*, 45, 2, 61–73.
- Paul B (1963) ‘Planar Librations of an Extensible Dumbbell Satellite’, *AIAA Journal*, 1, 2, 411–18.
- Pearson J (1975) ‘The Orbital Tower: A Spacecraft Launcher Using Earth’s Potential Energy’, *Acta Astronautica*, 2, 785–99.
- Pearson J (1979) ‘Anchored Lunar Satellites for Cislunar Transportation and Communication’, *Journal of the Astronautical Sciences*, 17, 1, 39–62.

- Pearson J (1984) ‘The Satellite Sail: A New Device for Applying Aerodynamic Forces to Spacecraft’, *Journal of the British Interplanetary Society*, 37, 4, 172–6.
- Pearson J, Levin E, Oldson J and Wykes H (2005) *Lunar Space Elevators for Cislunar Space Development*. Mount Pleasant, SC: Star Technology and Research.
- Pelaez J (1995a) ‘On the Dynamics of the Deployment of a Tether from an Orbiter – I. Basic Equations’, *Acta Astronautica*, 36, 2, 113–22.
- Pelaez J (1995b) ‘On the Dynamics of the Deployment of a Tether from an Orbiter – II. Exponential Deployment’, *Acta Astronautica*, 36, 6, 313–35.
- Pelaez J and Andres Y N (2005) ‘Dynamic Stability of Electrodynamic Tethers in Inclined Elliptical Orbits’, *Journal of Guidance, Control, and Dynamics*, 28, 4, 611–22.
- Pelt M van (2009) *Space Tethers and Space Elevators*. New York: Springer.
- Penzo P A and Mayer H L (1986) ‘Tethers and Asteroids for Artificial Gravity Assist in the Solar System’, *Journal of Spacecraft and Rockets*, 23, 79–82.
- Pirozhenko A V (2001a) ‘Chaotic Motions Modes in Dynamics of Space Tethering Systems. 1. Analysis of the Problem’ (in Russian), *Cosmic Science and Technology*, 7, 2/3, 83–9.
- Pirozhenko A V (2001b) ‘Chaotic Motions Modes in Dynamics of Space Tethering Systems. 2. Mechanical Image of Phenomenon’ (in Russian), *Cosmic Science and Technology*, 7, 2/3, 90–9.
- Pirozhenko A V (2001c) ‘Chaotic Motions Modes in Dynamics of Space Tethering Systems. 3. Influence of an Energy Dissipation’ (in Russian), *Cosmic Science and Technology*, 7, 5/6, 13–20.
- Polyakov G G (1999) *The Convention of Transactions. Vol. 1. Tethered Satellites, Space Elevators and Rings*.

- Astrakhan: Astrakhan State Pedagogical University (in Russian).
- Pugno N M (2006) ‘On the Strength of the Carbon Nanotube-Based Space Elevator Cable: From Nanomechanics to Megamechanics’, *Journal of Physics: Condensed Matter*, 18, S1971–S1990.
- Purdy W, Coffey S, Barnds W J, Kelm B and Davis M (1997) ‘TiPS: Results of a Tethered Satellite Experiment’, *Astrodynamic Spacialist Conference*, Sun Valley, ID, August 4–7, AAS-97-600.
- Radushkevich L V and Lukjanovich V M (1952) ‘About Structure of the Carbon Organised at Thermal Decomposition Carbon Monoxide on an Iron Contact’ (in Russian), *Journal of Physics and Chemistry*, 26, 88.
- Rauwolf G A, Pelaccio D G, Patel S and Sorensen K (2001) ‘Mission Performance of Emerging In-Space Propulsion Concepts for One-Year Crewed Mars Missions’, *Proceedings of 37th AIAA/ASME/SAE/ASEE Joint Propulsion Conference and Exhibit*, AIAA [AIAA 2001-3374].
- Robe T R (1968) ‘Stability of Two Tethered Unsymmetrical Earth-Pointing Bodies’, *AIAA Journal*, 6, 12, 2282–8.
- Rodnikov A V (2004) ‘Motion of a Load along a Cable Fastened to a Two-Body-Tethered Spacecraft’, *Cosmic Research*, 42, 427–31.
- Roy A E (2005) *Orbital Motion*. London: IOP Publishing.
- Rupp C C (1975) ‘A Tether Tension Control Law for Tethered Subsatellite Deployment along Local Vertical’, *NASATMX-64963*, Houston, TX, September.
- Sanmartin J R (2010) ‘A Review of Electrodynamic Tethers for Science Applications’, *Plasma Sources Science and Technology*, 19(3).
- Shcherbakov V I (2010) *Orbital Manoeuvres of Space Tethering Systems*. Sankt-Piterburg: A.F.Mozhaisky Military-space Academy (in Russian).

- Smith H F (1995) ‘The First and Second Flights of the Small Expendable Deployer System (SEDS)’, *Proceedings of the Fourth International Conference on Tethers in Space*, Smithsonian Inst., Washington, DC, 43–55.
- Sorensen K (2001) ‘Conceptual Design and Analysis of an MXER Tether Boost Station’, *Proceedings of 37th AIAA/ASME/SAE/ASEE Joint Propulsion Conference and Exhibit*, AIAA, 2001 [AIAA2001–3915].
- Sorensen K (2003) ‘Hyperbolic Injection Issues for MXER Tethers’, *Proceedings of the 39th AIAA/ASME/SAE/ASEE Joint Propulsion Conference and Exhibit*, AIAA [AIAA 2003–5221], 1–7.
- Sorensen K (2003) ‘Momentum Exchange ElectrodynamiC Reboost Tether. Technology Assessment Group Final Report’, *Space Propulsion Technologies Program*, July 24, 2003. NASA Marshall Space Flight Center, Huntsville, AL 35812.
- Tai C L and Loh M H (1965) ‘Planar Motion of a Rotating Cable-Connected Space Station in Orbit’, *Journal of Spacecraft and Rockets*, 2, 6, 889–94.
- Takeichi N, Natori M C, Okuzumi N and Higuchi K (2004) ‘Periodic Solutions and Controls of Tethered Systems in Elliptic Orbits’, *Journal of Vibration and Control*, 10, 1393–413.
- Troger H, Alpatov A P, Beletsky V V, Dranovskii V I, Khoroshilov V S, Pirozhenko A V and Zakrzhevskii A E (2010) *Dynamics of Tethered Space Systems*. Boca Raton, FL: CRC Press.
- Vas I E, Kelly T J and Scarl E A (2000) ‘Space Station Reboost with ElectrodynamiC Tethers’, *Journal of Spacecraft and Rockets*, 37, 2, 154–64.
- Vigneron F R, Jablonski A M, Chandrashaker R, Bergmans J L, McClure B A and Tyc G (1997) ‘Comparison of Analytical Modelling of OEDIPUS Tethers with Data

- from Tether Laboratory', *Journal of Guidance, Control, and Dynamics*, 20, 3, 471–8.
- Watanabe T, Makida T, Fujii H A, Kojima H and Singhose W (2004) 'An Application of Input Shaping for Electrodynamic Tether System', AIAA-2004-5313 AIAA/AAS Astrodynamics Specialist Conference, Aug. 16–19, Providence, RI.
- Wilbur P J and Laupa T G (1988) 'Plasma Contactor Design For Electrodynamic Tether Applications', *Advances in Space Research*, 8, 221–4.
- Williams P (2006) 'Energy Rate Feedback for Libration Control of Electrodynamic Tethers', *Journal of Guidance, Control, and Dynamics*, 29, 1, 221–3.
- Williams P, Blanksby C, Trivailoa P and Fujii H A (2005) 'In-Plane Payload Capture Using Tethers', *Acta Astronautica*, 57, 772–87.
- Williams P, Hyslop A, Stelzer M and Kruijff M (2009) 'YES2 Optimal Trajectories in Presence of Eccentricity and Aerodynamic Drag', *Acta Astronautica*, 64, 7–8, 745–69.
- Wisdom J (1987) 'Rotational Dynamics of Irregularly Shaped Natural Satellites', *Astronomical Journal*, 94, 1350–60.
- Zhou X, Li J, Baoyin H and Zakirov V (2006) 'Equilibrium Control of Electrodynamic Tethered Satellite Systems in Inclined Orbits', *Journal of Guidance, Control, and Dynamics*, 29, 6, 1451–4.
- Zhu R, Misra A K and Lin H (1993) 'Dynamics of Tether-Assisted Reentry Vehicle System', *Advances in the Astronautical Sciences*, 84, 2, 1387–402.
- Zhu R, Misra A K and Modi V J (1994) 'Dynamics and Control of Coupled Orbital and Librational Motion of Tethered Satellite Systems', *Journal of the Astronautical Sciences*, 42, 3, 319–42.
- Zimmermann F, Schottle U M and Messerschmid E (2005) 'Optimization of the Tether-Assisted Return Mission of a Guided Re-entry Capsule', *Aerospace Science and Technology*, 5, 713–21.

## Conclusion

The mechanics of space tether systems is an extensive area of the modern mechanics of space flight. In this book we have tried to show on the one hand a variety of tasks and areas of research related with space tether systems, and on the other, their practical feasibility based on modern technology, and their ability to solve existing problems.

In one book it is impossible to answer all questions related with dynamics of space cable systems. Therefore, we have tried to focus on problems that may find wide application in the coming decades: the delivery of cargo from an orbit without the cost of rocket fuel, exploring the atmosphere and surface of the Earth by a subsatellite lowered on a tether. The specificity of these problems require us to create new mathematical models that take into account the interaction of the tether with the atmosphere and the movement around the centre of the mass of the spacecraft. Practical implementation cannot be made without assessment of potential emergencies and their consequences. Therefore, we have developed models that take into account various abnormal situations. Presented in the book, models and analytical results were used in the preparation and post-flight analysis of the international experiment YES2.

The study of chaotic behaviour of a mechanical system in space is a relatively new direction of tether system's mechanics. The presence of orbital eccentricity and the phenomenon of elasticity of tethers are the cause of the chaos

in space tether system's motion. Chaos can be a serious obstacle to the successful implementation of the space missions, because it can lead to off-normal operation of the system and to accidents. Using the methods of chaotic dynamics allows us to carry out a selection of space tether system parameters that preclude the possibility of chaos.

Another new trend that is discussed in detail in the book, is the study of dynamics of motion, relative to the centre of mass of the spacecraft with an attached tether. Tether systems have a significant influence on spacecraft dynamics, despite the low weight of the tether and tethered payload in comparison with the mass of the spacecraft. In some cases the spacecraft can be observed swinging with a subsequent transition into the rotation. New analytical solutions describing the plane vibrations of the spacecraft are illustrated in the book. These solutions can be used for quick calculations and qualitative analysis of the spacecraft motion with a tether.

The authors wish to thank the readers for their patience. We hope that the book will not only broaden your horizons, but will also arouse an interest in further study of the dynamics of space tether systems.

# Mathematical models of space tethering systems

**Abstract:** This second chapter is devoted to the question of the mathematical modelling of space tethering systems consisting of two rigid bodies connected by a tether. The process of developing mathematical models is considered in detail. Various models are presented where the tether is represented in the form of: a massless bar, a ponderous bar, a heavy flexible thread, and a multipoint system connected by viscoelastic bars. Special attention is given to the question of a tether's interaction with the non-Newtonian gravitational field of Earth and with the atmosphere, and therefore whether the developed multipoint model can be applied to the analysis of a tether system's motion at rather low altitude.

**Key words:** space tethering systems; mathematical model; flexible thread; multipoint tether model; Lagrangian formalism.

In the scientific literature, steadfast attention is given to mathematical models of space tethering systems (STS). The great number of works on this theme is caused by a variety of problems: where STS can be used, perturbing factors, ways of modelling a tether and bodies connected by them.

All existing mathematical models of tether modelling can be divided into three groups. In the first group, it is possible to refer to models in which the tether is modelled as a bar

(Paul, 1963; Aslanov, 2010). Depending on the problem solved, the bar can be ponderous or massless, elastic or inelastic. Such models are often used for estimating calculations. Thanks to their simplicity, they enable us to obtain some analytical results.

Models in which the tether is represented as a heavy flexible thread are referred to in the second group (Beletsky and Levin, 1993; Ellis, 2010). These models most precisely describe the dynamics of a tether; however, their numerical integration requires great computing expenditure, although they can be used for exact control calculations. In models of the third group, the tether is substituted by a set of particles connected by segments of a massless viscoelastic bar. These models have a clear mechanical sense, and the calculations fulfilled with their help agree very well with the results received by means of models of the second group (Aslanov et al., 2007).

One more factor considerably influencing the complexity of a model is the way the bodies connected by a tether are represented. In the elementary cases, they can be considered as particles. In more exact models, it is necessary to consider the motion of rigid bodies concerning their centres of masses.

In this chapter, some models will be constructed that are different in the way the tether and its connected bodies are represented. As an additional perturbing factor in some models, aerodynamic force will be used. It allows for the use of these models for research of STS dynamics at low altitude.

## **2.1 Simple models of STS consisting of two point masses connected by a massless tether**

The models in which a tether is presented as a massless bar are the simplest kind of tether system models, and such

models were used in the early studies of STS dynamics (Paul, 1963). Despite their advanced age, until now these models have not lost their significance because in view of their complexity neither discrete models, nor models in which a tether is presented by a flexible thread, are suitable for obtaining analytical dependences and criteria. The simplicity of the models with a massless tether allows for the discovery of qualitative singularities of STS motions by rather simple methods. Besides, such models are often used for rough calculations.

### ***2.1.1 Model of a spacecraft with a tethered subsatellite in Keplerian orbit***

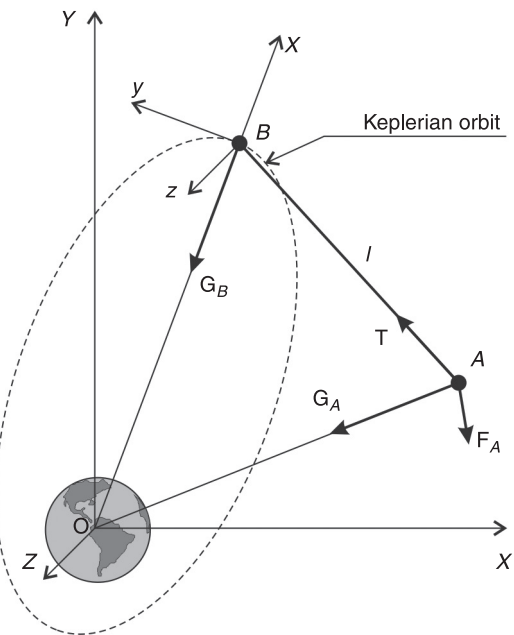
Let us begin our acquaintance with mathematical models of STS from the simple model given by Beletsky and Levin (1993). The considered STS consists of a massive spacecraft, a massless tether and a light subsatellite. Its movement occurs in the Newtonian gravitational field. The subsatellite and spacecraft are presented as particles with the masses  $m_A$  and  $m_B$  accordingly (see Figure 2.1). As the weight of the tether is ignored, the highly accurate description of the STS centre of mass movement is unnecessary. Therefore, in a case when  $m_B \gg m_A$ , it is possible to assume that the STS centre of mass coincides with particle B, which in turn moves in an unperturbed elliptic orbit defined only by a gravitational force action. In this case, the general equation of dynamics for particle B is:

$$m_B \mathbf{w}_B = \mathbf{G}_B,$$

where  $\mathbf{w}_A$  – the acceleration of particle B; and  $\mathbf{G}_B$  – the gravitational force acting on particle B.

$$\mathbf{G}_B = -m_B \frac{\mu \mathbf{r}_B}{r_B^3},$$

**Figure 2.1** STS consisting of two point masses connected by a massless tether in Keplerian orbit



where  $\mathbf{r}_B$  – the radius vector of particle B in a geocentric coordinate system OXYZ; and  $\mu$  – gravitational constant of Earth. NB: Hereinafter vectors are designated by **bold** letters.

Using these expressions, we get a differential equation defining the movement of particle B in an unperturbed elliptic orbit.

$$\ddot{\mathbf{r}}_B = -\frac{\mu \mathbf{r}_B}{r_B^3}, \quad [2.1]$$

The general equation of dynamics for the subsatellite has the form

$$m_A \mathbf{w}_A = \mathbf{T}_A + \mathbf{F}_A + \mathbf{G}_A, \quad [2.2]$$

where  $\mathbf{w}_A$  – the acceleration of particle A;  $\mathbf{T}_A$  – the tension force of the tether;  $\mathbf{F}_A$  – non-gravitational external forces; and  $\mathbf{G}_A$  – the gravitational force acting on particle A.

$$\mathbf{G}_A = -m_A \frac{\mu \mathbf{r}_A}{r_A^3}. \quad [2.3]$$

Let us find the equations describing the motion of a subsatellite in the orbital coordinate system connected with particle B. Axis Bx is directed along a geocentric radius vector of particle B, axis By – on a transversal, and Bz – on a binormal of the spacecraft's orbit (see Figure 2.1). Particle A makes a compound motion. Acceleration at this point, according to the Coriolis theorem, is a sum of relative  $\mathbf{w}_r$ , reference-frame  $\mathbf{w}_{rf}$  and Coriolis  $\mathbf{w}_c$  accelerations (Kleppner and Kolenkow, 1973).

$$\mathbf{w}_A = \mathbf{w}_r + \mathbf{w}_{rf} + \mathbf{w}_c. \quad [2.4]$$

Here,

$$\mathbf{w}_r = \ddot{\mathbf{p}}_A, \quad \mathbf{w}_{rf} = \ddot{\mathbf{r}}_B + \boldsymbol{\omega} \times (\boldsymbol{\omega} \times \mathbf{p}_A) + \dot{\boldsymbol{\omega}} \times \mathbf{p}_A, \quad \mathbf{w}_c = 2\boldsymbol{\omega} \times \dot{\mathbf{p}}_A, \quad [2.5]$$

where  $\boldsymbol{\omega}$  – vector of an angular velocity of orbital frame  $Bxyz$  rotation concerning inertial geocentric coordinate system OXYZ; and  $\mathbf{p}_A$  – radius vector of particle A in the orbital frame, cross denotes a vector product.

Substituting [2.5] and [2.1] into [2.4] and taking into account [2.3] we obtain:

$$\ddot{\mathbf{p}}_A + \boldsymbol{\omega} \times (\boldsymbol{\omega} \times \mathbf{p}_A) + \dot{\boldsymbol{\omega}} \times \mathbf{p}_A + 2\boldsymbol{\omega} \times \dot{\mathbf{p}}_A + \frac{\mu \mathbf{r}_A}{r_A^3} - \frac{\mu \mathbf{r}_B}{r_B^3} = \frac{\mathbf{T}_A + \mathbf{F}_A}{m_A}. \quad [2.6]$$

The difference of the two last parts of the left side of [2.6] can be calculated by expansion into a series with respect to  $\mathbf{p}_A$  and the cutting of the nonlinear term.

$$\frac{\mu \mathbf{r}_A}{r_A^3} - \frac{\mu \mathbf{r}_B}{r_B^3} = \mu \left( \frac{(\mathbf{r}_B + \mathbf{p}_A)}{|\mathbf{r}_B + \mathbf{p}_A|^3} - \frac{\mathbf{r}_B}{r_B^3} \right) \approx \mu \left( \frac{\mathbf{p}_A}{r_B^3} - 3 \frac{\mathbf{r}_B}{r_B^5} (\mathbf{p}_A \cdot \mathbf{r}_B) \right),$$

where the dot means a scalar product.

We substitute the last expression in [2.6], and the received vectorial equation we write in the projections to the axes of an orbital coordinate system (Beletsky and Levin, 1993).

$$\begin{aligned}\ddot{x} - 2\dot{y}\omega - \dot{\omega}y - (1+2k^{-1})\omega^2x &= (T_x + F_x)/m_A, \\ \ddot{y} + 2\dot{y}\dot{x}\omega + \dot{\omega}x - (1-k^{-1})\omega^2y &= (T_y + F_y)/m_A, \\ \ddot{z} + k^{-1}\omega^2z &= (T_z + F_z)/m_A,\end{aligned}\quad [2.7]$$

where  $x, y, z$  – coordinates of the vector  $\mathbf{p}_A$  in  $Bxyz$ ,  $k = 1 + e \cos \vartheta$ ;  $e$  and  $\vartheta$  – an eccentricity and an angle of true anomaly of spacecraft's orbit; and  $F_x, F_y, F_z$  – projections of the vector  $\mathbf{F}_A$  to axes  $Bxyz$ .

The module of angular velocity  $\omega$  can be found as:

$$\omega = \dot{\vartheta} = \sqrt{\frac{\mu}{p^3}} k^2,$$

where  $p$  – focal parameter of spacecraft orbit.

Because within the limits of model the tether is considered as a massless bar, the projections of tension force  $\mathbf{T}$  to the axes of  $Bxyz$  can be found as:

$$T_x = T \frac{x}{\sqrt{x^2 + y^2 + z^2}}, \quad T_y = T \frac{y}{\sqrt{x^2 + y^2 + z^2}}, \quad T_z = T \frac{z}{\sqrt{x^2 + y^2 + z^2}}.$$

The module of tension force  $T$  can be found by means of the Hooke law:

$$T = ES \left( \frac{\rho_A}{l_0} - 1 \right), \quad [2.8]$$

where  $E$  – the module of elasticity (see Table 1.2);  $S$  – cross-section area of strainless tether; and  $l_0$  – length of strainless tether.

Subsatellite motion is convenient for considering spherical co-ordinates  $\rho, \theta, \varphi$ , where  $\theta$  – a turn angle in a plane of the spacecraft orbit; and  $\varphi$  – an angle of a deflection from this plane. Cartesian coordinates  $x, y, z$  are connected with the spherical by the following relations:

$$x = -r \cos \theta \cos \varphi, \quad y = -r \sin \theta \cos \varphi, \quad z = -r \sin \varphi.$$

Substituting these expressions into [2.7] and calculating all necessary derivatives, we obtain:

$$\begin{aligned} \ddot{\theta} + \dot{\omega} + 2(\dot{\theta} + \omega)(\dot{\rho}_A \rho_A^{-1} - \dot{\varphi} t g \varphi) + 3k^{-1}\omega^2 \sin \theta \cos \theta = \\ -F_\theta (m_A \rho_A \cos \varphi)^{-1}, \\ \ddot{\varphi} + 2\dot{\varphi} \dot{\rho}_A \rho_A^{-1} + \sin \varphi \cos \varphi [(\dot{\theta} + \omega)^2 + 3k^{-1}\omega^2 \cos^2 \theta] = \\ -F_\varphi (m_A \rho_A)^{-1}, \\ \ddot{r} - r[\dot{\varphi}^2 + (\dot{\theta} + \omega)^2 \cos^2 \varphi + k^{-1}\omega^2 (3 \cos^2 \varphi \cos^2 \theta - 1)] \\ + T m_A^{-1} = -F_\rho m_A^{-1}. \end{aligned} \quad [2.9]$$

Projections of forces to the axes of a spherical frame are:

$$\begin{pmatrix} F_r \\ F_\theta \\ F_\varphi \end{pmatrix} = \begin{pmatrix} \cos \theta \cos \varphi & \sin \theta \cos \varphi & \sin \varphi \\ -\sin \theta & \cos \theta & 0 \\ -\cos \theta \sin \varphi & -\sin \theta \sin \varphi & \cos \varphi \end{pmatrix} \begin{pmatrix} F_x \\ F_y \\ F_z \end{pmatrix}.$$

Beletsky and Levin (1993) note that the suborbital motion is constrained in the sphere. The subsatellite makes a free motion in a sphere with the centre in point B and the radius of  $l_0$ . As soon as it goes outside of the sphere, a large tension force appears in the tether. This force aspires to return the subsatellite to the interior area of the sphere and is calculated in formula [2.8]. If the tension in the tether becomes more than the tensile strength  $\sigma_*$  (see Table 1.2), the tether will be broken off. The condition of tether breakage is:

$$\frac{T}{S} > \sigma_*.$$

From this inequality, by means of [2.8] the maximum distance  $\rho_*$  on which the subsatellite can move away from the spacecraft without a tether break can be found:

$$\rho_* = l_0 \left( \frac{\sigma_*}{E} + 1 \right).$$

The scalar equations [2.7] and [2.9], together with the vectorial equation [2.1], describe the motion of STS with a massless elastic tether in the case when the spacecraft is far heavier than the subsatellite, and the spacecraft moves in unperturbed Keplerian orbit.

### **2.1.2 Plane motion of a spacecraft and a tethered subsatellite in a wind coordinate system**

Numerous studies show that for many cases of STS, the out-of-plane oscillations are small in comparison with the oscillations in the orbital plane. Then it is possible to consider the STS motion as planar and to use the equations of motion recorded in a wind coordinate system. Without any restriction being imposed on the masses of the tethered spacecrafts, we write an equation of motion for one of them, for example corresponding to a particle A, in a vector form:

$$m_A \mathbf{w}_A = m_A \mathbf{g}_A + \mathbf{T} + \mathbf{F}_A, \quad [2.10]$$

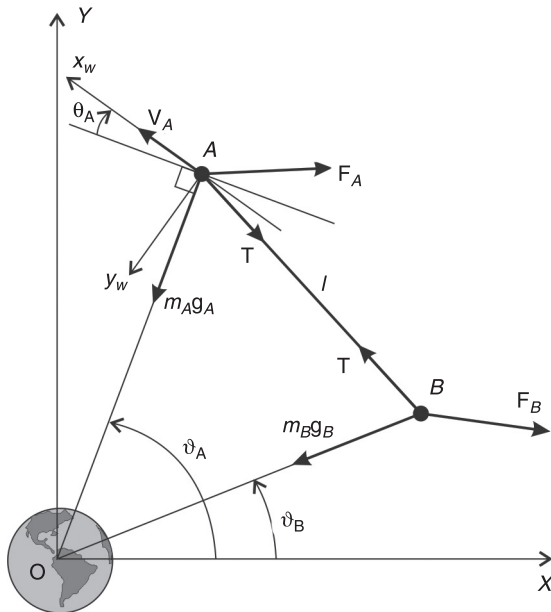
where  $\mathbf{g}_A$  – vector of gravitational acceleration on spacecraft at altitude  $H_A$  (see Figure 2.2).

It can be found as

$$\mathbf{g}_A = g_0 \left( \frac{R_E}{r_A} \right)^2 \mathbf{g}_0 \left( \frac{R_E}{R_E + H_A} \right)^2, \quad [2.11]$$

where  $g_0$  – acceleration of gravity on a surface of Earth; and  $R_E$  – radius of the Earth.

**Figure 2.2** STS consisting of two point masses connected by a massless tether



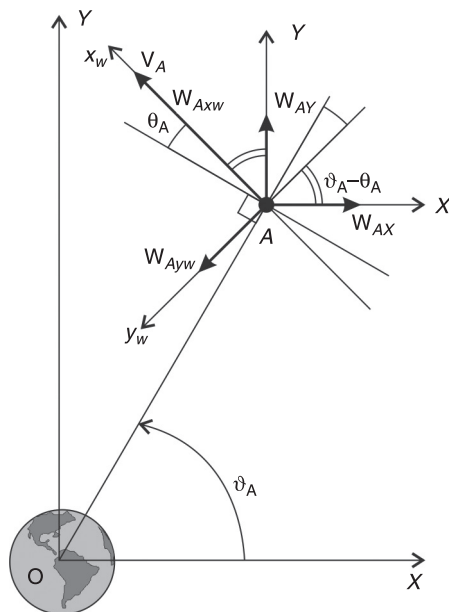
Let us write [2.10] in projections to the axes of a wind coordinate system  $Ax_wy_w$  related with the spacecraft. Axis  $Ax_w$  is directed along the velocity vector, and the axis  $Ay_w$  supplements the coordinate system to right-hand side.

$$\begin{aligned} m_A w_{Axw} &= -m_A g_A \sin \theta_A + T \sin(\theta_A + \varphi) + F_{Axw}, \\ m_A w_{Ayw} &= -m_A g_A \cos \theta_A - T \cos(\theta_A + \varphi) + F_{Ayw}, \end{aligned} \quad [2.12]$$

where  $\varphi$  is a slope angle of tether to radius vector of particle A;  $\theta_A$  – angle of trajectory inclination;  $w_{Axw}$ ,  $w_{Ayw}$  – coordinates of  $w_A$  in the wind coordinate system  $Ax_wy_w$ .  $F_{Axw}$ ,  $F_{Ayw}$  – projections of  $F_A$  to the  $Ax_wy_w$ .

We find projections of acceleration  $w_A$  to the axes of the wind coordinate system (see Figure 2.3). The absolute velocity of particle A can be set by coordinates in  $OXY$  related to the centre of the Earth:

$$\mathbf{V}_A = [-V_A \sin(\vartheta_A - \theta_A), V_A \cos(\vartheta_A - \theta_A)]^T,$$

**Figure 2.3** Wind coordinate system

where  $\vartheta_A$  – angle of true anomaly of particle A.

Here and below, the vector's coordinate will be represented in the form of a column matrix. The angle of true anomaly can be found from the differential equation:

$$\dot{\vartheta}_A = \frac{V_A \cos \theta_A}{R_E + H_A}. \quad [2.13]$$

By differentiating vector  $\mathbf{V}_A$  on time, we receive:

$$\mathbf{w}_A = [w_{AX}, w_{AY}]^T,$$

where projections to the fixed axes  $OXY$  are defined by the expressions:

$$\begin{aligned} w_{AX} &= -\dot{V}_A \sin(\vartheta_A - \theta_A) - V_A (\dot{\vartheta}_A - \dot{\theta}_A) \cos(\vartheta_A - \theta_A), \\ w_{AY} &= \dot{V}_A \cos(\vartheta_A - \theta_A) - V_A (\dot{\vartheta}_A - \dot{\theta}_A) \sin(\vartheta_A - \theta_A). \end{aligned} \quad [2.14]$$

Let us find coordinates of vector  $\mathbf{w}_A$  in the wind coordinate system  $Ax_wy_w$ :

$$\begin{aligned} w_{Axw} &= w_{AY} \cos(\vartheta_A - \theta_A) + w_{AX} \sin(\vartheta_A - \theta_A), \\ w_{Ayw} &= -w_{AX} \cos(\vartheta_A - \theta_A) - w_{AY} \sin(\vartheta_A - \theta_A). \end{aligned}$$

By substituting [2.14] into the last expressions, after simple transformations we obtain:

$$w_{xw} = \dot{V}_A, \quad w_{yw} = V_A (\dot{\theta}_A - \dot{\vartheta}_A). \quad [2.15]$$

Taking into account [2.15], the equations [2.12] can be written in the form:

$$\begin{aligned} m_A \dot{V}_A &= -m_A g_A \sin \theta_A + T \sin(\theta_A + \varphi) + F_{AXW}, \\ m_A V_A (\dot{\theta}_A - \dot{\vartheta}_A) &= -m_A g_A \cos \theta_A - T \cos(\theta_A + \varphi) + F_{AYW}. \end{aligned} \quad [2.16]$$

It is possible to add the kinematic relations to equations [2.16] (Andreevskiy, 1970):

$$\begin{aligned} \dot{H}_A &= V_A \sin \theta_A, \\ \dot{L}_A &= \frac{R_E}{R_E + H_A} V_A \cos \theta_A, \end{aligned} \quad [2.17]$$

where  $L_A$  – flight range.

If the tether is not attached to the spacecraft, the system consisting of equations [2.16] and [2.17] would be closed. For STS it is necessary to obtain similar equations for the second spacecraft, adding also equations [2.13]. Such a model is given in the article by Sidorov (2000):

$$\begin{aligned} m_i \dot{V}_i &= -\frac{g_0 R_E^2 m_i \sin \theta_i}{(R_E + H_i)^2} + j_i T \sin(\theta_i + \varphi) \\ m_i \dot{\theta}_i &= -\frac{g_0 R_E^2 m_i \cos \theta_i}{V_i (R_E + H_i)^2} + \frac{V_i m_i \cos \theta_i}{R_E + H_i} - \frac{j_i T \cos(\theta_i + \varphi)}{V_i}, \end{aligned}$$

$$\begin{aligned}\dot{\vartheta}_i &= \frac{V_i \cos \theta_i}{r_i}, \\ \dot{H}_i &= V_i \sin \theta_i, \\ \dot{L}_i &= \frac{R_E}{R_E + H_i} V_i \cos \theta_i, \quad i = A, B.\end{aligned}\tag{2.18}$$

In [2.18],  $j_A = 1$  and  $j_B = -1$ ,  $F_A = 0$ . The angle  $\varphi$  can be found by means of the law of sines:

$$\sin \varphi = \sin(\vartheta_A - \vartheta_B) \frac{H_B + R_E}{l}$$

or the cosine law:

$$\cos \varphi = \frac{(H_A + R_E)^2 + l^2 - (H_B + R_E)^2}{2l(H_A + R_E)}$$

where  $l = \sqrt{(H_A + R)^2 + (H_B + R)^2 - 2(H_A + R)(H_B + R)\cos(\vartheta_A - \vartheta_B)}$  – tether length.

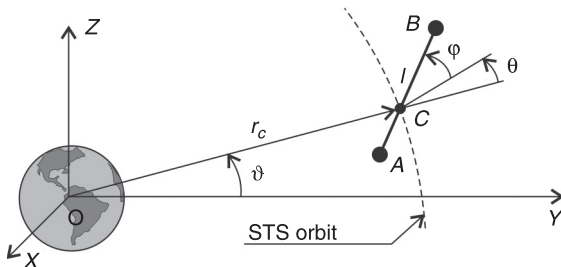
Tension force can be found from the equation similar to [2.8]:

$$T = ES \left( \frac{l}{l_0} - 1 \right)$$

## 2.2 Simple model of a STS consisting of two point masses connected by a heavy tether

The models discussed in section 2.1 appear to be the solution to many problems; however, if the tether mass is comparable to the mass of the end bodies, these models cannot adequately describe the dynamics of the system. One of the models taking account of the mass of the tether is the model obtained by Williams (2003). He obtained the equations of motion by

**Figure 2.4** STS consisting of two point masses connected by a heavy tether



means of Lagrangian formalism. This model illustrates the efficiency and beauty of application of the analytical mechanics methods for the solution of the current problems of the mechanics of space flight.

Let us make some assumptions. The cable is considered as a rigid, inextensible ponderous body. During the STS motion the tether length can vary. The deployment gear is mounted on one of the spacecraft, and it can deploy and retract the tether. From all exterior forces acting on the STS, only the influence of terrestrial gravitational force is considered, and this was assumed to be Newtonian. The tethered spacecrafts are considered as particles A and B (see Figure 2.4).

The state of the STS can be described by five generalised coordinates: the radius vector of the STS centre of mass  $r_C$ , the angle of true anomaly of the centre of mass  $\vartheta$ , an angle of tether deflection in the orbital plane  $\theta$ , an angle of deflection from the orbital plane  $\varphi$ , and a tether length  $l$ .

Let us obtain equations of the STS motion by means of the Lagrange equations. The total kinetic energy of the STS is the sum of the kinetic energy of its centre of masses  $T_C$  and the kinetic energy of the motion of the system concerning its centres of mass  $T_r$  (Taylor, 2005):

$$T_{tot} = T_C + T_r. \quad [2.19]$$

It is possible to present the last summand as the sum of the kinetic energy of the system's rotation concerning the centre of mass  $T_{rot}$  and the kinetic energy of extension about the centre of mass  $T_{ext}$ :

$$T_r = T_{rot} + T_{ext}. \quad [2.20]$$

The kinetic energy of centre of mass can be found as follows:

$$T_C = \frac{1}{2}m(\dot{r}_C^2 + \dot{\vartheta}^2 r_C^2), \quad [2.21]$$

where  $m = m_A + m_B + m_t$  – total mass of STS;  $m_A = m_A^0 - m_t$  – mass of spacecraft on which the reel with the tether is located;  $m_A^0$  – mass of the spacecraft when the tether is completely reeled on the reel;  $m_t = \rho_M S l$  – mass of the released site of the tether;  $\rho_M$  – density of the tether material (see Table 1.2); and  $S$  – cross-sectional area of the tether.

The kinetic energy of the STS rotation can be found by means of the matrix equation:

$$T_{rot} = \frac{1}{2}\omega^T \|I\|\omega, \quad [2.22]$$

where  $\omega$  – the vector of the angular velocity of the tether in relation to the spacecraft coordinate system,

$$\omega = \begin{bmatrix} (\dot{\theta} + \dot{\vartheta}) \sin \varphi \\ -\dot{\varphi} \\ (\dot{\theta} + \dot{\vartheta}) \cos \varphi \end{bmatrix},$$

and  $\|I\|$  – the matrix of the tensor of inertia of the STS,

$$\|I\| = \begin{bmatrix} 0 & 0 & 0 \\ 0 & I_{cm} & 0 \\ 0 & 0 & I_{cm} \end{bmatrix}.$$

Here,  $I_{cm}$  is the moment of inertia concerning the centres of mass which can be found by the definition:

$$I_{cm} = m_A \rho_A^2 + m_B \rho_B^2 + \int_{-\rho_A}^{\rho_B} \rho_M \rho^2 d\rho, \quad [2.23]$$

where distances from the centres of mass KTC to points A and B are:

$$\rho_A = (m_B + \frac{m_t}{2}) \frac{l}{m}, \quad \rho_B = (m_A + \frac{m_t}{2}) \frac{l}{m}.$$

After calculation of the integral in [2.23] and simple algebraic transformations, the moment of inertia  $I_{cm}$  can be written as:

$$I_{cm} = m_* l^2, \quad [2.24]$$

where  $m_* = (m_A + m_t/2)(m_B + m_t/2)/m - m_t/6$  – reduced mass of STS.

Substituting [2.23] into [2.22] we find a kinetic energy of the system's rotation:

$$T_{rot} = \frac{1}{2} m_* l^2 (\dot{\varphi}^2 + (\dot{\theta} + \dot{\vartheta})^2 \cos^2 \varphi). \quad [2.25]$$

The kinetic energy of extension about the centre of mass appears as the deploying and retrieval of the tether. For a tether considered as a rigid body, this energy can be found as:

$$T_{ext} = \frac{1}{2} \frac{m_A (m_B + m_t)}{m} j^2. \quad [2.26]$$

The potential energy of the STS in a terrestrial gravitational field can be found as the sum of the potential energies of the system's elements:

$$W = -\frac{\mu m_A}{r_A} - \frac{\mu m_B}{r_B} - \frac{\mu m_t}{r_C}. \quad [2.27]$$

The radius vectors  $\mathbf{r}_A$  and  $\mathbf{r}_B$  of particles A and B can be calculated as:

$$\mathbf{r}_A = \mathbf{r}_C + \boldsymbol{\rho}_A, \quad \mathbf{r}_B = \mathbf{r}_C + \boldsymbol{\rho}_B. \quad [2.28]$$

Vectors  $\mathbf{r}_C$ ,  $\boldsymbol{\rho}_A$  and  $\boldsymbol{\rho}_B$  are set in the fixed coordinate system:

$$\begin{aligned}\mathbf{r}_C &= [0, r_C \cos \vartheta, r_C \sin \vartheta]^T, \\ \boldsymbol{\rho}_A &= [\rho_A \sin \varphi, -\rho_A \cos \varphi \cos(\theta + \vartheta), -\rho_A \cos \varphi \sin(\theta + \vartheta)]^T, \\ \boldsymbol{\rho}_B &= [-\rho_B \sin \varphi, \rho_B \cos \varphi \cos(\theta + \vartheta), \rho_B \cos \varphi \sin(\theta + \vartheta)]^T.\end{aligned}$$

Whence, the lengths of the radius vectors can be found:

$$\begin{aligned}r_A &= \sqrt{r_C^2 + \rho_A^2 - 2r_C \rho_A \cos \varphi \cos \theta}, \\ r_B &= \sqrt{r_C^2 + \rho_B^2 + 2r_C \rho_B \cos \varphi \cos \theta}.\end{aligned}$$

Taking into account the last expressions, the potential energy [2.27] becomes:

$$\begin{aligned}W = -\frac{\mu m_A}{r_C \sqrt{1 - 2 \frac{\rho_A}{r_C} \cos \varphi \cos \theta + \frac{\rho_A^2}{r_C^2}}} \\ - \frac{\mu m_B}{r_C \sqrt{1 + 2 \frac{\rho_B}{r_C} \cos \varphi \cos \theta + \frac{\rho_B^2}{r_C^2}}} - \frac{\mu m_t}{r_C}. \quad [2.29]\end{aligned}$$

The presence of the square roots in the denominators of [2.29] leads to the conclusion that the Lagrange equations are lengthy enough. We note that in the majority of cases, the tether length is at least 10 times less than the radius vector of the centres of mass:  $\rho_{A,B}/r_C \ll 1$ . Therefore, within the limits of the simplified model, it is possible to develop the potential energy as the Maclaurin series in these parameters and to restrict consideration of the several first terms. Using expansion in the series

$$\frac{1}{\sqrt{1 \pm 2x \cos \varphi \cos \theta + x^2}} = 1 \mp x \cos \varphi \cos \theta + \frac{x^2}{2} (3 \cos^2 \varphi \cos^2 \theta - 1) + O(x^3)$$

we write the potential energy in the form:

$$W = -\frac{\mu m}{r_C} - \frac{\mu m_* l^2}{2r_C^3} (3 \cos^2 \varphi \cos^2 \theta - 1). \quad [2.30]$$

Let us note that the considered mechanical system is conservative, as it is independent of time (the kinetic energy is a quadratic function of the generalised velocities and does not depend on time obviously), all the forces of the system are potential, and the potential does not depend on time obviously. For the given system, there is the energy integral:

$$h = T_{tot} + W = \text{const.}$$

Using [2.19]–[2.21], [2.25], [2.26] and [2.30], we write the Lagrangian of the system:

$$\begin{aligned} L = T_{tot} - W &= \frac{m}{2} (\dot{r}_C^2 + \dot{\vartheta}^2 r_C^2) + \frac{1}{2} m_* l^2 (\dot{\varphi}^2 + (\dot{\theta} + \dot{\vartheta})^2 \cos^2 \varphi) \\ &+ \frac{1}{2} \frac{m_A (m_B + m_t)}{m} \dot{l}^2 + \frac{\mu m}{r_C} + \frac{\mu m_* l^2}{2r_C^3} (3 \cos^2 \varphi \cos^2 \theta - 1). \end{aligned} \quad [2.31]$$

The Lagrange equation has the form (Gantmacher, 1975):

$$\frac{d}{dt} \frac{\partial L}{\partial \dot{q}_i} - \frac{\partial L}{\partial q_i} = Q_i, \quad [2.32]$$

where  $q_i = r_C, \vartheta, \theta, \varphi, l$  – generalised coordinates; and  $Q_i$  – not potential generalised forces.

At evaluation of the Lagrange equations, it is necessary to remember that the masses  $m_A$  and  $m_t$  are functions of the tether length  $l$ . Substituting [2.31] into [2.32], we obtain a

system of the differential equations that describes the STS motion with a heavy tether as:

$$\ddot{r}_C = r_C \dot{\vartheta}^2 - \frac{\mu}{r_C^2} + \frac{3\mu\Phi_1 l^2 (1 - 3\cos^2 \theta \cos^2 \varphi)}{2r_C^4}, \quad [2.33]$$

$$\ddot{\vartheta} = -\frac{2\dot{\vartheta}\dot{r}_C}{r_C} + \frac{3\mu\Phi_1 l^2}{2r_C^5} \sin 2\theta \cos^2 \varphi, \quad [2.34]$$

$$\begin{aligned} \ddot{\theta} &= 2(\dot{\theta} + \dot{\vartheta}) \left[ \dot{\varphi} \tan \varphi - \Phi_2 \frac{\dot{l}}{l} \right] \\ &+ 2 \frac{\dot{r}_C}{r_C} \dot{\vartheta} - \frac{3\mu}{r_C^3} \sin \theta \cos \theta \left[ 1 + \frac{\Phi_1 l^2}{r_C^2} \cos^2 \varphi \right], \end{aligned} \quad [2.35]$$

$$\ddot{\varphi} = -2\Phi_2 \frac{\dot{l}}{l} \dot{\varphi} - \left[ (\dot{\theta} + \dot{\vartheta})^2 + \frac{3\mu}{r_C^3} \cos^2 \theta \right] \sin \varphi \cos \varphi, \quad [2.36]$$

$$\begin{aligned} \ddot{l} &= -\Phi_3 \frac{\dot{l}^2}{l} + \Phi_4 l \\ &\times \left[ \dot{\varphi}^2 + (\dot{\theta} + \dot{\vartheta})^2 \cos^2 \varphi + \frac{\mu}{r_C^3} (3 \cos^2 \theta \cos^2 \varphi - 1) \right] \\ &- \frac{mT}{m_A(m_B + m_t)}, \end{aligned} \quad [2.37]$$

where  $T$  – a controlling force of the tether's tension; and  $\Phi_i$  – the nondimensional coefficients set by expressions:

$$\begin{aligned} \Phi_1 &= \frac{m_*}{m}, \quad \Phi_2 = \frac{m_A(m_B + m_t / 2)}{mm_*}, \\ \Phi_3 &= \frac{(2m_A - m)m_t}{2m_A(m_B + m_t)}, \quad \Phi_4 = \frac{m_B + m_t / 2}{m_B + m_t}. \end{aligned}$$

If it is presumed that the centre of mass of the system moves on the unperturbed Keplerian orbit, then the system of the equations of motion [2.33]–[2.37] can be simplified essentially by transferring to a new independent variable – an angle of true anomaly. In this case, coordinates  $\vartheta$  and  $r_C$  are determined by the expressions (Curtis, 2005):

$$\dot{\vartheta} = \sqrt{\frac{\mu}{a^3(1-e^2)^3}}k^2, \quad r_C = \frac{a(1-e^2)}{k}, \quad [2.38]$$

where  $e$  – an eccentricity of orbit;  $a$  – apogee radius; and  $k = 1 + e\cos\vartheta$ .

Equations [2.35]–[2.37] take the form:

$$\theta'' = 2(\theta' + 1) \left[ \frac{e \sin \vartheta}{k} + \varphi' \tan \varphi - \Phi_2 \frac{l'}{l} \right] - \frac{3}{k} \sin \theta \cos \theta, \quad [2.39]$$

$$\begin{aligned} \varphi'' = & \frac{2e \sin \varphi}{k} \varphi' - 2\Phi_2 \frac{l'}{l} \varphi' \\ & - \left[ (\theta' + 1)^2 + \frac{3}{k} \cos^2 \theta \right] \sin \varphi \cos \varphi, \end{aligned} \quad [2.40]$$

$$\begin{aligned} l'' = & \frac{2e \sin \vartheta}{k} l' - \Phi_3 \frac{l'^2}{l} \\ & + \Phi_4 l \left[ \varphi'^2 + (\theta' + 1)^2 \cos^2 \varphi + \frac{1}{k} (3 \cos^2 \theta \cos^2 \varphi - 1) \right] \\ & - \frac{m T a^3 (1 - e^2)^3}{m_A (m_B + m_t) \mu k^4}. \end{aligned} \quad [2.41]$$

Here the accent means a derivative of a variable  $\vartheta$ .

For a case of flat motion, equations [2.33]–[2.37] definitely become simpler:

$$\ddot{r}_C = r_C \dot{\vartheta}^2 - \frac{\mu}{r_C^2} + \frac{3\mu\Phi_1 l^2 (1 - 3 \cos^2 \theta)}{2r_C^4}, \quad [2.42]$$

$$\ddot{\vartheta} = -\frac{2\dot{\vartheta}\dot{r}_C}{r_C} + \frac{3\mu\Phi_1 l^2}{2r_C^3} \sin 2\theta, \quad [2.43]$$

$$\ddot{\theta} = -2(\dot{\theta} + \dot{\vartheta})\Phi_2 \frac{\dot{l}}{l} + 2\frac{\dot{r}_C}{r_C} \dot{\vartheta} - \frac{3\mu}{r_C^3} \sin \theta \cos \theta \left[ 1 + \frac{\Phi_1 l^2}{r_C^2} \right], \quad [2.44]$$

$$\begin{aligned} \ddot{l} = & -\Phi_3 \frac{\dot{l}^2}{l} + \Phi_4 l \left[ \dot{\varphi}^2 + (\dot{\theta} + \dot{\vartheta})^2 + \frac{\mu}{r_C^3} (3 \cos^2 \theta - 1) \right] \\ & - \frac{mT}{m_A(m_B + m_t)}. \end{aligned} \quad [2.45]$$

For equations [2.39]–[2.41] we have:

$$\theta'' = 2(\theta' + 1) \left[ \frac{e \sin \vartheta}{k} - \Phi_2 \frac{l'}{l} \right] - \frac{3}{k} \sin \theta \cos \theta, \quad [2.46]$$

$$\begin{aligned} l'' = & -\Phi_3 \frac{l'^2}{l} + \Phi_4 l \left[ (\theta' + 1)^2 + \frac{1}{k} (3 \cos^2 \theta - 1) \right] \\ & - \frac{mTa^3(1-e^2)^3}{m_A(m_B + m_t)\mu k^4}. \end{aligned} \quad [2.47]$$

In a case in which the length of the tether remains invariable during motion, the systems of the equations become simpler. Equations [2.45] and [2.47] are degenerated, and [2.44] and [2.46] become accordingly:

$$\ddot{\vartheta} = 2\frac{\dot{r}_C}{r_C} \dot{\vartheta} - \frac{3\mu}{r_C^3} \sin \theta \cos \theta \left[ 1 + \frac{\Phi_1 l^2}{r_C^2} \right], \quad [2.48]$$

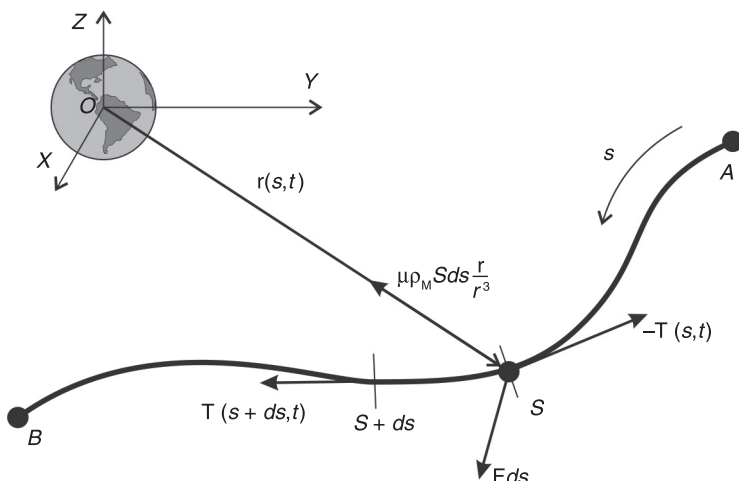
$$\theta'' = 2(\theta' + 1) \frac{e \sin \vartheta}{k} - \frac{3}{k} \sin \theta \cos \theta. \quad [2.49]$$

## 2.3 Model of a STS with a ponderous flexible tether

The majority of STS models are reduced to a system of two particles connected by a tether. Such a representation is quite reasonable, as the length of the tether makes several tens of kilometres, the sizes of the connected bodies several metres, and the thickness of the tether is only a few millimetres. For describing such a system, the model of two point masses connected by a heavy thread is used in many studies in the STS dynamics field (Alpatov et al., 1997; Beletsky and Levin, 1993). Let us consider a mechanical system of two particles A and B connected by a tether AB which is in the terrestrial gravitational field (see Figure 2.5). The tether length can vary at deployment or retraction by deploying gears mounted on the end bodies.

Let us separate the tether from the elemental section  $ds$  with density  $\rho_M(s)$  and cross-section area  $S$ . The tension

**Figure 2.5** STS consisting of two point masses connected by a flexible tether



forces act on this section from nearby parts of the tether:  $\mathbf{T}(s + ds, t)$  from  $sB$ , and  $-\mathbf{T}(s, t)$  from  $As$ . We denote  $\mathbf{r}(s, t)$  as the radius vector of a point  $s$  in an instant of time  $t$ . In a fixed geocentric coordinate system OXYZ, Newton's equation for the centre of mass of the viewed section has the form:

$$\rho_M(s)ds \frac{\partial^2 \mathbf{r}}{\partial t^2} S = \mathbf{T}(s + ds, t) - \mathbf{T}(s, t) - \rho_M(s)\mu ds \frac{\mathbf{r}}{r^3} S + \mathbf{F}ds,$$

where  $\mathbf{F}$  – vector of the external forces intensity.

From the last equation we obtain:

$$\rho_M \frac{\partial^2 \mathbf{r}}{\partial t^2} S = \frac{\partial \mathbf{T}}{\partial s} - \rho_M S \mu \frac{\mathbf{r}}{r^3} + \mathbf{F}. \quad [2.50]$$

This is the dynamical equation of the heavy flexible tether. The flexible tether, by definition, does not resist bending, and its tension is always directed along a tangent. The force of the tension in the tether is determined by Hooke's law:

$$\mathbf{T} = ES(\gamma - 1)\boldsymbol{\tau}, \quad [2.51]$$

where  $E$  – elastic modulus;  $\gamma = \left| \frac{\partial \mathbf{r}}{\partial s} \right|$  – unit elongation of the tether section; and  $\boldsymbol{\tau} = \left( \frac{\partial \mathbf{r}}{\partial s} \right) \left| \frac{\partial \mathbf{r}}{\partial s} \right|^{-1}$  – unit vector, tangential to tether line.

Substituting [2.51] into [2.50], we obtain:

$$\rho_M \frac{\partial^2 \mathbf{r}}{\partial t^2} = \frac{\partial}{\partial s} \left[ ES \frac{\partial \mathbf{r}}{\partial s} \left( 1 - \left| \frac{\partial \mathbf{r}}{\partial s} \right|^{-1} \right) \right] - \rho_M \mu \frac{\mathbf{r}}{r^3} S + \mathbf{F}. \quad [2.52]$$

This vector differential equation in partial derivatives of the wave type which is resolved in a strip with variables boundaries. For this equation, the boundary conditions are the equations of the motion of the end bodies:

$$\begin{aligned}
 m_A(t) \frac{d^2 \mathbf{r}_A}{dt^2} &= \boldsymbol{\tau}_A \left[ T_A - \rho_M(s_A) \gamma_A \left( \frac{ds_A}{dt} \right)^2 S \right] \\
 -m_A(t) \mu \frac{\mathbf{r}_A}{r_A^3} + \mathbf{F}_A, \\
 m_B(t) \frac{d^2 \mathbf{r}_B}{dt^2} &= -\boldsymbol{\tau}_B \left[ T_B - \rho_M(s_B) \gamma_B \left( \frac{ds_B}{dt} \right)^2 S \right] \\
 -m_B(t) \mu \frac{\mathbf{r}_B}{r_B^3} + \mathbf{F}_B. \tag{2.53}
 \end{aligned}$$

If, within the limits, the model of the rigid bodies at the tips of the tether is considered in the boundary conditions of equation [2.52], instead of points A and B (the corresponding centres of mass of the bodies), it is necessary to use mounting points of the tether  $A_k$  and  $B_k$ .

Let us write the dynamic equations of the end bodies concerning their centres of mass (Alpatov et al., 1997).

$$\begin{aligned}
 \|I_A\| \dot{\boldsymbol{\omega}}_A &= -\boldsymbol{\omega}_A \times \|I_A\| \cdot \boldsymbol{\omega}_A + \mathbf{d}_A \times \boldsymbol{\tau}_{A_k} T_{A_k} + 3 \frac{\mu}{r_A^3} \boldsymbol{\tau}_A \times \|I_A\| \boldsymbol{\tau}_A + \mathbf{M}_A, \\
 \|I_B\| \dot{\boldsymbol{\omega}}_B &= -\boldsymbol{\omega}_B \times \|I_B\| \cdot \boldsymbol{\omega}_B + \mathbf{d}_B \times \boldsymbol{\tau}_{B_k} T_{B_k} + 3 \frac{\mu}{r_B^3} \boldsymbol{\tau}_B \times \|I_B\| \boldsymbol{\tau}_B + \mathbf{M}_B, \tag{2.54}
 \end{aligned}$$

where,  $\|I_A\|$ ,  $\|I_B\|$  – the matrix of the tensors of inertia of the end bodies;  $\boldsymbol{\omega}_A$ ,  $\boldsymbol{\omega}_B$  – the vectors of the absolute angular velocities concerning the centre of mass;  $\mathbf{d}_A$ ,  $\mathbf{d}_B$  – vectors of the defining position of the tether mounting points concerning the centre of mass;  $\mathbf{M}_A$ ,  $\mathbf{M}_B$  – moments of external forces; and  $\boldsymbol{\tau}_i = \left( \frac{\partial \mathbf{r}_i}{\partial s} \right) \left| \frac{\partial \mathbf{r}_i}{\partial s} \right|^{-1}$ .

Motion of points  $A_k$  and  $B_k$ , can be found from the equations:

$$\begin{aligned}
 \ddot{\mathbf{r}}_{A_k} &= \ddot{\mathbf{r}}_A + \boldsymbol{\omega}_A \times \mathbf{d}_{A_k} + \boldsymbol{\omega}_A \times (\boldsymbol{\omega}_A \times \mathbf{d}_{A_k}), \\
 \ddot{\mathbf{r}}_{B_k} &= \ddot{\mathbf{r}}_B + \boldsymbol{\omega}_B \times \mathbf{d}_{B_k} + \boldsymbol{\omega}_B \times (\boldsymbol{\omega}_B \times \mathbf{d}_{B_k}),
 \end{aligned}$$

where  $\mathbf{r}_{A_k}$ ,  $\mathbf{r}_{B_k}$  – radius vectors of the points of the mounting points in the coordinate system.

Irrespective of whether the account of the spatial motion of rigid bodies is necessary or if it is possible to consider the bodies as particles, the received model has some essential singularities. A principal singularity is that the order of derivatives in the boundary conditions equal to the order of the partial differential equation. Implementation of the algorithms of numerical integration of this partial equation is a difficult task.

Another not less considerable difficulty is the indispensable condition that the integration step on time  $\Delta t$  must be very small. Its step is defined by the velocity of distribution of the longitudinal oscillations along the tether  $v_E$ :

$$\Delta t < \frac{\Delta s}{v_E} = \frac{\Delta s}{\sqrt{ES / \rho_M}},$$

where  $\Delta s$  – distance between mesh nodes.

This time appears very small in comparison with the time of the STS operation (the 100th fractions of a second), and taking into account the high dimension of the differential system, the volume of required computations becomes enormous (Beletsky and Levin, 1993).

## 2.4 Model of a STS consisting of a point mass connected by a heavy tether with a rigid body

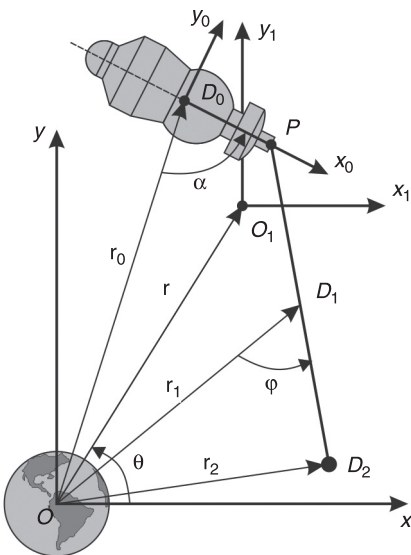
The models which are connected by tether bodies which were considered as mass points have been given above. Such an approach is reasonable when the motion of the connected bodies concerning their centres of mass is not a matter of principle. However, there are problems for which it is

impossible to disregard this angular motion; for example, as the solution of the problem of photographing the Earth's surface from the subsatellite lowered on the tether, or at an influence estimation of the tether system on the level of microgravitation on board the multipurpose spacecraft. For these examples it is possible to disregard an angular motion of one of the connected bodies and consider it as a mass point; for example, owing to the large difference between their masses or because of the work of the system of the stabilisation keeping the angular position of one of the bodies. For such problems, the mechanical system should consist of a rigid body, a mass point and a tether connecting them.

#### ***2.4.1 Development of a mathematical model by means of the Lagrange procedure***

Let us assume that the STS moves in a plane. We will consider a case when the tether length can vary, in other words, it can deploy from or be retrieved from one of the connected bodies. We will term the body which carries the tether and deployer the base spacecraft. It is represented as a rigid body with mass  $m_0$  (see Figure 2.6) on which the gravitational force, the gravitational moment and the moment of the tether's tension force act. In a dynamic sense, the spacecraft is defined by the moments of inertia  $I_x, I_y, I_z$  ( $I_{xy} = I_{xz} = I_{yz} = 0$ ) and by location of the centre of mass. The point of the tether's outlet  $P$  does not coincide with the spacecraft's centre of mass  $D_0$ . For simplicity we make the assumption that point  $P$  is on the spacecraft's axis of symmetry. The second end body will be termed the payload. It is represented as a mass point  $D_2$  with mass  $m_2$ . At the derivation of the equations of motion we will neglect the flexibility of an elastic tether. The tether is considered as an elastic heavy rod.

**Figure 2.6** STS consisting of a point mass connected by a heavy tether with a rigid body



Its mass varies proportionally to its length  $m_1(l)$ , and the centre of mass is in a point  $D_1$ .

As the length of the tether changes during the STS motion, so the mass of the spacecraft is a variable. The full mass of the system is defined as:

$$m = \sum_{i=0}^2 m_i = m_0^0 + m_2, \quad [2.55]$$

where  $m_0^0$  – initial mass of spacecraft; and  $m_0 = m_0^0 - m_1$  – current mass of spacecraft.

Let us introduce the coordinate systems (see Figure 2.6). The reference point O of a fixed geocentric coordinate system  $Oxyz$  corresponds to the centre of mass of Earth O, the axis  $Ox$  is directed on an orbit perigee, the axis  $Oz$  is in a perpendicular plane of orbit and directed on us,  $Oy$  supplements the system to the right. The axis connected with

the spacecraft coordinate systems  $D_0x_0y_0z_0$  has a reference point in the centre of the masses of the spacecraft  $D_0$ . The axis  $D_0x_0$  is directed along the axis of symmetry to the point of the tether's outlet, the axis  $D_0z_0$  is in a perpendicular plane of orbit and directed on us,  $D_0y_0$  supplements the system to the right. The coordinate system  $O_1x_1y_1z_1$  has its beginning in the STS centre of mass, and its axes are parallel to the axes of  $Oxyz$ .

For construction of the mathematical model we will use the Lagrange equations of the second kind. As generalised coordinates we will use an angle of deflection of the spacecraft's axis from its local vertical  $\alpha$ , an angle of deflection of the tether from its local vertical  $\varphi$ , the length of the deployed part of the tether  $l = PD_2$ , an angle of true anomaly of the STS centre of mass  $\theta$ , the distance from the centre of mass of Earth to the centre of mass of the STS  $r=OO_1$ . These parameters unambiguously define the position of the system.

$$q_1 = \alpha, \quad q_2 = \varphi, \quad q_3 = l, \quad q_4 = \theta, \quad q_5 = r. \quad [2.56]$$

For construction of the Lagrange equations it is necessary to find the kinetic and potential energy of the STS. For obtaining the kinetic energy we will use the Koenig theorem according to which the kinetic energy of the mechanical system is equal to the sum of the kinetic energy of the centre of mass and the kinetic energy of motion of the system concerning the centres of mass. For consideration of the STS, the Koenig theorem can be written as:

$$T_{tot} = T_C + \sum_{i=0}^2 T_i, \quad [2.57]$$

where  $T_{tot}$  – total kinetic energy of STS;  $T_C$  – kinetic energy of the centre of mass; and  $T_i$  kinetic energy of the STS elements in the coordinate system  $O_1x_1y_1$ .

The kinetic energy of the centre of mass of system is equal to:

$$T_C = \frac{1}{2}m(\dot{r}^2 + r^2\dot{\theta}^2) \quad [2.58]$$

The kinetic energies of the relative motion of the spacecraft  $T_0$ , the tether  $T_1$  and the payload  $T_2$  are:

$$T_0 = \frac{1}{2}m_0V_{0r}^2 + \frac{1}{2}I_z\omega_0^2, \quad [2.59]$$

$$T_1 = \frac{1}{2}m_1V_{1r}^2 + \frac{1}{2}I_{z1}\omega_1^2, \quad [2.60]$$

$$T_2 = \frac{1}{2}m_2V_{2r}^2, \quad [2.61]$$

where  $V_{ir}$  – velocity of particle  $D_i$  ( $i=0, 1, 2$ ) in the coordinate system  $O_1x_1y_1$ ;  $\omega_0$  and  $\omega_1$  – absolute angular velocities of the spacecraft and the tether;  $I_z$  – principal central moment of inertia of the spacecraft concerning axis  $D_0z_0$  in the coordinate system  $D_0x_0y_0z_0$ ; and  $I_{z1}=m_1l^2/12$  – moment of inertia of the tether concerning its centre of mass.

For definition of the kinetic energy of the STS [2.57] through generalised coordinates [2.56], we introduce a review of the radius vectors of the centre of mass of the STS  $O_1$  and the centres of mass of its elements  $D_i$  in the polar coordinates (see Figure 2.6):

$$\begin{aligned} \mathbf{r} &= \mathbf{OO}_1 = (r \cos \theta, r \sin \theta), \quad \mathbf{r}_i = \mathbf{OD}_i \\ &= (r_i \cos \theta_i, r_i \sin \theta_i), \quad (i = 0, 1, 2) \end{aligned} \quad [2.62]$$

and vectors

$$\begin{aligned} \mathbf{l} &= \mathbf{PD}_2 = (l \sin(\varphi + \theta_1 - \pi/2), -l \cos(\varphi + \theta_1 - \pi/2)) \\ &= (-l \cos(\varphi + \theta_1), -l \sin(\varphi + \theta_1)), \\ \Delta &= \mathbf{D}_0\mathbf{P} = (\Delta \sin(\alpha + \theta_0 - \pi/2), -\Delta \cos(\alpha + \theta_0 - \pi/2)) \\ &= (-\Delta \cos(\alpha + \theta_0), -\Delta \sin(\alpha + \theta_0)). \end{aligned} \quad [2.63]$$

where  $\Delta$  – distance between the centre of mass of the spacecraft  $D_0$  and the point of tether outlet  $P$ ; and  $\theta_i$  – angle of true anomaly of the centre of mass  $D_i$ .

Vectors [2.62] and [2.63] are connected by expressions which follow from the definition of the centre of mass of the system and its geometry:

$$m\mathbf{r} = \sum_{i=0}^2 m_i \mathbf{r}_i, \quad [2.64]$$

$$\mathbf{r}_1 = \mathbf{r}_0 + \Delta + \frac{1}{2}\mathbf{l}, \quad \mathbf{r}_2 = \mathbf{r}_0 + \Delta + \mathbf{l}. \quad [2.65]$$

Substituting the expressions [2.65] into [2.64] and considering that  $m=m_0+m_1+m_2$ , we obtain:

$$(m_0 + m_1 + m_2)\mathbf{r} = m_0\mathbf{r}_0 + m_1\left(\mathbf{r}_0 + \Delta + \frac{1}{2}\mathbf{l}\right) + m_2\left(\mathbf{r}_0 + \Delta + \mathbf{l}\right).$$

Expressing from the last formula the vector  $\mathbf{r}_0$ , we receive the expressions establishing connection between the coordinates of the point and the generalised  $D_0$  coordinates [2.56]:

$$\mathbf{r}_0 = \mathbf{r} - \frac{m_1 + m_2}{m}\Delta - \frac{m_1/2 + m_2}{m}\mathbf{l} \quad [2.66]$$

Substituting [2.66] into [2.65], we obtain similar expressions for the vectors  $\mathbf{r}_1$  and  $\mathbf{r}_2$ :

$$\mathbf{r}_1 = \mathbf{r} + \frac{m_0}{m}\Delta + \frac{m_0 - m_2}{2m}\mathbf{l}, \quad [2.67]$$

$$\mathbf{r}_2 = \mathbf{r} + \frac{m_0}{m}\Delta + \frac{m_0 + m_1/2}{m}\mathbf{l}. \quad [2.68]$$

By means of [2.66]–[2.68] it is possible to define the position of points  $D_i$  in the coordinate system  $O_1x_1y_1$  connected with the centre of mass of the STS

$$\begin{aligned}\rho_0 &= \mathbf{r}_0 - \mathbf{r} = -\frac{m_1 + m_2}{m} \Delta - \frac{m_1 / 2 + m_2}{m} \mathbf{l}, \\ \rho_1 &= \mathbf{r}_1 - \mathbf{r} = \frac{m_0}{m} \Delta + \frac{m_0 - m_2}{2m} \mathbf{l}, \\ \rho_2 &= \mathbf{r}_2 - \mathbf{r} = \frac{m_0}{m} \Delta + \frac{m_0 + m_1 / 2}{m} \mathbf{l}.\end{aligned}\quad [2.69]$$

Velocities of points  $D_i$  can be found as:

$$\mathbf{V}_{ir} = \dot{\rho}_i. \quad [2.70]$$

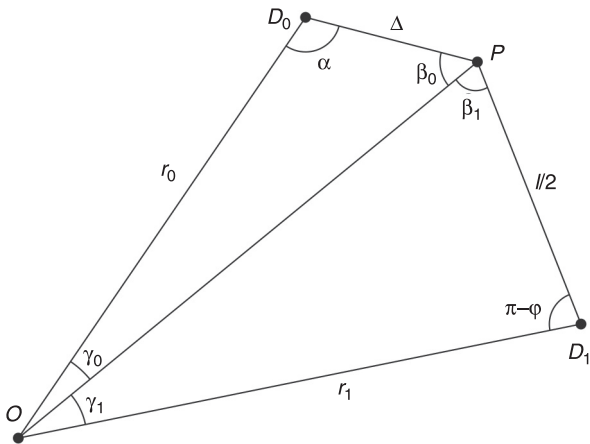
The angular velocities of the spacecraft and the tether entering into the formulas in [2.59] and [2.60] are equal:

$$\omega_0 = \dot{\alpha} + \dot{\theta}_0, \quad [2.71]$$

$$\omega_1 = \dot{\varphi} + \dot{\theta}_1. \quad [2.72]$$

The derivatives  $\dot{\theta}_0$  and  $\dot{\theta}_1$  can be found with the help of projections of [2.66] and [2.67] on the axis of  $O_1x_1y_1$ :

$$\begin{aligned}r_0 \cos \theta_0 &= r \cos \theta + \frac{m_1 + m_2}{m} \Delta \cos(\theta_0 + \alpha) \\ &+ \frac{m_1 / 2 + m_2}{m} l \cos(\theta_1 + \varphi), \\ r_0 \sin \theta_0 &= r \sin \theta + \frac{m_1 + m_2}{m} \Delta \sin(\theta_0 + \alpha) \\ &+ \frac{m_1 / 2 + m_2}{m} l \sin(\theta_1 + \varphi), \\ r_1 \cos \theta_1 &= r \cos \theta + \frac{m_0}{m} \Delta \cos(\theta_0 + \alpha) \\ &+ \frac{m_0 - m_2}{2m} l \cos(\theta_1 + \varphi), \\ r_1 \sin \theta_1 &= r \sin \theta + \frac{m_0}{m} \Delta \sin(\theta_0 + \alpha) \\ &+ \frac{m_0 - m_2}{2m} l \sin(\theta_1 + \varphi).\end{aligned}\quad [2.73]$$

**Figure 2.7** Geometry of points of a STS

To these equations, two equations received by means of the sine theorem from triangles  $OD_0P$  and  $OPD_1$  (Figure 2.7) can be added:

$$\frac{\sin \beta_0}{r_0} = \frac{\sin \gamma_0}{\Delta}, \quad \frac{\sin \beta_1}{r_1} = \frac{2 \sin \gamma_1}{l}.$$

Considering  $\gamma_0 = \theta_0 - \theta$ ,  $\gamma_1 = \theta - \theta_1$ ,  $\beta_0 = \pi - \alpha - \gamma_0 = \pi - \alpha - \theta_0 + \theta$ , and  $\beta_1 = \pi - (\pi - \phi) - \gamma_1 = \phi + \theta_1 - \theta$ , from the last equations we have:

$$r_0 = \Delta \frac{\sin(\alpha + \theta_0 - \theta)}{\sin(\theta_0 - \theta)}, \quad r_1 = \frac{l \sin(\phi + \theta_1 - \theta)}{2 \sin(\theta - \theta_1)}. \quad [2.74]$$

Angles  $\theta_0$  and  $\theta_1$  can be expressed from the trigonometrical equations [2.73] and [2.74] through generalised coordinates [2.56].

Finally, by means of the formulas [2.58]–[2.61] and [2.68]–[2.70], we write the kinetic energy of the STS [2.58] as functions of the generalised coordinates [2.56] and their velocities:

$$T_{tot} = \frac{1}{2}m(\dot{r}^2 + r^2\dot{\theta}^2) + \frac{1}{2}\sum_{i=0}^2 m_i\dot{\rho}_i^2 + \frac{1}{2}[I_z(\dot{\alpha} + \dot{\theta}_0)^2 + I_{z1}(\dot{\varphi} + \dot{\theta}_1)^2]. \quad [2.75]$$

Let us move to the construction of the potential energy of the STS. The gravitational force and the gravitational moment (which aspires to superimpose a principal axis of the body with the greatest moment of inertia, with a line connecting the centre of mass of the body with the centre of the Earth) operate on a body in orbit. We write a potential, allowing for the gravitational field influence on the spacecraft (Beletsky and Levin, 1993)

$$W_0 = -\frac{\mu m_0}{r_0} + \frac{3\mu}{2r_0^3}(I_x - I_y)\cos^2\alpha, \quad [2.76]$$

where  $I_x, I_y$  – principal central moments of inertia in the tether connected with the spacecraft coordinate system  $D_0x_0y_0z_0$  concerning axes  $D_0x_0$  and  $D_0y_0$  accordingly.

A similar potential can be written for the tether. As the tether is considered as a heavy homogeneous bar, its principal central moments of inertia are defined by the expressions  $I_{x1} = 0, I_{y1} = I_{z1} = m_1 l^2 / 12$ . Substituting these values into the formula for a gravitational field potential, we have:

$$W_1 = -\frac{\mu m_1}{r_1} \left(1 + \frac{l^2}{8r_1^2} \cos^2\varphi\right). \quad [2.77]$$

As within the limits of our model payload it is considered as a particle, its potential energy looks like:

$$W_2 = -\frac{\mu m_2}{r_2}. \quad [2.78]$$

Besides gravitational forces and the moments at the mechanical system there is an elastic force for which the potential energy is (Kleppner and Kolenkow, 1973):

$$W_E = \frac{c}{2}(l - l_0)^2, \quad [2.79]$$

where  $c = ES/l_0$  – coefficient of stiffness;  $l_0$  – length of unstressed tether;  $S$  – tether's cross-section area.

Uniting the expressions [2.76]–[2.79], we obtain the formula for potential energy:

$$W = -\mu \sum_{i=0}^2 \frac{m_i}{r_i} + \frac{3\mu}{2r_0^3} (I_x - I_y) \cos^2 \alpha - \frac{\mu m_1 l^2}{8r_1^3} \cos^2 \varphi + \frac{c}{2} (l - l_0)^2. \quad [2.80]$$

Let us write the Lagrangian using the expressions in [2.75] and [2.80]:

$$\begin{aligned} L = T - W = & \frac{1}{2} m (\dot{r}^2 + r^2 \dot{\theta}^2) + \frac{1}{2} \sum_{i=0}^2 m_i \dot{r}_i^2 \\ & + \frac{1}{2} [I_z (\dot{\alpha} + \dot{\theta}_0)^2 + I_{z1} (\dot{\varphi} + \dot{\theta}_1)^2] \\ & + \mu \sum_{i=0}^2 \frac{m_i}{r_i} - \frac{3\mu}{2r_0^3} (I_x - I_y) \cos^2 \alpha + \frac{\mu m_1 l^2}{8r_1^3} \cos^2 \varphi - \frac{c}{2} (l - l_0)^2. \end{aligned} \quad [2.81]$$

The Lagrange equations of the second kind have the form (Gantmacher, 1975):

$$\frac{d}{dt} \frac{\partial L}{\partial \dot{q}_j} - \frac{\partial L}{\partial q_j} = Q_j, \quad j = \overline{1, 5}, \quad [2.82]$$

where  $q_j$  – generalised coordinates [2.65];  $Q_j$  – nonpotential forces, including forces of control, damping, aerodynamic forces and others.

We will notice that the Lagrangian [2.81] depends on the generalised coordinates  $q_j$  and the generalised velocities  $\dot{q}_j$ , although implicitly. The Lagrangian equations [2.82] represent a system of five differential equations of the second order.

The basic difficulty in obtaining the equations in [2.82] is the determination of derivatives  $\dot{\theta}_0$  and  $\dot{\theta}_1$  from equations [2.73]

and [2.74]. The problem essentially becomes simpler if one makes the assumption  $r \gg l$ . In this case it is possible to consider approximately that  $\theta_0 \approx \theta_1 \approx \theta$ . The specified assumption is quite reasonable, as modern technologies allow for space tethers to be made in the order of several hundreds of kilometres, and orders of magnitudes  $r$  and  $l$  differ at least by two.

When the task involves deployment or retrieval of the tether, it is necessary to consider the length of the unstressed tether entering into the Lagrangian [2.81] as the time function  $l_0 = l_0(t)$ . This function is defined by the control law of the development gear and is considered as given. In this case, the masses of development tether and satellite will be also development time functions; for example, in the case of a homogeneous tether:

$$m_0 = m_0^0 - l_0(t)S\rho_M, \quad m_1 = l_0(t)S\rho_M.$$

Variability of development length of the deployed part of the tether and its mass leads to development of essential complication of the equations in [2.82].

## 2.4.2 The Lagrange equations for a deployed STS

Let us consider the case when the length of the deployed part of the tether remains invariable:

$$l_0 = \text{const}, \quad m_0 = \text{const}, \quad m_1 = \text{const}.$$

We also introduce some assumptions. Let the length of the tether considerably exceed the distance from the spacecraft's centre of mass to a point of introducing tether outlet:

$$\frac{\Delta}{l} \ll 1. \quad [2.83]$$

The given statement is fair for an overwhelming majority of the projects with space tethers, because the physical

phenomena incidental in cases of a large number of mechanical systems lie in their basis. For example, in the YES2 experiment (Williams et al., 2009), the tether had a length of about 30 km, and the size of the spacecraft was some metres. Thanks to [2.83], it is possible to consider that the centre of masses of all the system lies on a line  $PD_2$  (see Figure 2.6).

Let us disregard also the tether mass. In this case the mass of the STS is defined by a relation:

$$m = m_0 + m_2, \quad [2.84]$$

where  $m_0, m_2 = \text{const}$ .

For definition of the kinetic energy of the spacecraft [2.59] at first we find projections of point  $D_0$  on the axes of the translatory moving coordinate system  $O_1x_1y_1$ . According to [2.63] and [2.69] we have:

$$\begin{aligned} x_0 &= \bar{m}_2(l \cos(\varphi + \theta) + \Delta \cos(\alpha + \theta)), \\ y_0 &= \bar{m}_2(l \sin(\varphi + \theta) + \Delta \sin(\alpha + \theta)), \end{aligned} \quad [2.85]$$

where  $\bar{m}_2 = m_2/m$ .

It is obvious that the velocity of point  $D_0$  in  $O_1x_1y_1$  is:

$$V_{0r} = \left( \dot{x}_0^2 + \dot{y}_0^2 \right)^{\frac{1}{2}}, \quad [2.86]$$

where derivatives of the coordinates in [2.85] on time have the form:

$$\begin{aligned} \dot{x}_0 &= \bar{m}_2(l \cos(\varphi + \theta) - l\omega_1 \sin(\varphi + \theta) - \Delta\omega_0 \sin(\alpha + \theta)), \\ \dot{y}_0 &= \bar{m}_2(l \sin(\varphi + \theta) + l\omega_1 \cos(\varphi + \theta) + \Delta\omega_0 \cos(\alpha + \theta)), \end{aligned}$$

Substituting these expressions into [2.86], we write the kinetic energy of the spacecraft [2.59] as:

$$\begin{aligned} T_0 &= \frac{m_0 \bar{m}_2^2}{2} \left[ \dot{l}^2 + l^2 \omega_1^2 + 2\Delta l \omega_0 \sin(\varphi - \alpha) \right. \\ &\quad \left. + 2\Delta l \omega_0 \omega_1 \cos(\varphi - \alpha) \right] + \frac{I_{z0}}{2} \omega_0^2, \end{aligned} \quad [2.87]$$

where  $I_{z0} = I_z + m_0 \bar{m}^2 \Delta^2$ .

Similarly, using [2.69] we find coordinates of  $D_2$  in  $O_1x_1y_1$ :

$$\begin{aligned} x_2 &= -\bar{m}_0(l \cos(\varphi + \theta) + \Delta \cos(\alpha + \theta)), \\ y_2 &= -\bar{m}_0(l \sin(\varphi + \theta) + \Delta \sin(\alpha + \theta)). \end{aligned} \quad [2.88]$$

Using an assumption that the centre of mass lies on the line  $PD_2$ , we rewrite [2.88] as:

$$x_2 = -\bar{m}_0 l \cos(\varphi + \theta), \quad y_2 = -\bar{m}_0 l \sin(\varphi + \theta). \quad [2.89]$$

Then,

$$\begin{aligned} \dot{x}_2 &= \bar{m}_0(l\omega_1 \sin(\varphi + \theta) - \dot{l} \cos(\varphi + \theta)), \\ \dot{y}_2 &= -\bar{m}_0(\dot{l} \sin(\varphi + \theta) + l\omega_1 \cos(\varphi + \theta)) \end{aligned}$$

and the kinetic energy of the relative motion of the tethered payload  $D_2$  [2.61] becomes:

$$T_2 = \frac{m_2 \bar{m}_0^2}{2} [l^2 \omega_1^2 + \dot{l}^2]. \quad [2.90]$$

Finally, by means of the expressions [2.57], [2.58], [2.87] and [2.90] we obtain the kinetic energy of the STS:

$$\begin{aligned} T_{tot} &= \frac{m}{2}(\dot{r}^2 + r^2 \dot{\theta}^2) + \frac{m_*}{2} \dot{l}^2 + \frac{I_{z0}}{2} \omega_0^2 + \frac{I_{z2}}{2} \omega_1^2 \\ &\quad + \Delta m_0 \bar{m}_0^2 \omega_0 [\dot{l} \sin(\varphi - \alpha) + l \omega_1 \cos(\varphi - \alpha)], \end{aligned} \quad [2.91]$$

where  $m_* = m_0 m_2 m^{-1}$ ; and  $I_{z2} = m_* l^2$ .

According to [2.80], the potential energy at  $m_1 = 0$  takes the form:

$$W = -\mu \left( \frac{m_0}{r_0} + \frac{m_2}{r_2} \right) + \frac{3\mu}{2r_0^3} (I_x - I_y) \cos^2 \alpha + \frac{c}{2} (l - l_0)^2. \quad [2.92]$$

Using  $\Delta = 0$  and by means of [2.66], [2.68], [2.85], [2.89] we define the coordinates of vectors  $\mathbf{r}_0$  and  $\mathbf{r}_2$ :

$$\begin{aligned} \mathbf{r}_0 &= [r \cos \theta + \bar{m}_2 l \cos(\alpha + \theta), r \sin \theta + \bar{m}_2 l \sin(\alpha + \theta)]^T, \\ \mathbf{r}_2 &= [r \cos \theta - \bar{m}_0 l \cos(\varphi + \theta), r \sin \theta - \bar{m}_0 l \sin(\varphi + \theta)]^T, \end{aligned}$$

whence after a series of simple transformations we receive:

$$\begin{aligned} r_0 &= r \sqrt{1 + 2\bar{m}_2 \frac{l}{r} \cos \varphi + \bar{m}_2^2 \frac{l^2}{r^2}}, \\ r_2 &= r \sqrt{1 - 2\bar{m}_2 \frac{l}{r} \cos \varphi + \bar{m}_0^2 \frac{l^2}{r^2}}. \end{aligned} \quad [2.93]$$

Owing to the assumptions made, the ratio  $l/r$  is small. We substitute [2.64] into the first summand in [2.63] and then expand the result into the Maclaurin series in  $l/r$ . Disregarding the members of the third order of smallness, we obtain:

$$\begin{aligned} \frac{m_0}{r_0} + \frac{m_2}{r_2} &= \frac{m}{r} - \frac{m_2 m_0 l^2}{2mr^3} (1 - 3\cos^2 \varphi) \\ &+ O\left(\frac{l^3}{r^3}\right) \approx \frac{m}{r} - \frac{I_{z2}}{2r^3} (1 - 3\cos^2 \varphi). \end{aligned} \quad [2.94]$$

With a similar expansion for  $r_0^{-3}$  we make:

$$\frac{1}{r_0^3} = \frac{1}{r^3} - \frac{3\bar{m}_2 l \cos \varphi}{r^4} + O\left(\frac{l^5}{r^5}\right) \approx \frac{1}{r^3}. \quad [2.95]$$

Substituting [2.94] and [2.95] into [2.92], we obtain:

$$W = -\frac{\mu m}{r} + \frac{\mu I_*}{2r^3} (1 - 3\cos^2 \varphi) + \frac{3\mu}{2r^3} (I_x - I_y) \cos^2 \alpha + \frac{c}{2} (l - l_0)^2. \quad [2.96]$$

Taking into account [2.91] and [2.66], the Lagrangian can be written as:

$$\begin{aligned} L &= \frac{m}{2} (\dot{r}^2 + r^2 \dot{\theta}^2) + \frac{m_*}{2} \dot{l}^2 + \frac{I_{z0}}{2} \omega_0^2 + \frac{I_{z2}}{2} \omega_1^2 \\ &+ \Delta m_* \omega_0 \left[ l \sin(\varphi - \alpha) + l \omega_1 \cos(\varphi - \alpha) \right] \\ &+ \frac{\mu m}{r} - \frac{\mu I_{z2}}{2r^3} (1 - 3\cos^2 \varphi) - \frac{3\mu}{2r^3} (I_x - I_y) \\ &\times \cos^2 \alpha - \frac{c}{2} (l - l_0)^2. \end{aligned} \quad [2.97]$$

Substituting [2.97] into [2.82], we obtain differential equations:

$$\begin{aligned} I_{z0}\ddot{\alpha} + \left[ I_{z0} + \Delta m_0 \bar{m}_2^2 l \cos(\varphi - \alpha) \right] \ddot{\theta} + \Delta m_0 \bar{m}_2^2 l \cos(\varphi - \alpha) \ddot{\varphi} \\ + \Delta m_0 \bar{m}_2^2 \sin(\varphi - \alpha) \ddot{l} + 2 \Delta m_0 \bar{m}_2^2 l (\dot{\varphi} + \dot{\theta}) \cos(\varphi - \alpha) \\ - \Delta m_0 \bar{m}_2^2 l (\dot{\varphi} + \dot{\theta})^2 \sin(\varphi - \alpha) - \frac{3\mu}{r^3} (I_x - I_y) \sin \alpha \cos \alpha = Q_\alpha, \end{aligned} \quad [2.98]$$

$$\begin{aligned} \Delta m_0 \bar{m}_2^2 l \cos(\varphi - \alpha) \ddot{\alpha} + \left[ I_{z2} + \Delta m_0 \bar{m}_2^2 l \cos(\varphi - \alpha) \right] \ddot{\theta} + 2 m_* l \dot{l} (\dot{\varphi} + \dot{\theta}) \\ + I_{z2} \ddot{\varphi} + \Delta m_0 \bar{m}_2^2 l (\dot{\alpha} + \dot{\theta})^2 \sin(\varphi - \alpha) + \frac{3\mu I_{z2}}{r^3} \sin \varphi \cos \varphi = Q_\varphi, \end{aligned} \quad [2.99]$$

$$\begin{aligned} \Delta \bar{m}_2 \sin(\varphi - \alpha) (\ddot{\alpha} + \ddot{\theta}) + \ddot{l} + \frac{c}{m_*} (l - l_0) + \frac{\mu l}{r^3} (1 - 3 \cos^2 \varphi) \\ - l (\dot{\varphi} + \dot{\theta})^2 - \Delta \bar{m}_2 (\dot{\alpha} + \dot{\theta})^2 \cos(\varphi - \alpha) = Q_l, \end{aligned} \quad [2.100]$$

$$\ddot{r} - r \dot{\theta}^2 + \frac{\mu}{r^2} - \frac{3\mu I_{z2}}{2mr^4} (1 - 3 \cos^2 \varphi) - \frac{9\mu}{2mr^4} (I_x - I_y) \cos^2 \alpha = Q_r. \quad [2.101]$$

We use a method of transition from time variable to a new independent variable – an angle of true anomaly  $\theta$ . This way is widely applied to solving the problem of the spacecraft's motion research in an orbit (Beletsky and Levin, 1993; Curtis, 2005). In this result, the differential equation system's order is decreased. We will suppose that the motion of the centre of mass of the STS and the motion concerning the centre of mass do not influence each other, and the centre of mass of the STS moves in an elliptic trajectory. The assumptions made allow the equation for an angular velocity of true anomaly to be written as:

$$\dot{\theta} = nk^2, \quad [2.102]$$

where  $n = \sqrt{\mu p^{-3}}$ ;  $p = rk$  – focal parameter of orbit,  $k = 1 + e \cos \theta$ ; and  $e$  – eccentricity of orbit.

Parameters  $n$ ,  $p$  and  $e$  are constants for each concrete orbit and can be found from the initial conditions (Curtis, 2005).

$$p = \frac{(\dot{\theta}_0 r_0)^2}{\mu}, \quad e = \sqrt{1 + \frac{(\dot{r}_0^2 + r_0^2 \dot{\theta}_0^2)r_0^2 \dot{\theta}_0^2}{\mu^2}} \quad [2.103]$$

where 0 – an initial moment of time.

Equation [2.102] establishes the connection between the old and new independent variables. For the arbitrary function  $f(t)$ , the first and second derivatives owing to [2.102] can be calculated as:

$$\begin{aligned} \dot{f} &= nk^2 f', & \ddot{f} &= n^2 k^3 (kf'' - 2ef' \sin \theta), \\ \text{where } (\ )' &= \frac{d(\ )}{d\theta} \text{ and } (\ )'' = \frac{d^2(\ )}{d\theta^2}. \end{aligned} \quad [2.104]$$

Let us notice also that the differentiation on the time of the equation [2.103] gives:

$$\ddot{\theta} = -2n^2 k^3 e \sin \theta. \quad [2.105]$$

Let us rewrite the equations of motion of the STS [2.98]–[2.100] taking into account formulas [2.102]–[2.105] as follows:

$$\begin{aligned} I_{z0} (k\alpha'' - 2e\alpha' \sin \theta) + \Delta m_0 \bar{m}_2^2 l \cos(\varphi - \alpha) (k\varphi'' - 2e\varphi' \sin \theta) \\ + \Delta m_0 \bar{m}_2^2 \sin(\varphi - \alpha) (kl'' - 2el' \sin \theta) + 2k \Delta m_0 \bar{m}_2^2 l' \\ \times (1 + \varphi') \cos(\varphi - \alpha) \\ - k \Delta m_0 \bar{m}_2^2 l (1 + \varphi')^2 \sin(\varphi - \alpha) - 2e \\ \times [I_{z0} + \Delta m_0 \bar{m}_2^2 l \cos(\varphi - \alpha)] \sin \theta \\ - 3(I_x - I_y) \sin \alpha \cos \alpha = \frac{Q_\alpha}{n^2 k^3}, \end{aligned} \quad [2.106]$$

$$\begin{aligned} \Delta m_0 \bar{m}_2^2 l \cos(\varphi - \alpha) (k\alpha'' - 2e\alpha' \sin \theta) + I_{z2} (k\varphi'' - 2e\varphi' \sin \theta) \\ + 2km_* ll' (1 + \varphi') + \Delta km_0 \bar{m}_2^2 l (1 + \alpha')^2 \sin(\varphi - \alpha) \\ - 2e [I_{z2} + \Delta m_0 \bar{m}_2^2 l \cos(\varphi - \alpha)] \sin \theta + 3I_{z2} \\ \times \sin \varphi \cos \varphi = \frac{Q_\varphi}{n^2 k^3}, \end{aligned} \quad [2.107]$$

$$\begin{aligned}
 & \Delta\bar{m}_2 \sin(\varphi - \alpha) [k\alpha'' - 2e(1 + \alpha') \sin \theta] + kl'' - 2el' \sin \theta \\
 & + \frac{c}{n^2 k^3 m_*} (l - l_0) + l(1 - 3 \cos^2 \varphi) - kl(1 + \varphi')^2 \\
 & - \Delta\bar{m}_2 k (1 + \alpha')^2 \cos(\varphi - \alpha) = \frac{Q_l}{n^2 k^3}. \tag{2.108}
 \end{aligned}$$

The differential equation systems [2.106]–[2.108] describe the attitude motion of the STS when its centre of mass is on an elliptic orbit. These equations are essentially easier than the systems [2.98]–[2.102]. As a result of their integration, we obtain the functions  $\alpha(\theta)$ ,  $\varphi(\theta)$ ,  $l(\theta)$  and the derivatives  $\alpha'(\theta)$ ,  $\varphi'(\theta)$ ,  $l'(\theta)$ . The distance from the centre of mass of the STS to the Earth's centre of mass for the elliptic orbit is defined by the relation:

$$r(\theta) = \frac{p}{1 + e \cos \theta}.$$

If it is necessary to receive dependence of the generalized coordinates from the time, it is necessary to integrate [2.102] and to substitute the outcome into that found from the functions in [2.106]–[2.108].

For a circular orbit when  $e = 0$  and  $k = 1$ , we have  $r = \text{const}$  and  $\theta(t) = nt + \theta_0$ . In this case equations [2.106]–[2.108] take the form:

$$\begin{aligned}
 & I_{z0} \alpha'' + \Delta m_0 \bar{m}_2^2 l \cos(\varphi - \alpha) \varphi'' + \Delta m_0 \bar{m}_2^2 \sin(\varphi - \alpha) l'' \\
 & + \Delta m_0 \bar{m}_2^2 l' (1 + \varphi') \cos(\varphi - \alpha) - \Delta m_0 \bar{m}_2^2 l (1 + \varphi')^2 \sin(\varphi - \alpha) \\
 & - 3(I_x - I_y) \sin \alpha \cos \alpha = \frac{Q_\alpha}{n^2}, \tag{2.109}
 \end{aligned}$$

$$\begin{aligned}
 & \Delta m_0 \bar{m}_2^2 l \cos(\varphi - \alpha) \alpha'' + I_{z2} \varphi'' + 2m_* ll' (1 + \varphi') \\
 & + \Delta m_0 \bar{m}_2^2 l (1 + \alpha')^2 \sin(\varphi - \alpha) + 3I_{z2} \sin \varphi \cos \varphi = \frac{Q_\varphi}{n^2}, \tag{2.110}
 \end{aligned}$$

$$\Delta \bar{m}_2 \sin(\varphi - \alpha) \alpha'' + l'' + \frac{c}{n_*^2 m_*} (l - l_0) + l(1 - 3 \cos^2 \varphi) - l(1 + \varphi')^2 - \Delta \bar{m}_2 (1 + \alpha')^2 \cos(\varphi - \alpha) = \frac{Q_l}{n_*^2}. \quad [2.111]$$

### 2.4.3 Estimation of the influence of a tether's elasticity on the motion of a STS

Let us consider that the angular position of the tether and the generalised force  $Q_\phi$  do not influence the angular position of the spacecraft ( $\Delta = 0$ ,  $Q_\phi = 0$ ). Then equations [2.107] and [2.108] become:

$$\varphi'' + 2 \frac{l'}{l} (1 + \varphi') + \frac{3}{k} \sin \varphi \cos \varphi = 2 \frac{e}{k} (1 + \varphi') \sin \theta, \quad [2.112]$$

$$l'' + \frac{c}{m_* n_*^2 k^4} (l - l_0) + \frac{l}{k} (1 - 3 \cos^2 \varphi) - l(1 + \varphi')^2 = 2 \frac{e}{k} l' \sin \theta. \quad [2.113]$$

For a circular orbit  $e = 0$ , equations [2.112] and [2.113] can be written as:

$$\varphi'' + 3 \sin \varphi \cos \varphi = -2 \frac{l'}{l} (1 + \varphi'), \quad [2.114]$$

$$l'' + \frac{c}{m_* n_*^2} (l - l_0) + l(1 - 3 \cos^2 \varphi) - l(1 + \varphi')^2 = 0. \quad [2.115]$$

If the centre of mass moves in an elliptic orbit with a small eccentricity, the tether is deployed along the local vertical and its unit elongation is small, then taking into account [2.83] we estimate that the following magnitudes have the order of smallness  $\varepsilon$ :

$$\delta = \frac{\Delta}{l}, \frac{l - l_0}{l_0} \varphi, \varphi', \varphi'', e. \quad [2.116]$$

At the performance of conditions in [2.116], and at  $Q_\phi = 0$ , we rewrite equations [2.106] and [2.108] disregarding members of an order  $O(\varepsilon^2)$ :

$$\alpha'' - 3 \frac{I_x - I_y}{k I_{z0}} \sin \alpha \cos \alpha = \varepsilon F_a, \quad [2.117]$$

$$\bar{l}'' + \frac{c}{n^2 k^4 m_*} (\bar{l} - 1) - 3 = \varepsilon F_L, \quad [2.118]$$

where

$$\varepsilon F_a = -\delta J \left[ (1 - \bar{l}'') \sin \alpha + 2 \bar{l}' \cos \alpha \right] + 2e(1 + \alpha') \sin \theta;$$

$$\varepsilon F_L = \delta \left[ \sin \alpha \alpha'' + (1 + \alpha')^2 \cos \alpha \right] - 2e(\cos \theta - \bar{l}' \sin \theta); \text{ and}$$

$$\bar{l} = \frac{l}{l_0}, \quad J = \frac{m_* l_0^2}{I_{z0}}.$$

Let us find the approximate law of the tether's length. For this purpose we consider the equation obtained from [2.118] as a term of neglect of the order of smallness  $\varepsilon$ :

$$\bar{l}'' + \Omega^2 \bar{l} = 3 + \Omega^2, \quad [2.119]$$

$$\text{where } \Omega = \frac{1}{n} \sqrt{\frac{c}{m_*}}.$$

As the value  $\varepsilon = 0$  corresponds to the motion in a circular orbit, for which  $k = 1$ , the equilibrium position of the tether is defined by the formula:

$$\bar{l}_1 = \frac{3 + \Omega^2}{\Omega^2}.$$

Under initial conditions  $t_0 = 0 : \bar{l} = \bar{l}_1, \bar{l}' = \bar{l}'_0$ , the solution of [2.119] takes the form:

$$\bar{l} = \bar{l}_1 + \frac{\bar{l}'_0}{\Omega} \sin \Omega \theta. \quad [2.120]$$

We will consider the case when the tether is always in the stretched position ( $\bar{l} > 1$ ), then the initial velocity of the payload should not exceed:

$$\bar{l}'_0 < \frac{3}{\Omega}.$$

Let us estimate the influence of the tether's elasticity on the motion of the STS (Aslanov, 2010). We find the derivatives [2.120] and substitute them into the right side of equation [2.117]:

$$\begin{aligned} \alpha'' - 3 \frac{I_x - I_y}{I_{z0}} \sin \alpha \cos \alpha = \\ -\delta J \left[ \left( 1 + \bar{l}'_0 \Omega \sin \Omega \theta \right) \sin \alpha + 2 \bar{l}'_0 \cos \Omega \theta \cos \alpha \right] \\ + e \left[ 2 \left( 1 + \alpha' \right) \sin \theta - 3 \frac{I_x - I_y}{I_{z0}} \sin \alpha \cos \alpha \cos \theta \right]. \end{aligned} \quad [2.121]$$

Equation [2.121] allows for the estimation of the influence of a tether's elasticity and an orbit ellipticity on the motion of the spacecraft concerning its centre of mass. The equation of unperturbed motion (at  $\varepsilon = 0$ ) corresponds to the disturbed equation [2.121]:

$$\alpha'' + \lambda^2 \sin \alpha \cos \alpha = 0, \quad [2.122]$$

where  $\lambda^2 = -3 \frac{I_x - I_y}{I_{z0}} = 3 \frac{I_x - I_y}{I_z + m_0 \bar{m}_2 \Delta^2}$  – natural frequency of tether oscillations.

Equation [2.122] is well studied, and it has a known analytical solution.

We will make some numerical calculations to show how the orbit's eccentricity and the tether's elasticity influence the oscillations of the spacecraft with a tethered payload. Let us take parameter  $p = 6700$  km, spacecraft's parameters  $I_x = 1000$  kg·m<sup>2</sup>,  $I_y = I_{z0} = 10^5$  kg·m<sup>2</sup>,  $m_0 = 6000$  kg,  $m_2 = 30$  kg,

$\Delta = 3$  m and the tether parameters  $l_0 = 20$  km,  $d_T = 0.5$  mm, where  $d_T$  – diameter of the tether. The natural frequency of the unperturbed system [2.122] for given parameters is equal to  $\lambda = 0.222$ . The hyperbolic points of the system [2.93]  $\alpha_* = \frac{\pi}{2} \pm N\pi$  ( $N = 0, 1, 2, \dots$ ) ( $N = 0, 1, 2, \dots$ ) correspond to the unstable position of equilibrium. We choose the following initial conditions:

$$\alpha = 1.57, \alpha' = 0, \varphi = 0, \varphi' = 0, l = l_0, l' = 0.9 \frac{3}{\Omega} l_0.$$

In Figure 2.8, the phase trajectories of the system are shown at various values of eccentricity as  $E = 15$  GPa. With an increase of the eccentricity, an amplitude of the spacecraft oscillations increases too. At great values of eccentricity the spacecraft passes from an oscillation into a rotational motion (see Figure 2.8c). In a case shown in Figure 2.11c, some passages between the rotational and oscillating motions' modes are observed. These passages can be considered as manifestations of the chaotic behaviour of the mechanical system in a separatrix neighbourhood.

In Figure 2.9 the phase trajectories of the system are shown at various values of modulus of elasticity for  $e = 0.1$ . At rather small values of  $E$ , both oscillation and rotation are observed (see Figure 2.9(a)). At great values of  $E$ , only one oscillation (see Figure 2.9(b) and Figure 2.9(c)) take place.

## 2.5 Model of a STS consisting of two rigid bodies connected by a heavy elastic multipoint tether

At the base of a multipoint model of a tether lies the simple idea – the continuous tether is substituted by a set of the

**Figure 2.8** Phase portraits of [2.121] at various values of eccentricity

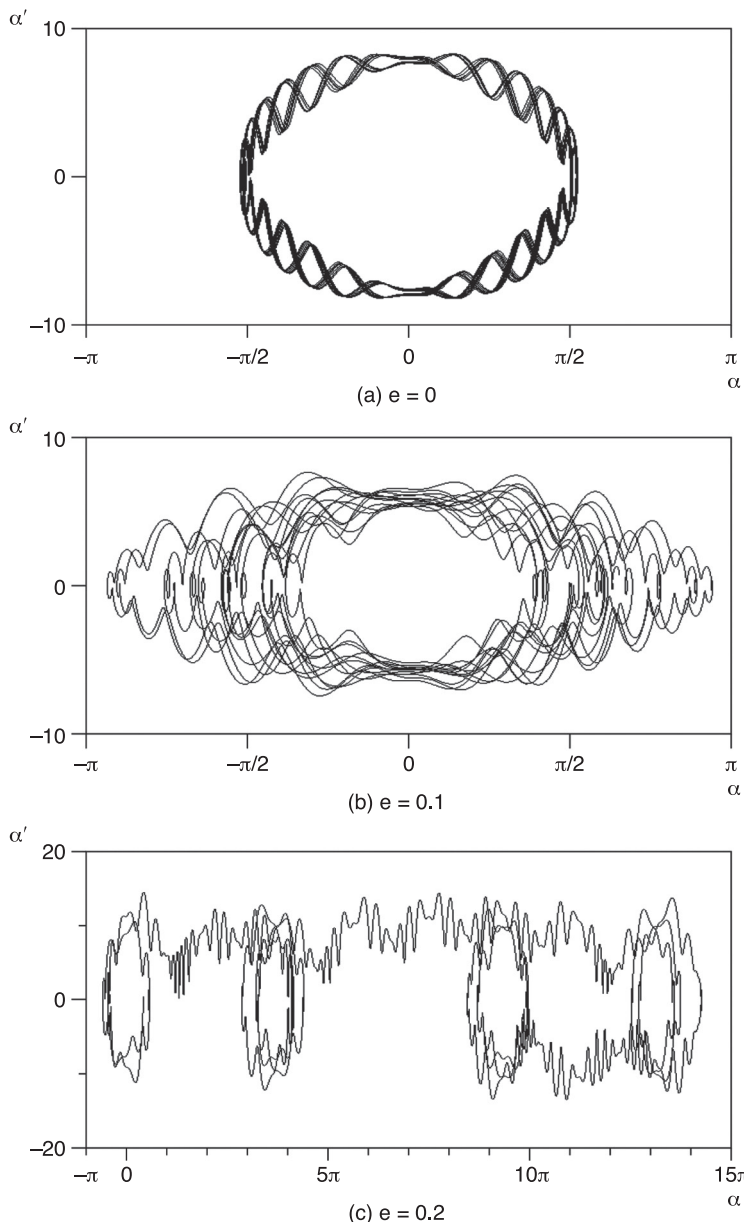
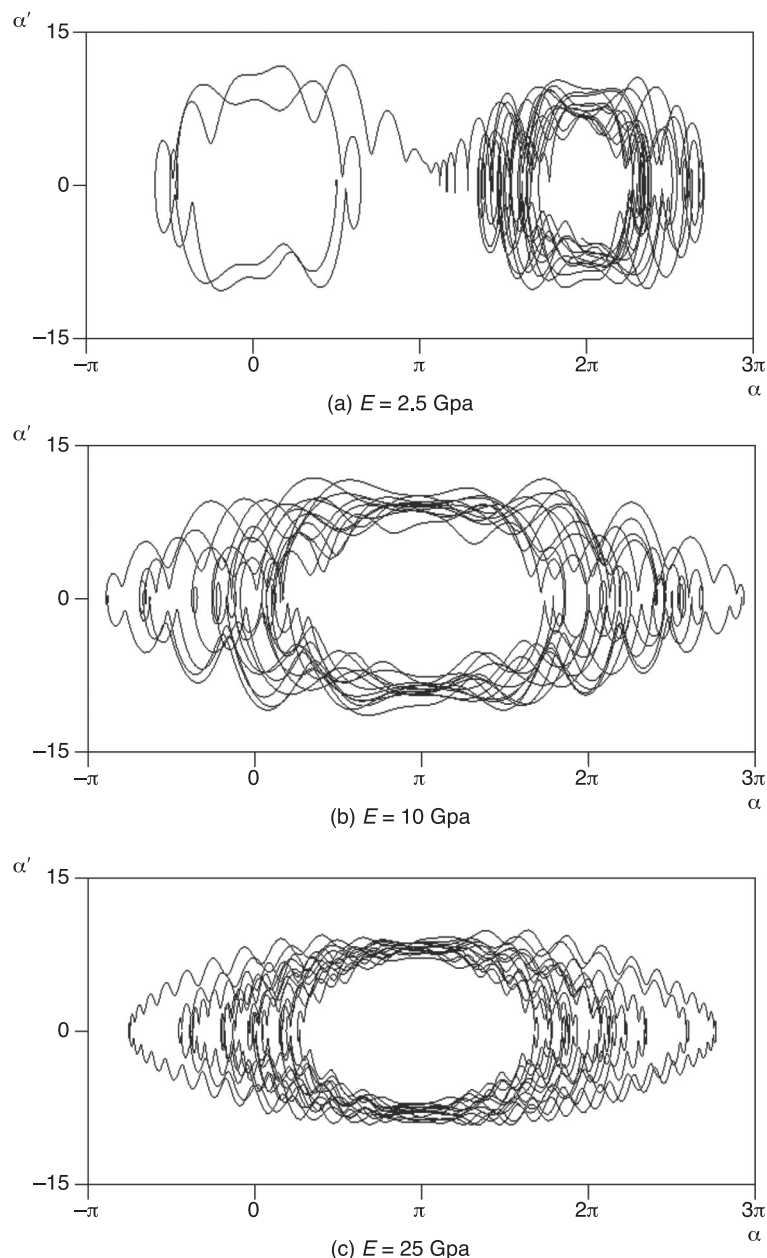


**Figure 2.9** Phase portraits of [2.121] at various values of tether elastic modulus



particles connected among themselves by massless springs. Such an approach ensures a result of an acceptable accuracy at a fairly small computing expenditure.

### ***2.5.1 Substantiation of the introduction of a tether's multipoint model***

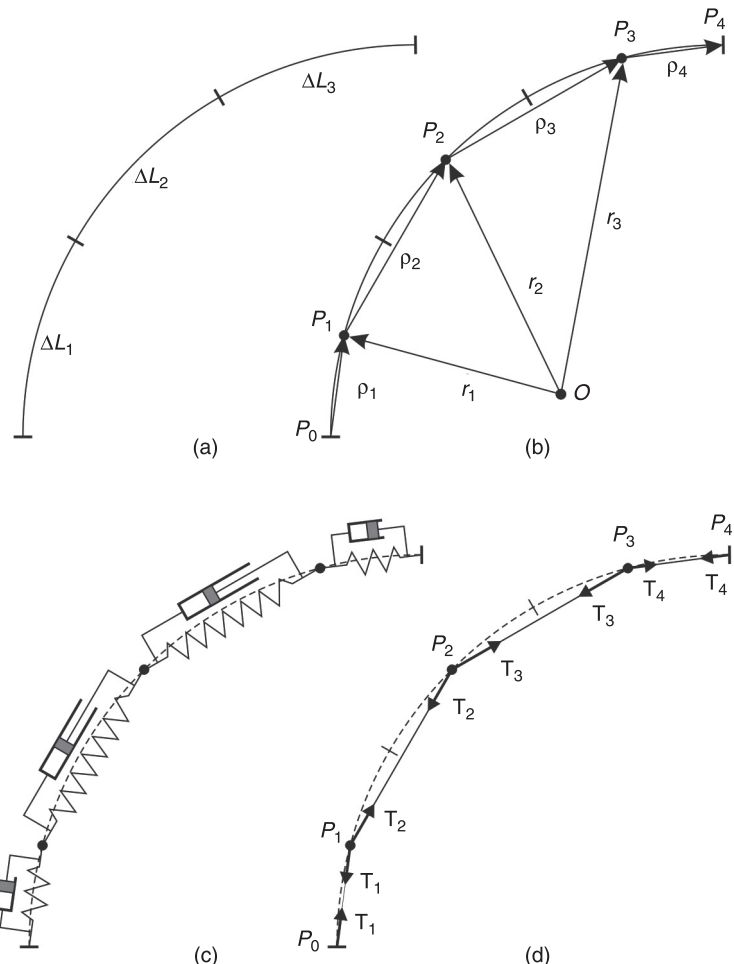
Two different mathematical models of tether systems were considered above. In one of them, the tether was represented as a bar; in another, as a heavy flexible thread. Both models are used for the study of the dynamics of a STS; however, they possess enough essential disadvantages.

In the model with a bar, the influence of the tether on the end bodies' motion is limited to the single function of the transmission of the stress along a line connecting the bodies. Such an approach considerably simplifies the numerical modelling and enables the retrieving of some analytical results to carry out the qualitative analysis of the tether system's motion. However, replacement of the tether by the bar leads to the fact that many of the physical phenomena of real tethers cannot be reflected by means of this model. For example, it is impossible to show the tether curving; the model is inapplicable for a case of a weak tension of the tether. The neglect of the mass-inertial and elastic-damping properties in the model of a massless bar does not allow the influence of the tether to be considered, which has distinct elastic properties on the motion of the tethered bodies. Certainly, it is not so important for problems where a tether mass is of some orders less than the mass of the connected bodies, but it is impossible to forget that there is a whole class of problems implying the use of comparable bodies on a mass with a tether. The simplified model does not allow interaction of a tether with the atmosphere to be considered.

As will be shown, this factor makes a strong impact on the STS at low altitudes.

Specified singularities lead to the necessity to develop more complicated models. More correctly, the physics of the process is reflected by a model in which the tether is presented as a heavy flexible thread. This model allows us to obtain the most exact results, but considerable computing difficulties accompany its use. The compromise model, in which the heavy elastic tether is substituted by a chain of the particles connected by segments of an elastic massless bar, can become a way out from the current situation. The distributed mechanical system with an infinite number of degrees of freedom is substituted by a discrete system in which the number of degrees of freedom is limited. Such a model has an intuitively clear mechanical sense, in that it can be programmed easily, and it requires much less computing resources. In the limiting expressions it is reduced to the model of an elastic massless bar, when the number of particles of a tether is equal to zero, and to the model of a heavy flexible thread when this number aspires to infinity. The results obtained by use of this model, even in case of the weak tension of a tether, could well agree with calculations on a nonlinear model with the distributed parameters (Alpatov et al., 1997).

Let us divide the tether into  $N$  parts with finite length  $\Delta L_i$  ( $i = \overline{1, N}$ ) (see Figure 2.10a). Each part is substituted by particle  $P_i$  with the mass equal to the mass of the tether's part  $m_i$ . The radius vectors of these particles we designate as  $r_i$  (see Figure 2.10b). The force interaction of two adjacent parts  $\Delta L_i$  and  $\Delta L_{i+1}$  on their boundary is transformed to viscoelastic interaction of the particles  $P_i$  and  $P_{i+1}$ . From the point of view of the mechanics between point masses, there is a pair of spring-dampers, whose parameters (stiffness and viscosity) are equal to the corresponding part of the tether

**Figure 2.10** A multipoint tether

(see Figure 2.10c). To each point  $P_i$ , the tension forces  $T_i, T_{i+1}$  equal to the forces in tether's parts  $P_{i-1}P_i$  and  $P_iP_{i+1}$  will act. Points  $P_0$  and  $P_{N+1}$  correspond to the tether tips (see Figure 2.10d). A part of the tether  $P_{i-1}P_i$  we will term the  $i$ -th part.

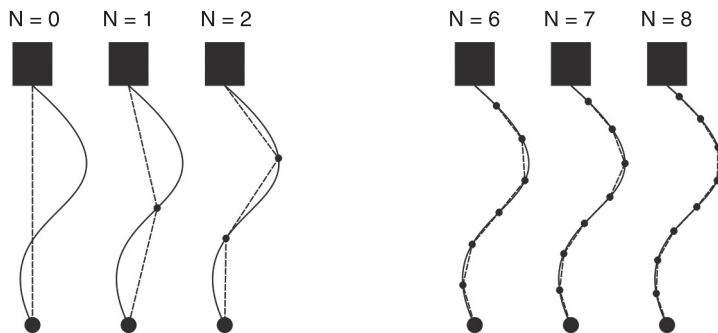
The tension of the  $i$ -th part of the tether  $T_i$  can be specified by means of the law (Beletsky and Levin, 1993):

$$T_i = \begin{cases} ES_i(\gamma_i - 1) + D_i \frac{\partial \gamma_i}{\partial t}, & \gamma_i > 1, \\ 0, & \gamma_i \leq 1, \end{cases} \quad [2.123]$$

where  $E$  – modulus of elasticity;  $\gamma_i = \rho_i/l_{0i}$  – elongation;  $\rho_i = |\mathbf{r}_i - \mathbf{r}_{i-1}|$  – length of the  $i$ -th tether part;  $l_{0i}$  – length of the unstrained  $i$ -th tether part;  $S_i$  – cross-section area of the  $i$ -th tether part;  $D_i = \sqrt{\frac{ES_i m_i}{l_{0i}}}\eta$  – factor of an interior friction for a case of longitudinal oscillations of the tether's part;  $\eta$  – loss factor (Lazan, 1968); and  $m_i$  – mass of the  $i$ -th tether part.

From the point of view of practical application of a multipoint model, the problem of a choice of the number of particles, by which the tether is modelled, and the length of the tether's parts is essential. According to the authors, there is no universal recipe and these parameters should be fitted for each specific problem proceeding with the required accuracy. The results of numerous numerical calculations for various STS have shown that by increasing the number of  $N$  (at large  $N$ ) the difference between the results, which were obtained by use of models with  $N-1$  particles, decreases. For example, for project YES2 where a 30 km tether was used, 20 particles were enabled to find the tethered payload location at the end of deployment with an accuracy of one metre (Aslanov et al., 2007). This result corresponds to an estimation obtained by Dignath and Schiehlen (2000). At small values of  $N$ , the difference between outcomes can grow with an increasing number of particles. It happens because at low values of  $N$ , the introduction of an additional point essentially changes the model geometry; and when the cable is modelled by a great number of points, the adding of a new point poorly changes the picture (see Figure 2.11).

**Figure 2.11** Effect of increasing the number of particles on the geometry of a tether in a multipoint model



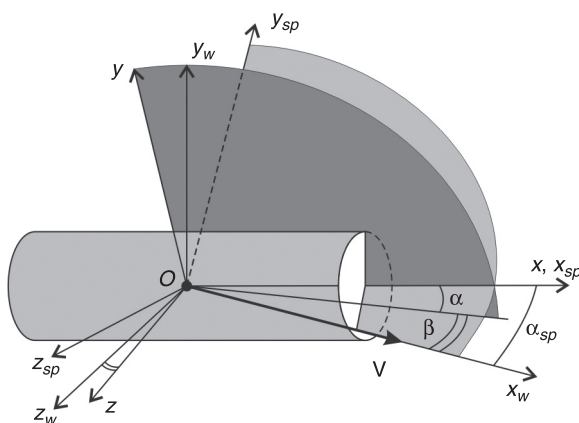
## 2.5.2 Interaction of a tether's part with the atmosphere

Some of the most essentially disturbing factors for a STS working at low altitudes are aerodynamic forces and moments. Calculations often consider the aerodynamic forces operating only on the end bodies, but neglect the influence of the atmosphere on the tether. This is not absolutely true. Though modern technologies enable us to make space tethers with a diameter of an order of the tenth part of a millimetre, owing to their long length the influence of aerodynamic forces on a tether as a whole can appear rather appreciable. Taking account of the atmosphere's influence complicates the fact that the density of the atmosphere depends on the height and, as a tether's length can reach hundreds of kilometres, the influence of the atmosphere on different parts of a tether can strongly differ.

When in motion in the atmosphere, any body feels the force action which can be reduced to the resultant vector and the resultant moment of the aerodynamic forces (Krasnov et al., 1968). These forces usually are defined by projections to the axes of the wind or body coordinate system. Let us

consider these coordinate systems in more detail. The beginning of the body coordinate system  $O$  coincides with the centre of masses of the body, axis  $Ox$  is directed along the longitudinal axis,  $Oy$  is perpendicular to  $Ox$  and lies in the body's plane of symmetry. Axis  $Oz$  supplements the system to the right-hand side. Axis  $Ox_w$  of a wind coordinate system is directed along a vector of the velocity of the centre of mass  $V$ , axis  $Oy_w$  lies in the body's plane of symmetry and is perpendicular to  $Ox_w$ ,  $Oz_w$  supplements the system to the right-hand side (see Figure 2.12). Mutual orientation of the axes of the body and the wind coordinate systems is defined by means of an angle of attack  $\alpha$  and a slip angle  $\beta$ . The angle of attack is an angle between the longitudinal axis of the body and a projection of the velocity vector to the plane of symmetry. The slip angle is an angle between the vector of velocity and this plane. Actually, these angles set a deflection of the longitudinal axis of the body from the direction of the centre of mass motion. For axisymmetric bodies, the coordinate system connected with a spatial angle of attack  $\alpha_{sp}$  is often used. The axis  $Ox_{sp}$  is directed along the body's

**Figure 2.12** Coordinate systems



axis of symmetry, the axis  $Oy_{sp}$  lies in the plane formed by  $Ox_{sp}$  and the velocity vector,  $Oz_{sp}$  supplements the system to the right-hand side. The spatial angle of attack is an angle between the body's axis of symmetry and vector of velocity of the centre of mass.

Projections of the resultant vector of the aerodynamic forces to the axes of the body coordinate system are named the longitudinal (axial)  $X$ , the normal  $Y$  and the cross-section  $Z$  forces, and the projections of the same vector to the axes of a wind coordinate system are drag  $X_w$ , the aerodynamic lift  $Y_w$  and the side force  $Z_w$ , and for the coordinate system connected with a spatial angle of attack the tangential force  $\tau$  and the normal force  $N$ . Projections of the resultant moment of the aerodynamic forces to the axes of the body and the wind coordinate systems have identical titles: rolling moment  $M_x$ ,  $M_{xw}$  and  $M_{xsp}$ , hunting moment  $M_y$ ,  $M_{yw}$  and  $M_{ysp}$ , and pitching moment  $M_z$ ,  $M_{zw}$  and  $M_{zsp}$ .

In aerodynamics, the dimensionless parameters characterising the forces and moments are used. They are termed as aerodynamic coefficients:

$$\begin{aligned} c_x &= \frac{X}{qS}, \quad c_y = \frac{Y}{qS}, \quad c_z = \frac{Z}{qS}, \quad c_{xa} = \frac{X_w}{qS}, \quad c_{ya} = \frac{Y_w}{qS}, \\ c_{za} &= \frac{Z_w}{qS}, \quad c_\tau = \frac{-\tau}{qS}, \quad c_n = \frac{N}{qS}, \end{aligned}$$

$$m_j = \frac{M_j}{qSl}, \quad (j = x, y, z, xa, ya, za, xsp, ysp, zsp),$$

where  $c_x, c_y, c_z$  – coefficients of longitudinal, normal and cross-section forces;  $c_{xw}, c_{yw}, c_{zw}$  – coefficients of drag, aerodynamic lift and side force;  $c_\tau, c_n$  – coefficients of tangential and normal forces;  $m_x, m_{xw}, m_{xsp}$  – coefficients of rolling moment;  $m_y, m_{yw}, m_{ysp}$  – coefficients of hunting moment;  $m_z, m_{zw}, m_{zsp}$  – coefficients of pitching moment;

$q = \rho_a V^2/2$  – dynamic pressure;  $\rho_a$  – atmosphere density;  $V$  – velocity of the centre of mass;  $S$  – frontal area; and  $l$  – characteristic dimension.

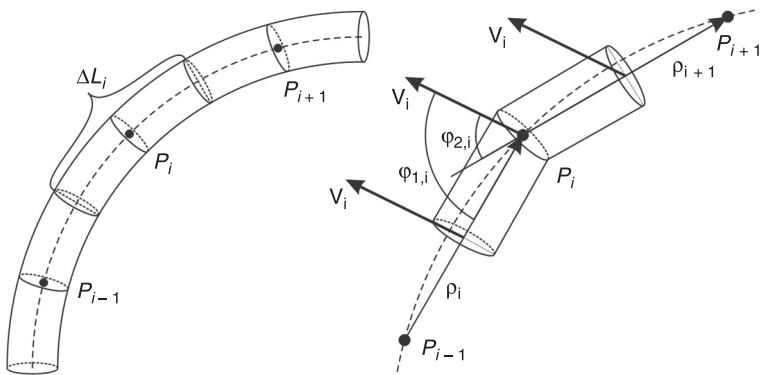
There are various models of atmosphere density. For example, for exact calculations the tables of the standard atmosphere are used. In this, the influence of a geographical position, environmental conditions, seasonal and daily modifications, solar activity and other parameters are considered. In a case when such high accuracy is not required, more simple models of the atmosphere are used. One such model is the isothermal atmosphere for which the density is calculated by means of the exponential functions of height:

$$\rho_a = \rho_{a0} \exp\left(-\frac{H}{H_*}\right),$$

where  $\rho_{a0}$  – an atmosphere density at sea level,  $H_* = 7.11$  km.

Aerodynamic coefficients do not depend on the size of a body. It enables us to obtain them as a result of experiments in a wind tunnel, and then to use them for the analysis of the motion of real spacecrafts. The greatest influence on the aerodynamic coefficient values is provided by body orientation in relation to an incident flow. Therefore, aerodynamic coefficients are usually set in the form of functions from an angle of attack and the slip angle for the body of the arbitrary form and functions from a spatial angle of attack  $\alpha_{sp}$  for the axisymmetric body.

Let us consider a tether part  $\Delta L_i$  and define the aerodynamic forces acting on it (see Figure 2.13). We present this part in the form of a bend in the middle of a cylindrical bar. We will suppose that diameter of the bar is equal to the diameter of the tether. Such a presentation of the tether's part is not quite correct because in general it is described by a quartic curve. However, in case of the tense tether and the great number of

**Figure 2.13** Velocities of a part of a tether

particles by which it is modelled, the gain in accuracy from use of a nonlinear representation is insignificant.

In calculating aerodynamic forces, for simplicity, we will consider that half of parts  $\rho_i$  and  $\rho_{i+1}$  adjoining to point  $P_i$  moves translational with the velocity of this point (see Figure 2.13). We will consider also that the cable is divided into rather small parts so that the atmosphere density in each point of the tether's part is constant.

At a hypersonic flow in the rarefied atmosphere good results are given by use of this method of calculation of the aerodynamic coefficients of a body, based on use of Newton's impact theory. The calculation of aerodynamic coefficients is carried out by integration of the dynamic pressure on the unshaded exterior surface of a body. It is considered that the impact of particles of gas with a body has an inelastic character, and there is a normal damping to the body's surface component of the momentum of flow.

For the cylinder, by means of Newton's method (Krasnov et al., 1968), it is possible to obtain these dependences:

$$c_\tau = 0, c_n(\alpha_{sp}) = \frac{2}{3} k \sin^2 \alpha_{sp}, \quad [2.124]$$

where factor  $k$  depends on the velocity and atmosphere properties:

$$k = \frac{2}{\chi M_\infty^2} \left[ \left( \frac{\chi+1}{2} M_\infty^2 \right)^{\frac{\chi}{\chi-1}} \cdot \left( \frac{\chi+1}{2\chi M_\infty^2 - \chi + 1} \right)^{\frac{1}{\chi-1}} - 1 \right],$$

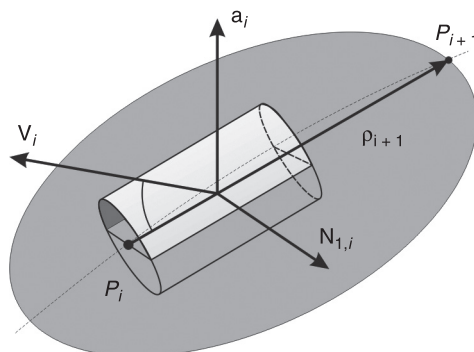
where  $M_\infty$  – Mach number of an unperturbed flow; and  $\chi$  – adiabatic index of the atmosphere.

Let us view one of the cylinders of the tether's part  $\Delta L_i$  (see Figure 2.13). At motion in the atmosphere, the aerodynamic force, having only the normal component  $\mathbf{N}_{1,i}$  in  $Oxyz$ , acts on it. Vector  $\mathbf{N}_{1,i}$  is perpendicular to vector  $\rho_{i+1}$  and lies in a plane formed by vectors  $\mathbf{V}_i$  and  $\rho_{i+1}$  (see Figure 2.14). The first index of the vector  $\mathbf{N}_{j,i}$  means the number of cylinders of the tether's part ( $j = 1$  or  $2$ ), and second, the part's number. The module of  $\mathbf{N}_{1,i}$  is:

$$N_{1,i} = q_i S_{1,i} c_n,$$

where –  $q_i$  dynamic pressure of a point  $P_i$ ;  $S_{j,i}$  – the area of dilatational section of the  $j$ -th cylinder.

**Figure 2.14** The relative position of vectors



Substituting [2.124] here we obtain:

$$N_{1,i} = \frac{\rho_{ai} V_i^2}{2} c_n S_{1,i} = \frac{\rho_{ai} V_i^2 k d_T \rho_{i+1}}{6} \sin^2 \varphi_{1,i},$$

where  $\rho_{ai}$  – atmosphere density in the point  $P_i$ ;  $d_T$  – diameter of the tether; and  $\varphi_{1,i}$  – an angle between vectors  $\rho_{i+1}$  and a velocity vector  $\mathbf{V}_i$ .

Let us express vector  $\mathbf{N}_{1,i}$  through  $\mathbf{V}_i$  and  $\rho_{i+1}$ . The vector  $\mathbf{a}_{1,i} = \mathbf{V}_i \times \rho_{i+1}$  is perpendicular to vectors  $\mathbf{V}_i$  and  $\rho_{i+1}$ . Its module is:

$$|\mathbf{a}_{1,i}| = V_i \rho_{i+1} \sin \varphi_{1,i}.$$

The direction of vector  $\mathbf{n}_{1,i+1} = \mathbf{a}_{1,i} \times \rho_{i+1}$  coincides with vector  $\mathbf{N}_{1,i}$  and its module is equal:

$$|\mathbf{n}_{1,i+1}| = a_{1,i} \rho_{i+1} \sin \frac{\pi}{2} = V_i \rho_{i+1}^2 \sin \varphi_{1,i}.$$

Taking into account the last expression, vector  $\mathbf{N}_{1,i}$  can be presented as:

$$\begin{aligned} \mathbf{N}_{1,i} &= \frac{\rho_{ai} V_i k d_T}{6 \rho_{i+1}} \sin \varphi_{1,i} \mathbf{n}_{1,i+1} \\ &= \frac{\rho_{ai} V_i k d_T}{6 \rho_{i+1}} \sin \varphi_{1,i} (\mathbf{V}_i \times \rho_{i+1}) \times \rho_{i+1}. \end{aligned} \quad [2.125]$$

Similar expression can be obtained for the second cylinder of  $\Delta L_i$ :

$$\mathbf{N}_{2,i} = \frac{\rho_{ai} V_i k d_T}{6 \rho_i} \sin \varphi_{2,i} (\mathbf{V}_i \times \rho_i) \times \rho_i. \quad [2.126]$$

By summation of the vectors [2.125] and [2.126] we will receive a resultant vector of the aerodynamic forces acting on the tether's part  $\Delta L_i$ :

$$\mathbf{F}_{Ai} = \mathbf{N}_{1,i} + \mathbf{N}_{2,i} = \frac{\rho_{ai} V_i k d_T}{6} \left( \frac{\sin \varphi_{1,i}}{\rho_i} \mathbf{n}_{1,i+1} + \frac{\sin \varphi_{2,i}}{\rho_{i+1}} \mathbf{n}_{2,i} \right), \quad [2.127]$$

where  $\mathbf{n}_{i,j} = (\mathbf{V}_i \times \rho_j) \times \rho_j$ .

For definition of angles  $\varphi_{1,i}$  and  $\varphi_{2,i}$ , it is necessary to use the formula of the module of a scalar product:

$$\cos \varphi_{1,i} = \frac{\mathbf{V}_i \cdot \mathbf{\rho}_i}{V_i \rho_i}, \quad \cos \varphi_{2,i} = \frac{\mathbf{V}_i \cdot \mathbf{\rho}_{i+1}}{V_i \rho_{i+1}}.$$

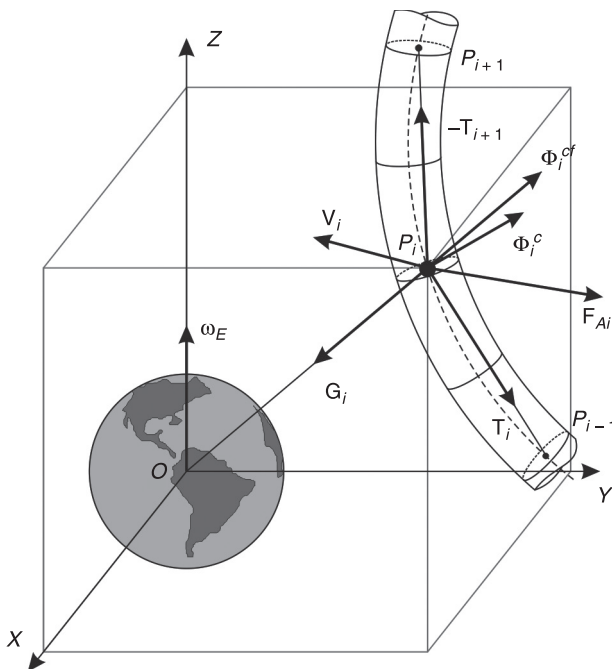
### **2.5.3 The equation for the motion of a particle in a multipoint model of a tether**

If we consider the tethered bodies as particles, the equations for the motion of a tether's points and of the connected bodies have the same form. This assumption is quite reasonable in the case of a fast spinning STS, or when the motion of the end bodies concerning their centres of mass is insignificant for a considered problem. We will construct the equation of motion of  $P_i$  point of the system, remembering that the end bodies correspond to  $P_0$  and  $P_{N+1}$  (see Figure 2.10).

To obtain the equations of motion we will use a rotating Greenwich coordinate system OXYZ. Its beginning coincides with the Earth's centre of mass. The plane OXY coincides with an equatorial plane, the axis OX is directed to the Greenwich meridian, the axis OZ is directed along the spin axis of the Earth, OZ supplements the system to the right-hand side. This system is noninertial because it rotates along the axis OZ with a constant angular velocity  $\omega_E$ .

Several forces act on point  $P_i$ : gravitational  $\mathbf{G}_i$ ; aerodynamic  $\mathbf{F}_{Ai}$ ; forces of the tension from the adjacent tether's parts  $\mathbf{T}_i$ ,  $-\mathbf{T}_{i+1}$ ; and also the forces of inertia caused by rotation of the coordinate system;  $\Phi_i^{cf}$  – centrifugal and  $\Phi_i^C$  – Coriolis (see Figure 2.15).

As Earth rotates with a constant angular velocity, on one point the rotational force of inertia does not act –  $\Phi_i^{rot} = 0$ .

**Figure 2.15** The forces acting on a part of the tether

We write Newton's second law for noninertial system  $OXYZ$ :

$$m_i \ddot{\mathbf{r}}_i = \mathbf{G}_i + \mathbf{F}_{Ai} + \mathbf{T}_i - \mathbf{T}_{i+1} + \Phi_i^{cf} + \Phi_i^c. \quad [2.128]$$

Gravitational force is potential. The coordinates of a vector of this force depend on one scalar function  $U$ , called a gravitational potential

$$\mathbf{G}_i = \text{grad } U,$$

where  $\text{grad}$  – a gradient.

Often at rough calculations, the Earth is represented in the form of a sphere. In this case the gravitational field is central, and its potential corresponds to the Newtonian potential and depends only on the distance from the Earth's centre to the considerable point  $r_i$ :

$$U = \frac{\mu}{r_i}, \quad [2.129]$$

where  $\mu$  – gravitational parameter of Earth.

In this case, the vector of gravitational forces  $\mathbf{G}_i$  in OXYZ has coordinates:

$$\mathbf{G}_i = \left[ -\frac{\mu m_i}{r_i^3} x_i, -\frac{\mu m_i}{r_i^3} y_i, -\frac{\mu m_i}{r_i^3} z_i \right]^T, \quad [2.130]$$

where  $r_i = \sqrt{x_i^2 + y_i^2 + z_i^2}$ ,  $x_i, y_i, z_i$  – coordinates of  $i$ -th point in OXYZ.

Actually, the form of the Earth differs from a sphere and for the correct exposition of its gravitational field a more complicated potential is required. The gravitational field of a rigid body in a general case can be presented by means of the decomposition of spherical functions:

$$U = \frac{\mu}{r_i} \left( 1 - \sum_{n=2}^{\infty} J_n \left( \frac{R_E}{r_i} \right)^n P_n \sin \varphi + \sum_{n=2}^{\infty} \sum_{k=1}^n \left( \frac{R_E}{r_i} \right)^n P_n^{(k)} \sin \varphi (C_{nk} \cos k\lambda + S_{nk} \sin k\lambda) \right),$$

where  $\phi, \lambda$  – geocentric latitude and longitude;  $P_n$  – Legendre polynomial of  $n$  order;  $R_E$  – semimajor axis of a common terrestrial ellipsoid;  $P_n^{(k)}$  – associated function of Legendre;  $J_n$  – coefficient of zonal harmonic;  $C_{nk}, S_{nk}$  – dimensionless coefficients, termed at  $n \neq k$  the coefficients of tesseral harmonics, and at  $n = k$  the coefficients of a sectoral harmonics. These coefficients characterise differences of the body from a sphere. There are some models of the gravitational field of the Earth, which are tables with groups of numbers, allowing us to calculate the coefficients  $J_n, C_{nk}, S_{nk}$  (Lerch et al., 1994; Tapley et al., 1996).

The basic disturbing term in the decomposition of the potential  $U$  is the second zonal harmonic, which defined oblateness of the planet at the poles. It exceeds all remaining terms of decomposition on three orders. If the Earth is viewed as a body with a rotational symmetry and is symmetrical relative to the equator, only the even coefficients of zonal harmonics will be nonzero in decomposition of the potential.

$$U = \frac{\mu}{r_i} \left( 1 - \sum_{n=1}^{\infty} J_{2n} \left( \frac{R_E}{r_i} \right)^{2n} P_{2n} \sin \varphi \right).$$

Using the last formula, we write the projections of gravitational force  $\mathbf{G}_i$  in the coordinate system  $OXYZ$ , considering the influence of only the second and fourth zonal harmonic:

$$\mathbf{G}_i = \begin{bmatrix} -\frac{\mu m_i}{r_i^3} x_i - \left( \frac{3\bar{c}_{20} R_E^2}{2r_i^4} \left( 5 \frac{z_i^2}{r_i^2} - 1 \right) \right. \\ \left. + \frac{5\bar{c}_{40} R_E^4}{8r_i^6} \left( 3 + \left( 63 \frac{z_i^2}{r_i^2} - 42 \right) \frac{z_i^2}{r_i^2} \right) \right) \frac{\mu m_i x_i}{r_i} \\ -\frac{\mu m_i}{r_i^3} y_i - \left( \frac{3\bar{c}_{20} R_E^2}{2r_i^4} \left( 5 \frac{z_i^2}{r_i^2} - 1 \right) \right. \\ \left. + \frac{5\bar{c}_{40} R_E^4}{8r_i^6} \left( 3 + \left( 63 \frac{z_i^2}{r_i^2} - 42 \right) \frac{z_i^2}{r_i^2} \right) \right) \frac{\mu m_i y_i}{r_i} \\ -\frac{\mu m_i}{r_i^3} z_i - \left( \frac{3\bar{c}_{20} R_E^2}{2r_i^4} \left( 5 \frac{z_i^2}{r_i^2} - 3 \right) \right. \\ \left. + \frac{5\bar{c}_{40} R_E^4}{16r_i^6} \left( 30 + \left( 63 \frac{z_i^2}{r_i^2} - 70 \right) \frac{z_i^2}{r_i^2} \right) \right) \frac{\mu m_i z_i}{r_i} \end{bmatrix} [2.131]$$

where  $\bar{c}_{20}$ ,  $\bar{c}_{40}$  – coefficients from models of a gravitational field of Earth.

They allow us to find the coefficients of zonal harmonics:

$$J_{2n} = -\bar{c}_{n0} \sqrt{2n+1}.$$

Coordinates of the vector of aerodynamic force [2.127] are determined by coordinates of vectors  $\mathbf{n}_{1,i+1}$  and  $\mathbf{n}_{2,i}$  which in system OXYZ are:

$$\mathbf{n}_{i,j} = \begin{bmatrix} [(x_j - x_{j-1})\dot{z}_i - (z_j - z_{j-1})\dot{x}_i](z_j - z_{j-1}) \\ -[(y_j - y_{j-1})\dot{x}_i - (x_j - x_{j-1})\dot{y}_i](y_j - y_{j-1}) \\ [(y_j - y_{j-1})\dot{x}_i - (x_j - x_{j-1})\dot{y}_i](x_j - x_{j-1}) \\ -[(z_j - z_{j-1})\dot{y}_i - (y_j - y_{j-1})\dot{z}_i](z_j - z_{j-1}) \\ [(z_j - z_{j-1})\dot{y}_i - (y_j - y_{j-1})\dot{z}_i](y_j - y_{j-1}) \\ -[(x_j - x_{j-1})\dot{z}_i - (z_j - z_{j-1})\dot{x}_i](x_j - x_{j-1}) \end{bmatrix}. \quad [2.132]$$

The tension force is directed along vector  $\rho_i$  (see Figure 2.10) and has the following coordinates in OXYZ:

$$\mathbf{T}_i = \left[ T_i \frac{x_i - x_{i-1}}{\rho_i}; \quad T_i \frac{y_i - y_{i-1}}{\rho_i}; \quad T_i \frac{z_i - z_{i-1}}{\rho_i} \right]^T, \quad [2.133]$$

where  $\rho_i = \sqrt{(x_i - x_{i-1})^2 + (y_i - y_{i-1})^2 + (z_i - z_{i-1})^2}$ ; for end bodies  $T_0 = T_{N+2} = 0$ .

Besides the active forces, the inertial forces caused by rotation of the Earth act on a tether's part. The centrifugal force of inertia is:

$$\Phi_i^{cf} = -m_i \omega_E \times (\omega_E \times \mathbf{r}_i),$$

where  $\omega_E = [0, 0, \omega_E]^T$  – defined in the OXYZ vector of the angular velocity of the Earth's rotation.

The Coriolis force of inertia can be found as:

$$\Phi_i^C = -2m_i \omega_E \times V_i.$$

In OXYZ, vectors  $\Phi_i^{cf}$  and  $\Phi_i^C$  have coordinates

$$\begin{aligned}\Phi_i^{cf} &= [m_i \omega_E^2 x_i; m_i \omega_E^2 y_i; 0]^T, \\ \Phi_i^C &= [2m_i \omega_E \dot{y}_i; -2m_i \omega_E \dot{x}_i; 0]^T.\end{aligned}\quad [2.134]$$

Let us write the vector equation [2.128] in the scalar form, leading it to a normal view:

$$\dot{x}_i = V_{X,i},$$

$$\dot{y}_i = V_{Y,i}, \quad i = 0, \dots, N+1$$

$$\dot{z}_i = V_{Z,i},$$

$$\dot{V}_{X,i} m_i = -\left( \frac{3\bar{c}_{20} R_E^2}{2r_i^4} \left( 5 \frac{z_i^2}{r_i^2} - 1 \right) + \frac{5\bar{c}_{40} R_E^4}{8r_i^6} \left( 3 + \left( 63 \frac{z_i^2}{r_i^2} - 42 \right) \frac{z_i^2}{r_i^2} \right) \right)$$

$$\begin{aligned}&\times \frac{\mu m_i x_i}{r_i} - \frac{\mu m_i}{r_i^3} x_i + F_{Aix} + T_i \frac{x_i - x_{i-1}}{\rho_i} - T_{i+1} \frac{x_{i+1} - x_i}{\rho_{i+1}} \\&+ m_i \omega_E^2 x_i + 2m_i \omega_E y_i\end{aligned}$$

$$\begin{aligned}\dot{V}_{Y,i} m_i &= -\left( \frac{3\bar{c}_{20} R_E^2}{2r_i^4} \left( 5 \frac{z_i^2}{r_i^2} - 1 \right) \right. \\&\left. + \frac{5\bar{c}_{40} R_E^4}{8r_i^6} \left( 3 + \left( 63 \frac{z_i^2}{r_i^2} - 42 \right) \frac{z_i^2}{r_i^2} \right) \right) \frac{\mu m_i y_i}{r_i} \\&-\frac{\mu m_i}{r_i^3} y_i + F_{Aiy} + T_i \frac{y_i - y_{i-1}}{\rho_i}\end{aligned}\quad [2.135]$$

$$\begin{aligned}&-T_{i+1} \frac{y_{i+1} - y_i}{\rho_{i+1}} + m_i \omega_E^2 y_i - 2m_i \omega_E \dot{x}_i, \\&\dot{V}_{Z,i} m_i = -\left( \frac{3\bar{c}_{20} R_E^2}{2r_i^4} \left( 5 \frac{z_i^2}{r_i^2} - 3 \right) + \frac{5\bar{c}_{40} R_E^4}{16r_i^6} \left( 30 + \left( 63 \frac{z_i^2}{r_i^2} - 70 \right) \frac{z_i^2}{r_i^2} \right) \right)\end{aligned}$$

$$\begin{aligned}&\times \frac{\mu m_i z_i}{r_i} - \frac{\mu m_i}{r_i^3} z_i + F_{Aiz} + T_i \frac{z_i - z_{i-1}}{\rho_i} - T_{i+1} \frac{z_{i+1} - z_i}{\rho_{i+1}}.\end{aligned}$$

where  $F_{Aix}$ ,  $F_{Aiy}$ ,  $F_{Aiz}$  – projections of the resultant vector of aerodynamic forces [1.127] to system OXYZ axes.

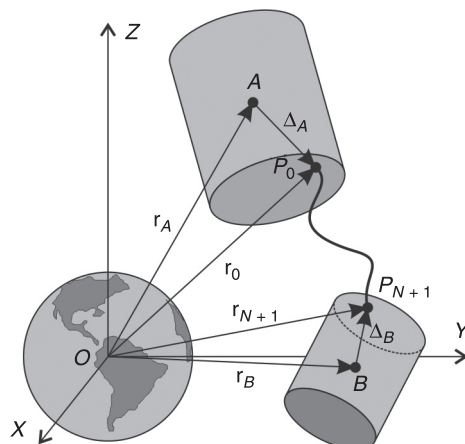
## 2.5.4 The equation of motion of end bodies

In section 2.5.3 the mathematical model for a STS, not taking into account the motion of the tethered bodies concerning their centres of mass, has been constructed. Let us consider a case when the end bodies cannot be presented in the form of particles (see Figure 2.16). The fixing points of the tether,  $P_0$  and  $P_{N+1}$ , will no longer coincide with the centres of mass of the bodies. The radius vectors of these points are defined by relations:

$$\mathbf{r}_0 = \mathbf{r}_A + \Delta_A, \quad \mathbf{r}_{N+1} = \mathbf{r}_B + \Delta_B, \quad [2.136]$$

where points A and B correspond to bodies' centres of masses;  $\mathbf{r}_A$  and  $\mathbf{r}_B$  – their radius vectors; and  $\Delta_A$  and  $\Delta_B$  – vectors connecting the centres of mass of bodies with the fixing points of the tether  $P_0$  and  $P_{N+1}$ .

**Figure 2.16** STS consisting of two rigid bodies connected by a tether



The motion of the centres of mass is described by equations similar to [2.128]:

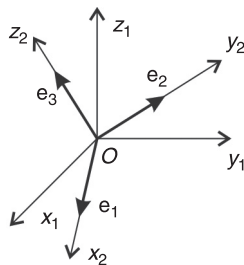
$$\begin{aligned} m_A \ddot{\mathbf{r}}_A &= \mathbf{G}_A + \mathbf{F}_{AA} + \mathbf{T}_1 + \Phi_A^{cf} + \Phi_A^C, \\ m_B \ddot{\mathbf{r}}_B &= \mathbf{G}_B + \mathbf{F}_{AB} - \mathbf{T}_{N+1} + \Phi_B^{cf} + \Phi_B^C. \end{aligned} \quad [2.137]$$

Projections of the forces  $\mathbf{G}_j$ ,  $\Phi_j^{cf}$ ,  $\Phi_j^C$ ,  $T_i$  are defined as in section 2.5.3. The aerodynamic force  $\mathbf{F}_{Aj}$  depends on the orientation of the body and will be described later.

Before starting to develop the equations describing the motion of the end bodies concerning their centres of mass, we will talk about the methods of a body's orientation representation (Bear, 1952). Let us take two coordinate systems  $Ox_1y_1z_1$  and  $Ox_2y_2z_2$  (see Figure 2.17). The vector  $\mathbf{a}$  has coordinates  $[a_{x1}, a_{y1}, a_{z1}]^T$  in the system  $Ox_1y_1z_1$ , and  $[a_{x2}, a_{y2}, a_{z2}]^T$  in the system  $Ox_2y_2z_2$ . Transition from  $Ox_1y_1z_1$  to  $Ox_2y_2z_2$  can be made by means of the rotation matrix  $\|A_2^1\|$ . To find the coordinates of vector  $\mathbf{a}$  in system  $Ox_2y_2z_2$ , it is necessary to multiply the matrix  $\|A_2^1\|$  by the column matrix with the vector's coordinates in  $Ox_1y_1z_1$ :

$$\begin{bmatrix} a_{x2} \\ a_{y2} \\ a_{z2} \end{bmatrix} = \|A_2^1\| \begin{bmatrix} a_{x1} \\ a_{y1} \\ a_{z1} \end{bmatrix}.$$

**Figure 2.17** The relative position of coordinate systems



The matrix components are cosines of the angles between the axes of the first and second coordinate systems:

$$\|A_2^1\| = \begin{bmatrix} \cos(x_2 \wedge x_1) & \cos(x_2 \wedge y_1) & \cos(x_2 \wedge z_1) \\ \cos(y_2 \wedge x_1) & \cos(y_2 \wedge y_1) & \cos(y_2 \wedge z_1) \\ \cos(z_2 \wedge x_1) & \cos(z_2 \wedge y_1) & \cos(z_2 \wedge z_1) \end{bmatrix}, \quad [2.138]$$

Therefore, in the mechanics, this matrix is called a matrix of direction cosines. It is possible to notice that the columns of matrix  $\|A_2^1\|$  contain coordinates of the basis vectors of the first coordinate system in the second system, and the rows contain coordinates of the basis vectors of the second system in the first one.

To fulfil the inverse transition from the system  $Ox_2y_2z_2$  to  $Ox_1y_1z_1$ , it is necessary to use a matrix  $\|A_1^2\|$  which is connected with the matrix  $\|A_2^1\|$  by relation:

$$\|A_1^2\| = \|A_2^1\|^{-1} = \|A_2^1\|^T. \quad [2.139]$$

The last relation is fair owing to the orthogonality of a rotation matrix.

The matrix  $\|A_2^1\|$  contains nine components, however only three out of nine of the direction cosines are independent. The remaining six can be found from a condition of orthogonality of the coordinate system's axes. For example, we take a vector of the base of the second system  $e_i$  (see Figure 2.7) to which rows in the matrix  $\|A_2^1\|$  correspond:

$$\|A_2^1\| = \begin{bmatrix} e_{1x} & e_{1y} & e_{1z} \\ e_{2x} & e_{2y} & e_{2z} \\ e_{3x} & e_{3y} & e_{3z} \end{bmatrix}. \quad [2.140]$$

As we use the Cartesian coordinate systems, the length of the basis vector  $e_i$  is equal to one, whence:

$$\mathbf{e}_i \cdot \mathbf{e}_i = 1, \quad i = 1, 2, 3. \quad [2.141]$$

The basis vectors are mutually orthogonal, therefore their paired scalar product is equal to zero:

$$\mathbf{e}_i \cdot \mathbf{e}_j = 0, \quad i \neq j, \quad i, j = 1, 2, 3. \quad [2.142]$$

Orthogonality of vectors  $\mathbf{e}_i$  allows us to write out three vector products:

$$\mathbf{e}_1 = \mathbf{e}_2 \times \mathbf{e}_3, \quad \mathbf{e}_2 = \mathbf{e}_3 \times \mathbf{e}_1, \quad \mathbf{e}_3 = \mathbf{e}_1 \times \mathbf{e}_2. \quad [2.143]$$

Equations [2.141]–[2.143] allow us to define nine components of the matrix [2.140] if three of them are known.

If the coordinate system  $Ox_2y_2z_2$  rotates around  $Ox_1y_1z_1$  with an angular velocity  $\omega$  for a basis vector of the second system  $\mathbf{e}_i$  then the relation is fair:

$$\frac{d\mathbf{e}_i}{dt} + \boldsymbol{\omega} \times \mathbf{e}_i = 0, \quad [2.144]$$

where  $\mathbf{e}_i$  and  $\boldsymbol{\omega}$  are defined in  $Ox_1y_1z_1$ .

Let us construct the equation system for describing the motion of the end bodies concerning their centres of mass. Further, for brevity we will consider one of the bodies, for example, with the centre of mass in point  $A$ . The equations for the second body can be similarly received. For a rigid body of the arbitrary form moving in the atmosphere, the equations system in the direction of the cosines is effective from the point of view of minimization of the volume of the calculations at integration. A similar system was presented for the first time in the article by Shilov and Vasiliev (1971).

Let us write the theorem of a moment of momentum modification for the body coordinate system  $Oxyz$ , taking into account that the aerodynamic moment  $\mathbf{M}_A$ , the moment of tension force  $\Delta_A \times \mathbf{T}_1$ , and the gravitational moment  $\mathbf{M}_G$  act on the body.

$$\frac{d\mathbf{K}}{dt} + \boldsymbol{\omega} \times \mathbf{K} = \mathbf{M}_A + \mathbf{M}_G + \Delta_A \times \mathbf{T}_1, \quad [2.145]$$

where  $\mathbf{K} = \|I\| \cdot \boldsymbol{\omega}$  – body's moment of momentum; and  $\|I\|$  – inertia tensor:

$$\|I\| = \begin{bmatrix} I_x & I_{xy} & I_{xz} \\ I_{xy} & I_y & I_{yz} \\ I_{xz} & I_{yz} & I_z \end{bmatrix},$$

where  $I_x, I_y, I_z$  – axial moment of inertia;  $I_{xy}, I_{xz}, I_{yz}$  – product of inertia;  $\boldsymbol{\omega} = \boldsymbol{\omega}_r + \boldsymbol{\omega}_E$  – defined in  $Oxyz$  body's angular velocity vector; and  $\boldsymbol{\omega}_r$  – vector of angular velocity of the body concerning an air.

It is equal to an angular velocity of the body coordinate system's  $Oxyz$  rotating around the Greenwich coordinate system OXYZ.

Orientation of the body around the Greenwich coordinate system can be set by means of a matrix of direction cosines:

$$\|A_{Gr}^b\| = \begin{bmatrix} l_x & l_x & l_x \\ m_x & m_y & m_z \\ n_x & n_y & n_z \end{bmatrix},$$

where  $\mathbf{e}_i = [\mathbf{l}, \mathbf{m}, \mathbf{n}]^T$  – basis vectors of the Greenwich coordinate system which are defined in projections to axes of the body coordinate system:

$$\begin{bmatrix} \mathbf{l} \\ \mathbf{m} \\ \mathbf{n} \end{bmatrix} = \|A_{Gr}^b\| \begin{bmatrix} \mathbf{i} \\ \mathbf{j} \\ \mathbf{k} \end{bmatrix},$$

where  $\mathbf{i}, \mathbf{j}, \mathbf{k}$  – basis vectors of the body coordinate system.

Notice incidentally that in equation [2.137], the coordinates of vector  $\mathbf{F}_{Aj}$  can be obtained by means of the expression:

$$\mathbf{F}_{Ai} = q_i S_i \|A_{Gr}^b\| \begin{bmatrix} c_{xi} \\ c_{yi} \\ c_{zi} \end{bmatrix}, \quad [2.146]$$

where  $q_i$  – dynamic pressure of  $i$ -th body;  $S_i$  – frontal area of  $i$ -th body; and  $c_{xi}$ ,  $c_{yi}$ ,  $c_{zi}$  – coefficients of aerodynamic forces.

Let us write equation [2.145] in the form:

$$\dot{\omega} = \|I\|^{-1} (\mathbf{M}_A + \mathbf{M}_G + \Delta_A \times \mathbf{T}_1 + (\|I\| \cdot \omega) \times \omega). \quad [2.147]$$

The vector

$$\mathbf{M}_A = \left[ \frac{q_A S_A}{l_A} m_x, \frac{q_A S_A}{l_A} m_y, \frac{q_A S_A}{l_A} m_z \right]^T$$

is set in the body coordinate system and depends on the aerodynamic coefficients, which in turn are functions of an angle of attack  $\alpha$  and a slip angle  $\beta$  for a body of the arbitrary form, or functions of a spatial angle of attack  $\alpha_{sp}$  for an axisymmetric body, where  $l_A$  – characteristic dimension of body A.

These angles can be discovered from relations (Aslanov, 2004)

$$\begin{aligned} \sin \alpha &= -\frac{V_y}{\sqrt{V_x^2 + V_y^2}}, & \cos \alpha &= \frac{V_x}{\sqrt{V_x^2 + V_y^2}}, \\ \sin \beta &= \frac{V_z}{V}, & \cos \beta &= \frac{\sqrt{V_x^2 + V_y^2}}{V}, \\ \sin \alpha_{sp} &= \frac{\sqrt{V_y^2 + V_z^2}}{V}, & \cos \alpha_{sp} &= \frac{V_x}{V}, \end{aligned}$$

where  $V = \sqrt{V_x^2 + V_y^2 + V_z^2}$ ,  $V_x, V_y, V_z$  – projections of the velocity vector of the body's centre of mass to the axes of the body coordinate system.

As a result of integration of the system in [2.135], we receive projections of a velocity to the axes of the Greenwich

coordinate system  $V_x, V_y, V_z$ . To obtain these coordinates of the velocity in the body system, it is necessary to use the rotation matrix  $\|A_c^{Gr}\|$  which is a matrix of transition from the coordinate system  $Oxyz$  to  $OXYZ$ :

$$\begin{bmatrix} V_x \\ V_y \\ V_z \end{bmatrix} = \|A_b^{Gr}\| \begin{bmatrix} V_X \\ V_Y \\ V_Z \end{bmatrix}.$$

The vector of gravitational moment  $\mathbf{M}_G$  is set in the body system by the coordinates:

$$\mathbf{M}_G = \left[ \frac{3\mu}{r_A^3} (I_z - I_y) a_{32} a_{33}, \frac{3\mu}{r_A^3} (I_x - I_z) a_{33} a_{31}, \frac{3\mu}{r_A^3} (I_y - I_x) a_{31} a_{32} \right]^T, \quad [2.148]$$

where  $a_{ij}$  – components of a matrix of passage from body to a barycentric coordinate system  $\|A_{bc}^b\|$ .

This approximate expression received for a gravitational field with a potential [2.129] in which the magnitudes which order less than  $(l_A/r_A)^2$  are removed. In addition, it is considered that the body's centrifugal moments of inertia are equal to zero.

Let us obtain a transition matrix  $\|A_{bc}^b\|$  from the body to a barycentric coordinate system  $A\tau bn$ . At the beginning of the barycentric system it is possible to choose any point of the mechanical system. For certainty, we take the point  $A$  as the centre of mass of the body. Axis  $An$  is directed along the radius vector of point  $A$  towards its increase, axis  $Ab$  is normal to the orbit plane and colinear to the vector of an integral of the squares  $C$ , and the axis  $A\tau$  supplements the system to the right-hand side (see Figure 2.18). Let us write the formulas for transition of the point's coordinates from  $OXYZ$  to  $A\tau bn$  (Narimanov and Tihonov, 1972):

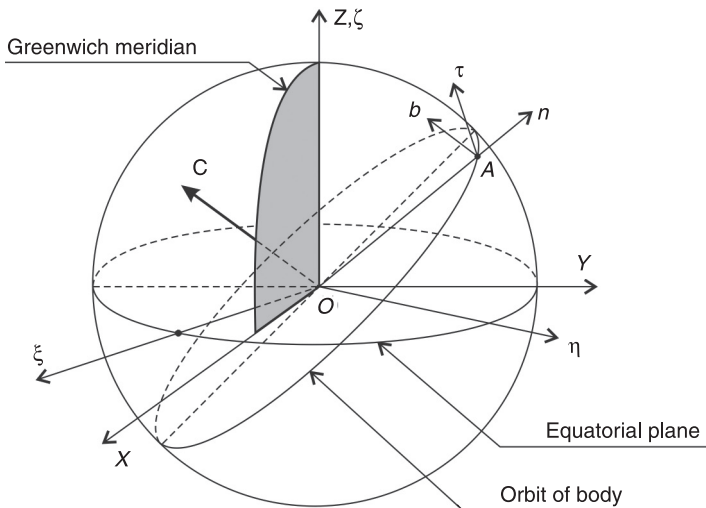
$$\begin{bmatrix} \tau \\ b \\ n \end{bmatrix} = \|A_{bc}^{eq}\| \begin{bmatrix} \xi - \xi_0 \\ \eta - \eta_0 \\ \zeta - \zeta_0 \end{bmatrix}, \quad \begin{bmatrix} \xi \\ \eta \\ \zeta \end{bmatrix} = \|A_{eq}^{Gr}\| \begin{bmatrix} x \\ y \\ z \end{bmatrix}, \quad \begin{bmatrix} \xi_A \\ \eta_A \\ \zeta_A \end{bmatrix} = \|A_{eq}^{Gr}\| \begin{bmatrix} x_A \\ y_A \\ z_A \end{bmatrix},$$

$$\begin{bmatrix} V_{\xi A} \\ V_{\eta A} \\ V_{\zeta A} \end{bmatrix} = \|A_{eq}^{Gr}\| \begin{bmatrix} V_{xA} \\ V_{yA} \\ V_{zA} \end{bmatrix} + \omega_E \begin{bmatrix} -\eta_A \\ \xi_A \\ 0 \end{bmatrix}, \quad \|A_{eq}^{Gr}\| = \begin{bmatrix} \cos \gamma & -\sin \gamma & 0 \\ \sin \gamma & \cos \gamma & 0 \\ 0 & 0 & 1 \end{bmatrix},$$

$$\|A_{eq}^{bc}\| = \begin{bmatrix} \frac{1}{Cr_A} (C_2 \xi_A - C_3 \eta_A) & \frac{C_1}{C} & \frac{\xi_A}{r_A} \\ \frac{1}{Cr_A} (C_3 \xi_A - C_1 \eta_A) & \frac{C_2}{C} & \frac{\eta_A}{r_A} \\ \frac{1}{Cr_A} (C_1 \eta_A - C_2 \xi_A) & \frac{C_3}{C} & \frac{\zeta_A}{r_A} \end{bmatrix}, \quad \begin{aligned} C &= \sqrt{C_1^2 + C_2^2 + C_3^2}, \\ C_1 &= \eta_A V_{\xi A} - \zeta_A V_{\eta A}, \\ C_2 &= \zeta_A V_{\xi A} - \xi_A V_{\zeta A}, \\ C_3 &= \xi_A V_{\eta A} - \eta_A V_{\xi A}, \\ \gamma &= S_0 + \omega_E (t - t_0); \end{aligned}$$

$$\|A_{bc}^b\| = \|A_{bc}^{eq}\| \cdot \|A_{eq}^{Gr}\| \cdot \|A_{eq}^b\|.$$

**Figure 2.18** Coordinate systems



Here  $\tau, b, n$  – coordinates of an arbitrary point in  $A\tau bn$ ;  $x, y, z$  – coordinates of the same point in the Greenwich coordinate system OXYZ;  $\xi, \eta, \varsigma$  – coordinates of the same point in the equatorial coordinate system  $O\xi\eta\varsigma$ ;  $x_A, y_A, z_A$  and  $V_{xA}, V_{yA}, V_{zA}$  – coordinates and components of a velocity of the point A in OXYZ;  $S_0$  – sidereal time at moment  $t_0$ ;  $t$  – current time; and  $t_0$  – mean solar time.

In practice, the use of a barycentric system coordinate is convenient because the coordinates of a point set in it are easily interpreted.

To the equations of the body's centre of mass motion, [2.137], and the dynamic equations of its motion [2.147], it is necessary to add the kinematic equations. From the point of view of minimisation of the calculations and the uniqueness of the results interpretation, as a rule, six differential and three algebraic equations are used. These equations are acquired from following three vector equations (Aslanov, 2004):

$$\dot{\mathbf{l}} = \mathbf{l} \times \boldsymbol{\omega}, \quad \dot{\mathbf{m}} = \mathbf{m} \times \boldsymbol{\omega}, \quad \mathbf{n} = \mathbf{l} \times \mathbf{m}. \quad [2.149]$$

Let us write the kinematic equations [2.149] in a scalar form:

$$\begin{aligned} \dot{l}_x &= l_y \omega_z - l_z \omega_y, & \dot{l}_y &= l_z \omega_x - l_x \omega_z, & \dot{l}_z &= l_x \omega_y - l_y \omega_z, \\ \dot{m}_x &= m_y \omega_z - m_z \omega_y, & \dot{m}_y &= m_z \omega_x - m_x \omega_z, \\ \dot{m}_z &= m_x \omega_y - m_y \omega_z, \end{aligned} \quad [2.150]$$

$$\begin{aligned} n_x &= l_y m_z - l_z m_y, & n_y &= l_z m_x - l_x m_z, & n_z &= l_x m_y - l_y m_z, \end{aligned} \quad [2.151]$$

Three scalar differential equations, [2.147], six scalar differential equations, [2.150], and three algebraic equations, [2.151], describe the motion of the rigid body concerning its centre of mass.

Let us note that besides the direction of the cosines there are also alternative approaches to obtaining the equations of

motion of a rigid body concerning its centre of mass. The greatest distribution in classical mechanics was received by the approach based on the use of Euler's angles (Curtis, 2005) which implies transition from the body coordinate system to a fixed system by means of three consecutive turns. The simplicity and clearness of this approach has brought about its wide distribution; however, this approach has one essential disadvantage hampering its use in problems of space flight mechanics. The equations received by means of Euler's angles have a singular point of zero value at one of the angles. To solve this difficulty it is necessary to constantly watch the value of the given angle during integration and at its approach to the singular value it is necessary to pass to the alternative system of the differential equations received from a coordinate system turned 90 degrees to the starting point. The new system of differential equations will have a singular point too, but it will correspond to the other orientations of the body.

Another approach to the representation of the orientation of a body is based on the use of quaternions (Kuipers, 2002). From the computing point of view, this approach is more effective in comparison with the direction cosines. For this reason, quaternions are widely used in computer graphics. The system of differential equations received by means of quaternions, as well as the system in the direction cosines, has no singular points and degenerations. However, quaternions are not so obvious as the direction cosines, and they demand additional efforts for the interpretation of results.

### **2.5.5 Singularities of a tether deployment algorithm**

The multipoint model developed in this section can be applied if the length of undistorted tether does not vary

during motion. Certainly, the tether can be stretched, but its mass remains invariable. If the length of the undistorted tether increases (the tether is deploying from a spacecraft) or decreases (the tether is retracting into a spacecraft) so it is necessary to make some modifications to the model. The question is whether the number of particles presenting the tether varies during calculation. In the case of development, their number increases by one each time as soon as the distance between the tether's outlet point and the particle nearest to it reaches the appointed magnitude  $\Delta L_{k+1}$ , where  $k$  is number of particles modelling at the current moment on the tether. In the case of retrieval, the number of point masses decreases, when the distance between the tether's outlet point and the nearest particle becomes equal to zero.

Let us consider in more detail the process of tether deployment. Let us assume that the tether is presented as  $k$  particles in a moment  $\tau$ . Tethered bodies represent particles. At this moment, the distance between the tether's outlet point and the  $k$ -th particle is less than  $\Delta L_{k+1}$ :

$$\rho_{k+1} < \Delta L_{k+1}$$

If the numerical integration of the differential equation system [2.135] is carried out with a pitch on the time of  $\Delta t$ , and in the time *moment*  $\tau + \Delta t$  the distance  $\rho_{k+1}$  becomes more than  $\Delta L_{k+1}$ , the number of the tether's particles needs to be increased by one. Thus, the dimension of system [2.135] will increase by six equations. From the point of view of mechanics, there will be a division of the body from which the tether is deploying, into two parts. The majority of the body, whose mass is  $m_B - m_{k+1}$ , remains in the same point of space in which the body was before separation in the moment  $\tau$ . The velocity of this point keeps its value. The smaller part, whose mass is equal to  $m_{k+1}$ , is transferred to a point defined by a radius vector  $\mathbf{r}_{k+1}$ .

Let us use the conservation laws of momentum and of the moment of momentum for the definition of position and velocity of  $(k + 1)$ -th particle (energy in system does not remain constant because of the deployment gear works):

$$\begin{aligned} m_A \mathbf{V}_A + m_1 \mathbf{V}_1 + \dots + m_k \mathbf{V}_k + m_B \mathbf{V}_B &= \\ = m_A \mathbf{V}_A + m_1 \mathbf{V}_1 + \dots + m_k \mathbf{V}_k + m_{k+1} \mathbf{V}_{k+1} + (m_B - m_{k+1}) \mathbf{V}_B, \\ m_A \mathbf{r}_A \times \mathbf{V}_A + m_1 \mathbf{r}_1 \times \mathbf{V}_1 + \dots + m_k \mathbf{r}_k \times \mathbf{V}_k + m_B \mathbf{r}_B \times \mathbf{V}_B &= \\ = m_A \mathbf{r}_A \times \mathbf{V}_A + m_1 \mathbf{r}_1 \times \mathbf{V}_1 + \dots + m_k \mathbf{r}_k \times \mathbf{V}_k + m_{k+1} \mathbf{r}_{k+1} \\ \times \mathbf{V}_{k+1} + (m_B - m_{k+1}) \mathbf{r}_B \times \mathbf{V}_B. \end{aligned}$$

From the first expression, we obtain  $\mathbf{V}_{k+1} = \mathbf{V}_B$ , and from the second,  $\mathbf{r}_{k+1} = \mathbf{r}_B$ . Such a choice of location and the velocity of a new point introduced into the system ensures observance of the laws of mechanics. Nevertheless, it leads to serious problems. In equation [2.133], magnitude  $\rho_i$  costs in a denominator, and at a choice  $\mathbf{r}_{k+1} = \mathbf{r}_B$  it becomes equal to zero. A traditional way of elimination of this singularity is the disposition of a new particle a small distance  $\Delta L_{k+1}$  from the point  $B$ . At  $\rho_{k+1} = \Delta L_{k+1} \neq 0$  entry conditions will become:

$$\mathbf{r}_{k+1} = \mathbf{r}_B + \Delta L_{k+1} \frac{\mathbf{r}_k - \mathbf{r}_B}{|\mathbf{r}_k - \mathbf{r}_B|}, \quad \mathbf{V}_{k+1} = \mathbf{V}_B + \frac{\Delta L_{k+1}}{|\mathbf{r}_k - \mathbf{r}_B|} (\mathbf{V}_k - \mathbf{V}_B). \quad [2.152]$$

At modelling of the tether deployment, the tension  $\mathbf{T}_{k+1}$  acting on the  $k$ -th particles (that is closer than others to the body with the deployer) cannot be found by means of expression [2.123], as it is defined not only by the elastic properties of the tether's part, but also by the force created by the mechanism of development. Additionally, the length of the undistorted tether's part changes during deployment  $l_{k+1} = l_{k+1}(t) \neq \text{const}$ . At modelling of the STS motion, with a variable tether  $\mathbf{T}_{k+1}$ , this is considered as a given function of time of a control force.

It is important to define precisely the input moment of a new particle in the system to avoid a saltus in the tension force of the tether. In other words, the tension force acting on the  $k$ -th point mass before input of a new point should not vary after that input. The new particle appears in the moment when the distance between the new point and  $k$ -th point corresponds to the length of the deformed tether ensuring this tension force:

$$\rho_{k+1} = \left( \frac{T_{k+1} - D_{k+1}\dot{\gamma}}{ES_{k+1}} + 1 \right) l_{k+1} + \Delta L_{k+1}, \quad [2.153]$$

where  $T_{k+1}$  is defined by the law of tension control.

Let us also consider the question of computer modelling of the tether deploying process. The considerable mechanical system consists of the spacecraft in which the mechanism of development and a spool with a tether are located, and the payload is connected with it by tether. For simplicity, we will assume that the spacecraft and the payload are represented by particles. In an initial moment of time, the tether and the payload are in the spacecraft. The impulse under which the operation payload begins movement is affixed to it. At this stage, the STS is modelled by two particles corresponding to the spacecraft and the payload. The tension force of the tether  $T_1$  is defined by the control law and it is a known function of time. The STS motion is described by a system of twelve ordinary differential equations of the first order in [2.135]. When the distance  $\rho_1$  between the spacecraft and the payload reaches values [2.153], the new tether's particle is introduced into the model. Six new equations are added to the system [2.135]. Between the payload and the first point, the tension force  $T_1$  acts. It is defined by the relation [2.123]. The force of tension  $T_2$  is defined by the control law. Input of the following particles is made under the same scheme. If the tether is completely deployed, and all the particles are

emitted ( $k = N$ ), the development mechanism ceases to work. The tension force  $T_{N+1}$  between the  $N$ -th particle and the spacecraft is defined by the formula [2.123].

## 2.6 References

- Alpatov A P, Dranovskii V I, Zakrzhevskii A E and Pirozhenko A V (1997) ‘Space Tether Systems. The Problem Review’ (in Russian), *Cosmic Science and Technology*, 3, 5/6, 21–9.
- Andreevskiy V V (1970) *Dynamics of Spacecraft Descent on Earth*. Moscow: Mashinostroenie (in Russian).
- Aslanov V S (2004) *Spatial Motion of a Body at Descent in the Atmosphere*. Moscow: FIZMATLIT (in Russian),
- Aslanov V S (2007) ‘The Oscillations of a Body with an Orbital Tethered System’, *Journal of Applied Mathematics and Mechanics*, 71, 926–32.
- Aslanov V S (2010) ‘The Effect of the Elasticity of an Orbital Tether System on the Oscillations of a Satellite’, *Journal of Applied Mathematics and Mechanics*, 74, 416–24.
- Aslanov V S, Ledkov A S and Stratilatov N R (2007) ‘Spatial Motion of a Space Rope Cargo Transport System’ (in Russian), *Polyot* (‘Flight’), ISSN 1684–1301, 2, 28–33.
- Bear R (1952) *Linear Algebra and Projective Geometry*. New York: Academic Press.
- Beletsky V V and Levin E M (1993) *Dynamics of Space Tether Systems*, San Diego, CA: American Astronautical Society.
- Curtis H (2005) *Orbital Mechanics for Engineering Students*. Norfolk, VA: Elsevier Butterworth-Heinemann.
- Dignath F and Schiehlen W (2000) ‘Control of the Vibrations of a Tethered Satellite System’, *Journal of Applied Mathematics and Mechanics*, 64, 5, 715–22.

- Ellis J R (2010) ‘Modeling, Dynamics, and Control of Tethered Satellite Systems’, *Dissertation of Doctor of Philosophy in Aerospace Engineering*, Blacksburg, VA.
- Gantmacher F (1975) *Lectures in Analytical Mechanics*. Moscow: MIR Publisher.
- Kleppner D and Kolenkow R J (1973) *An Introduction to Mechanics*. New York: McGraw-Hill.
- Krasnov N F, Koshevoy V N, Danilov A N and Zakharchenko (1968) *Rocket Aerodynamics*. Moscow: ‘Vysshaya Shkola’ Press.
- Kuipers J B (2002) *Quaternions and Rotation Sequences: A Primer with Applications to Orbits, Aerospace and Virtual Reality*, Princeton, NJ: Princeton University Press.
- Lazan B J (1968) *Damping of Material and Members in Structural Mechanics*. Oxford: Pergamon Press.
- Lech F J, Nerem R S, Putney B H, Felsentreger T L, Sanchez B V, Klosko S M, Patel G B, Williamson R G, Chinn D S, Chan J C, Rachlin K E, Chandler N L, Mc Carthy J J, Marshall J A, Luthcke S B, Pavlis D E, Robbins J W, Kapoor S and Pavlis E C (1994) ‘Geopotential Models from Satellite Tracking, Altimeter and Surface Gravity Data: GEM-T3 and GEM-T3S’, *Journal of Geophysical Research*, 99, 82, 2815–39.
- Narimanov G S and Tihonov M K (1972) *Bases of the Theory of Flight of Space Vehicles*. Moscow; Mashinostroenie (in Russian).
- Paul B (1963) ‘Planar Librations of an Extensible Dumbbell Satellite’, *AIAA Journal*, 1, 2, 411–18.
- Shilov A A and Vasiliev A F (1971) ‘Dynamic Stability of Spatial Motion of Flying Vehicle on the Big Angles of Attack of Inertionno-Aerodynamic Asymmetry’ (in Russian), *TsAGI Transactions*, vol. 1345.
- Sidorov I M (2000) ‘About Application of Tether Systems for Creation of Constantly Operating Transport Channel

- in Space' (in Russian), *Polyot* ('Flight'), ISSN 1684–1301, 8, 36–9.
- Tapley B D, Watkins M M, Ries J C, Davis G W, Eanes R J, Poole S R, Rim H J, Schutz B E, Shum C K, Nerem R S, Lerch F J, Marshall J A, Klosko S M, Pavlis N K and Williamson R G (1996) 'The Joint Gravity Model 3', *Journal of Geophysical Research*, 101, 28029–49.
- Taylor J R (2005) *Classical Mechanics*. University Science Books, [www.uscibooks.com](http://www.uscibooks.com)
- Williams P, Hyslop A, Stelzer M and Kruijff M (2009) 'YES2 Optimal Trajectories in the Presence of Eccentricity and Aerodynamic Drag', *Acta Astronautica*, 64, 7–8, 745–69.
- Williams P (2003) 'Tethered Planetary Capture: Controlled Maneuvers', *Acta Astronautica*, 53, 681–708.



## Conclusion

The mechanics of space tether systems is an extensive area of the modern mechanics of space flight. In this book we have tried to show on the one hand a variety of tasks and areas of research related with space tether systems, and on the other, their practical feasibility based on modern technology, and their ability to solve existing problems.

In one book it is impossible to answer all questions related with dynamics of space cable systems. Therefore, we have tried to focus on problems that may find wide application in the coming decades: the delivery of cargo from an orbit without the cost of rocket fuel, exploring the atmosphere and surface of the Earth by a subsatellite lowered on a tether. The specificity of these problems require us to create new mathematical models that take into account the interaction of the tether with the atmosphere and the movement around the centre of the mass of the spacecraft. Practical implementation cannot be made without assessment of potential emergencies and their consequences. Therefore, we have developed models that take into account various abnormal situations. Presented in the book, models and analytical results were used in the preparation and post-flight analysis of the international experiment YES2.

The study of chaotic behaviour of a mechanical system in space is a relatively new direction of tether system's mechanics. The presence of orbital eccentricity and the phenomenon of elasticity of tethers are the cause of the chaos

in space tether system's motion. Chaos can be a serious obstacle to the successful implementation of the space missions, because it can lead to off-normal operation of the system and to accidents. Using the methods of chaotic dynamics allows us to carry out a selection of space tether system parameters that preclude the possibility of chaos.

Another new trend that is discussed in detail in the book, is the study of dynamics of motion, relative to the centre of mass of the spacecraft with an attached tether. Tether systems have a significant influence on spacecraft dynamics, despite the low weight of the tether and tethered payload in comparison with the mass of the spacecraft. In some cases the spacecraft can be observed swinging with a subsequent transition into the rotation. New analytical solutions describing the plane vibrations of the spacecraft are illustrated in the book. These solutions can be used for quick calculations and qualitative analysis of the spacecraft motion with a tether.

The authors wish to thank the readers for their patience. We hope that the book will not only broaden your horizons, but will also arouse an interest in further study of the dynamics of space tether systems.

## Motion of a spacecraft with a tethered payload

**Abstract:** The third chapter is devoted to examination of the influence of tether systems with an attached payload on the base spacecraft's motion concerning its centre of mass. The mathematical model of the STS motion is developed. For a case of a slow modification of the tether's tension force and an angle of deflection of a tether from the vertical, the approximate analytical solutions and also the formula for an estimate of microaccelerations on board the spacecraft are obtained. The spacecraft's motion, taking into account activity of the attitude engines, is studied. The analysis of the influence of elasticity of the tether on the base spacecraft's motion is carried out.

**Key words:** spacecraft with tethered payload; vertical tether; analytical solution for tether oscillation; additional acceleration; adiabatic invariant.

In the latest astronautics, multipurpose spacecrafts are widely used. During flight they conduct a great number and variety of technological operations and experiments. Some of them have hard constraint parameters of the spacecraft's motion such as its orientation, the angular velocity and the level of microaccelerations.

This chapter is devoted to the study of the tether system's influence on the motion of the spacecraft. We will consider a STS that consists of the base spacecraft, the tether and the

payload attached to it. On the spacecraft, the deployment gear controlling the tension force of the tether is mounted. As the tether's outlet point does not coincide with the spacecraft's centre of mass, the moment of tether tension acts on the spacecraft. Under the influence of this moment, the spacecraft oscillates around the centre of mass with a variable frequency and amplitude. This, in turn, can lead to the appearance of additional microaccelerations on board and be a serious obstacle for the conducted experiments.

The results given in this chapter can be used to estimate the influence of the tether deployment, intended for delivery of a payload to the Earth, on the angular motion of the base spacecraft.

### 3.1 Mathematical model of a base spacecraft with a tethered payload

In the majority of the works devoted to space tether systems, the studied objects are the tether and the connected payload, and a spacecraft is considered as a particle (Beletsky and Levin, 1993; Sazonov, 2006; Misra, 2008). In some cases, such simplification is quite reasonable, as the spacecraft's mass considerably exceeds the mass of the tether and the payload, and its size is much less than the tether length. Under such circumstances, the tether weakly influences the spacecraft's centre of mass motion, and the attitude motion of the spacecraft concerning its centre of masses on the payload position. As for us, our basic interest represents the motion of the spacecraft under the influence of the tether's tension, so such simplification is unacceptable.

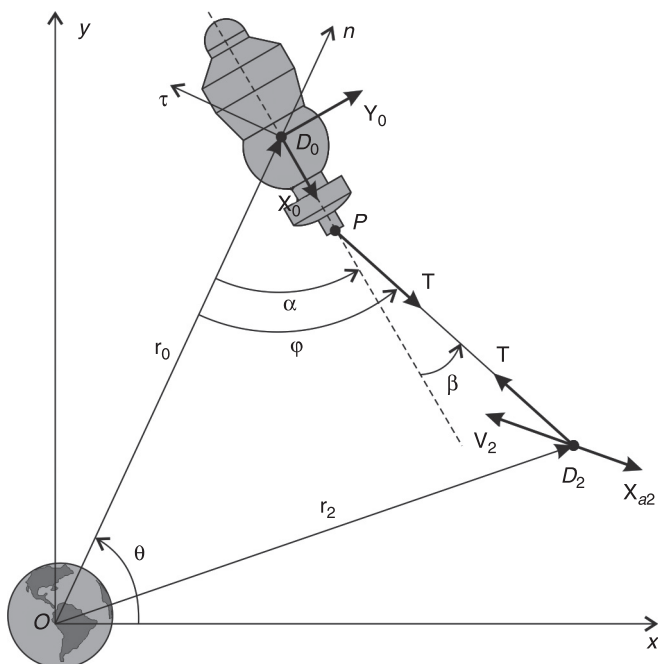
Let us construct the mathematical model describing the motion around the centres of mass of the spacecraft with a tether system of variable length. Defining the influence on

the STS motion is provided by gravitational and Coriolis forces which lie in the orbital plane. Numerical calculations show that for this type of system the amplitude of out-of-plane oscillations is many times less than the amplitude of in-plane oscillation (Aslanov et al., 2007). Therefore the motion of the STS can be considered as flat.

The question of selection of a tether model is important. As the studied object is the spacecraft, therefore we will use the elementary model of a massless, thin, elastic bar.

We will examine the mechanical system shown in Figure 3.1. As we did in section 2.4, we will assume that  $r \gg l$ . In this case, it is possible to consider approximately that  $\theta_0 \approx \theta_1 \approx \theta$ . The angle  $\varphi$  in Figure 3.1 does not coincide

**Figure 3.1** Base spacecraft with a tethered payload



with a corresponding corner  $\varphi$  in Figure 2.12. We did not introduce a new label as in the case of concurrence of the angles  $\theta$ , as the angles  $\varphi$  also coincide.

Let us write the Lagrangian [2.81], using expressions [2.69] and [2.96]:

$$\begin{aligned} L = & \frac{1}{2}m(\dot{r}^2 + r^2\dot{\theta}^2) + \frac{I_z(\dot{\alpha} + \dot{\theta})^2}{2} + \frac{m_0m_2}{2m}(\Delta^2(\dot{\alpha} + \dot{\theta})^2 \\ & + 2\Delta(\dot{\alpha} + \dot{\theta})(l(\dot{\varphi} + \dot{\theta})\cos(\alpha - \varphi) - \dot{l}\cos(\alpha - \varphi)) \\ & + \dot{l}^2 + l^2(\dot{\varphi} + \dot{\theta})^2) - \frac{\mu m}{r} - \frac{\mu}{2r^3} \frac{m_0m_2l^2}{m} (1 - 3\cos^2 \varphi) \\ & - \frac{3\mu}{2r^3}(I_x - I_y)\cos^2 \alpha. \end{aligned} \quad [3.1]$$

In the Lagrangian [3.1], the term caused by action of the potential force of the tether elasticity is absent. This force will be included in the nonpotential control force created by the deployment gear.

The right side of the Lagrange equations [2.82] includes the generalised nonpotential forces  $Q_j$ . We determine them as coefficients of variations of the generalised forces in the expression for the elementary work.

$$\delta A = \sum_{v=1}^N \mathbf{F}_v \cdot \delta \mathbf{r}_v + \sum_{v=1}^N \mathbf{M}_v \cdot \delta \boldsymbol{\varphi}_v = \sum_j Q_j \delta q_j, \quad [3.2]$$

where  $v$  – index of the body of the mechanical system;  $j$  – index of the generalized coordinate;  $\mathbf{F}_v$  – resultant force acting on a point  $v$ ;  $\mathbf{M}_v$  – resultant moment acting on a point  $v$ ;  $\delta \mathbf{r}_v$ ,  $\delta \boldsymbol{\varphi}_v$  – variation of the radius vector and the angle of turn of the body; and  $\delta q_j$  – variation of the generalized coordinate.

Let us pick out three points in the mechanical system:  $v = D_0, D_2, P$ ,  $\mathbf{F}_0, \mathbf{F}_2, \mathbf{F}_P$  – resultant force acting to these

points,  $\mathbf{r}_0, \mathbf{r}_2, \mathbf{r}_p$  – their radius vectors. The aerodynamic force  $\mathbf{F}_{A0}$  is applied to point  $D_0$ . Its force has the tangential and normal component in the body coordinate system connected with the spatial angle of attack:

$$X_0 = q_0 S_0 c_t, Y_0 = q_0 S_0 c_n,$$

where  $S_0$  – spacecraft's frontal area;  $q_0$  – dynamic pressure of the spacecraft.

The dimensionless aerodynamic coefficients  $c_t, c_n$  depend on the shape of the spacecraft, and they are functions of the angle between the spacecraft's axis and a vector of velocity of an incident flow. In coordinate system  $Oxy$ , related to the centre of the Earth, the aerodynamic force has coordinates:

$$\begin{aligned} \mathbf{F}_0 = \mathbf{F}_{A0} &= \begin{bmatrix} X_0 \sin(\alpha + \theta - \frac{\pi}{2}) + Y_0 \cos(\alpha + \theta - \frac{\pi}{2}) \\ -X_0 \cos(\alpha + \theta - \frac{\pi}{2}) + Y_0 \sin(\alpha + \theta - \frac{\pi}{2}) \end{bmatrix} \\ &= \begin{bmatrix} -X_0 \cos(\alpha + \theta) + Y_0 \sin(\alpha + \theta) \\ -X_0 \sin(\alpha + \theta) - Y_0 \cos(\alpha + \theta) \end{bmatrix}. \end{aligned}$$

Besides the aerodynamic forces, the pitching moment also acts on the spacecraft

$$M_z = m_{zsp} q_0 S_0 L_0,$$

where  $m_{zsp}$  – coefficients of pitching moment; and  $L_0$  – characteristic dimension of the spacecraft.

Control force  $T$  is enclosed to point  $P$ :

$$\mathbf{F}_P = \begin{bmatrix} T \sin(\varphi + \theta - \frac{\pi}{2}) \\ -T \cos(\varphi + \theta - \frac{\pi}{2}) \end{bmatrix} = \begin{bmatrix} -T \cos(\varphi + \theta) \\ -T \sin(\varphi + \theta) \end{bmatrix}.$$

Similarly, the module force is enclosed to a point  $D_2$ . The aerodynamic force is also enclosed to this point. We will consider the payload as the homogeneous sphere. In this case, the aerodynamic force acting on it has only the tangential component  $X_{a2}$  corresponding to the frontal resistance. This force is directed opposite to the vector of velocity.

$$X_{a2} = q_2 S_2 c_{xa},$$

where  $S_0$  – payload's frontal area;  $q_0$  – dynamic pressure of the payload.

For the sphere  $c_{xa} = 1$ . We write down force  $X_{a2}$  in projections to axes of  $Oxy$ :

$$\mathbf{X}_{a2} = \begin{bmatrix} -q_2 S_2 c_{xa} \frac{V_{2x}}{V_2} \\ -q_2 S_2 c_{xa} \frac{V_{2y}}{V_2} \end{bmatrix} = \begin{bmatrix} X_2 \\ Y_2 \end{bmatrix},$$

where  $\mathbf{V}_2 = [V_{2x}, V_{2y}]^T$  – vector of velocity of the payload whose coordinates can be found by means of [2.68], as:

$$\mathbf{V}_2 = \dot{\mathbf{r}}_2.$$

Considering the last expression, the vector of the resultant force enclosed to a point  $D_2$  takes the form:

$$\mathbf{F}_2 = \begin{bmatrix} T \cos(\varphi + \theta) - q_2 S_2 c_{xa} \frac{V_{2x}}{V_2} \\ T \sin(\varphi + \theta) - q_2 S_2 c_{xa} \frac{V_{2y}}{V_2} \end{bmatrix}.$$

Let us find the variations  $\delta\mathbf{r}_0$ ,  $\delta\mathbf{r}_2$ ,  $\delta\mathbf{r}_p$ , using expressions [2.66] and [2.68] and considering that  $\mathbf{r}_p = \mathbf{r}_0 + \Delta$ :

$$\begin{aligned}\delta \mathbf{r}_0 &= \begin{bmatrix} \delta r \cos \theta - \delta \theta r \sin \theta - \bar{m}_2 \Delta \sin(\alpha + \theta)(\delta \alpha + \delta \theta) \\ + \bar{m}_2 \delta l \cos(\varphi + \theta) - \bar{m}_2 l \sin(\varphi + \theta)(\delta \varphi + \delta \theta) \\ \delta r \sin \theta + \delta \theta r \cos \theta + \bar{m}_2 \Delta \cos(\alpha + \theta)(\delta \alpha + \delta \theta) \\ + \bar{m}_2 \delta l \sin(\varphi + \theta) + \bar{m}_2 l \cos(\varphi + \theta)(\delta \varphi + \delta \theta) \end{bmatrix}, \\ \delta \mathbf{r}_p &= \begin{bmatrix} \delta r \cos \theta - \delta \theta r \sin \theta + \bar{m}_2 \delta l \cos(\varphi + \theta) - \bar{m}_2 l \sin(\varphi + \theta)(\delta \varphi + \delta \theta) \\ + \bar{m}_0 \Delta \sin(\alpha + \theta)(\delta \alpha + \delta \theta) \\ \delta r \sin \theta + \delta \theta r \cos \theta + \bar{m}_2 \delta l \sin(\varphi + \theta) + \bar{m}_2 l \cos(\varphi + \theta)(\delta \varphi + \delta \theta) \\ - \bar{m}_0 \Delta \cos(\alpha + \theta)(\delta \alpha + \delta \theta) \end{bmatrix}, \\ \delta \mathbf{r}_2 &= \begin{bmatrix} \delta r \cos \theta - \delta \theta r \sin \theta + \bar{m}_0 \Delta \sin(\alpha + \theta)(\delta \alpha + \delta \theta) - \bar{m}_0 \delta l \cos(\varphi + \theta) \\ + \bar{m}_0 l \sin(\varphi + \theta)(\delta \varphi + \delta \theta) \\ \delta r \sin \theta + \delta \theta r \cos \theta - \bar{m}_0 \Delta \cos(\alpha + \theta)(\delta \alpha + \delta \theta) - \bar{m}_0 \delta l \sin(\varphi + \theta) \\ - \bar{m}_0 l \cos(\varphi + \theta)(\delta \varphi + \delta \theta) \end{bmatrix}.\end{aligned}$$

Substituting the found variations  $\delta \mathbf{r}_0$ ,  $\delta \mathbf{r}_2$ ,  $\delta \mathbf{r}_p$  and the vectors  $\mathbf{F}_0$ ,  $\mathbf{F}_2$ ,  $\mathbf{F}_p$  in [3.2], after a series of transformations we obtain the generalised forces as coefficients of the corresponding variations of the generalised coordinates:

$$\begin{aligned}\mathcal{Q}_l &= -T - \bar{m}_2 (X_0 \cos(\alpha - \varphi) - Y_0 \sin(\alpha - \varphi)) \\ &\quad + \bar{m}_0 (X_2 \cos(\varphi + \theta) + Y_2 \sin(\varphi + \theta)), \\ \mathcal{Q}_\theta &= M_z - (\bar{m}_2 L \sin(\alpha - \varphi) + r \sin \alpha) X_0 \\ &\quad - (\bar{m}_2 L \cos(\alpha - \varphi) + r \cos \alpha + \bar{m}_2 \Delta) Y_0 \\ &\quad + (-\bar{m}_0 \Delta \sin(\alpha + \theta) - \bar{m}_0 L \sin(\varphi + \theta) + r \sin \theta) X_2 \\ &\quad + (\bar{m}_0 \Delta \cos(\alpha + \theta) + \bar{m}_0 L \cos(\varphi + \theta) - r \cos \theta) X_2, \quad [3.3] \\ \mathcal{Q}_\alpha &= M_z - \bar{m}_2 \Delta Y_0 - \bar{m}_0 \Delta (X_2 \sin(\alpha + \theta) - Y_2 \cos(\alpha + \theta)), \\ \mathcal{Q}_\varphi &= \bar{m}_0 L (Y_2 \cos(\varphi + \theta) - X_2 \sin(\varphi + \theta)) \\ &\quad - \bar{m}_2 L (Y_0 \cos(\alpha - \varphi) - X_0 \sin(\alpha - \varphi)), \\ \mathcal{Q}_r &= -X_0 \cos \alpha + Y_0 \sin \alpha - X_2 \cos \theta - Y_2 \sin \theta.\end{aligned}$$

Substituting [3.2] and [3.3] in [2.82] we obtain the equations of motion of the STS with a variable length tether in the atmosphere.

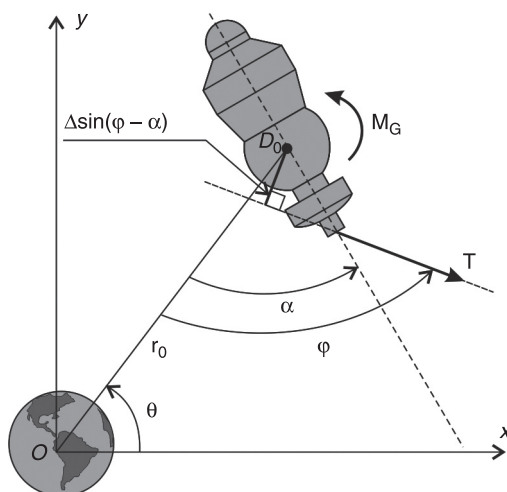
Let us consider the spacecraft separately from the tether and the payload. We will assume that its mass essentially exceeds the tether and the payload masses, and it moves in a circular orbit. In this case, according to [2.103], the motion of the centre of mass of the spacecraft is described by the equations:

$$\dot{\theta} = \sqrt{\frac{\mu}{r^3}} = \omega, \quad r = \text{const.} \quad [3.4]$$

To obtain an equation of the motion of the spacecraft concerning its centre of mass, we will use the theorem of the change of the moment of momentum (Taylor, 2005) in a projection to an axis  $D_0z$ , with perpendicular planes  $Oxy$  (see Figure 3.2):

$$\dot{K}_z = M_T + M_G, \quad [3.5]$$

**Figure 3.2** The arm of the tension force



where  $K_z = I_z(\dot{\alpha} + \omega)$  – moment of momentum of spacecraft concerning axis  $D_0z$ ;  $M_G = 3\omega^2(I_x - I_y)\sin\alpha\cos\alpha$  – gravitational moment (Beletsky, 1965); and  $M_T = T\Delta\sin(\varphi - \alpha)$  – the moment of tension force of the tether concerning  $D_0z$ .

Let us enter the coefficients

$$\Omega^2 = \frac{T(t)\Delta}{I_z}, \quad \kappa = \frac{3\omega^2(I_x - I_y)}{2I_z}. \quad [3.6]$$

With the help of [3.4], the moments  $M_G$  and  $M_T$  can be written as:

$$M_T = I_z\Omega^2\sin(\varphi - \alpha), \quad M_G = I_z\kappa\sin 2\alpha. \quad [3.7]$$

Let us substitute the derivative  $\dot{K}_z = I_z\ddot{\alpha}$  and the moments [3.7] into [3.5]. After simple transformations we will obtain the equation of motion of the spacecraft concerning its centre of mass.

$$\ddot{\alpha} = \Omega^2\sin(\varphi - \alpha) + \kappa\sin 2\alpha, \quad [3.8]$$

In equation [3.8], as well as  $\alpha$  it includes an angle  $\varphi$ . Therefore to the equations [3.7] it is necessary to add the equations [3.4], and the Lagrange equations:

$$\begin{aligned} \ddot{l} &= \Delta(\dot{\alpha} + \omega)^2\cos(\alpha - \varphi) + \frac{3}{4}\Delta\omega^2(I_x - I_y)(\cos(\alpha + \varphi) \\ &\quad - \cos(3\alpha - \varphi)) + l(\dot{\varphi} + \omega)^2 - \frac{\Delta^2T}{I_z}\sin^2(\alpha - \varphi) \\ &\quad - \frac{mT}{m_0m_2} + \omega^2l(3\cos^2\varphi - 1), \\ \ddot{\varphi} &= \frac{\Delta^2T}{I_z}\sin(\alpha - \varphi)\cos(\alpha - \varphi) \\ &\quad - \frac{1}{l}\left(\frac{3}{4}\Delta\omega^2(I_x - I_y)(\sin(3\alpha - \varphi) + \sin(\alpha + \varphi))\right. \\ &\quad \left.+ 2l(\dot{\varphi} + \omega) - \Delta\sin(\alpha - \varphi)(\dot{\alpha} + \omega)^2\right) - 3\omega^2\cos\varphi\sin\varphi. \end{aligned} \quad [3.9]$$

If the tether is deployed on enough length, the motion of the spacecraft concerning its centres of mass will make little impact on the payload motion. In this case, it is possible to simplify the equations [3.9] by means of representation of the spacecraft as particle ( $\Delta = 0$ ).

$$\begin{aligned}\ddot{l} &= l(\dot{\varphi} + \omega)^2 - \frac{mT}{m_0 m_2} + \omega^2 l(3 \cos^2 \varphi - 1), \\ \ddot{\varphi} &= -\frac{2\dot{l}(\dot{\varphi} + \omega)}{l} - 3\omega^2 \cos \varphi \sin \varphi.\end{aligned}\quad [3.10]$$

The equations [3.4], [3.8] and [3.10] form the simplified system which approximately describes the STS dynamics. The given system is unsuitable for exact calculations; however, with its help it is possible to obtain the analytical results qualitatively characterising the motion of a mechanical system. The remarkable feature of the equations [3.10] is their lack of a variable on their right side. It allows for integration of the equations [3.10] separately from [3.8].

## 3.2 Analytical solution in case of a slow changing of the parameters

Let us suppose that the tether's tension force and an angle between the line of action of the tension force and the local vertical are slowly changing functions:

$$T = T(\tau), \quad \varphi = \varphi(\tau),$$

where  $\tau = \varepsilon t$  – slow time; and  $\varepsilon$  – small parameter.

We will consider a case when the gravitational moment is substantially less than the moment of tether tension. We will assign to the gravitational moment an order of smallness  $\varepsilon$ , than the equation [3.8]:

$$\ddot{\alpha} + \omega^2(\tau) \sin(\alpha - \varphi(\tau)) = -\varepsilon \kappa \sin 2\alpha, \quad [3.11]$$

where  $\varepsilon \kappa = \frac{3}{2} \omega^2 (I_y - I_x) / I_z$ .

Let us rewrite the equation of the perturbed motion of the spacecraft concerning its centre of mass in the form:

$$\ddot{\alpha} + \eta(\tau) \sin \alpha - v(\tau) \cos \alpha = -\varepsilon \kappa \sin 2\alpha = \varepsilon \Phi(\alpha), \quad [3.12]$$

$$\eta(\tau) = \omega^2(\tau) \cos \varphi(\tau), \quad v(\tau) = \omega^2(\tau) \sin \varphi(\tau). \quad [3.13]$$

At  $\varepsilon = 0$  we obtain the equation of the unperturbed motion:

$$\ddot{\alpha} + \eta \sin \alpha - v \cos \alpha = 0, \quad [3.14]$$

where  $\eta, v$  – some constants.

Let us find a general solution of the equation [3.14]. This equation has the first integral as an energy integral:

$$\frac{\dot{\alpha}^2}{2} - \eta \cos \alpha - v \sin \alpha = h. \quad [3.15]$$

We will consider only an oscillative motion which is made between the two positions:  $\alpha_1 = \alpha_{\min}$  and  $\alpha_2 = \alpha_{\max}$ . We will choose the following initial conditions:  $t = 0, \alpha_0 = \alpha_2, \dot{\alpha}_0 = 0$ , and then from [3.15] we have:

$$h = -\eta \cos \alpha_2 - v \sin \alpha_2. \quad [3.16]$$

Taking into account [3.16], we rewrite [3.15] as follows:

$$\dot{\alpha}^2 = a + b \sin \alpha + c \cos \alpha = f(\alpha), \quad [3.17]$$

where  $a = 2h, b = 2v$ ; and  $c = 2\eta$ .

Let us note that  $\alpha_1 = \alpha_{\min}$  and  $\alpha_2 = \alpha_{\max}$  are roots of the equation  $f(\alpha) = 0$ . Separating the variables in [3.17] we obtain the quadrature:

$$t = - \int_{\alpha_2}^{\alpha} \frac{d\alpha}{\sqrt{f(\alpha)}}. \quad [3.18]$$

We use substitution of variables (Gradshteyn and Ryzhik, 2000):

$$\alpha = 2\psi + \delta, \quad [3.19]$$

where  $\delta = \arctan(b/c) = \arctan(v/\eta) = \varphi$  for calculation of integral [3.18]:

$$t = -\frac{2}{\sqrt{a+p}} \int_{\psi_2}^{\psi} \frac{d\psi}{\sqrt{1-q^2 \sin^2 \psi}}, \quad [3.20]$$

$$p = \sqrt{b^2 + c^2}, \quad q^2 = \frac{2p}{a+p}. \quad [3.21]$$

From formulas [3.13], [3.16] and [3.17], it follows that the module is always equal to or greater than one:

$$q^2 = \frac{1}{\sin^2(\frac{\varphi - \alpha_2}{2})} \geq 1. \quad [3.22]$$

Let us reduce the elliptic integral [3.20] in a normal form with the  $q$  module which does not exceed one, and for this purpose we use a new replacement:

$$\sin \psi = \frac{1}{q} \sin \gamma, \quad [3.23]$$

As a result we obtain:

$$\omega t = - \int_{\pi/2}^{\gamma} \frac{d\gamma}{\sqrt{1-k^2 \sin^2 \gamma}}, \quad [3.24]$$

$$\omega(\tau) = \sqrt{\frac{p}{2}} = \sqrt{T(\tau) \frac{\Delta}{C}}, \quad [3.25]$$

$$k^2 = \frac{1}{q^2} = \sin^2\left(\frac{\varphi - \alpha_{1,2}}{2}\right). \quad [3.26]$$

Introducing the Jacobi amplitude function (Jahnke et al., 1960), we can rewrite equation [3.24] as follows:

$$\gamma = \operatorname{am}(K(k) - \omega t, k),$$

where  $K(k) = \int_0^{\pi/2} (1 - k^2 \sin^2 y)^{-1/2} dy$  – the complete elliptic integral of the first kind.

Further, by means of replacements [3.19] and [3.23] we will obtain the general solution of the equation of the unperturbed motion [3.14] in the form:

$$\alpha = \varphi - 2 \arcsin(\operatorname{sn}(\omega t - K(k), k)), \quad [3.27]$$

where  $\operatorname{sn}(u, k) = \sin(\operatorname{am}(u, k))$  – elliptic sine.

The solution [3.27] can be simplified by means of approximation of the elliptic sine by the elementary functions (Jahnke et al. 1960):

$$\operatorname{sn}(u, k) \approx \sin y(1 + 4d \cos^2 y)$$

where  $d = \exp\left(-\pi \frac{K(k')}{K(k)}\right)$ ;  $y = \frac{\pi u}{2K(k)}$ ; and  $k' = \sqrt{1 - k^2}$  – the complementary module.

Let us obtain an action integral (Volosov, 1963) for the perturbed system with slowly changing parameters [2.3]. It is possible to present it in two forms which are accurate within a factor:

$$I(\tau) = \int_t^{t+T_\alpha} \dot{\alpha}^2 dt = 2 \int_{\alpha_1}^{\alpha_2} \dot{\alpha} d\alpha, \quad [3.28]$$

where  $T_\alpha = 4K(k)/\omega$  – period of oscillation of variable  $\alpha$  on time  $t$ .

The behaviour of the action integral for the perturbed system [3.12] is defined by an average differential equation of a form (Volosov, 1963):

$$\dot{I} = \varepsilon \int_t^{t+T_\alpha} \Phi_\alpha(\alpha) \dot{\alpha} dt, \quad [3.29]$$

The subintegral expression on the right side of the equation [3.29] owing to a solution [3.27] is an odd periodic function

of time, therefore the right side is converted to zero, and the action integral [3.28] keeps its value. It is an adiabatic invariant of the perturbed motion:

$$I = \text{const.} \quad [3.30]$$

Let us write the action integral [3.28] by means of [3.17] in the form:

$$I = 2 \int_{\alpha_1}^{\alpha_2} \dot{\alpha} d\alpha = 2 \int_{\alpha_1}^{\alpha_2} \sqrt{f(\alpha)} d\alpha.$$

With the help of sequential replacements [3.19] and [3.23], we have:

$$I = 16\omega \int_0^{\pi/2} \frac{\cos^2 \gamma d\gamma}{\sqrt{1 - k^2 \sin^2 \gamma}}.$$

With this integral, after simple transformations, it is possible to lead to a linear combination of the complete elliptic integrals of the first and second kind:

$$I = 16\omega [E(k) - (1 - k^2)K(k)], \quad [3.31]$$

where  $E(k) = \int_0^{\pi/2} (1 - k^2 \sin^2 \gamma)^{1/2} d\gamma$  – complete elliptic integrals of the second kind.

The perturbed motion magnitude of the tether's tension force and its direction are known to be slowly changing functions. It is obvious that the peak values of an angle of deflection of the spacecraft's axis from the local vertical  $\alpha_1 = \alpha_{\min}$ ,  $\alpha_2 = \alpha_{\max}$  will slowly vary too. If one value is known, for example  $\alpha_2 = \alpha_{\max}$ , another value  $\alpha_1 = \alpha_{\min}$  can be found by the equation:

$$h(\alpha_1) = h(\alpha_2), \quad [3.32]$$

where  $h = -\eta \cos \alpha - v \sin \alpha$ .

The formula establishes a connection between the frequency  $\omega$  and the module  $k$ . According to [3.25] and

[3.26], the frequency  $\omega$  depends upon a known force  $T(\tau)$ , and the module  $k$  depends upon a known angle  $\varphi(\tau)$  and an unknown amplitude  $\alpha_m$  ( $\alpha_1 = \alpha_{\min}$  or  $\alpha_2 = \alpha_{\max}$ ). In other words, the formula [3.31] represents an implicit dependence of the amplitude  $\alpha_m$  on known functions. We will use the method given by Aslanov (2004) and find the approximate analytical dependence of the spacecraft's oscillation amplitude on slow time  $\tau$  in an explicit form. We will consider separately the expression standing in square brackets in [3.31]:

$$D = [E(k) - (1 - k^2)K(k)] \quad [3.33]$$

Let us use the known expansion formulas for the full elliptic integrals of the first and second kind into a power series (Jahnke et al. 1960) to present the expression [3.33] in the form:

$$D = \frac{\pi}{2} \left\{ \frac{1}{2} k^2 + \left( \frac{1}{2} \right)^2 \frac{k^4}{4} + \dots + \left[ \frac{1 \cdot 3 \dots (2i-3)}{2 \cdot 4 \dots (2i-2)} \right] \frac{k^{2i}}{2i} + \dots \right\}. \quad [3.34]$$

Further, from [3.32]–[3.34] we have:

$$\frac{h}{\omega} = k^2 + \frac{k^4}{8} + \dots + \left[ \frac{3 \cdot 5 \dots (2i-3)}{4 \cdot 6 \dots (2i-2)} \right] \frac{k^{2i}}{2i} + \dots, \quad [3.35]$$

where  $h = \text{const}$ .

Let us make an ascending power series inversion (Dwight, 1957):

$$k^2 = \frac{h}{\omega} - \frac{1}{2\pi} \left( \frac{h}{\omega} \right)^2 - \frac{1}{4\pi^2} \left( \frac{h}{\omega} \right)^3 - \dots \quad [3.36]$$

Comparing relations [3.26] and [3.36], we obtain the expression for the minimum and maximum angle of deflection of the spacecraft from a local vertical:

$$\alpha_{1,2} = \varphi(\tau) \mp 2 \arcsin \sqrt{\frac{h}{\omega(\tau)} - \frac{1}{2\pi} \left[ \frac{h}{\omega(\tau)} \right]^2 - \frac{1}{4\pi^2} \left[ \frac{h}{\omega(\tau)} \right]^3 - \dots} \quad [3.37]$$

If it is to be limited to two members in expansion [3.35], it is possible to obtain a more simple formula:

$$\alpha_{1,2} = \varphi(\tau) \mp 2 \arcsin 2 \sqrt{\sqrt{1 + \frac{b}{\omega(\tau)}} - 1}. \quad [3.38]$$

### 3.3 The approximate analytical solutions in the variables of the amplitude-phase

Let us consider a case when the moment of the tension force sizeably exceeds the gravitational moment, so that the condition is satisfied:

$$\Omega^2 \gg |\kappa|. \quad [3.39]$$

Let us introduce a vector:

$$\mathbf{z} = [\theta, r, \varphi, l, \dot{\varphi}, \dot{l}]^T,$$

which defines parameters of the spacecraft's motion, and also a deflection angle, the length of the tether and their derivatives. Let the components of this vector change slowly:

$$\dot{\mathbf{z}} = O(\varepsilon), \quad [3.40]$$

where  $\varepsilon$  – small parameter.

At performance of the conditions [3.39] and [3.40], the system of equations [3.4], [3.8] and [3.10] is reduced to a perturbed system with one fast variable:

$$\begin{cases} \ddot{\alpha} + \Omega(\mathbf{z})^2 \sin(\alpha - \varphi) = \varepsilon \Phi_\alpha(\mathbf{z}, \alpha), \\ \dot{\mathbf{z}} = \varepsilon \Phi_z(\mathbf{z}), \end{cases} \quad [3.41]$$

where  $\varepsilon \Phi_\alpha(\mathbf{z}, \alpha) = \kappa(\mathbf{z}) \sin 2\alpha$ ; and  $\varepsilon \Phi_z(\mathbf{z})$  – right sides of equations [3.4] and [3.8].

The equations for the slow variable  $z$  in the system [3.12] do not contain fast variable  $\alpha$  and can be integrated separately.

Let us make the replacement  $\beta = \varphi - \alpha$  in the perturbed system [3.41]:

$$\begin{cases} \ddot{\beta} + \Omega^2(z) \sin(\beta) = \varepsilon \Phi_\beta(z, \beta), \\ \dot{z} = \varepsilon \Phi_z(z), \end{cases} \quad [3.42]$$

where

$$\varepsilon \Phi_\beta(z, \beta) = \ddot{\varphi} - \kappa(z) \sin(2\varphi - 2\beta). \quad [3.43]$$

The angle  $\beta$  is an angle of the deflection of the spacecraft's longitudinal axis from the line of action of the tension force (see Figure 3.1).

In the first equation of system [3.42], the term  $\Omega^2(z) \sin(\beta)$  represents the restoring moment of the tether's tension accurate to within a factor. In the right side of the equation [3.43], the first term is caused by non-uniformity of the tether deflection from a local vertical, and the second term is the gravitational moment acting on the spacecraft.

Let us consider that, throughout all movement, the angle  $\beta$  is small, then the system [3.42] will become:

$$\begin{cases} \ddot{\beta} + \Omega^2(z)\beta = \varepsilon \Phi_\beta(z, \beta), \\ \dot{z} = \varepsilon \Phi_z(z). \end{cases} \quad [3.44]$$

At  $\varepsilon = 0$  the perturbed system [3.44] is reduced to one equation of the unperturbed motion

$$\ddot{\beta} + \Omega^2 \beta = 0, \quad [3.45]$$

where  $\Omega = \text{const}$ .

Let us name [3.45] a generating equation for system [3.44], and let us use the Van der Pol method (Mitropolsky and Dao, 1999). For this purpose we write a solution of the equation [3.45] in the form:

$$\beta = \xi \cos \eta, \quad [3.46]$$

where  $\eta = \Omega t + \eta_0$ ; and  $\xi$ , and  $\eta_0$  – arbitrary constants.

The equation [3.46] describes the oscillations with a frequency  $\Omega$ . Magnitude  $\xi$  is called the amplitude, and the function  $\eta(t)$  is called the phase. In case of small values  $\varepsilon$ , the solution of the first equation [3.44] describes the oscillating process of a view [3.46], but the amplitude of this process varies more slowly when  $\varepsilon$  is less. The frequency  $\Omega$  also changes in time. Thus, if in each moment of time investigated, the process has an oscillating character then it is defined completely by the instantaneous values of its amplitude  $\xi$  and the phase  $\eta$ . For this reason the amplitude and the phase can be accepted as the new variables describing the process.

The transition in the equation [3.44] to the new variables amplitude-phase, we find the time derivative of equation [3.46], considering  $\xi$  and  $\eta$  as constants.

$$\dot{\beta} = -\xi \Omega \sin \eta \quad [3.47]$$

Let us build differential equations, in which the amplitude is  $\xi(t)$  and phase,  $\eta(t)$  describing a state of the perturbed system. Differentiating [3.46] and equating the result to [3.47], we obtain:

$$\frac{d}{dt}(\xi(t) \cos \eta(t)) = \dot{\xi} \cos \eta - \xi \dot{\eta} \sin \eta = -\Omega \xi \sin \eta,$$

whence we receive a condition of compatibility of the formulas [3.46] and [3.47]:

$$\dot{\xi} \cos \eta - \xi \dot{\eta} \sin \eta + \Omega \xi \sin \eta = 0. \quad [3.48]$$

Differentiating [3.47] and substituting the result in the first equation of [3.44], we obtain:

$$\begin{aligned} \ddot{\beta} &= -\dot{\xi} \Omega \sin \eta - \Omega \xi \dot{\eta} \cos \eta + \Omega^2 \xi \cos \eta \\ &= \varepsilon \Phi_\beta(z, \xi \cos \eta) - \Omega^2 \xi \cos \eta. \end{aligned} \quad [3.49]$$

The equations [3.48] and [3.49] represent a system of two equations of the first order concerning two unknown functions  $\xi(t)$  and  $\eta(t)$ . Resolving it around derivatives  $\dot{\xi}$  and  $\dot{\eta}$ , we obtain:

$$\begin{cases} \dot{\xi} = -\frac{1}{\Omega(\mathbf{z})} \left( \varepsilon \Phi_\beta(\mathbf{z}, \xi \cos \eta) \sin \eta + \dot{\Omega}(\mathbf{z}) \xi \sin^2 \eta \right), \\ \dot{\eta} = \Omega(\mathbf{z}) - \frac{1}{\Omega(\mathbf{z})} \left( \frac{\varepsilon \Phi_\beta(\mathbf{z}, \xi \cos \eta)}{\xi} \cos \eta + \dot{\Omega}(\mathbf{z}) \sin \eta \cos \eta \right), \end{cases} \quad [3.50]$$

where  $\dot{\Omega}(\mathbf{z}) = \frac{d\Omega}{dt} = \sum_{z_i} \frac{\partial \Omega}{\partial z_i} \dot{z}_i = \varepsilon \sum_{z_i} \left( \frac{\partial \Omega}{\partial z_i} \Phi_{z_i} \right)$ . Let us notice that the system [3.50] is completely equivalent to the first equation of the system [3.44].

The first equations of the system [3.50] show that the amplitude  $\xi$  changes slowly because its derivative is of the  $\varepsilon$  order of smallness. The right side of the second equation of [3.41] is of the single order of smallness, therefore a phase  $\eta$  is a fast variable. The right sides of the equations of the system are  $2\pi$ -periodic functions of the phase  $\eta$ .

As during one oscillation the amplitude and frequency vary a little, it is possible to expect that we do not make a big error if we substitute the right side of the system [3.50] by their average values over the phase. As a result, we will receive the truncated equations:

$$\begin{cases} \dot{\xi} = -\frac{\dot{\Omega}(\mathbf{z}) \xi}{2\omega(\mathbf{z})}, \\ \dot{\eta} = \Omega - \frac{1}{2\pi\xi\Omega(\mathbf{z})} \int_0^{2\pi} \varepsilon \Phi_\beta(\mathbf{z}, \xi \cos \eta) \cos \eta d\eta. \end{cases} \quad [3.51]$$

The described method is widely used in the theory of nonlinear oscillations.

The average equations [3.51] do not contain high-frequency components in the solution, therefore their

numerical integration can be made with one big step. Regardless that the slow and fast movements are separated, the second equation can be integrated after the solution for slow variables to be obtained. Often in practice it is enough to know the amplitude of oscillations. In such cases, the second equation of system [3.51] can generally be excluded from review.

Let us pass to the building of the approximate analytical solution. We write for the perturbed system [3.44] action integral:

$$I = \int_0^{2\pi} \Omega \frac{\partial \beta(\xi, \eta)}{\partial \eta} d\eta. \quad [3.52]$$

where  $\beta(\xi, \eta)$  is the solution of the generating equation [3.45]. We calculate an integral [3.52] using [3.46]:

$$I = \frac{1}{2\pi} \int_0^{2\pi} \Omega \xi^2 \sin^2 \eta d\eta = \frac{\Omega(z) \xi^2}{2}. \quad [3.53]$$

From the theory of oscillations, it is known that for the systems of the considered type the action integral is an adiabatic invariant (Mitropolsky and Dao, 1999), that is a function of the amplitude and the phase, the total time derivative calculated owing to the truncated equations is equal to zero. In other words, the adiabatic invariant is a function of the amplitude and the phase which varies more slowly than system parameters. Substituting solutions of the system [3.51] into [3.53], we obtain:

$$I = \frac{\Omega(z) \xi^2}{2} = \text{const.}$$

Let us calculate in some moment of time  $t = t_0$  the integral [3.53]:

$$I_0 = \frac{\Omega_0 \xi_0^2}{2}, \quad [3.54]$$

where  $\Omega_0 = \sqrt{\frac{T_0 \Delta}{I_z}}$ ,  $T_0 = T(t_0)$ ; and  $\xi_0$  – the value of amplitude

of the angle  $\beta$  in the moment  $t = t_0$ .

From [3.53], taking into account [3.54], we have in an explicit form the analytical expression for the amplitude of an angle of deflection of the spacecraft's longitudinal axis from a line of operation of the tether's tension force:

$$\xi(t) = \sqrt{\frac{2I_0}{\Omega(\mathbf{z}(t))}} = \left( \frac{4I_0^2 I_z}{T(t)\Delta} \right)^{1/4}$$

or

$$\xi(t) = \xi_0 \left( \frac{T_0}{T(t)} \right)^{1/4}. \quad [3.55]$$

### 3.4 Analytical solutions for small oscillations

In the case of slow changing of the force of the tether's tension and the angle between a line of operation of the tension force and the local vertical, the equation [3.8] can be written as:

$$\ddot{\alpha} + a(\tau) \sin \alpha - b(\tau) \cos \alpha + 2\kappa \sin \alpha \cos \alpha = 0, \quad [3.56]$$

where

$$a(\tau) = T(\tau) \frac{\Delta}{I_z} \cos \varphi(\tau), \quad [3.57]$$

$$b(\tau) = T(\tau) \frac{\Delta}{I_z} \sin \varphi(\tau).$$

We will be limited to reviewing the case when the module of the tether deflection angle from the vertical during its deployment is always less than the value  $\pi/2$  (payload is always below the spacecraft). In this case for the

variable factor entering into the equation [3.56] it is fairly unequal:

$$a(\tau) > 0.$$

Let us also suppose that the angle of deflection of the spacecraft's axis of symmetry from a local vertical is small, then:

$$\sin \alpha \approx \alpha, \quad \cos \alpha \approx 1,$$

and the equation [3.56] can be written as:

$$\ddot{\alpha} + (a(\tau) + 2\kappa)\alpha - b(\tau) = 0. \quad [3.58]$$

At the unperturbed motion ( $\varepsilon = 0$ ), factors  $a(\tau)$  and  $b(\tau)$  are constant, and the equation [3.58] has an energy integral. To obtain this, we transfer the second and third items [3.58] to the right side of the equation and we multiply all on  $d\alpha$ :

$$\ddot{\alpha}d\alpha = bd\alpha - (a + 2\kappa)\alpha d\alpha. \quad [3.59]$$

In consideration of:

$$\ddot{\alpha}d\alpha = \frac{d\dot{\alpha}}{dt}d\alpha = d\dot{\alpha}\frac{d\alpha}{dt} = \dot{\alpha}d\dot{\alpha} = \frac{1}{2}d\dot{\alpha}^2,$$

we take integrals from both sides of equation [3.59]:

$$\int \frac{1}{2}d\dot{\alpha}^2 = \int (b - (a + 2\kappa)\alpha)d\alpha.$$

As a result of taking the integrals, we receive an energy integral:

$$\frac{\dot{\alpha}^2}{2} + (a + 2\kappa)\frac{\alpha^2}{2} - b\alpha = h = \text{const}, \quad [3.60]$$

where  $a, b, \kappa, h$  – some constants.

Let us find a solution of the equation of the unperturbed motion, considering only what oscillates between two positions:  $\alpha_1 = \alpha_{\min}$  and  $\alpha_2 = \alpha_{\max}$ . We will choose the following initial conditions:

$$t = 0 : \quad \alpha_0 = \alpha_2, \quad \dot{\alpha}_0 = 0.$$

Then we have:

$$h = \Omega^2 \frac{\alpha_2^2}{2} - b\alpha_2, \quad [3.61]$$

where:

$$\Omega = \sqrt{a+c}. \quad [3.62]$$

Dividing the variables in the equation [3.60], we obtain:

$$t = - \int_{\alpha_2}^{\alpha_1} \frac{d\alpha}{\sqrt{a_0\alpha^2 + a_1\alpha + a_2}}, \quad [3.63]$$

where  $a_0 = -\Omega^2$ ,  $a_1 = 2b$ ,  $a_2 = 2h$ .

Let us calculate a quadrature [3.63] (Gradshteyn and Ryzhik, 2000):

$$\Omega t = \arcsin \left( \frac{b - \Omega^2 \alpha}{\sqrt{b^2 + 2h\Omega^2}} \right) \Big|_{\alpha_2}^{\alpha_1}.$$

Taking into account [3.61], we present the generating solution (general solution of unperturbed equation) in the form:

$$\alpha(t) = \frac{b}{\Omega^2} + \left( \alpha_2 - \frac{b}{\Omega^2} \right) \cos(\Omega t). \quad [3.64]$$

The action integral reviewing is of interest for the perturbed system [3.58] with slowly changing parameters:

$$I(\tau) = \int_0^{T_a} \dot{\alpha}^2 dt, \quad [3.65]$$

where  $T = 2\pi/\Omega$  – instant period of oscillations of the angle  $\alpha$ .

The perturbed equation [3.58] contains slowly changing parameters, and if the right side of this equation is equal to zero then, according to (Volosov, 1963), the action integral [3.65] keeps the value. It is an adiabatic invariant of the perturbed motion.

$$I = \text{const.}$$

Let us use a solution [3.64] for the action integral [3.65] calculation.

$$\begin{aligned} I &= \Omega^2 \left( \alpha_2 - \frac{b}{\Omega^2} \right)^2 \int_0^{T_a} \sin^2(\Omega t) dt = \Omega \left( \alpha_2 - \frac{b}{\Omega^2} \right)^2 \int_0^{2\pi} \sin^2(y) dy \\ &= \pi \Omega \left( \alpha_2 - \frac{b}{\Omega^2} \right), \end{aligned}$$

whence, taking into account [3.62], we find:

$$\sqrt{a+2\kappa} \left( \alpha_2 - \frac{b}{a+2\kappa} \right) = \text{const.} \quad [3.66]$$

In some cases, at the perturbed motion the tension force of the tether and its direction can be defined by the known, slowly changing functions (Aslanov et al., 2009). It is obvious that the peak values of an angle of the spacecraft's deflection can vary too. Taking into account these notes, we will rewrite [3.66] in the form:

$$\sqrt{a(\tau)+2\kappa} \left( \alpha_{\max}(\tau) - \frac{b(\tau)}{a(\tau)+2\kappa} \right) = \text{const.}$$

Resolving this equation relative to  $\alpha_{\max}(\tau)$ , we obtain the equation of an envelope of the maximum angle of the spacecraft's deflection concerning its local vertical:

$$\alpha_{\max}(\tau) = \frac{\text{const}}{\sqrt{a(\tau)+2\kappa}} + \frac{b(\tau)}{a(\tau)+2\kappa}$$

Let us use relations [3.57] and write the expression for the maximum angle of the spacecraft's deflection as a function of the tension force and the angle of deflection of this force from the local vertical:

$$\begin{aligned} \alpha_{\max}(\tau) &= \frac{T(\tau)\Delta \sin \varphi(\tau)}{T(\tau)\Delta \cos \varphi(\tau) + 3\omega^2(I_x - I_y)} \\ &+ \frac{\text{const} \sqrt{I_z}}{\sqrt{T(\tau)\Delta \cos \varphi(\tau) + 3\omega^2(I_x - I_y)}}. \end{aligned} \quad [3.67]$$

Let us notice that the values of the minimum and maximum angles of deflection are connected by the energy integral [3.60]:

$$h(\alpha_{\max}, \dot{\alpha} = 0) = h(\alpha_{\min}, \dot{\alpha} = 0). \quad [3.68]$$

Resolving [3.68] relative to  $\alpha_{\min}$ , we obtain:

$$\alpha_{\min}(\tau) = \frac{2b}{a + 2\kappa} - \alpha_{\max}(\tau).$$

Substituting here [3.68], we have:

$$\alpha_{\min}(\tau) = \frac{T(\tau)\Delta \sin \varphi(\tau)}{T(\tau)\Delta \cos \varphi(\tau) + 3\omega^2(I_x - I_y)} - \frac{\text{const} \sqrt{I_z}}{\sqrt{T(\tau)\Delta \cos \varphi(\tau) + 3\omega^2(I_x - I_y)}}.$$

### 3.5 Estimation of the microaccelerations level on board the spacecraft

During deployment of the tether system, the normal and tangential additional accelerations arise on board the spacecraft:

$$W_n = \dot{\alpha}^2 r_C, \quad W_\tau = \ddot{\alpha} r_C,$$

where  $r_C$  – distance from the spacecraft's centre of mass to a point in which additional accelerations are defined.

Transforming the new variable  $\beta = \varphi - \alpha$  and considering [3.43] and [3.44], we obtain accuracy within  $O(\varepsilon)$ :

$$\begin{aligned} W_n &= (\dot{\varphi} - \dot{\beta})^2 r_C, \\ W_\tau &= (\ddot{\varphi} - \ddot{\beta}) r_C = (\kappa \sin(2\varphi - 2\beta) + \Omega^2 \beta) r_C. \end{aligned} \quad [3.69]$$

Then the additional acceleration is:

$$W = \sqrt{W_n^2 + W_\tau^2} = r_C \sqrt{(\ddot{\alpha})^2 + (\dot{\alpha})^4} \quad [3.70]$$

or taking into account [3.69]:

$$W = r_C \sqrt{(\dot{\phi} - \dot{\beta})^4 + (\kappa \sin(2\phi - 2\beta) + \Omega^2 \beta)^2}.$$

In the case of the performance of conditions [3.39] and [3.40], the magnitudes  $\dot{\phi}$  and  $\kappa \sin(2\phi - 2\beta)$  are small in comparison; accordingly, with  $\dot{\beta}$  and  $\omega^2 \beta$ , therefore it is possible to write:

$$W_n \approx \dot{\beta}^2 r_C, \quad W_\tau \approx \Omega^2 \beta r_C.$$

Passing on these formulas to the variables amplitude-phase by means of replacementa [3.46] and [3.47], we obtain the following expression for additional acceleration:

$$W = \xi \Omega^2 r_C \sqrt{\xi^2 \sin^4 \eta + \cos^2 \eta}. \quad [3.71]$$

Earlier it was supposed that the angle of deflection of the spacecraft's axis from a line of operation of the tension force  $\beta$  is small, and hence the amplitude  $\xi$  is small. It is possible to show that  $\pi$ -periodic function of a phase  $f(\eta) = \sqrt{\xi^2 \sin^4 \eta + \cos^2 \eta}$ , reaches maximum value  $f_{\max} = 1$  at  $\xi \leq 1$ , therefore maximum value of an additional overload is:

$$W_{\max}(t) = \xi(t) \Omega(t)^2 r.$$

Using [3.55] in the last formula, we obtain the analytical association for the maximum additional acceleration caused by deployment of the tether system:

$$W_{\max}(t) = \frac{\xi_0 \Delta r_C}{I_z} \sqrt[4]{T(t)^3 T_0}. \quad [3.72]$$

At performance of the conditions [3.39] and [3.40], the formula [3.72] gives an estimation of the maximum additional acceleration, thus it is not required to make numerical integration of the initial [3.44] or the truncated [3.51] system of equations.

In case of small oscillations of the spacecraft in the points of a trajectory corresponding to the extreme values of an angle of the spacecraft's deflection from a local vertical, the time derivative of this angle is equal to zero. Then the estimation of full acceleration is:

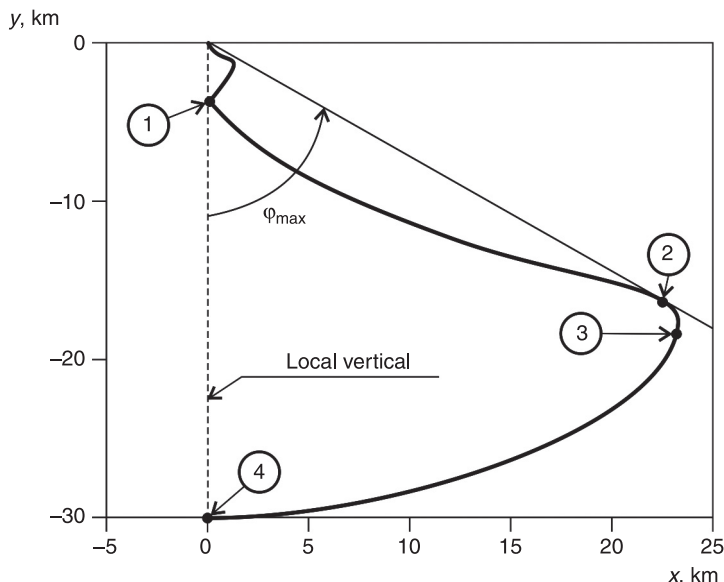
$$\langle W \rangle = \langle W_\tau \rangle = \langle \ddot{a} r_C \rangle = r_C (b(\tau) - (a(\tau) + 2\kappa) \alpha_{\max}(\tau)), \quad [3.73]$$

where  $\alpha_{\max}(\tau)$  is defined by [3.67].

As an example, we will consider development of the tether system having the following parameters:  $l_{\max} = 3 \cdot 10^4$  m – full length of the tether;  $I_x = 10^3$  kg·m<sup>2</sup>;  $I_y = I_z = 10^4$  kg·m<sup>2</sup>;  $m_B = 6000$  kg;  $m_A = 15$  kg;  $\Delta = 2$  m;  $V_B = 7.7 \cdot 10^3$  m/s;  $\theta_0 = 0.15^\circ$ ;  $r_B = 6.671 \cdot 10^6$  m;  $l_0 = 4$  m;  $\dot{l}_0 = 2.5$  m/s;  $\alpha_0 = 0$ ;  $\dot{\alpha}_0 = 0$  s<sup>-1</sup>;  $\varphi_0 = 0$ ; and  $\dot{\varphi}_0 = 0$  s<sup>-1</sup>.

We will execute the tether development under the other development of the dynamic scheme corresponding to project YES-2 (see Figure 3.3), which consists of three phases: slow

**Figure 3.3** Trajectory of the payload in  $D_0\tau n$

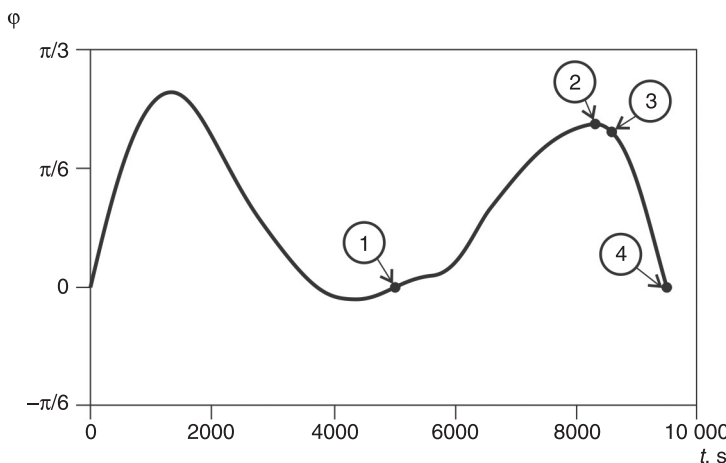


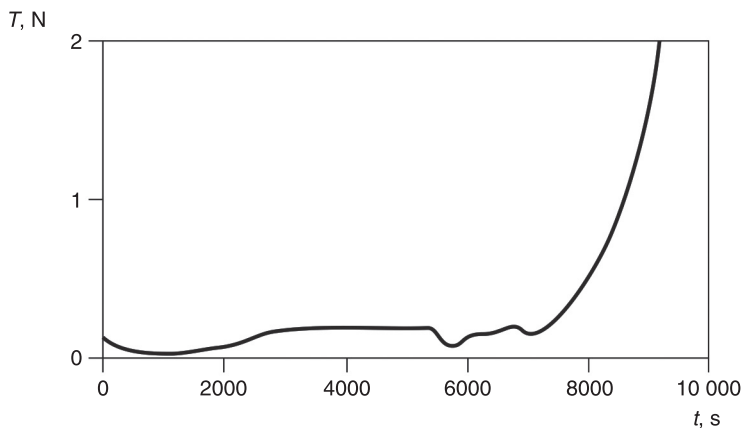
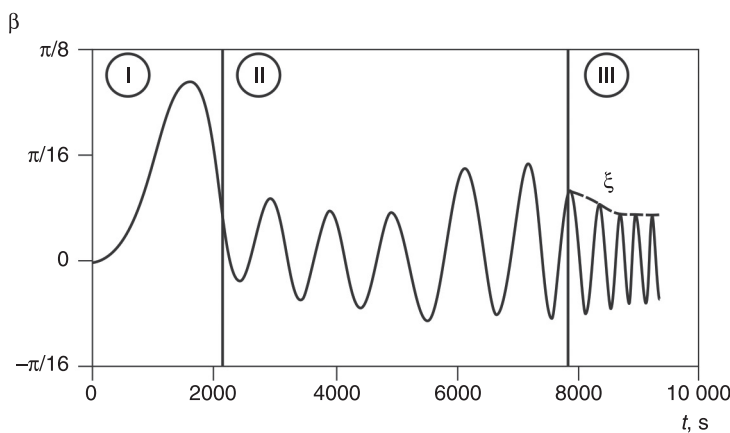
deployment (to a point 1); the fast deployment leading to a deflection of the tether from a local vertical in the direction of flight (to a point 3); and a return oscillation of the tether (to a point 4). The point 2 corresponds to a maximum angle of deflection of the tether from a vertical. In Figure 3.4, the angle  $\varphi$  as time function is shown. The scheme of deployment described is provided by the tension force of the tether, shown in Figure 3.5 (Kruijff and Stelzer, 2007).

The graphs shown in Figure 3.3 and Figure 3.4 can be received by numerical integration of the systems [3.4], [3.8] and [3.9] with use of the dependence shown in Figure 3.5 as the law of tension force. The graphs obtained as a result of numerical integration of systems [3.42] for the angles  $\beta = \beta(t)$  and  $\alpha(t) = \varphi(t) - \beta(t)$  are presented in Figure 3.6 and Figure 3.7.

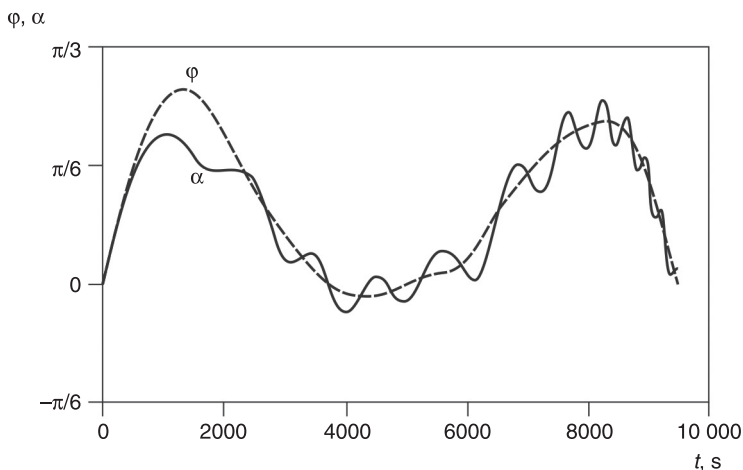
In Figure 3.6, the process of deploying of the STS is divided into three sites.

**Figure 3.4** Dependence of the tether deflection  $\varphi$  on time



**Figure 3.5** The law of tension force**Figure 3.6** Dependences of  $\beta$  and  $\xi$  on time

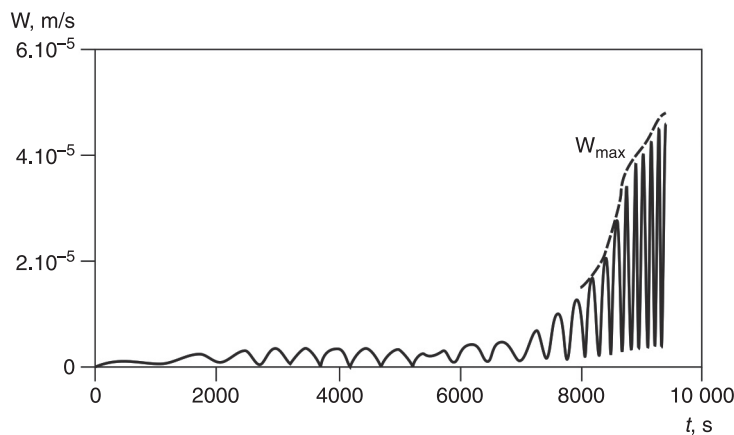
1. On site I, the tension force and frequency are insignificant. The gravitational moment provides considerable influence on the spacecraft motion.
2. On site II, the influence of the gravitational moment is insignificant in comparison with the influence of

**Figure 3.7** Dependences of  $\alpha$  and  $\varphi$  on time

the moment of tether tension; however, it still does not allow for application of the approximate analytical solution [3.55] as the condition [3.39] is not satisfied.

3. On site III, the tension moment is predominant in comparison with other factors, and as  $\Omega^2 \gg |\kappa|, |\ddot{\varphi}|$  the conditions [3.39] and [3.40] are satisfied. In this case, it is possible to use the approximate formulas [3.55] and [3.72] for an estimation of the amplitude of the spacecraft's oscillation and additional acceleration.

Let us pass to an estimation of the additional acceleration. In Figure 3.8, the dependence of the acceleration on time for a point at a distance  $r_C = 1$  m from the spacecraft's centres of mass is shown. It is obvious that maximum additional accelerations are observed at the closing stage of movement of the system when the tether's force of tension has the greatest value. Thus, the approximate

**Figure 3.8** Dependence of additional acceleration on time

Equation [3.55] gives a good approximation of the exact outcome (see Figure 3.8).

### 3.6 Motion of the spacecraft with a propulsion system

If on board the spacecraft the propulsion system works, it creates the moment  $M_{PS}$ , and the theorem of changing of a moment of momentum [3.5] can be written as:

$$\dot{K}_z = M_T + M_G + M_{PS}. \quad [3.74]$$

The moment  $M_{PS}$  we will determine as a couple

$$M_{PS} = P \cdot h_{PS},$$

where  $P$  – thrust of the propulsion system;  $h_{PS}$  – arm of the thrust.

Let the thrust be constant, and the duration of actuation of the propulsion system  $T_{PS}$  depends on an angle of deflection of the spacecraft's axis from a vertical  $\alpha$  and an angular velocity  $\dot{\alpha}$ :

$$T_{PS} = k_\alpha \alpha + k_{\dot{\alpha}} \dot{\alpha},$$

where  $k_\alpha, k_{\dot{\alpha}}$  – control coefficients.

For an orbit of the spacecraft close to circular ( $\omega = const$ ), the equation [3.74] becomes similar to [3.6]:

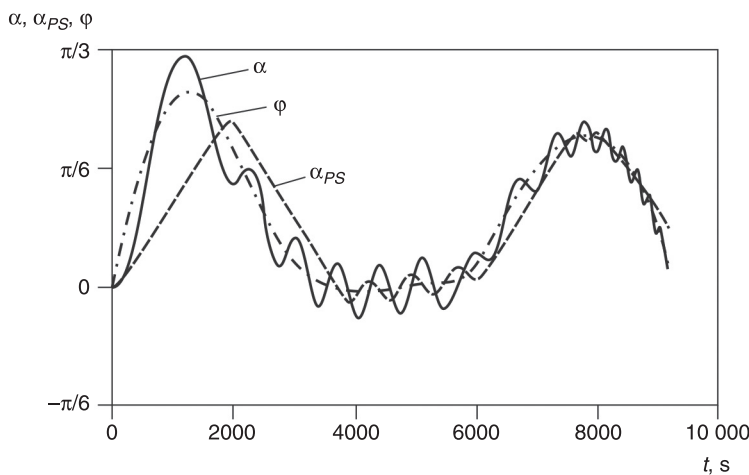
$$I_z \ddot{\alpha} = T \Delta \sin(\varphi - \alpha) + 3\omega^2 (I_x - I_y) \sin \alpha \cos \alpha + M_{PS} \quad [3.8]$$

The total additional acceleration arising during deployment of the tether system on board the spacecraft can be find under formula [3.70].

Let us do numerical modelling of the STS with the control engine. We will view deployment of the tether system having the parameters and initial conditions, corresponding to those given above. Assume that  $k_\alpha = 1, k_{\dot{\alpha}} = 0$ .

The laws of tether deflection from a local vertical  $\varphi(t)$  (dash-dot curve), the angle of deflection from a vertical taking into account the attitude control system activity  $\alpha_{PS}(t)$  (shaped curve) and without control  $\alpha(t)$  (solid curve) are given in Figure 3.9. The results are obtained by numerical integration of [3.75].

**Figure 3.9** Deflection of the tether  $\varphi$  and the spacecraft  $\alpha$ ,  $\alpha_{PS}$  from the local vertical



### 3.7 Motion of a spacecraft around its centre of mass in a circular orbit with a vertically deployed elastic tether

Let us consider a particle case of the STS motion when the tether is constantly parallel to the local vertical transiting through the centres of mass of the base spacecraft. The equations [3.10] have two pairs of stationary solutions (Avdeev et al., 1990), one of which corresponds to an inconvertible (vertical) disposition of the tether.

$$\varphi = 0, \pi; \quad T = 3\omega^2 m_2 l \quad [3.76]$$

In case  $\varphi = 0$ , the tethered payload moves below the spacecraft, but in case  $\varphi = \pi$  it moves above.

We will represent the tether as the massless elastic bar whose length varies according to Hooke's law:

$$T = c(l - l_0), \quad [3.77]$$

where  $c = ES_T / l_0$  – stiffness of the tether;  $E$  – an elastic modulus;  $S_T$  – the area of tether cross-section; and  $l_0$  – length of the strained tether. Let the payload move stringently on a local vertical in the neighbourhoods of the equilibrium position [3.76]. Then the first equation [3.10], taking into account [3.77], becomes:

$$\ddot{l} + \Omega_1^2 l = \frac{T}{m_2}, \quad [3.78]$$

$$\text{where } \Omega_1^2 = \frac{c}{m_2} - 3\omega^2 > 0.$$

For the materials used for manufacturing of the space tethers, this requirement is carried out (see Table 1.2). The equilibrium position of the payload is determined by the formula:

$$\rho_0 = \frac{cl_0}{c - 3m_2\omega^2}.$$

For the initial conditions:  $t_0 = 0$ :  $l = \rho_0$ ,  $\dot{l} = V_0$  the solution of the equation [3.78] takes the form:

$$l = \rho_0 + V_0\Omega_1^{-1} \sin \Omega_1 t. \quad [3.79]$$

The tether is in the stretched state if the initial velocity of the payload does not exceed the value:

$$V_0 \leq \frac{3\omega^2 \sqrt{m_2 l_0^2}}{\sqrt{c - 3m_2\omega^2}}. \quad [3.80]$$

The tension force of the tether according to [3.77] and [3.79] varies under the harmonious law

$$T = T_0 + T_t \sin \Omega_1 t, \quad [3.81]$$

$$T_0 = \frac{3m_2\omega^2 cl_0}{c - 3m_2\omega^2}, \quad T_t = \frac{V_0 c \sqrt{m_2}}{\sqrt{c - 3m_2\omega^2}}. \quad [3.82]$$

Substituting these expressions in [3.8], we obtain the equation of the spacecraft's motion concerning its centre of mass with the vertically organised tether:

$$I_z \ddot{\alpha} = 3\omega^2 (I_x - I_y) \sin \alpha \cos \alpha - T_0 \Delta \sin \alpha - T_m \Delta \sin \alpha \sin \Omega_1 t, \quad [3.83]$$

Equations [3.79] and [3.83], together with [3.4], describe the motion of the spacecraft with an elastic vertical tether. Let us rewrite [3.83]:

$$\ddot{\alpha} = -a \sin \alpha - b \sin \alpha \cos \alpha - \varepsilon \sin \alpha \sin \Omega_1 t, \quad [3.84]$$

$$a = \frac{\Delta T_0}{I_z}, \quad b = 3\omega^2 \frac{I_y - I_x}{I_z}, \quad \varepsilon = \frac{\Delta T_m}{I_z}. \quad [3.85]$$

Let us make the numerical modelling of the motion of the spacecraft with the vertical tether. The spacecraft has the following quantities-geometrical parameters:  $m_1 = 6000$  kg,

$A = 2500 \text{ kg}\cdot\text{m}^2$ ,  $B = C = 10^4 \text{ kg}\cdot\text{m}^2$ ,  $\Delta = 2 \text{ m}$ . It moves on a circular orbit at the altitude  $H = 250 \text{ km}$  ( $p = 6621 \text{ km}$ ), and its angular velocity is  $\omega = 1172 \cdot 10^{-3} \text{ s}^{-1}$ . The length of the unstrained tether is  $l_0 = 30 \text{ km}$ , the tether diameter is  $d_T = 0.5 \text{ mm}$ , and the payload mass is  $m_2 = 100 \text{ kg}$ . We assume that during motion the tether at all times remains parallel to the local vertical, transiting through the centre of mass of the spacecraft. In this case, the dynamics of the STS is described by equations [3.79] and [3.84]. For a system with the given parameters  $\gamma = b/a = 1.234 \cdot 10^{-3}$ , therefore, the coefficient  $b$  in equation [3.84] appears as two orders less than  $a$ .

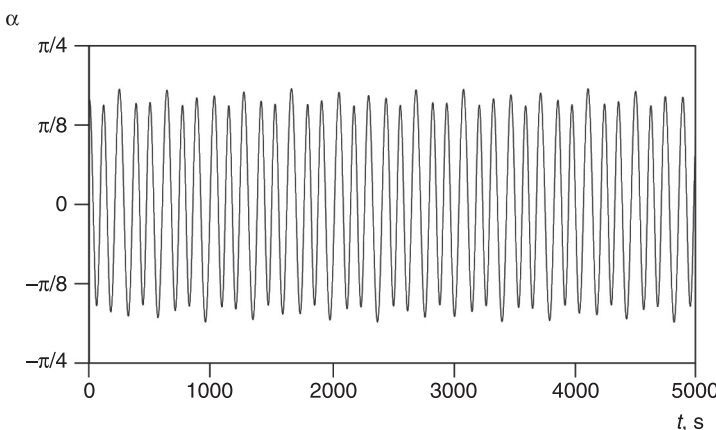
We explore the influence of the coefficient  $E$  on the system motion, and decide on the initial instant:

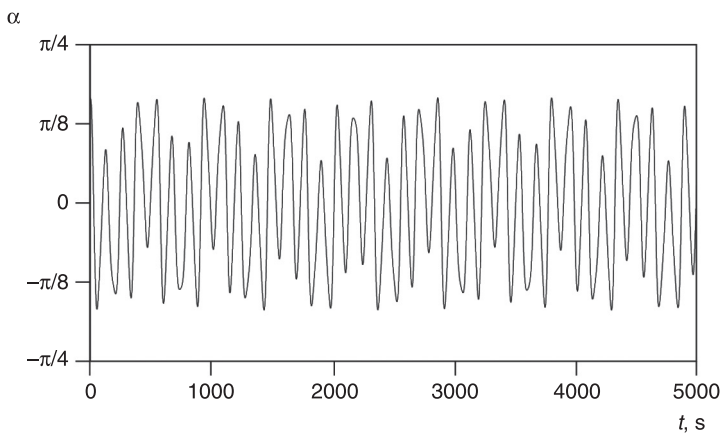
$$\alpha = \frac{\pi}{6}, \dot{\alpha} = 0, r = r_0, V_0 = 2 \text{ m/s.}$$

In Figures 3.10–3.12, the modification of the angle of spacecraft deflection is shown.

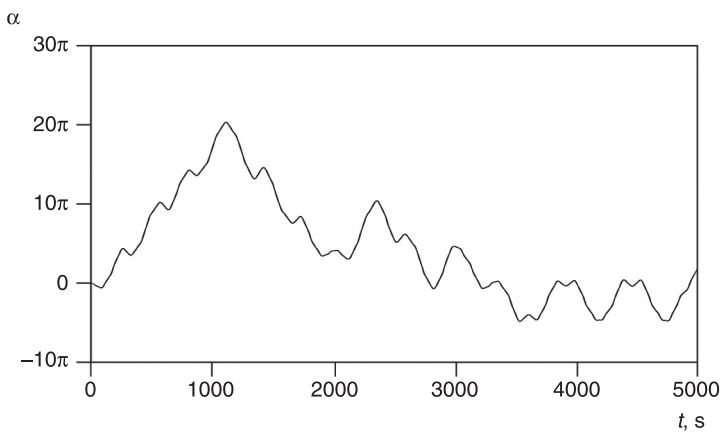
At the small  $E$  in the equation [3.84], the coefficient  $\varepsilon$  is 10 times less than  $a$ ; therefore, in Figure 3.10, oscillations

**Figure 3.10** Dependence of  $\alpha$  on time at  $E = 5 \text{ GPa}$



**Figure 3.11** Dependence of  $\alpha$  on time at  $E = 50$  GPa

close to the harmonious are observed. With an increase of  $E$ , the odds between  $\varepsilon$  and  $\alpha$  decrease, and the oscillations adopt a more complicated form (see Figure 3.11). At further growth of  $E$ , the phase trajectories start to intercross a separatrix of the unperturbed system ( $\varepsilon = 0$ ), transferring from the field of oscillations into the field of rotation (see Figure 3.12).

**Figure 3.12** Dependence of  $\alpha$  on time at  $E = 100$  GPa

At value:

$$E_* = \frac{3m_2\omega^2l_0(V_0^2 + 3\omega^2l_0)}{V_0^2S_T},$$

curves  $T_0(E)$  and  $T_t(E)$  are intercrossed (see Figure 3.13). Thus the biggest influence on the STS dynamics starts to provide the last addend on the right-hand side of [3.84], which already cannot be viewed as a small disturbance, and a spacecraft's oscillations essentially differ from the oscillations of the unperturbed system.

In this example, the initial velocity of the tether satisfied the requirement of [3.80], thus the tether at all times was in the stretched state.

It is similarly possible to estimate the influence of other parameters of the system on the spacecraft's motion. In Figure 3.14 and Figure 3.15, curves of  $T_0$  and  $T_t$  to mass of the payload and tether length are shown. With an increase of the payload's mass, the odds between the coefficients  $\varepsilon$  and  $\alpha$  increase, and oscillations come nearer to the harmonious. For short tethers, when  $l_0 < l_*$  the inequalities  $T_t > T_0$  and  $\varepsilon > \alpha$  are

**Figure 3.13** Dependences of  $T_0$ ,  $T_t$  on the tether elastic modulus at  $l_0 = 30$  km,  $m_2 = 100$  kg

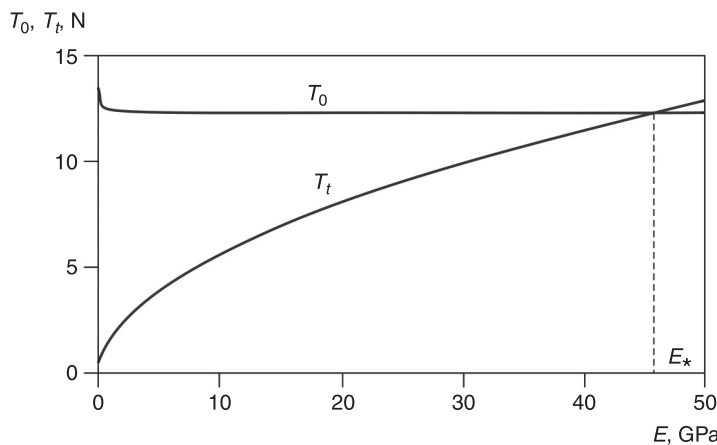


**Figure 3.14** Dependences of  $T_0$ ,  $T_t$  on mass of the payload at  $l_0 = 30 \text{ km}$ ,  $E = 50 \text{ GPa}$

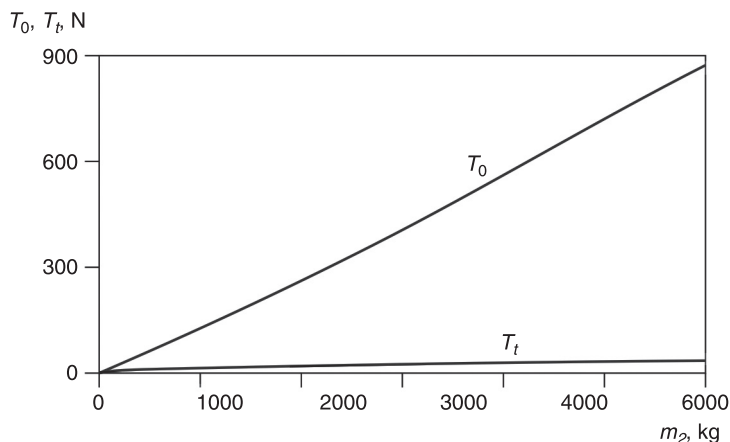
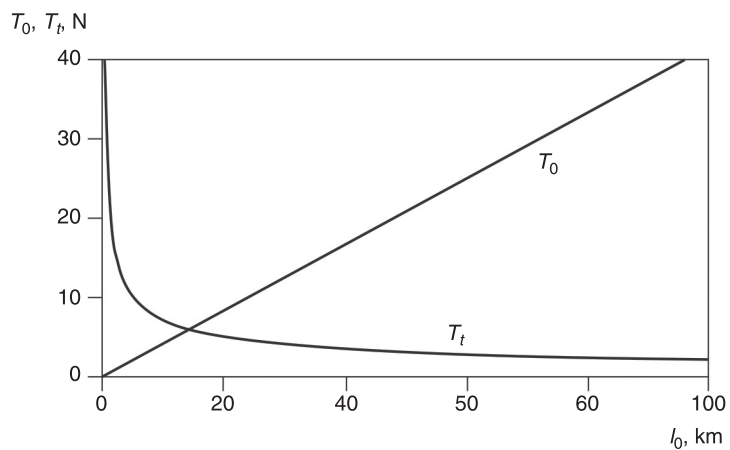


**Figure 3.15** Dependences of  $T_0$ ,  $T_t$  on the tether length at  $m_2 = 100 \text{ kg}$ ,  $E = 50 \text{ GPa}$

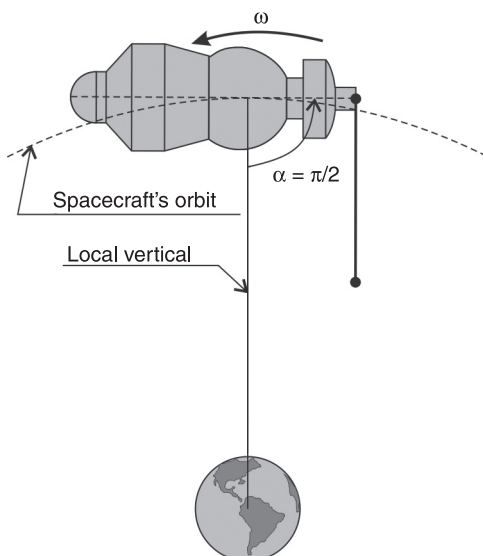


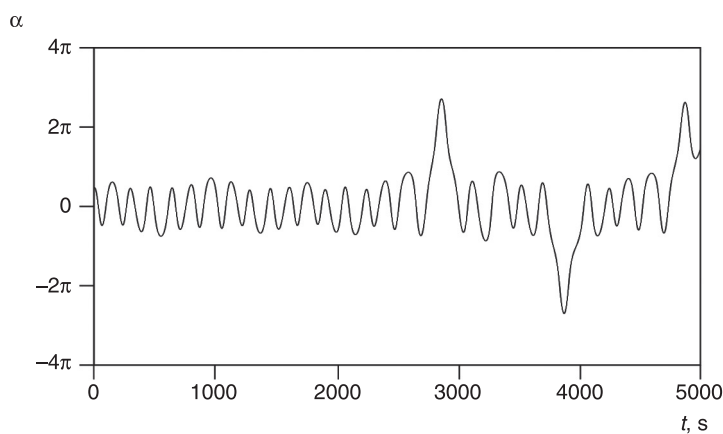
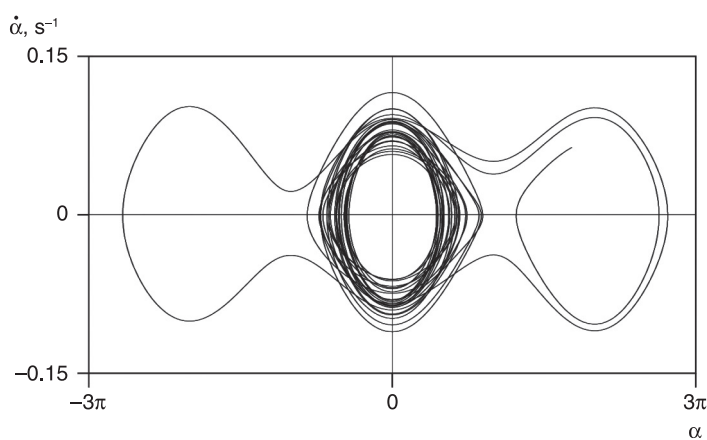
fair (where  $l_*$  – intersection point of curves in Figure 3.15). Thus the STS oscillations have an essentially non-linear character. With growth of the tether length, the coefficient  $\varepsilon$  decreases, and the oscillations come nearer to the harmonious.

Let us consider the STS motion when the base spacecraft is orientated perpendicularly to the local vertical (see Figure 3.16). Under the influence of the periodic disturbance caused by the third addend on the right-hand side of [3.84], the phase trajectory can intercross the unperturbed separatrix, transferring from the field of oscillative motions into the field of rotation and the inverse. Such a succession of events is very dangerous, as it leads to the tether winding on the spacecraft.

In Figure 3.17 and Figure 3.18, there are dependences of the angle  $\alpha$  to time and a phase portrait of the system for  $E = 15 \text{ GPa}$ . Even for such a low value of  $E$ , the spacecraft's transition into a rotation mode is observed. It is necessary to use tethers of smaller rigidity, or to orientate the spacecraft along a local vertical, to prevent occurrence of such situations.

**Figure 3.16** Spacecraft with a vertical tether



**Figure 3.17** Dependence of  $\alpha$  on time**Figure 3.18** Phase portrait

## 3.8 References

Aslanov V S, Ledkov A S and Stratilatov N R (2007) ‘Spatial Motion of Space Rope Cargo Transport System’, *Polyot* (*Flight*) (in Russian), ISSN 1684–1301, 2, 28–33.

- Aslanov V S, Ledkov A S and Stratilatov N R (2009) ‘The Influence of the Cable System Dedicated to Deliver Freights to the Earth of the Rotary Motion of Spacecraft’, *Polyot* (‘Flight’) (in Russian), ISSN 1684–1301, 1, 54–60.
- Aslanov V S (2004) *Spatial Motion of Body at Descent in Atmosphere*. Moscow: FIZMATLIT (in Russian).
- Avdeev Yu Yu, Belyakov A I, Brykov A V, Gorkov V L, Grigoriev M M, Zhurin B L, Ivanov V A, Titov G S and Yagudin V M (1990) *Flight of Space Vehicles. Examples and Tasks*. Moscow: Mashinostroenie (in Russian).
- Beletsky V V and Levin E M (1993) *Dynamics of Space Tether Systems*, San Diego, CA: American Astronautical Society.
- Beletsky V V (1965) *Motion of an Artificial Satellite about its Center of Mass*. Moscow: Nauka (in Russian). (English translation: Israel Program for Scientific Translation, Jerusalem, 1966.)
- Dwight H B (1957) *Tables of Integrals and Other Mathematical Data*. New York: Macmillan.
- Gradshteyn I S and Ryzhik I M (2000) *Tables of Integrals, Sums, Series, and Products*. New York: Academic Press.
- Jahnke J, Emde E and Losch F (1960) *Tables of Higher Functions*. New York: McGraw-Hill.
- Kruijff M and Stelzer M (2007) *TN0113-YES2 Post Flight Analysis Summary, Version: 2.0*, 12/12/07.
- Misra A K (2008) ‘Dynamics and Control of Tethered Satellite Systems’, *Acta Astronautica*, 63, 1169–77.
- Mitropolsky Yu A and Dao N V (1999) *Applied Asymptotic Methods in Nonlinear Oscillations*. London: Springer.
- Sazonov V V (2006) *Mathematical Modelling of Deployment of Tether System with Taking into Account of Tether*

*Mass.* Moscow: Keldysh Institute of Applied Mathematics  
(in Russian).

Volosov V M (1963) ‘Some forms of calculations in the theory of non-linear oscillations related with averaging’, *Zhurnal Vychislitel’noi Matematiki i Matematicheskoi Fiziki*, 3, 3–53.

## Conclusion

The mechanics of space tether systems is an extensive area of the modern mechanics of space flight. In this book we have tried to show on the one hand a variety of tasks and areas of research related with space tether systems, and on the other, their practical feasibility based on modern technology, and their ability to solve existing problems.

In one book it is impossible to answer all questions related with dynamics of space cable systems. Therefore, we have tried to focus on problems that may find wide application in the coming decades: the delivery of cargo from an orbit without the cost of rocket fuel, exploring the atmosphere and surface of the Earth by a subsatellite lowered on a tether. The specificity of these problems require us to create new mathematical models that take into account the interaction of the tether with the atmosphere and the movement around the centre of the mass of the spacecraft. Practical implementation cannot be made without assessment of potential emergencies and their consequences. Therefore, we have developed models that take into account various abnormal situations. Presented in the book, models and analytical results were used in the preparation and post-flight analysis of the international experiment YES2.

The study of chaotic behaviour of a mechanical system in space is a relatively new direction of tether system's mechanics. The presence of orbital eccentricity and the phenomenon of elasticity of tethers are the cause of the chaos

in space tether system's motion. Chaos can be a serious obstacle to the successful implementation of the space missions, because it can lead to off-normal operation of the system and to accidents. Using the methods of chaotic dynamics allows us to carry out a selection of space tether system parameters that preclude the possibility of chaos.

Another new trend that is discussed in detail in the book, is the study of dynamics of motion, relative to the centre of mass of the spacecraft with an attached tether. Tether systems have a significant influence on spacecraft dynamics, despite the low weight of the tether and tethered payload in comparison with the mass of the spacecraft. In some cases the spacecraft can be observed swinging with a subsequent transition into the rotation. New analytical solutions describing the plane vibrations of the spacecraft are illustrated in the book. These solutions can be used for quick calculations and qualitative analysis of the spacecraft motion with a tether.

The authors wish to thank the readers for their patience. We hope that the book will not only broaden your horizons, but will also arouse an interest in further study of the dynamics of space tether systems.

## Delivery of a payload from an orbit by means of a space tether

**Abstract:** This fourth chapter is devoted to the problem of payload delivery from an orbit to the Earth's surface without expenditure of fuel, by means of a tether. Two essentially different schemes of deployment of tethers are considered. In one example, using the YES2 experiment, the high potential of this method of payload delivery is shown. Various abnormal situations which can arise in the course of cable deployment are viewed: wrong orientation of a spacecraft at payload separation, a tether jamming, breakage of a spacecraft's attitude control system, and premature breakage of the tether.

**Key words:** YES2; tether deployment; abnormal situations; tether jamming; tether breakage.

The problem of experimental delivery of a payload from orbit is close to being solved. The first such experiment was carried out in 1993 by NASA. At the second stage of a Delta rocket, the SEDS-1 gear which perform tether deployment was erected. Within the limits of this experiment, the payload with a mass of 25 kg was lowered from orbit by means of a 20 km tether. In 2007, another experiment was carried out by ESA. A tether of 31.7 km and a capsule weighing 12 kg were used in it. These experiments showed a

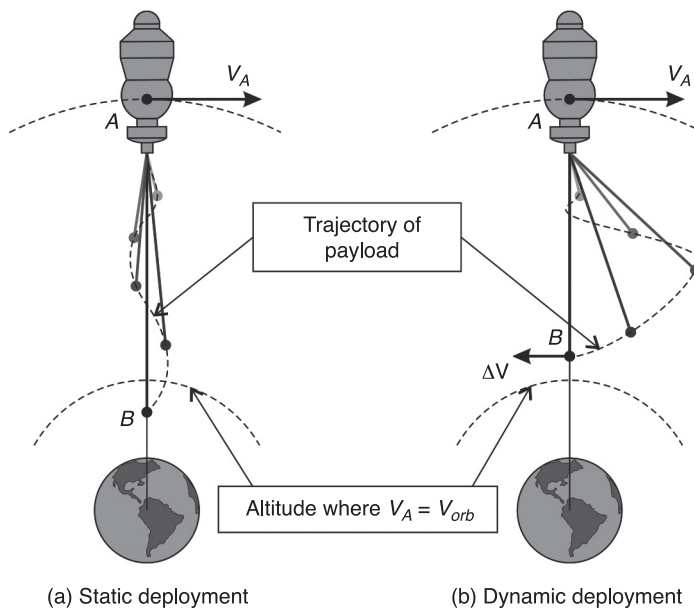
basic capability of payload delivery by means of a tether system. However, for wide practical use, it is necessary to answer some questions related to gear reliability and the safety of such systems.

## 4.1 Tether deployment schemes

In the literature, two different types of tether control during deployment are considered. They are called static and dynamic deployment (Zimmermann et al., 2005).

At static deployment, the payload during manoeuvre is in the neighbourhood of the local vertical of the base spacecraft. When the payload altitude becomes small enough for transfer to a ballistic trajectory, the tether is cut (see Figure 4.1a). In other words, at static deployment the payload transfers to a

**Figure 4.1** Tether deployment schemes

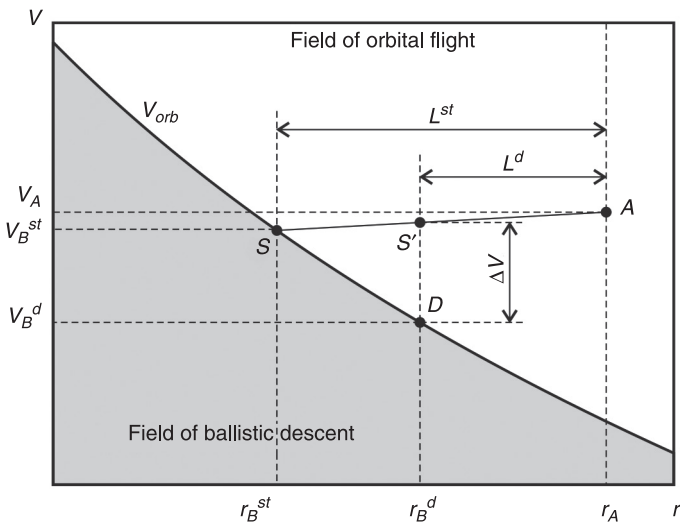


descent trajectory without decreasing its velocity, but because it appears at the altitude where its velocity is not enough for motion in a circular orbit. It is possible to tell that at low altitudes gravitational forces make more noticeable impact on dynamics of a body, than at higher altitudes.

The basic idea of dynamic deployment consists of additional diminution of payload velocity at the expense of return oscillation. The cause of transition of payload in a descent trajectory is the diminution of both altitude and velocity. The tether deployment is implemented with a fast enough speed. Under the influence of the Coriolis force, the payload deflects from the local vertical of the base spacecraft in the direction of motion of the system's centre of mass. In the process of increasing the tether's length, the payload altitude will decrease and the gravitational acceleration operating on it will be increased in comparison with a similar acceleration operating on the base spacecraft and, because of this, the payload makes a return oscillation in the direction of the local vertical. Being close to the vertical, the payload will have a lower velocity than that of the base spacecraft. In other words, at the expense of the return motion, the payload receives the negative gain to the orbital velocity, equivalent to a braking momentum. On the other hand, the orbital velocity at the altitude of the payload exceeds the orbital velocity at the altitude of the spacecraft. At this stage it breaks off from the tether and the payload makes its descent into the atmosphere (see Figure 4.1b).

The dynamic deployment in comparison with the static deployment allows it to receive the necessary diminution of the perigee of the payload orbit by means of tethers of considerably smaller length (Dignath and Schiehlen, 2000). In Figure 4.2, the parameter space (radius of an orbit and an absolute velocity of the spacecraft)

**Figure 4.2** Comparison of the length of tethers required for payload descent at static and dynamic deployment



is shown. The curve of the orbital velocity is set by the equation:

$$V_{orb} = \sqrt{\frac{\mu}{r}}$$

This curve divides the parameter space into two fields. If velocity  $V$  and the radius of an orbit of the spacecraft  $r$  correspond to a point on this curve, the spacecraft moves in a circular orbit round the Earth. If the point  $(r, V)$  lies in the upper (white) field, the spacecraft moves in an elliptical orbit. If the point is in the grey field, the spacecraft carries out its descent to the Earth in a ballistic trajectory. Prior to the beginning of tether deployment, the payload moves with the velocity of the base spacecraft (point A). To transfer the payload in a ballistic trajectory at static deployment, it is necessary to unreel the tether at a length

larger than  $L^{st}$ . The payload's velocity at the altitude  $r_B^{st}$  will be less than the velocity at altitude  $r_A$  on a value  $\Delta V^{st} = \dot{\theta}L^{st}$  (where  $\dot{\theta}$  – angular velocity of tether system's centre of mass round the Earth; and  $L^{st}$  – tether length sufficient for deorbiting at static deployment). At dynamic deployment, the necessary length of the tether is less than at static, because of the cost of a return oscillative motion the payload's velocity decreases by value  $\Delta V$ , and the payload can transfer to a ballistic trajectory on a greater altitude  $r_B^d$ . Thus the velocity is:

$$V_B^d = V_A - \dot{\theta}L^d - \Delta V$$

and

$$V_B^d < V_B^{st},$$

where  $L^d$  – tether length sufficient for deorbiting at dynamic deployment.

The detailed analysis of the dynamic scheme of deployment at various control laws is given in Shcherbakov (2010).

## 4.2 Project YES2

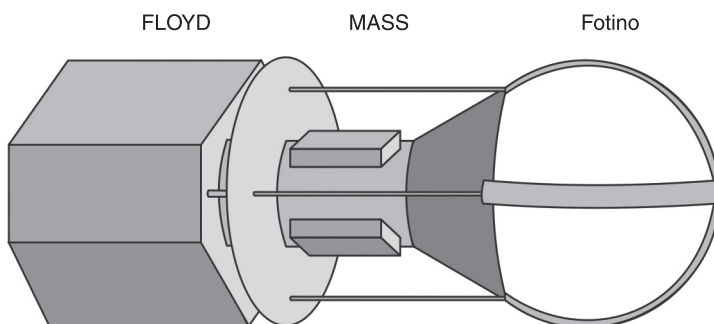
In 2007, similar experiments were carried out by ESA. During project YES2, students and young scientists from Europe and Russia created a satellite for delivery of a payload from an orbit to the Earth. Five universities from Great Britain, Greece, Italy, Germany and Russia took part in the project. YES2 was managed by Delta-Utec SRC. Formed by the efforts of this international team, the module was attached to the Russian space vehicle Foton-3M. On 14 September 2007, it was launched into space. The experiment of payload deliveries commenced eleven days after this.

We took part in the project, carrying out an estimation of the safety of the YES2 experiment for the Foton-3M vehicle at the request of SRPSRC ‘TsSKB-Progress’. The mathematical models and the scientific results obtained during this work are given in this book.

The module YES2 consisted of three parts (see Figure 4.3) (Kruijff and Stelzer, 2007):

1. FOTINO – a spherical re-entry capsule with a diameter of 40 cm and a mass of approximately 5.5 kg. It had a small parachute and a heat-resistant coating of flexible alumina and rigid ceramic. At the beginning of the experiment, the capsule was fastened into the module MASS funnel. In the capsule, there were tools for communication and coordinates determination.
2. MASS – Mechanical and data Acquisition Support System. This contained the transmitter and the auxiliary scientific equipment. MASS consisted of the round foundation, the cylinder consolidated on it, and the funnel installed on the cylinder. Boxes with electronics and the transmitter are consolidated round the cylinder.
3. FLOYD – the component disposed on Foton-3M contained the coil with the tether, the deploying system,

**Figure 4.3** Construction of the Young Engineers Satellite 2



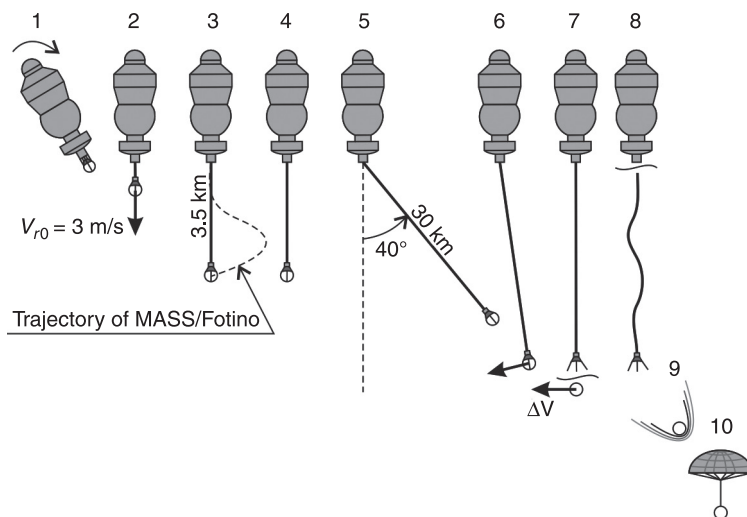
the ejection system and control electronics. FLOYD supplied linking of the YES2 module with the subsystems of the power supplies and telecontrol/telemetry of Foton-3M.

In the experiment, a tether made from Dyneema, a polymer nonconducting material, was used. The tether length was 31.7 km, the diameter 0.5 mm, and the mass 5.8 kg.

A dynamic scheme of the tether deployment was used in YES2. All programs can be split up conditionally into 10 stages (see Figure 4.4).

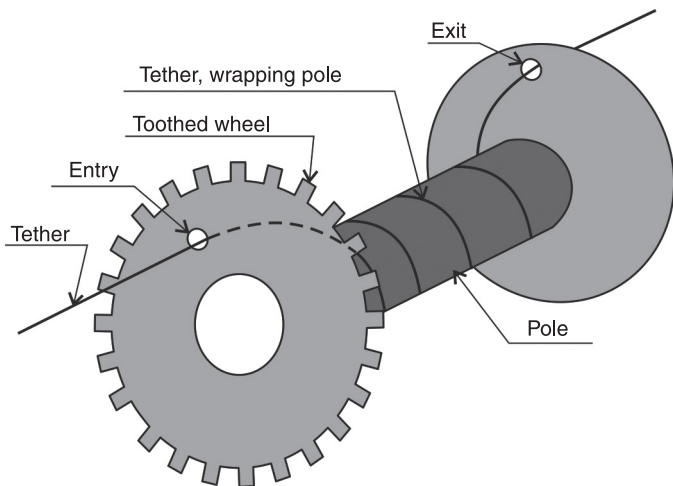
1. Directly ahead of activation of module YES2, the spacecraft Foton-3M is directed along a local vertical.
2. By means of three springs, the unit MASS/FOTINO separates from the spacecraft with a relative velocity of about 3 m/s.

**Figure 4.4** The scheme of YES2



3. For 90 minutes the tether deploys to a length of 3.5 km.
4. The braking gear blocks the tether, and the system is retained in that state for some minutes.
5. The braking gear unblocks, and the tether deploys to a length of 30 km. The MASS/FOTINO unit deflects from the local vertical at an angle of 40°.
6. The braking gear is again activated, and the MASS/FOTINO unit makes a return oscillation.
7. When the tether is near the local vertical, the FOTINO separates from the MASS.
8. FLOOD cuts the tether which, together with the MASS, burns up in the atmosphere.
9. FOTINO enters the atmosphere.
10. At an altitude of 5 km, the brake parachute is opened and FOTINO soft-lands on the Earth.

For control of the deploying process, a special brake was disposed on FLOYD (Lennert and Cartmell, 2006). The gear had a very simple construction as it allowed only deployment of the tether without the capability of inverse retraction. At the heart of the braking gear lies the idea stated by Carroll (1993). He suggested using the friction between the tether and the cylindrical surface around which some turns of the tether are made. The more the length of the tether touching with the cylinder, the more the friction force action. Thus, by changing the number of turns, it is possible to change the tension force of the tether. The tether falls on the cylinder through a toothed wheel which can rotate round an axis of the cylinder; turning the wheel, it is possible to change the number of tether turns (see Figure 4.5). The braking mechanism is well reviewed in the article by Lennert and Cartmell (2006).

**Figure 4.5** Brake gear

As a control law the following relation is used:

$$T = T_{cp} (1 + k_1(l - l_{cp}) + k_2(V - V_{cp})), \quad [4.1]$$

where  $l_{cp}$ ,  $V_{cp}$ ,  $T_{cp}$  – calculated tension force of the tether, length of the tether deployed and velocity of tether's outlet;  $l$ ,  $V$  – measured length of the tether deployed and the velocity of the tether's outlet;  $k_1$ ,  $k_2$  – control coefficients.

Curves of the relations of the calculated parameters are given in Figures 4.6–4.8. They are grounded on data given in Kruijff and Stelzer (2007).

Unfortunately, it is impossible to term the YES2 experiment as completely successful because the FOTINO capsule was lost. After telemetry data processing, it became clear that the tether was deployed more slowly than was planned. To validate this data, the tether was deployed only to 8.5 km at the time of cutting off. In this case, the capsule should remain in orbit; however this did not happen and the FOTINO entered the atmosphere. After additional analysis, the estimate was made that the information on incomplete

**Figure 4.6** Calculated tether length used in control law [4.1]

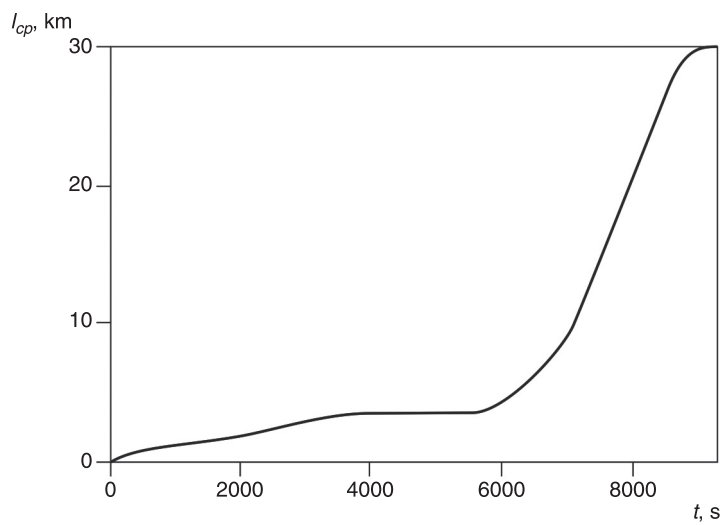


**Figure 4.7** Fig. 4.7 Calculated tether outlet velocity used in control law [4.1]

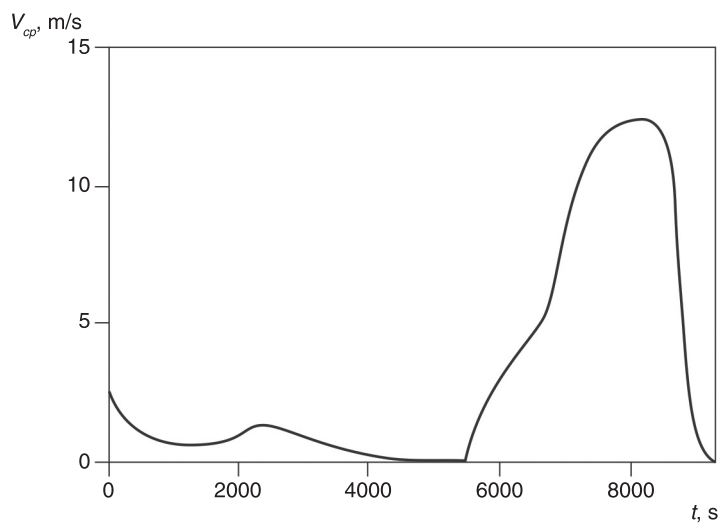
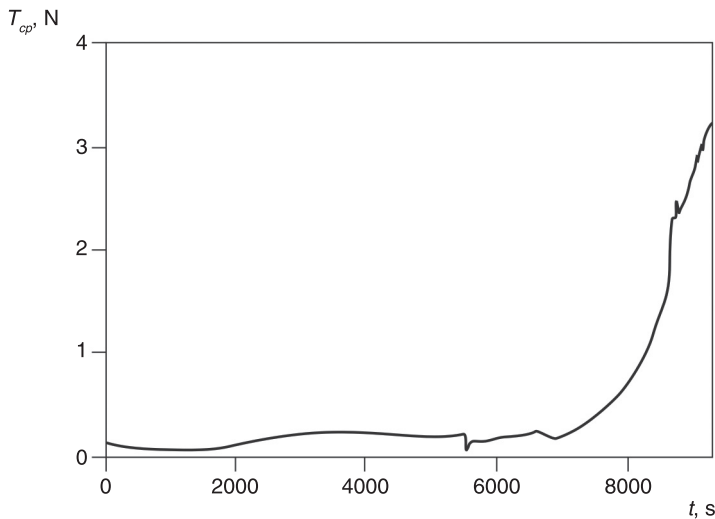


**Figure 4.8** Calculated tension force used in control law [4.1]



deploying of the tether was received owing to the wrong indications of the sensor measuring the velocity of the tether outlet. Actually, the tether was deployed to its overall length, but with a higher velocity; therefore the capsule did not appear in the prospective landing area.

As a result of this experiment, the capability of the implementation of a payload delivery by means of a tether was shown. However, the loss of the capsule indicates the necessity of a more detailed study of a tether system's dynamics.

### 4.3 Modelling of the YES2 tether deployment

Let us consider the problem of payload delivery from an orbit which was solved within the limits of the

YES2 international project. During the experiment, the Foton-M3 spacecraft was retained by its engines in a vertical position; therefore, the tether deployment feebly influenced its spatial orientation. In this connection, we will view Foton-M3 as a particle. We will also consider the tethered capsule as a mass point. For the motion analysis, we will use the multipoint model [2.135] given in Chapter 2 of this book.

As a control law of tether deployment, we will use [4.1]. In this equation the measured velocity of the tether's outlet represents the relative velocity of the  $k$ -th tether particle concerning the  $(k + 1)$ -th particle corresponding to the spacecraft:

$$V = |V_{k+1} - V_k|.$$

Curves of the calculated parameters  $l_{cp}$ ,  $V_{cp}$ ,  $T_{cp}$  are given in Figures 4.6–4.8.

We will conduct the modelling under the following starting conditions and parameters: the limiting length of the tether – 31.7 km; linear density of the tether – 0.18 kg/km; diameter of the tether – 0.5 mm; rigidity of the tether – 5 kN; damping coefficient – 0.06; mass of Foton-3M – 6300 kg; mass of MASS/FOTINO – 12 kg; and its ballistic coefficient – 0.0123 m<sup>2</sup>/kg.

We set initially the coordinates and velocities of the base spacecraft in the Greenwich coordinate system  $x_0 = -3724.741$  km,  $y_0 = 5492.645$  km,  $z_0 = 0$ ,  $V_{x0} = -2503.02$  m/s,  $V_{y0} = -1718.50$  m/s, and  $V_{z0} = 6912.06$  m/s. The payload separates from the Foton-3M on a local vertical downwards with an initial relative velocity of  $V_r = 2.58$  m/s. Because of the coefficients in control law [4.1], we accept  $k_1 = 1$ ,  $k_2 = 2$ . For modelling the STS we will use 40 particles. Results of the modelling are given in Figures 4.9–4.17.

**Figure 4.9** Motion of MASS/Fotino in a barycentric coordinate system connected with the base spacecraft

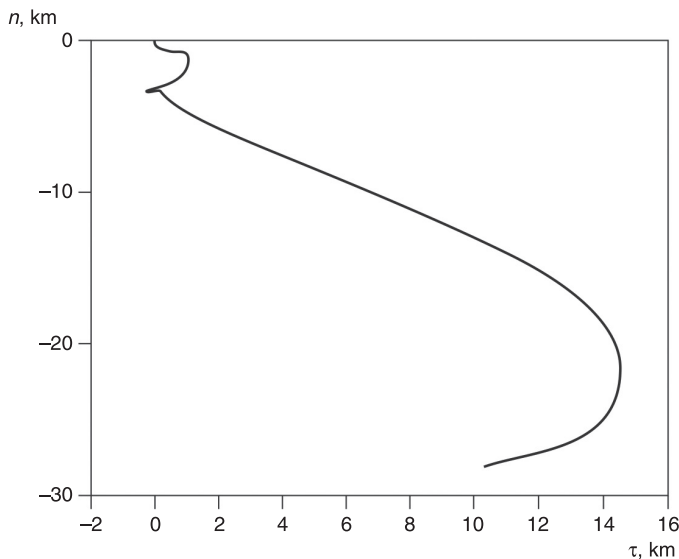


**Figure 4.10** Motion of MASS/Fotino in a barycentric coordinate system connected with the base spacecraft

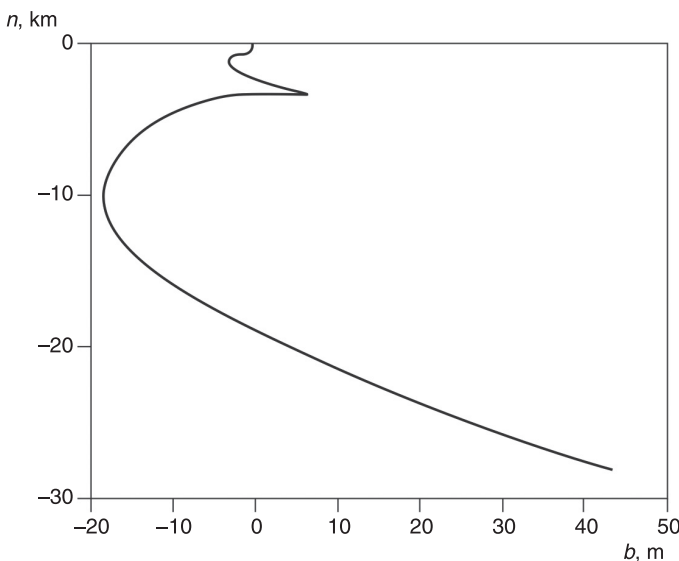


**Figure 4.11** Dependences of a spacecraft and MASS/Fotino velocities on time

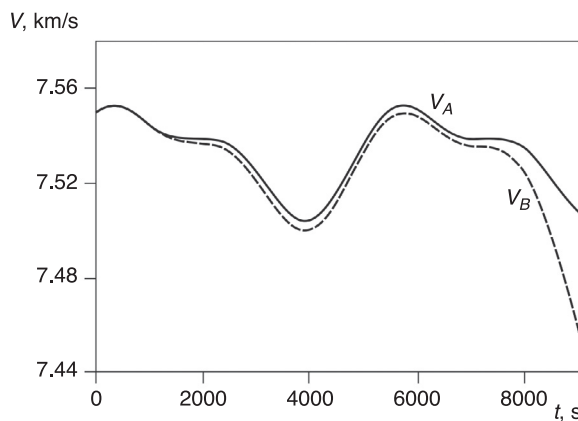
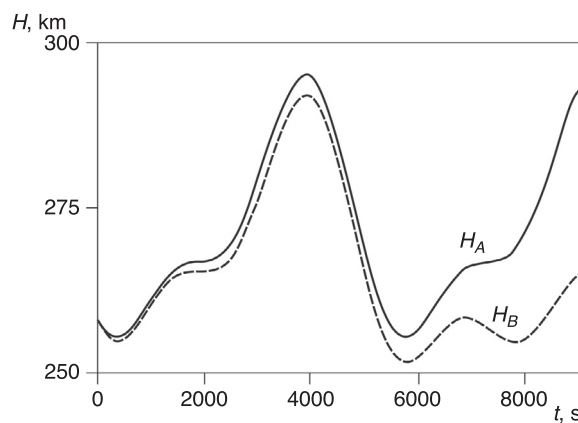


**Figure 4.12** Dependences of spacecraft and MASS/Fotino altitude on time



In Figure 4.9 and Figure 4.10, the trajectories of the MASS/FOTINO motion in the barycentric coordinate system  $Atnb$  related to the base spacecraft are shown. The oscillations of the tethered payload in the plane  $Atn$  on the three orders exceed the oscillations in the plane  $Anb$ . Therefore, when

**Figure 4.13** Dependence of the angle of tether deflection from a spacecraft's local vertical on time

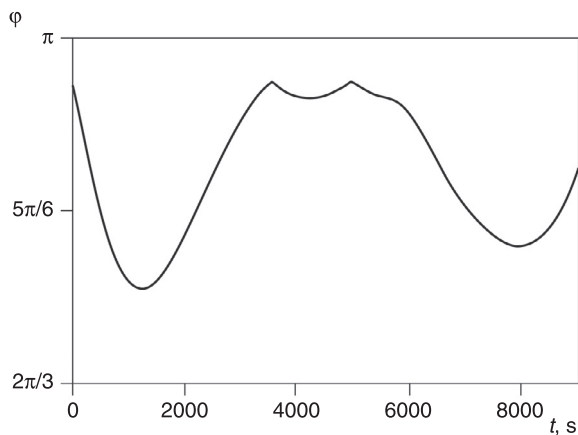


**Figure 4.14** Dependence of the distance between tether points and the line connecting a spacecraft with MASS/Fotino, on a number of rejected points

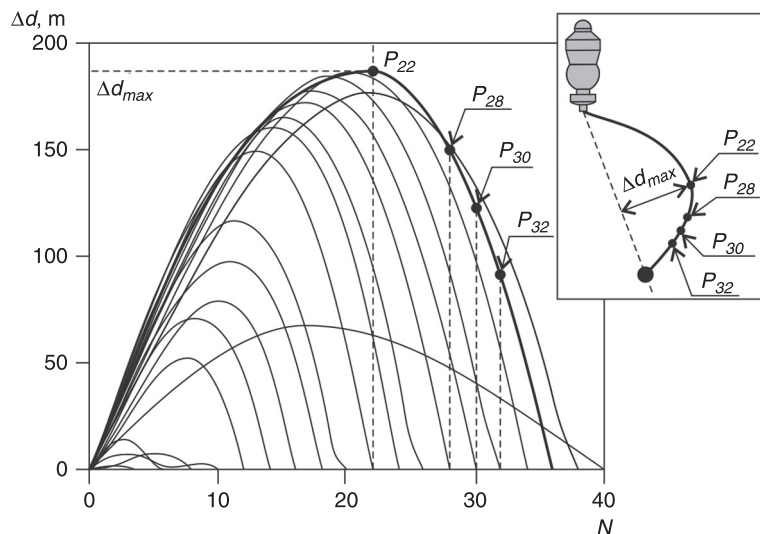


**Figure 4.15** Comparison of the model tether length (dashed curve) with the design value (solid curve)

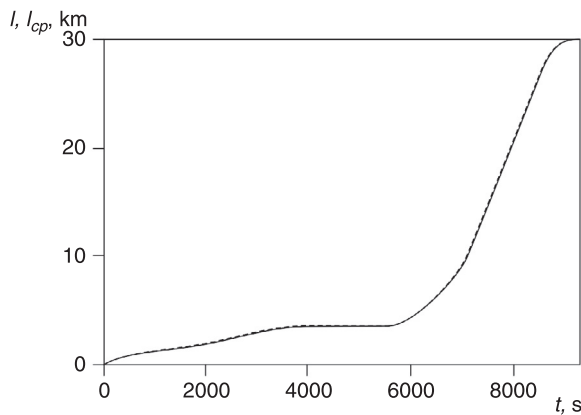
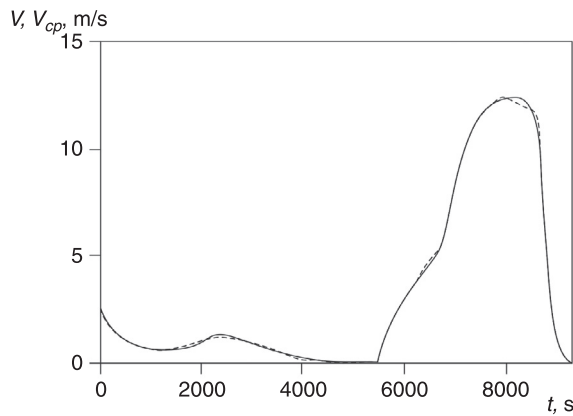


**Figure 4.16** Comparison of the model tether outlet velocity (dashed curve) with the design value (solid curve)

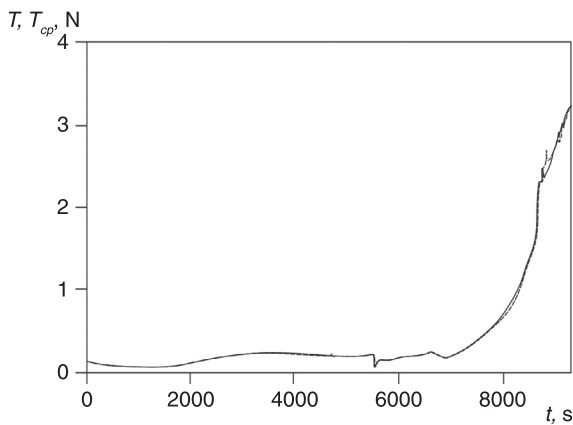


estimating calculations that do not demand high accuracy, it is possible to consider the STS motion as a plane.

In Figure 4.11 and Figure 4.12, the curves of the velocity and altitude of the spacecraft and the tethered payload are

**Figure 4.17**

Comparison of the model tension force (dashed curve) with the design value (solid curve)



shown. It is seen that the separation of FOTINO happens at an altitude of 246.83 km with a velocity of 7455,20 m/s. The orbital velocity at this altitude is equal to  $V_{orb} = 7756$  m/s, therefore FOTINO transfers to a ballistic trajectory and will descend from an orbit. Use of the STS allows for deceleration of the motion of the descent capsule by more than 100 m/s. In Figure 4.13, the modification of the angle of deflection of the payload from a vertical of the base spacecraft during tether deployment is shown.

In Figure 4.14 the deflection of the tether's points from a line joining the spacecraft with the payload is shown. On an abscissa axis, the quantity of the deployment points is put aside. On an ordinate axis, the deflection of the tether's particles is shown. Lines are constructed for the moments of issue of the new particle. It can be seen that the peak deflection happens when 36 particles are deployed and the 21st point deviates at a distance of 186.5 m.

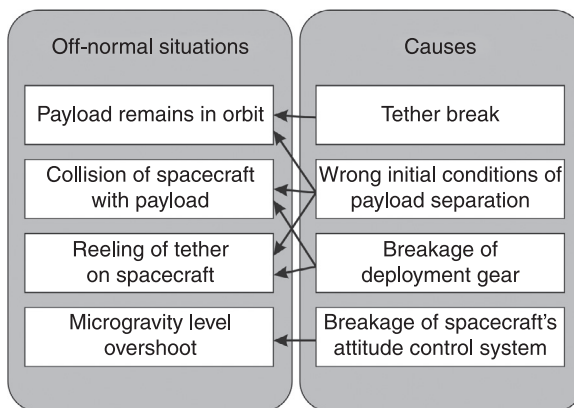
A comparison of the length, velocity of outlet and tension force to their design values is shown in Figures 4.15–4.17,

and the design values are shown by solid curves. It can be noticed that the chosen coefficients of control  $k_1$ ,  $k_2$  provide quite good results. During deployment, no sharp oscillations of the tension force of the tether are observed.

## 4.4 Abnormal situations during tether deployment

In the latest astronautics, multipurpose spacecraft are widely used. Operation of a payload delivery from orbit can be one of the many tasks in a spacecraft's mission. Therefore the problems related to activity of the tether system should not hinder the realisation of other mission objectives. It is important to envision a capability of the occurrence of an abnormal situation, to detect it at an early design stage, and to take all necessary measures for its elimination in actual flight, up to a forced cutting of a tether and loss of the payload. In most cases, the last measure can be quite justified.

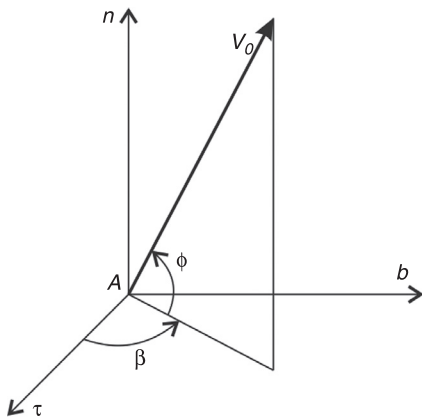
Abnormal situations can be divided conditionally into two groups: dangerous to the payload; and dangerous to the base spacecraft, and to the mission as a whole. In the first group, it is possible to include malfunctions during an impossible delivery of the payload to the Earth when the payload transfers to an orbit higher in relation to the spacecraft or when it enters into orbit. The second group includes the abnormal situations leading to collision of the spacecraft with the payload and to reeling of the tether on the spacecraft. Here it is possible to include sharp increases in the tension force leading to growth of the on board microgravity level and hindering the carrying out of the experiments. Among the causes leading to occurrence of indicated abnormal situations, it is possible to note the wrong initial conditions of payload separation (the relative velocity and its direction),

**Figure 4.18** Abnormal situations at tether deployment

failure of the tether's deployment gear, and failure of the stabilisation system of the spacecraft (see Figure 4.18).

#### **4.4.1 The incorrect orientation of a spacecraft at payload separation**

Normal operational mode of an STS implies that at the moment of the payload's separation its initial velocity is directed along a local vertical to the centre of the Earth. Obviously, the base spacecraft should be orientated in an appropriate way. Let us consider a situation when, at the moment of payload separation, the spacecraft is incorrectly orientated. In this case, there can be abnormal situations of two types: the payload can transfer to higher-altitude orbit that makes its delivery to the Earth impossible (abnormal situation A); the payload can collide with the spacecraft or the tether can be reeled onto it (abnormal situation B). Let us consider that the module of the relative velocity of separation does not depend on orientation of the spacecraft. We will set the direction of the initial velocity of the payload  $V_0$  by

**Figure 4.19** Direction of the initial velocity of a payload

means of angles  $\phi$  and  $\beta$  in an orbital coordinate system *Atbn* (see Figure 4.19). The normal operational mode of the STS corresponds to  $\phi = -\frac{\pi}{2}$ , when the initial velocity of the payload is along vector  $-\mathbf{n}$ .

For the analysis of abnormal situations, we use a multipoint mathematical model of the STS. As an example, we will consider the STS with the parameters given in section 4.3. Let us view two ways of tether deployment. The first way is characterised by a large initial velocity of separation of the payload and the deployment proceeds until the moment the payload reaches a separation point about a local vertical (see Figure 4.20). It is shown by the dashed curve. The second way corresponds to the scheme of deployment applied in YES2, and it is described above. In Figure 4.20 it is shown by a solid curve.

In Figure 4.21, the trajectory of payload motion is shown for two ways of tether control. The initial velocity of the payload was directed along the local vertical in both cases.

Let us make a series of numerical calculations of tether deployment at various values of angles  $\beta \in [0; 2\pi]$  and

**Figure 4.20** Calculated velocities of the tether outlet for control law [4.1]

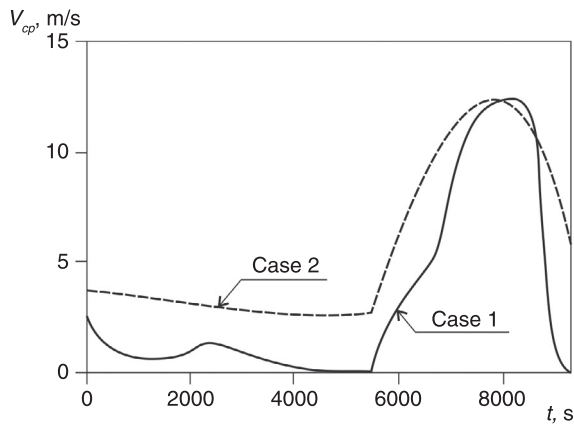
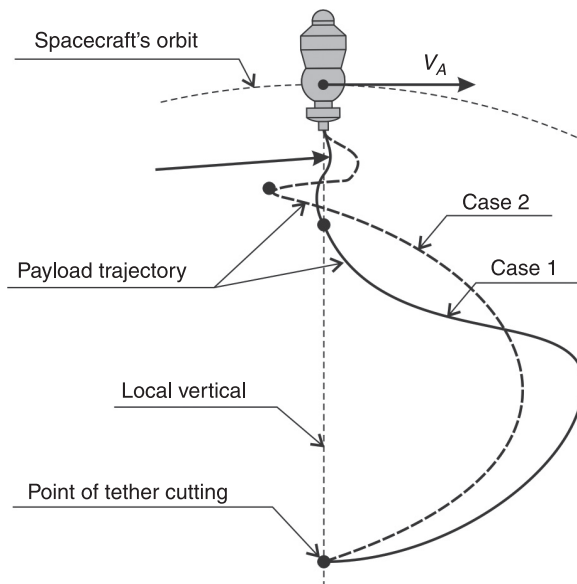


**Figure 4.21** Scheme of payload descent



$\phi \in [-\pi/2; \pi/2]$ . We will divide the space of the parameters into dangerous (A, B) and safe regions (see Figure 4.22 and Figure 4.23). If the values of angles  $\beta$  and  $\phi$  in the payload separation moment correspond to a point lying in region A, then during tether deployment the payload transfers to a higher-altitude orbit. If the point  $(\beta, \phi)$  belongs to region B, the tether reels in the spacecraft. By reeling, we understand a situation when during motion the angle between a plus direction of axis  $A\tau$  and a direction on the first particle of the tether varies more than on the  $\pi$  radian. In Figure 4.24 the

**Figure 4.22** Safe and danger regions in space of the initial parameters for case 1

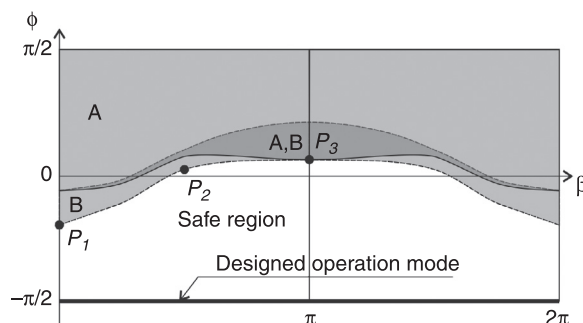


**Figure 4.23** Safe and danger regions in space of the initial parameters for case 2

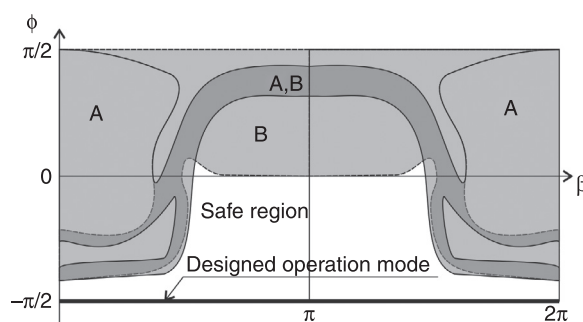
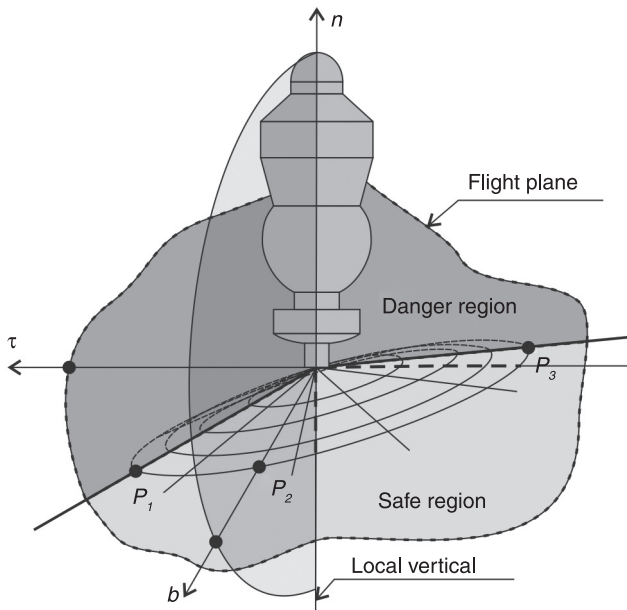


**Figure 4.24** Safe separation region for first method of deployment



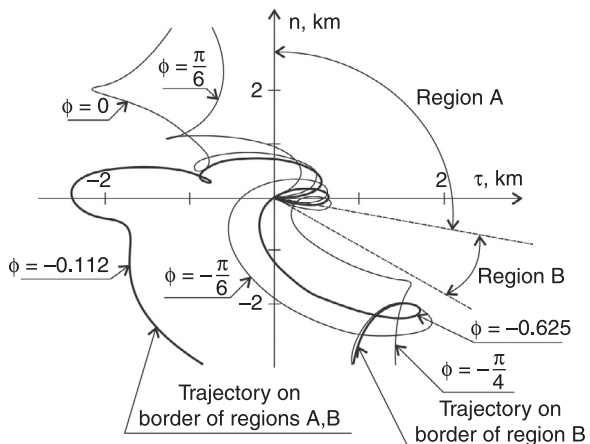
region of safe separation, corresponding to the first way of deployment, is shown schematically. Points  $P_1$ ,  $P_2$  and  $P_3$  lie on the border of the safety area at  $\beta = 0$ ,  $\beta = \pi/2$ ,  $\beta = \pi$  (see Figure 4.22).

In Figure 4.25 some trajectories of the payload and the dangerous regions for the first way of deployment are shown for  $\beta = 0$ .

Comparing Figure 4.22 and Figure 4.23, we see that with the second method of deployment the total area of the dangerous regions is a little more than with the first. Thus, in the second method in case of the wrong orientation of spacecraft, the probability of an abnormal situation is higher.

Influence of the deflection of the payload's initial velocity from the orbital plane  $\beta = 0$  at its separation from the spacecraft was studied at the various values of  $\phi = 0$

**Figure 4.25** Payload trajectories at various angles  $\phi$  ( $\beta = 0$ ) for first method of deployment



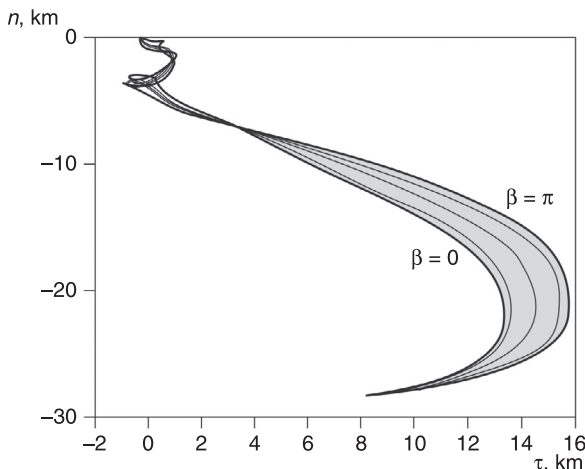
corresponding to safe region (see Figure 4.22 and Figure 4.23). As a result of a series of numerical experiments, it was revealed that the out-of-plane deflection of the initial velocity direction at payload separation made little impact on the final stage of motion. The trajectories received for angles  $\beta = 0$  and  $\beta = \pi$  organise on a plane field where all other trajectories lie (see Figure 4.26).

Numerical calculations show that, at both envisaged ways of deployment, the force of the tether's tension reaches values of the order of one Newton, and the spacecraft's known acceleration is of the order of  $10^{-4}$  m/s<sup>2</sup>. It leads to an abnormal situation related to excess of the admissible level of microaccelerations on board the spacecraft.

#### 4.4.2 Tether jamming

Along with the wrong orientation of a spacecraft, the malfunction of the deployment gear can be the cause of an

**Figure 4.26** Payload trajectories at various angles  $\beta$  ( $\phi = \pi/3$ ) for first method of deployment



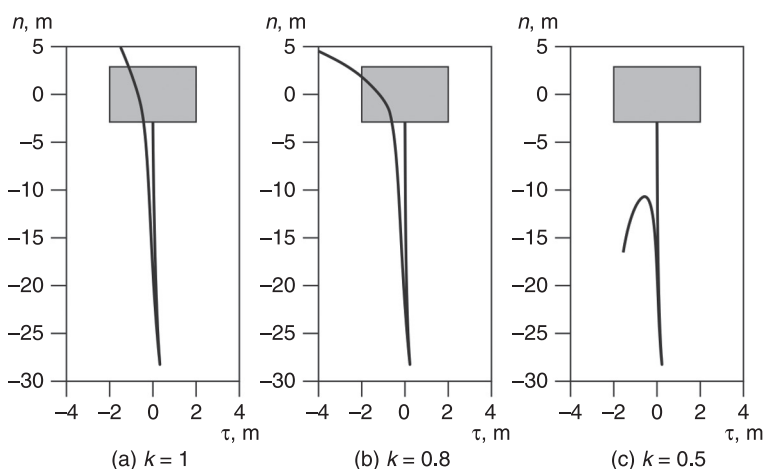
abnormal situation. Let us look at the jamming of the tether (Dyukov, 2010).

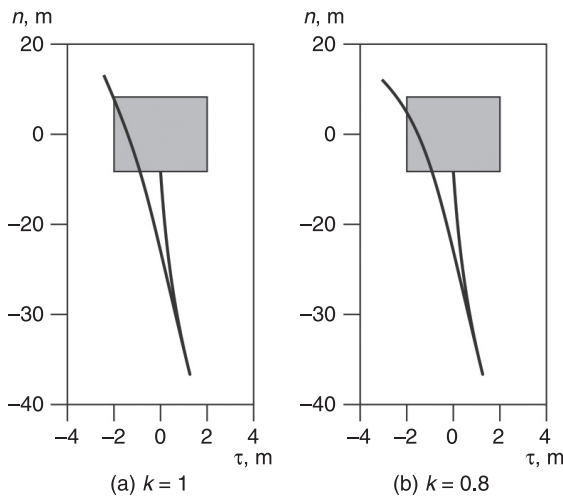
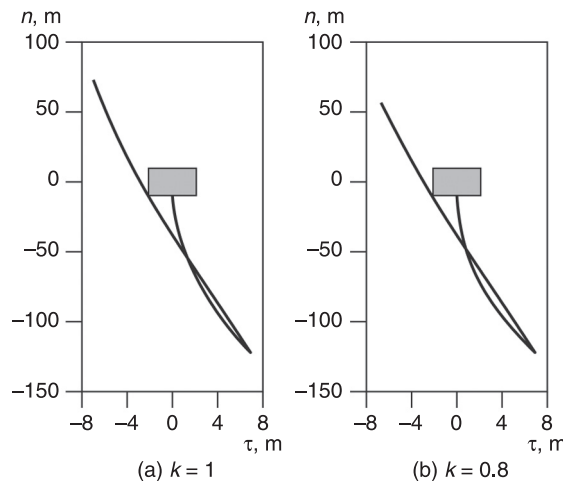
Motion of the payload after jamming is caused by the elasticity force of the tether, and the velocity of a backward motion of the payload is determined according to the shock theory. The modification of the bodies' velocity at collision depends on the elastic properties of the bodies, which are characterised by a value termed the coefficient of restitution  $k \in [0;1]$ . This coefficient is equal to the ratio of the module of velocity *after* collision to the module of velocity *before* it. The coefficient of restitution does not depend either on the size of the bodies, or on their relative velocity; and it is determined only by the properties of their material. Let us describe the process of modelling of an abnormal situation. The system motion is described by the elementary model [2.18] where the tension force is determined by the control law [4.1]. At the moment of jamming, the direction of the relative velocity of the payload changes to the opposite, and its value is multiplied by a coefficient of restitution. As the

payload's motion happens in the opposite direction the tether appears slack and  $T = 0$  in [2.18].

We make numerical calculations with various values of the coefficients of restitution. We will figure the spacecraft in the form of the cylinder with a size 6 m by 2 m. Initial conditions we will take to be similar to those used in the previous section (the first way of the tether's deployment). In Figures 4.27–4.29 the results of the calculations are shown. The rectangle designates the spacecraft, and the line the a trajectory of the payload motion. In Figures 4.27–4.29 the trajectory of the payload motion is shown at different values of a coefficient of restitution and at the various moments of jamming over 10 s. In Figure 4.30, the dependence of the distance between the spacecraft's symmetry axis and a collision point at the time of jamming is shown with different values of a coefficient of restitution. From Figure 4.30, it can be seen that jamming is most dangerous if it happens within 50 s after commencement of the deployment, as the collision of the payload with the spacecraft is very probable. The

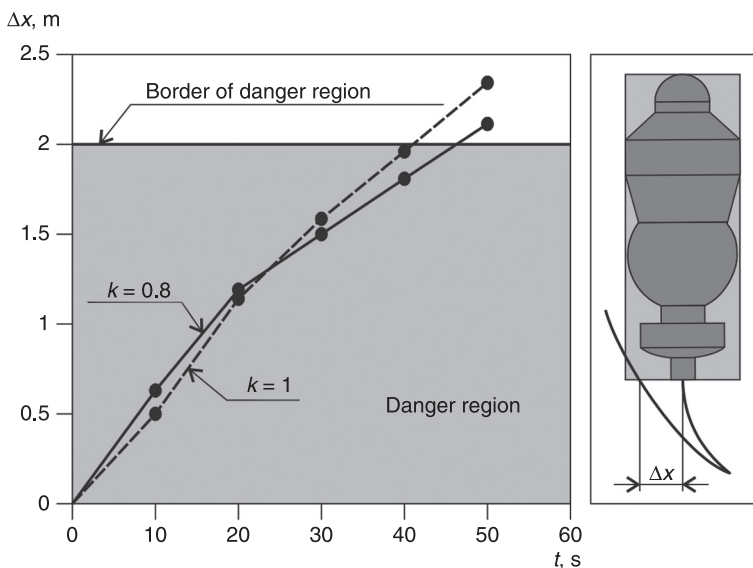
**Figure 4.27** Tether jamming at 10 s



**Figure 4.28** Tether jamming at 20 s**Figure 4.29** Tether jamming at 50 s

frontier value of a coefficient of restitution at which the collision does not happen is  $k = 0.63$ .

Thus, for diminution of the probability of collision of the payload and the spacecraft, it is necessary to reduce the

**Figure 4.30** Comparison of results of jamming modelling

coefficient of restitution. This can be done using various constructive methods, for example the use of tethers with rupturing loops.

#### 4.4.3 Breakage of a spacecraft's attitude control system

In the previous calculations, it was supposed that throughout deployment the spacecraft is retained in a vertical state ( $\alpha = 0$ ) by means of an attitude control system. In Figure 4.31, the behaviour of the spacecraft at failure of this system is shown. The breakage occurred when a tether was deflected on the peak angle from a local vertical (point 2 in Figure 3.3). In this case additional accelerations (see Figure 4.32) on the order exceed the accelerations at the free motion of the spacecraft (see Figure 3.8). Hence, if there is a probability of failure of

**Figure 4.31** Dependences of  $\beta$  and  $\xi$  on time at breakage of a spacecraft's attitude control system

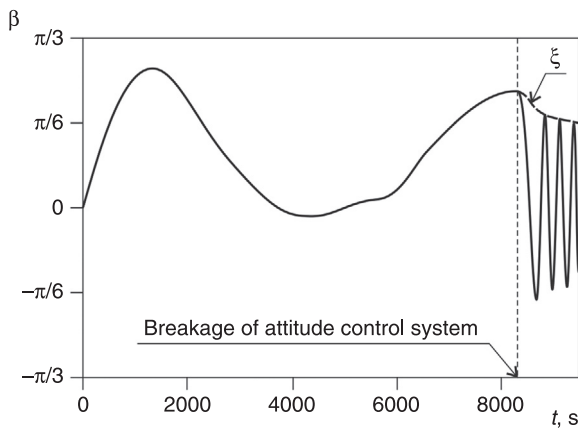
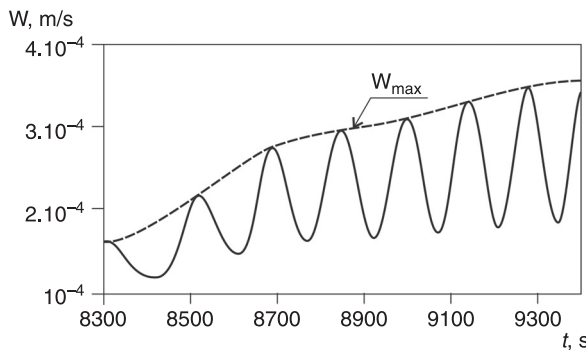


**Figure 4.32** Additional acceleration at breakage of a spacecraft's attitude control system



the attitude control system, from the point of view of minimisation of additional accelerations it is better not to use the attitude control system at all, allowing the spacecraft to make the free oscillations.

A series of numerical experiments showed that failure of the attitude control system after the beginning of deployment influences only the level of microgravitation on board the spacecraft and does not lead to collision and tether reeling.

#### 4.4.4 Premature breakage of the tether

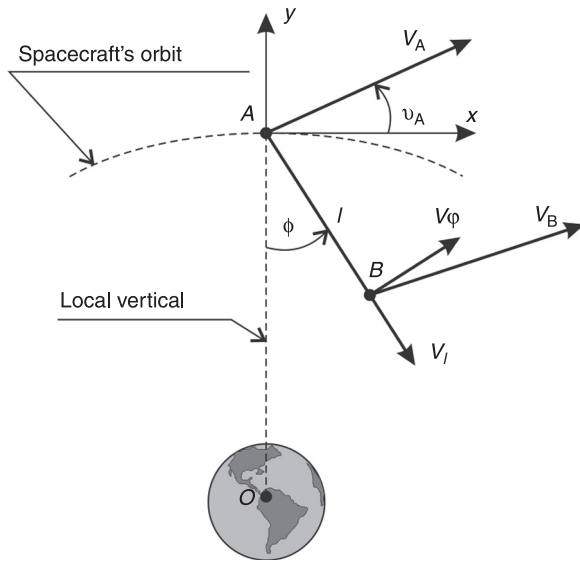
Let us view an abnormal situation of tether breakage and estimate its influence on the capability of the payload delivery to the Earth. Tether breakage can be caused by misoperation of a deployment gear, excess of the admissible value of tension force or, as happened in the SEDS-2 experiment, as a result of collision with space debris (Aslanov et al., 2010).

Let us consider the spacecraft and the payload as two particles connected by a massless, perfectly inelastic tether. The force of tension is determined by the law of deployment [4.1]. We write the equation of motion for the spacecraft in a geocentric coordinate system (Andreevskiy, 1970):

$$\begin{aligned}\dot{V}_A &= -\frac{c_{xA}\rho_a(H_A)V_AS_A}{2m_A} - g(H_A)\sin v - \frac{T}{m_A}\sin(v_A - \phi), \\ \dot{v}_A &= \omega - \frac{1}{V_A}\left(g(H_A)\cos v_A + \frac{T}{m_A}\cos(v_A - \phi)\right), \\ \dot{H}_A &= V_A \sin v_A, \\ \dot{L}_A &= R_3 V_A \cos v_A (R_E + H_A)^{-1},\end{aligned}\quad [4.2]$$

where  $V_A$  – velocity of spacecraft;  $H_A$  – its altitude;  $c_{xA}$  – drag aerodynamic coefficient of spacecraft;  $\rho_a(H) = \rho_{a0} \exp(-H/H_*)$  – atmosphere density;  $\rho_{a0} = 1.225 \text{ kg/m}^3$  – an atmosphere density at a sea level,  $H_* = 7.11 \text{ km}$ ;  $S_A$  – spacecraft's frontal area;  $m_A$  – spacecraft's mass;  $g(H) = g_0 R_E^2 (R_E + H)^{-2}$  acceleration of gravity;  $g_0 = 9.81 \text{ m/s}^2$ ;  $v_A$  – spacecraft's trajectory slope angle;  $\omega = V_A (H_A + R_E)^{-1} \cos v_A$  – angular velocity of spacecraft's centre of mass orbital motion;  $L_A$  – flight range; and  $R_E$  – radius of the Earth.

For the payload equations of motion we insert the coordinate system related to the spacecraft (see Figure 4.33). As independent variables, we use the length of the tether  $l$

**Figure 4.33** Wind coordinate system

and an angle of deflection of the tether from a local vertical  $\phi$  (Aslanov et al., 2009):

$$\begin{aligned}
 \ddot{l} &= -2\omega\rho(H_A)\dot{\phi} - \frac{T}{m_2} + \frac{\rho(H_A)}{2} \left( \frac{c_{xA}S_AV_A^2}{m_A} - \frac{c_{xB}S_BV_B^2}{m_B} \right) \\
 &\quad \times \sin(\phi - v_A) + 3\omega^2 l \cos^2 \phi + l\dot{\phi}^2, \\
 \ddot{\phi} &= 2\omega \frac{\dot{l}}{l} + \dot{\omega} + \frac{\rho(H_A)}{2l} \left( \frac{c_{xA}S_AV_A^2}{m_A} - \frac{c_{xB}S_BV_B^2}{m_B} \right) \\
 &\quad \times \cos(\phi - v_A) - 3\omega^2 \cos \phi \sin \phi - 2\dot{\phi} \frac{\dot{l}}{l},
 \end{aligned} \tag{4.3}$$

where  $c_{xB}$  – drag aerodynamic coefficient of payload;  $V_B$  – velocity of payload; and  $S_B$  – payload's frontal area.

Equations [4.2] and [4.3] describe the motion of the considered STS.

The payload equations of motion in the atmosphere after separation from a tether look like [4.2]:

$$\begin{aligned}\dot{V}_B &= -c_{xB} \frac{\rho(H_B)V_B^2 S_B}{2m_B} - g(H_B) \sin v_B, \\ \dot{v}_B &= \frac{1}{V_B} \left( g(H_B) - \frac{V_B^2}{H_B + R_E} \right) \cos v_B, \\ \dot{H}_B &= V_B \sin v_B, \\ \dot{L}_B &= R_E V_B \cos v_B (R_E + H_B)^{-1},\end{aligned}\quad [4.4]$$

where  $m_B$  – payload's mass;  $v_B$  – payload's trajectory slope angle; and  $H_B, L_A$  – altitude and flight range of payload.

For modelling of the descent of the payload into the atmosphere, it is necessary to have the initial conditions of motion. The absolute velocity of the payload can be found as:

$$\mathbf{V}_B = \mathbf{V}_A + \mathbf{V}_l + \mathbf{V}_\phi,$$

where  $V_l = \dot{l}$ ,  $V_\phi = l\dot{\phi}$ .

The vector  $\mathbf{V}_B$  in the coordinate system  $Cxy$  (see Figure 4.33) has coordinates:

$$\begin{aligned}V_{Bx} &= V_A \cos v_A + \dot{l} \sin \phi + l\dot{\phi} \cos \phi, \\ V_{By} &= V_A \sin v_A - \dot{l} \cos \phi + l\dot{\phi} \sin \phi.\end{aligned}$$

Then

$$\begin{aligned}V_B &= \sqrt{V_{Bx}^2 + V_{By}^2}, \\ v_B &= \operatorname{arctg}(V_{By} / V_{Bx}), \\ H_B &= H_A - l \cos \phi, \\ L_B &= L_A + l \sin \phi.\end{aligned}\quad [4.5]$$

In [4.5] we substitute the parameters of the system's motion in the payload separation moment, and we receive the initial conditions necessary for integration of the system [4.4].

Let us consider the motion of the system with the following parameters:  $m_A = 6300$  kg,  $m_B = 15$  kg,  $c_{xA} = c_{xB} = 2$ ,  $S_A = 10$  m<sup>2</sup>,  $S_B = 0.785$  m<sup>2</sup>. We will suggest that in an initial instant:  $H_A = 250$  km,  $V_A = 7760$  m/s,  $v = 0$ ,  $L_A = 0$ ,  $\phi = 0$ ,  $\dot{\phi} = 0$ ,  $l = 0$ ,  $\dot{l} = 3$  m/s.

Integrating equation systems [4.2] and [4.3], we obtain dependence of the parameters of the tethered payload motion on time (see Figures 4.34–4.36). Substituting the corresponding results to an instant  $t_R$  in [4.5], and using it as the initial conditions for equations [4.4] we obtain a trajectory of the payload motion after tether breakage in the

**Figure 4.34** Dependence of payload velocity on time

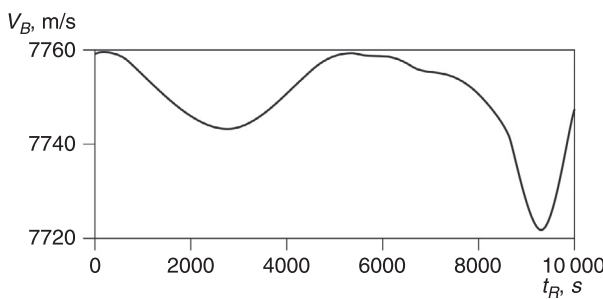


**Figure 4.35** Dependence of a payload's trajectory slope angle on time

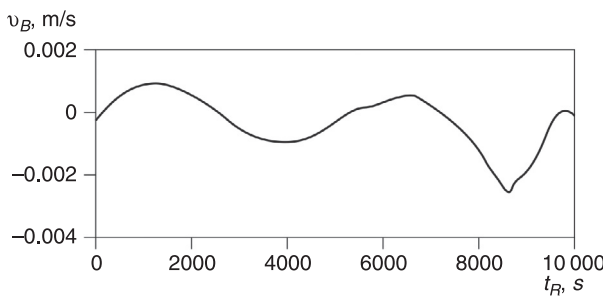


**Figure 4.36** Dependences of a payload's and a spacecraft's altitude on time

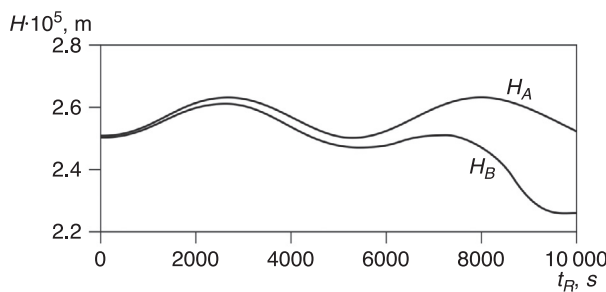
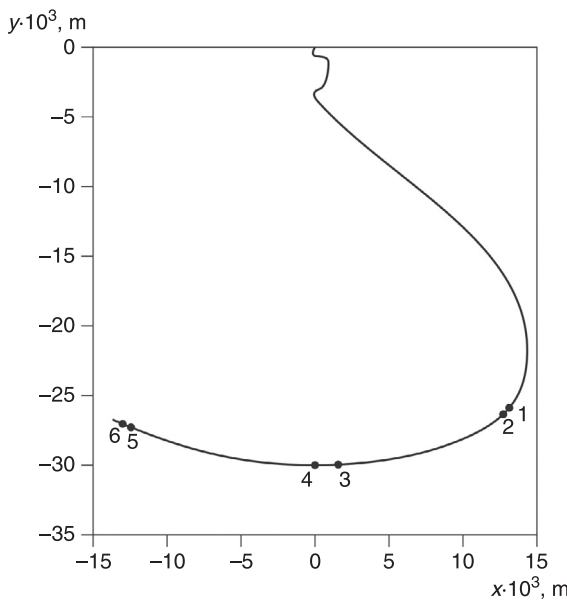


**Figure 4.37** Trajectory of a payload in a barycentric coordinate system connected with the base spacecraft

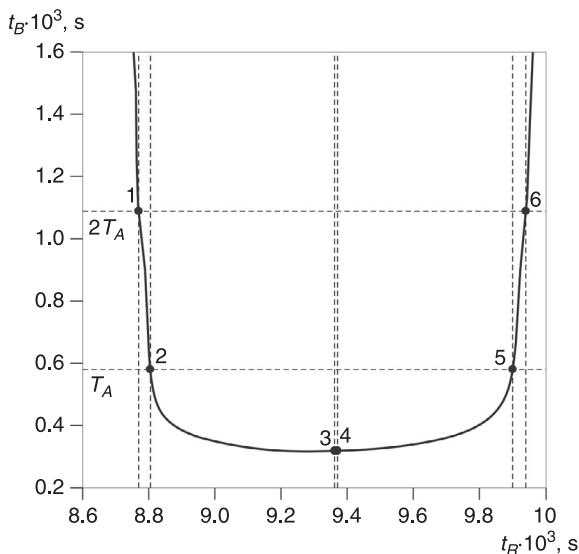


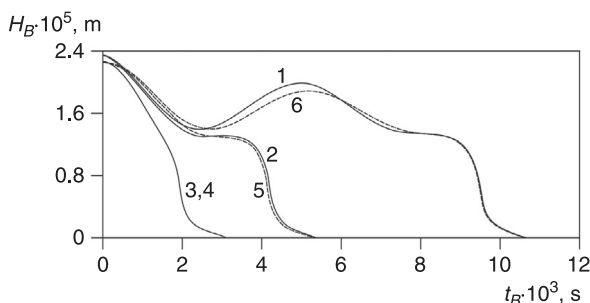
moment  $t_R$ . In Figure 4.37, the trajectory of the payload motion in the coordinate system related to the spacecraft is shown.

Let us study the influence of the moment of tether breakage on the time of the payload descent into the atmosphere  $t_B$ .

We will consider that the landing transited successfully if the payload reached the surface of the Earth in a time  $t_B$  not exceeding two periods of revolution of the spacecraft around the Earth  $T_A$ . Let us denote in Figure 4.37 and Figure 4.38 some characteristic points. Points 1 and 6 correspond to the trajectories of descent by a time of  $2T_A$ . If tether breakage happens before that time, corresponding to a point 1, or after time, corresponding to a point 6, the payload will be lost. Points 2 and 5 correspond to trajectories of the descent by a time of  $T_A$ . Point 3 corresponds to the fastest descent of the payload from an orbit, and point 4 relates to separation in a point lying on a local vertical of the spacecraft ( $\phi = 0$ ). The difference between the descent time at tether breakage in points 3 and 4 is 8 seconds. In Figure 4.39 the dependence of the payload altitude on the time of descent for the trajectories corresponding to the denoted points is shown.

**Figure 4.38** Dependence of the time of payload descent in the atmosphere on time of the tether breakage



**Figure 4.39** Dependence of altitude of the payload on time

Thus, for the viewed transport operation, from the point of view of payload loss, the cases of tether breakage at early stages of deployment are inadmissible. Breakage at a stage of the tether's return oscillative motion and some time after transiting by the payload of the local vertical is quite admissible. The point corresponding to the quickest descent does not lie on the local vertical, and is disposed somewhere near it.

## 4.5 References

- Andreevskiy V V (1970) *The Dynamics of the Descent of Spacecraft to Earth*, Moscow: Mashinostroenie (in Russian).
- Aslanov V S, Ledkov A S and Stratilatov N R (2007) ‘Spatial Motion of Space Rope Cargo Transport System’ (in Russian), *Polyot* (‘Flight’), ISSN 1684–1301, 2, 28–33.
- Aslanov V S, Ledkov A S and Stratilatov N R (2009) ‘The Influence of the Cable System Dedicated to Deliver Freights to the Earth of the Rotary Motion of Spacecraft’ (in Russian), *Polyot* (‘Flight’), ISSN 1684–1301, 1, 54–60.
- Aslanov V S, Pirozhenko A V, Voloshenjuk O L, Kislov A V and Yaschuk A V (2010), ‘Definition of Survival Time of

- Space Cord System' (in Russian), *Izvestiia Samarskogo nauchnogo tsentra RAN*, 4, 138–43.
- Carroll J (1993) *SEDS Deployer Design and Flight Performance*, AIAA 93-4764.
- Dignath F and Schiehlen W (2000) 'Control of the vibrations of a tethered satellite system', *Journal of Applied Mathematics and Mechanics*, 64, 5, 715–22.
- Dyukov D I (2010) 'Movement of a space vehicle with tether system at supernumerary situations' (in Russian), *Izvestiia Samarskogo nauchnogo tsentra RAN*, 4, 267–71.
- Kruijff M and Stelzer M (2007) *TN0113-YES2 Post Flight Analysis Summary, Version: 2.0*, 12/12/07.
- Lennert S and Cartmell M P (2006) 'Analysis and design of a friction brake for momentum exchange propulsion tethers', *Acta Astronautica*, 59, 923–30.
- Shcherbakov V I (2010) *Orbital Manoeuvres of Space Tether Systems* (in Russian). St Petersburg: A. F. Mozhaysky Military-space Academy.
- Zimmermann F, Schottle U M, and Messerschmid E (2005) 'Optimization of the tether-assisted return mission of a guided re-entry capsule', *Aerospace Science and Technology*, 5, 713–21.



## Conclusion

The mechanics of space tether systems is an extensive area of the modern mechanics of space flight. In this book we have tried to show on the one hand a variety of tasks and areas of research related with space tether systems, and on the other, their practical feasibility based on modern technology, and their ability to solve existing problems.

In one book it is impossible to answer all questions related with dynamics of space cable systems. Therefore, we have tried to focus on problems that may find wide application in the coming decades: the delivery of cargo from an orbit without the cost of rocket fuel, exploring the atmosphere and surface of the Earth by a subsatellite lowered on a tether. The specificity of these problems require us to create new mathematical models that take into account the interaction of the tether with the atmosphere and the movement around the centre of the mass of the spacecraft. Practical implementation cannot be made without assessment of potential emergencies and their consequences. Therefore, we have developed models that take into account various abnormal situations. Presented in the book, models and analytical results were used in the preparation and post-flight analysis of the international experiment YES2.

The study of chaotic behaviour of a mechanical system in space is a relatively new direction of tether system's mechanics. The presence of orbital eccentricity and the phenomenon of elasticity of tethers are the cause of the chaos

in space tether system's motion. Chaos can be a serious obstacle to the successful implementation of the space missions, because it can lead to off-normal operation of the system and to accidents. Using the methods of chaotic dynamics allows us to carry out a selection of space tether system parameters that preclude the possibility of chaos.

Another new trend that is discussed in detail in the book, is the study of dynamics of motion, relative to the centre of mass of the spacecraft with an attached tether. Tether systems have a significant influence on spacecraft dynamics, despite the low weight of the tether and tethered payload in comparison with the mass of the spacecraft. In some cases the spacecraft can be observed swinging with a subsequent transition into the rotation. New analytical solutions describing the plane vibrations of the spacecraft are illustrated in the book. These solutions can be used for quick calculations and qualitative analysis of the spacecraft motion with a tether.

The authors wish to thank the readers for their patience. We hope that the book will not only broaden your horizons, but will also arouse an interest in further study of the dynamics of space tether systems.

# Use of chaotic dynamics for the analysis of tether system motion

**Abstract:** This final chapter is devoted to research into the chaotic motion of space tether systems. The Melnikov method and Poincaré sections are described briefly. It is shown that the presence of an eccentricity at a system's orbit leads to chaotisation of motion. For the biharmonic oscillator equation, which describes the motion of a spacecraft with an elastic tether, the analytical solutions for homoclinic and heteroclinic orbits are found. For some particle cases, the analytical representation of the Melnikov function is obtained. The motion of a spacecraft with a vertical elastic tether is investigated by means of the chaotic method, and the conditions for prevention of chaotic motions are found.

**Key words:** chaotic motion; Poincaré sections; Melnikov method; condition for prevention of chaotic motions.

For a long time, the study of chaos has been associated with an assumption that in a system of extreme excitation a great number of degrees of freedom are necessary. This concept was generated under the influence of the ideas which have developed in statistical mechanics: the movement of each separate particle in a gas can be predicted, but behaviour in a system with a great number of particles is extremely complicated and consequently the detailed dynamic approach

loses its meaning. Later, it became clear that this very complicated behaviour can be observed in nonlinear systems with a small number of freedoms.

Physically, the initial condition of the system in view of the inevitably small perturbations should be set by some distribution. If the system is stable, small perturbations do not increase in the course of time and the system's behaviour is predictable. If a system is exponentially unstable, so it possesses a sensitive dependence on the initial conditions, then the points located in the initial instant at a small distance from each other can after a while separate at a bigger distance. Thus having full information on the movement of any point of a phase space, we cannot tell anything about the movement of the close points. Poincaré (1912), in his works, has come to the conclusion that a system's movement has an extremely complicated character close to unstable fixed points of a phase space. This was the first indication that nonlinear dynamic systems can exhibit chaotic properties. At various resonances in a phase space there are stable and unstable fixed points. The resonances of high orders lead to the formation of a chain of separatrix loops. The classical theory of perturbations does not describe such resonances because the solutions near to them are strongly disturbed (Birkhoff, 1927). These reasons have been laid down as the basis of modern representations of dynamic chaos. The chaos, instead of exterior random disturbances, defines the behaviour of nonlinear systems. The number of scenarios of the birth of chaos is limited. Moreover, some of them submit to universal regularities and do not depend on a system's nature (Loskutov, 2007).

Chaotic properties can show diversified nonlinear systems, and if the chaos is not discovered, that is probably only because it arises in very small areas of parametrical space, or at values of the parameters corresponding to physically unrealised areas.

It is necessary to distinguish casual and chaotical movements. The casual motion is understood as situations when forces acting on a system and parameters of that system are previously unknown or only some of their statistical performances are known. Under chaotic movement, a situation is understood when there are no casual or unpredictable forces or parameters.

## 5.1 Some elements of chaotic dynamics

Before starting research on the chaotic motions of a STS, we need to become acquainted with the Melnikov method which allows for achieving the necessary condition of chaos existence for the deterministic systems with several stable positions of equilibrium, and also with the Poincaré maps which allow us to carry out the qualitative analysis of a nonlinear mechanical system's behaviour.

### 5.1.1 Melnikov function

Let us consider a conservative system with two degree of freedoms, whose movement is set by means of an ordinary differential equation:

$$\dot{\mathbf{x}} = \mathbf{f}(\mathbf{x}), \quad [5.1]$$

where  $\mathbf{x} = \mathbf{x}(t) = [x_1(t); x_2(t)]^T$  – vectorial function of an independent variable  $t$ ; and  $\mathbf{f} = [f_1; f_2]^T$  – the continuous vectorial function having continuous first and second derivatives.

We assume that the mechanical system is a Hamiltonian system with coefficients:

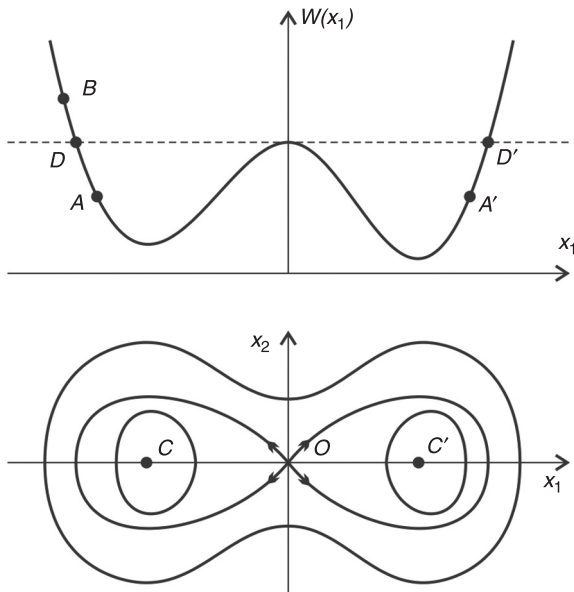
$$f_1 = x_2, \quad f_2 = -\frac{dW(x_1)}{dx_1},$$

where  $W(x_1)$  – the potential energy which is shown in Figure 5.1.

On a phase plane there are three singular points corresponding to local minimums and maximums of the potential energy – two centres (points C and C') and a saddle (point O). If, at the beginning, the particle is in a potential hole below a potential barrier, and starts to move with a zero velocity from the point A (or A') with ordinate  $W(x_1) < 0$ , then the particle will make periodic oscillations about the centre C (or C'), located at the bottom of that potential hole. On a phase plane  $(x_1, x_2)$ , the movement trajectory is represented by the closed curve around the centre C (or C'). If the particle begins its motion from the point B with ordinate  $W(x_1) > 0$ , it will make periodic oscillations around a saddle point O, and the particle will pass from one potential hole to another. Depending on the initial position and the initial velocity, the point will move in any periodic trajectory topologically similar to that presented in Figure 5.1.

Particles, whose total energy in an initial time is equal to  $x_2^2/2 - W(x_1) = W(0)$ , move on a trajectory with an infinitely large period. In Figure 5.1, the movement along this trajectory, termed a separatrix, is presented. The separatrix shown in Figure 5.1 has two branches connecting saddle point O to itself. Such trajectories, going out from a saddle point and entering into the same saddle point, are termed homoclinic. If the potential energy has more than one local minimum, there can be several saddle points on the phase portrait. The trajectories which are going out from one saddle point, and on entering the other saddle point they are termed heteroclinic (see Figure 5.2). Homoclinic and

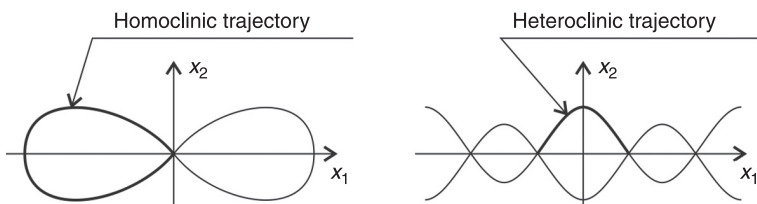
**Figure 5.1** Potential energy and phase portrait of some mechanical systems



heteroclinic trajectories will be designated by the index  $h$ :  $\mathbf{x}_h = [x_{h1}, x_{h2}]^T$ .

Motion along the homoclinic and heteroclinic trajectories can be considered as an extreme case of periodic motion arising in an area limited by these trajectories at periods tending to infinity. We will consider a system with homoclinic

**Figure 5.2** Homoclinic and heteroclinic trajectories

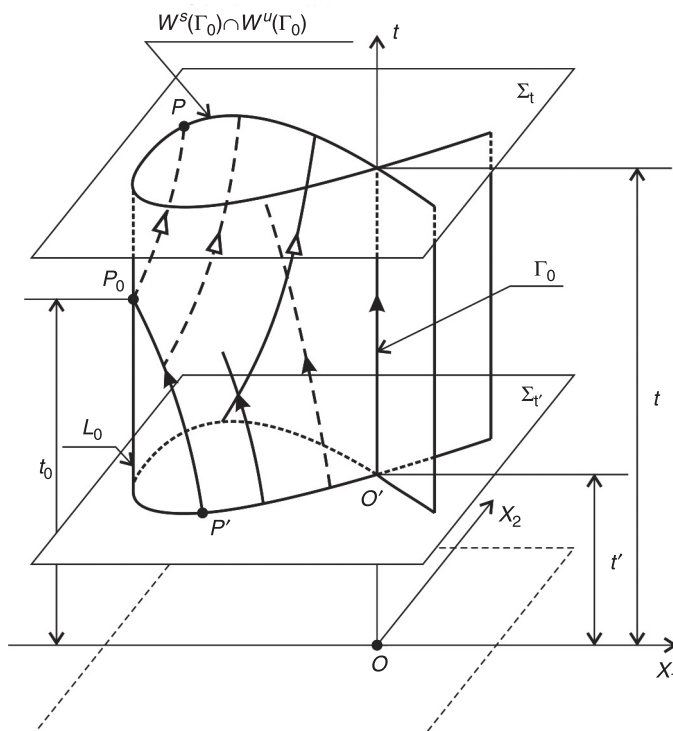


trajectories; however, all received results are fair and for the heteroclinic trajectories.

For an unperturbed system [5.1], the homoclinic trajectory is impenetrable. Other phase trajectories cannot intersect it and pass from one potential hole to another. If within the system there are perturbations or dissipations, this impermeability can be breached.

Let us consider the expanded phase space  $(x_1, x_2, t)$  with orthogonal axes of coordinates  $Ox_1, Ox_2, Ot$  (see Figure 5.3). We will construct in this space the homoclinic trajectories of the unperturbed system [5.1]. This set of trajectories form a

**Figure 5.3** Intersection of the manifolds of an unperturbed system



cylindrical surface. The intersection of this surface with a plane  $t = \text{const}$  creates homoclinic trajectories which coordinate in plane and are defined as  $(x_{h1}, x_{h2})$ . The intersection of an axis  $\Gamma_0 = Ot$  with a plane  $t = \text{const}$  corresponds to a saddle point of the homoclinic trajectory in this plane.

The specified cylindrical surface consists of two subsets. The first subset contains the trajectories which are asymptotically moving away from the axis  $\Gamma_0 = Ot$  and again coming nearer to it at  $t \rightarrow \infty$ ; that is, corresponding to trajectories on the plane  $(x_1, x_2)$  asymptotically coming to a saddle point in a direct time (see Figure 5.1). The second subset contains the trajectories which are coming nearer to the axis  $\Gamma_0 = Ot$  at  $t \rightarrow -\infty$ ; that is, corresponding to trajectories on the plane  $(x_1, x_2)$  asymptotically coming to the saddle point in an inverse time. These two subsets are termed unstable manifold  $W^u(\Gamma_0)$  and stable manifold  $W^s(\Gamma_0)$  of the system accordingly. For the considered unperturbed system [5.1], the stable and unstable manifolds coincide. The cylindrical surface of Figure 5.3 represents the intersection of the manifolds  $W^u(\Gamma_0) \cap W^s(\Gamma_0)$ . It is a three-dimensional analogue of coincidence of the homoclinic trajectories which are coming to a saddle point in direct and inverse time on a phase plane  $(x_1, x_2)$ .

Let us define the vertical reference axis  $L_0$  contained in the manifolds, and intersecting planes  $t = \text{const}$  in the points with coordinates  $\mathbf{x}_h(0)$ . The trajectory belonging to the manifolds is defined by coordinate  $t_0$  and a point  $P_0$  in which the trajectory is tangential to  $L_0$ . The arbitrary point  $P$  of this trajectory is defined by the coordinate  $t_0$  setting all of the trajectory as a whole, and by the coordinate  $t - t_0$  representing the shift in time between points  $P$  and  $P_0$ . The point coordinate  $P$  on a plane  $(x_1, x_2)$  is written as  $\mathbf{x}_h(t - t_0)$ . In particular, as is specified above, the coordinate of  $P_0$  in this plane is  $\mathbf{x}_h(t_0 - t_0) = \mathbf{x}_h(0)$ .

The unstable manifold can be considered as the unification of two subsets. The first subset is a surface contained in  $\varepsilon$ , close to  $\Gamma_0$  and termed as a local unstable manifold. The second subset is a global unstable manifold consisting of a set of trajectories developing in direct time with the initial conditions belonging to a local unstable manifold. Local and global stable manifolds are similarly defined.

Stable and unstable manifolds are invariant, that is they possess the following property: if some point of a trajectory belongs to a manifold then all points of the trajectory belong to it.

The trajectory, arising in a limited area coinciding with stable and unstable manifolds, cannot intersect these manifolds. It follows from the uniqueness of the solution: if such an intersection has happened, various trajectories of the system would pass through a cross point, one of them belonging to the manifolds, and another to the intersecting manifolds. As has already been said, the existence of a separatrix in a conservative system hinders the occurrence of motions with passages. Motions with passages can arise in systems with exterior excitation and dissipative forces.

Let us consider the perturbed system:

$$\dot{\mathbf{x}} = \mathbf{f}(\mathbf{x}) + \varepsilon \mathbf{g}(\mathbf{x}, t), \quad [5.2]$$

where  $\mathbf{g} = [g_1, g_2]^T$  – continuous vectorial function having continuous first and second derivatives.

Let us assume that the unperturbed system [5.1] corresponding to it has a homoclinic trajectory  $\mathbf{x}_h = [x_{h1}, x_{h2}]^T$  with saddle point O in an origin of coordinates. Nonautonomous perturbations convert the integrable system into a nonintegrable system. One of the effects generated by them is the splitting of the stable and unstable manifolds, in other words the homoclinic trajectories received in direct and inverse time are noncoincident.

The perturbation transforms the axis  $\Gamma_0$  to the smooth curve  $\Gamma_\varepsilon$ . The distance between  $\Gamma_0$  and  $\Gamma_\varepsilon$  depends on time  $t$  and has an order  $\varepsilon$  (see Figure 5.4). The perturbed system has local stable and unstable manifolds. The intersection of these manifolds with a cut plane  $C^r$  close to the intersection with this plane of corresponding local manifolds of the unperturbed system (two elements are called  $C^r$  which are nearby if the elements and  $r$  their first derivatives differ in magnitude of an order  $\varepsilon$ ). The set  $\Gamma_\varepsilon$ , as well as  $\Gamma_0$  is hyperbolic. The perturbed stable and unstable manifolds, unlike their unperturbed analogues, do not coincide. The distance between them depends on the position of the unperturbed manifold. In Figure 5.4, this distance in a point  $P$  of the unperturbed manifold is shown. Its intersection varies with a plane  $\Sigma_t$  which is represented by a dashed line. As a first approximation, the absolute value of this distance is proportional to the Melnikov function (Simiu, 2009):

$$M(t_0) = \int_{-\infty}^{\infty} (f_1(\mathbf{x}_b(\xi))g_2(\mathbf{x}_b(\xi), \xi + t_0) - f_2(\mathbf{x}_b(\xi))g_1(\mathbf{x}_b(\xi), \xi + t_0)) d\xi, [5.3]$$

where  $\mathbf{x}_b = [x_{b1}, x_{b2}]^T$  – homoclinic trajectory of unperturbed system.

Let us construct a cross-section  $\Sigma_t$  normal to an axis  $Ot$  in a point  $t'$  and consider its intersection with the stable and unstable manifolds coinciding in the unperturbed system (the dashed curve in Figure 5.5) and splitting the perturbed system (the solid curve in Figure 5.5). We fix the ordinate  $t'$ , and define a point  $P'$  by coordinates  $t_0$  and  $t'$  (see Figure 5.3). A straight line  $N$  is a normal to the intersection of the unperturbed manifolds with cross-section  $\Sigma_{t'}$  in the point  $P'$ . We consider the trajectories belonging to the stable and unstable manifolds of the perturbed system and intersecting the normal  $N$  in points  $A'$  and  $A''$  accordingly. The same

**Figure 5.4** Intersection of the manifolds of a perturbed system

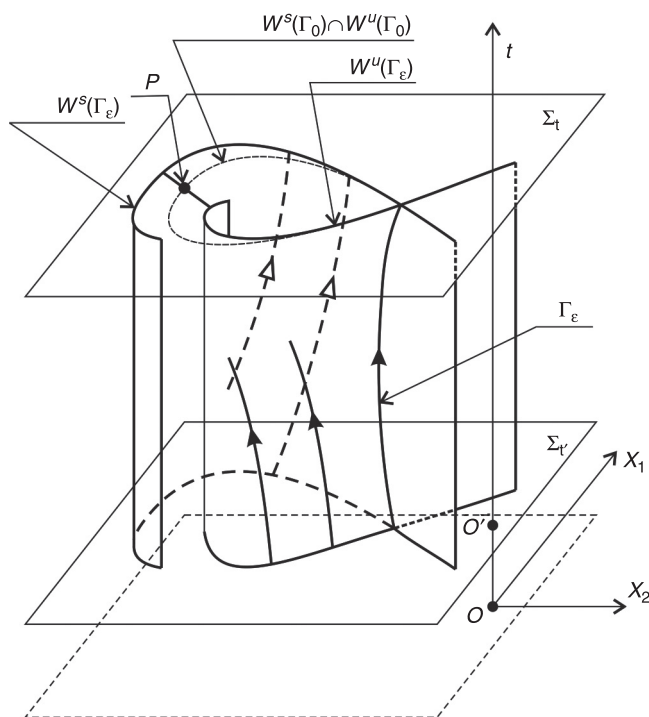
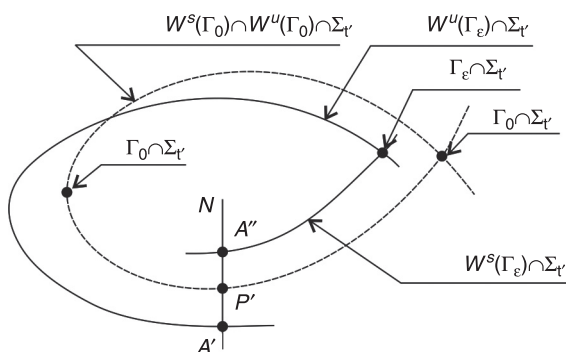


**Figure 5.5** The Melnikov distance in a point  $P$



trajectories intersect a plane of cross-section  $\Sigma_t$  with the ordinate  $t$  in points with coordinates:

$$\mathbf{x}^s(t; t_0, t', \varepsilon) = [x_1^s(t; t_0, t', \varepsilon), x_2^s(t; t_0, t', \varepsilon)]^T$$

and

$$\mathbf{x}^u(t; t_0, t', \varepsilon) = [x_1^u(t; t_0, t', \varepsilon), x_2^u(t; t_0, t', \varepsilon)]^T.$$

As was specified above, the trajectory belonging to the unperturbed manifolds and containing the point  $P'$ , intersects a plane  $\Sigma_t$  in a point with a coordinate  $\mathbf{x}_b(t - t_0)$ . Having supposed in equation [5.2] that  $\varepsilon = 0$ , we will prove that the vector  $\mathbf{f}(\mathbf{x}_b(t - t_0))$  in the point  $P$  is directed along a tangent to the intersection of the unperturbed manifolds with  $\Sigma_t$ .

Splitting of the manifolds on a plane  $\Sigma_t$  is defined by the function:

$$\Delta_\varepsilon(t; t_0, t') = \mathbf{f}(\mathbf{x}_b(t - t_0)) \wedge (\mathbf{x}^u(t; t_0, t', \varepsilon) - \mathbf{x}^s(t; t_0, t', \varepsilon)), \quad [5.4]$$

where  $\mathbf{a} \wedge \mathbf{b} = a_1 b_2 - a_2 b_1$ .

Equation [5.4] means that the function  $\Delta_\varepsilon(t; t_0, t')$  is equal to the vector product of  $\mathbf{f}(\mathbf{x}_b(t - t_0))$  on a projection of the difference  $(\mathbf{x}^u(t; t_0, t', \varepsilon) - \mathbf{x}^s(t; t_0, t', \varepsilon))$  to the normal  $N$ . The absolute value of this projection is called the Melnikov distance in the point  $P$  (see Figure 5.4). In particular,  $\Delta_\varepsilon(t'; t_0, t')$  represents the splitting of the manifolds in a point  $P'$  of the cross-section  $\Sigma_{t'}$ . The absolute value of the function  $\Delta_\varepsilon(t'; t_0, t')$  is proportional to the Melnikov distance in the point  $P'$ , that is equal by definition to the distance between points  $A'$  and  $A''$  (see Figure 5.5). Approximation of the function  $\Delta_\varepsilon$ , accurate within the first order of  $\varepsilon$ , gives (Simiu, 2009):

$$\Delta_\varepsilon(t'; t_0, t') = \varepsilon M(t_0) + O(\varepsilon^2), \quad [5.5]$$

where  $M(t_0)$  is defined by equation [5.3].

At the heart of the Melnikov theory lies the following statement: if the Melnikov function has a simple root at some value of  $t_0$  then at a small enough  $\varepsilon$ , stable  $W^s(\Gamma_\varepsilon(t))$ , and unstable  $W^u(\Gamma_\varepsilon(t))$ , the manifolds of the perturbed system are intersected transversally. If  $M(t_0) \neq 0$ , the manifolds are not intersected:

$$W^s(\Gamma_\varepsilon(t)) \cap W^u(\Gamma_\varepsilon(t)) = \emptyset.$$

The Smale-Birkhoff theorem states that the existence of a simple zero of the Melnikov function is a necessary condition of the origin of chaos. Arising from the chaotic motion with the passages exhibited at the intersection of the stable and unstable manifolds, is the homoclinic chaos. If the Melnikov function has no simple zero, the motion cannot be chaotic, and the passages do not arise (Simiu, 2009).

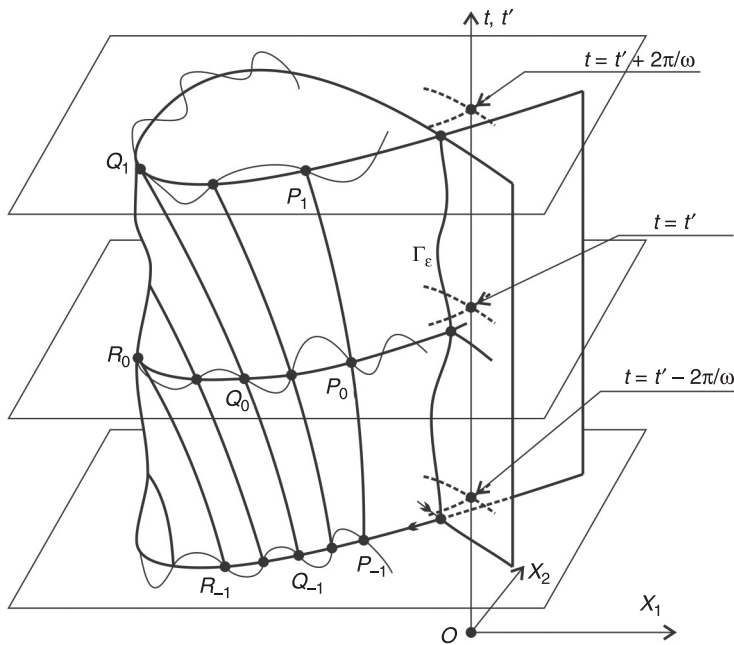
### 5.1.2 Poincaré mapping

Let us suppose that the disturbance in system [5.2] is a periodic function of time and the frequency  $\Omega$ . We designate a solution of equation [5.2] in the moment  $t$  with the initial condition  $\mathbf{x} = \mathbf{x}_0$  in the moment  $t_0$  as  $\mathbf{x}(\mathbf{x}_0, t_0; t)$ . Let  $t_0 = t' + 2k\pi/\Omega$ , where  $t'$  is the fixed instant of time,  $k$  is the integer, and we will also define  $t = t' + 2(k + 1)\pi/\Omega$ . As the periodic disturbance does not change at modification of the integer  $k$ , from equation [5.2] we will obtain that the vector:

$$\mathbf{x}(\mathbf{x}_0, t' + 2\pi k / \Omega; t' + 2\pi(k + 1) / \omega), \quad (k = \pm 1, \pm 2, \dots)$$

does not depend from  $k$ .

Coordinates of the intersections of the curve  $\Gamma_\varepsilon$  with planes having ordinates  $t' + 2\pi k / \Omega$  ( $k = 0, \pm 1, \pm 2, \dots$ ) are identical to all  $k$  (see Figure 5.6). We will term these planes the sections of Poincaré. In Figure 5.6, the identical intersections are

**Figure 5.6** Cross-sections of manifolds

presented with planes with the ordinates  $t' - 2\pi k/\Omega$  and  $t' + 2\pi k/\Omega$  at the fixed  $t'$ .

Let us consider the sequence of the intersections of a trajectory with parallel planes with ordinates  $t' + 2\pi k/\Omega$  ( $k = 0, \pm 1, \pm 2, \dots$ ).  $Q_{-1}, Q_0, Q_1, \dots$  are points of the intersections at direct motion, and  $Q_1, Q_0, Q_{-1}, \dots$  are points of the intersections at inverse motion. The point  $Q_1$  is called the direct iteration of  $Q_0$ , and the point  $Q_{-1}$  is the inverse iteration of  $Q_0$ . As at fixed  $x_0$ , the function  $x(x_0, t' + 2\pi k/\Omega; t' + 2\pi(k+1)/\Omega)$  does not depend on  $k$ , and the point  $Q_1$  can be characterised by its orthogonal projection  $R_0$  on the plane  $t = t'$ . Similarly, the point  $Q_{-1}$  is characterised by the projection  $P_0$ . It means that instead of the sequence of points  $Q_{-1}, Q_0, Q_1, \dots$  on the three parallel planes it is possible to consider the equivalent sequence  $P_0, Q_0, R_0$  on one plane.

Similar sections can be constructed for the nonautonomous system. Let us assume that  $T = 2\pi/\Omega$  is a period of nonautonomous disturbance of the system. We will write the equations of motion [5.2] in the expanded (autonomous) phase space  $(x_1, x_2, \theta)$ , where  $\theta = [\Omega t + \theta_0] \pmod{2\pi}$ :

$$\begin{aligned}\dot{x}_1 &= f_1(x_1, x_2) + \varepsilon g_1(x_1, x_2, \theta), \\ \dot{x}_2 &= f_2(x_1, x_2) + \varepsilon g_2(x_1, x_2, \theta), \\ \dot{\theta} &= \Omega.\end{aligned}\quad [5.6]$$

The equations [5.6] generate a stream  $\phi_t = \phi_t(\mathbf{x}(t), \theta(t))$ , and the intersection  $\phi_t$  with a plane  $\theta(t) = \theta_c = \text{const}$  will be designated as  $\Sigma$ . The Poincaré map  $\Sigma \rightarrow \Sigma$  is defined as:

$$\phi\left(\mathbf{x}\left(\frac{\theta_c - \theta_0}{\Omega}\right), \theta_c\right) \rightarrow \psi\left(\mathbf{x}\left(\frac{\theta_c - \theta_0 + 2\pi}{\Omega}\right), \theta_c + 2\pi\right).$$

Or, taking into account periodicity of disturbance,

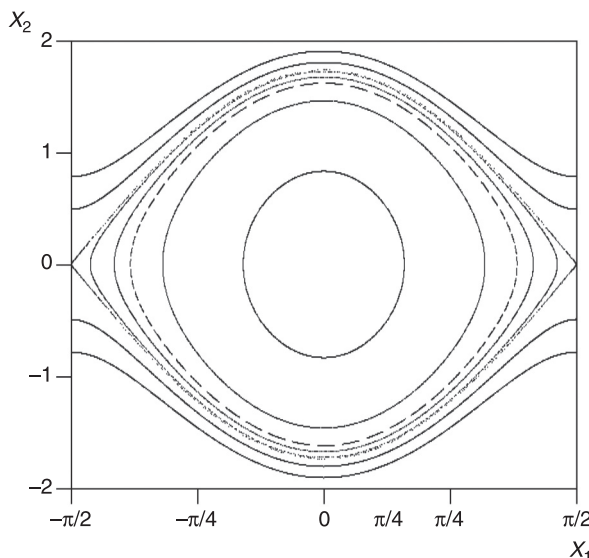
$$\phi\left(\mathbf{x}(\Omega), \theta_c\right) \rightarrow \psi\left(\mathbf{x}\left(\frac{\theta_c - \theta_0 + 2\pi}{\Omega}\right), \theta_c\right).$$

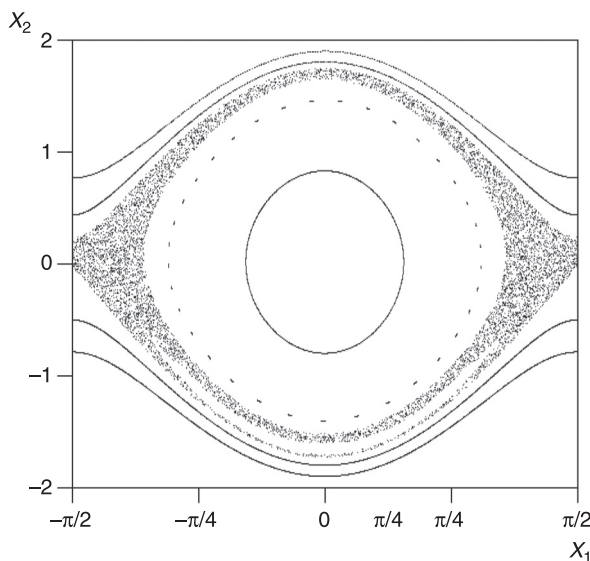
Construction of the Poincaré section for systems [5.2] or [5.6] allows us to estimate qualitatively the chaos presence in the system. Let us describe the procedure of construction of the section. The limited set of initial points on a phase plane is selected. Then numerical integration of the motion equations is made for each initial point. The points of intersection of each trajectory with the cross sections  $t' + 2\pi k/\Omega$  are plotted on a single phase plane  $(x_1, x_2)$ . Increasing the final time to which the trajectories are calculated, it is possible to increase the number of points on the received section. A similar result can be achieved by increasing the number of initial points and, accordingly, the trajectories. The question of a choice of the initial points is interesting.

The most obvious result occurs if we take some points in the  $\varepsilon$  neighbourhoods of a separatrix and also take some points away from it. If we take too many points, it will lead to an overloaded picture which is difficult, or occasionally impossible, to interpret.

The Poincaré section received thus allows us to make a conclusion on the chaos presence. If the points of intersection of the trajectories with the cross sections form lines, it is possible to tell that chaos is not present in the system. If the points organise the uniform cloud called a chaotic layer, there is chaos in the system. In Figure 5.7 and Figure 5.8, the Poincaré sections for the unperturbed system and the system in the presence of chaos are shown. In Figure 5.7, the points organise lines, therefore the motion is regular. In Figure 5.8, in the neighbourhood of the separatrix, the chaotic layer is observed. The trajectories passing far from a separatrix are feebly perturbed and the cross points organise

**Figure 5.7** Poincaré section of an unperturbed system



**Figure 5.8** Poincaré section of a perturbed system

lines. In addition, the new areas which were absent on the section of the unperturbed system are observed (a white spot in the bottom of the chaotic layer).

## 5.2 The chaotic approach in STS dynamics

We described above the Melnikov method and the Poincaré sections for research of the chaotic motion of a STS.

### 5.2.1 Chaotic oscillations of a STS in an elliptic orbit

In problems of the modern mechanics of space flight, great attention is paid to research into a spacecraft's motion in a

circular orbit. The assumption that the orbit is circular considerably simplifies the equations of motion and allows us to receive some analytical results. Meanwhile, the presence of a nonzero eccentricity can essentially affect the character of all the system motion. To estimate the influence of eccentricity on STS dynamics we use equations [2.106]–[2.108], which describe the STS motion around its centre of mass. Let us introduce some additional assumptions. We will disregard the sizes of the base spacecraft ( $\Delta = 0$ ) and the elasticity of a tether ( $l = \text{const}$ ). Thus, the eccentricity remains as the unique disturbing factor. Movement of the STS around its centre of mass in this case is described by one differential equation of the second order:

$$\varphi'' + \frac{3\sin\varphi\cos\varphi}{1+e\cos\vartheta} - \frac{2e\sin\vartheta}{1+e\cos\vartheta}(1+\varphi') = 0. \quad [5.7]$$

Equation [5.7] can be simplified. We will expand the expression into the series:

$$\frac{1}{1+e\cos\vartheta} = 1 - e\cos\vartheta + e^2\cos^2\vartheta + \dots$$

For small values of eccentricity, it is possible to consider only the first two terms of this series:

$$\frac{1}{1+e\cos\vartheta} \approx 1 - e\cos\vartheta.$$

Substituting the last expression into [5.7], we obtain the equation of a STS's perturbed motion around its centre of mass in an orbit plane for  $e \ll 1$ :

$$\varphi'' + 3\sin\varphi\cos\varphi = 2e(1+\varphi')\sin\vartheta + 3e\sin\varphi\cos\varphi\cos\vartheta = 0, \quad [5.8]$$

that coincides with the results obtained in Beletsky and Levin (1993).

Substituting  $e = 0$  into [5.8], we obtain the equation of the unperturbed movement:

$$\varphi'' + 3\sin\varphi\cos\varphi = 0, \quad [5.9]$$

corresponding to motion of the STS in a circular orbit. We will obtain an analytical solution for separatrix of [5.9], and for this purpose we write an energy integral:

$$\frac{\varphi'^2}{2} + W(\varphi) = h, \quad [5.10]$$

where  $W(\varphi) = -\frac{3}{2}\cos^2\varphi$  – potential energy; and  $h$  – total energy.

The curve of a potential energy and phase portrait of the system [5.9] is presented in Figure 5.9. The system [5.9], on a segment  $[-\pi/2, \pi/2]$ , has three positions of equilibrium: one centre  $\varphi_C = 0$ , and two saddles  $\varphi_{S-1} = -\pi/2$ ,  $\varphi_{S1} = \pi/2$ . It is necessary to note that the system is periodical within a period  $\pi$ : at  $\varphi \rightarrow -\pi/2$  and  $\varphi \rightarrow \pi/2$  the velocities coincide and the phase trajectories are closed, therefore we will investigate a cylindrical phase space for  $\varphi \in [-\pi/2, \pi/2]$ .

Let us integrate [5.10].

$$\frac{d\varphi}{d\vartheta} = \pm\sqrt{2h - 2W(\varphi)}.$$

We divide the variables:

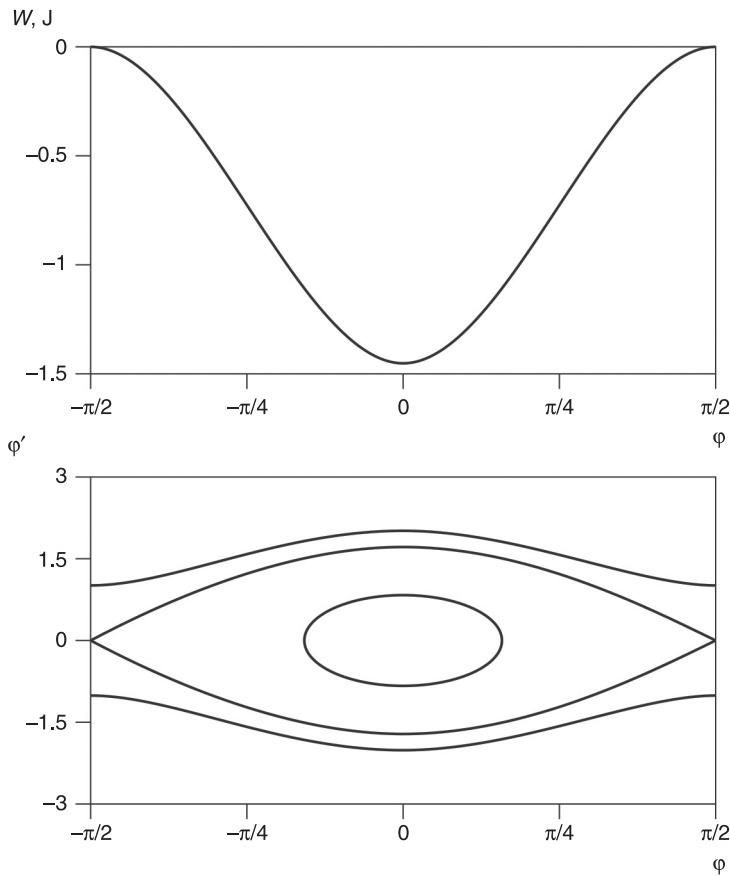
$$d\vartheta = \pm \frac{d\varphi}{\sqrt{2h - 2W(\varphi)}}. \quad [5.11]$$

In saddle points  $\varphi = \pi/2 + \pi n$ , ( $n \in \mathbb{Z}$ ),  $\varphi' = 0$ . Substituting these values in [5.10], we find the energy corresponding to the separatrix:

$$E_s = 0.$$

Then expression [5.11] takes the form:

$$d\vartheta = \pm \frac{d\varphi}{\sqrt{2h_s - 2W(\varphi)}} = \pm \frac{d\varphi}{\sqrt{3\cos\varphi}}.$$

**Figure 5.9** Potential energy and a phase portrait of [5.9]

This equation can be integrated:

$$\vartheta = \pm \frac{1}{2\sqrt{3}} \ln \left| \frac{1 + \sin \varphi}{1 - \sin \varphi} \right| + \vartheta_0.$$

where  $\vartheta_0$  – arbitrary constant: and we assume  $\vartheta_0 = 0$ .

From this last expression it is possible to find:

$$\varphi(\vartheta) = \arcsin \left( \frac{e^{\pm 2\sqrt{3}\vartheta} - 1}{e^{\pm 2\sqrt{3}\vartheta} + 1} \right). \quad [5.12]$$

Definitively, for the solution of the equation describing the unperturbed motion in the separatrix we write in a form convenient for use in the Melnikov method:

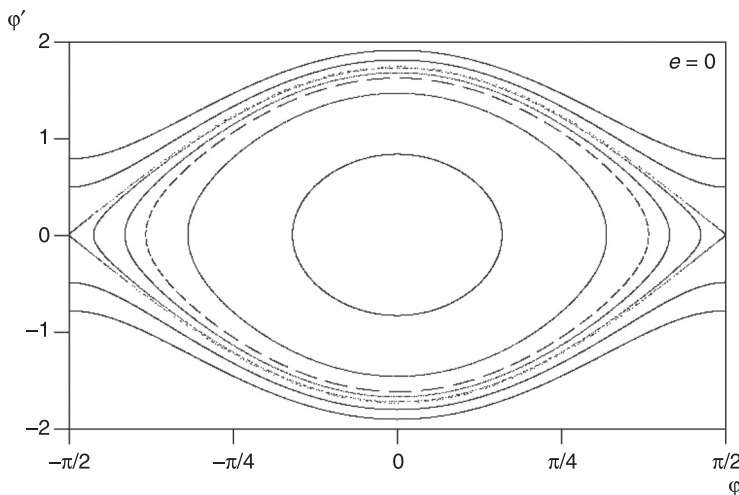
$$\varphi_{\pm}(\vartheta) = \arcsin(\tanh(\pm 2\sqrt{3}\vartheta)), \quad [5.13]$$

$$\sigma_{\pm}(\vartheta) = \frac{\pm 2\sqrt{3}e^{\pm\sqrt{3}\vartheta}}{e^{\pm 2\sqrt{3}\vartheta} + 1}. \quad [5.14]$$

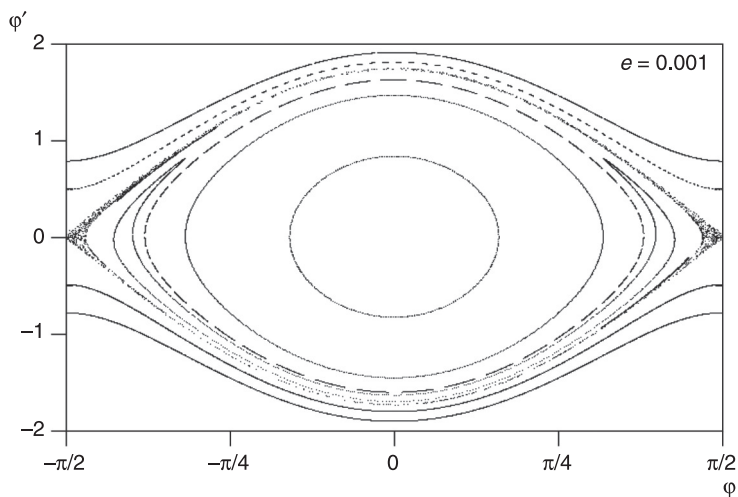
This solution is a more special case than the more common solution found in Aslanov (2009a).

Let us construct the Poincaré sections of equation [5.8] for various eccentricities. At  $e = 0$ , the motion is unperturbed, and in Figure 5.10 the lines corresponding to the phase trajectories of the unperturbed system are observed. With an increase in the eccentricity, the thickness of a chaotic layer in a neighbourhood of the separatrix which looks like a cloud of points, increases (see Figures 5.11–5.13). If the phase trajectory gets to this layer, the system motion becomes chaotic.

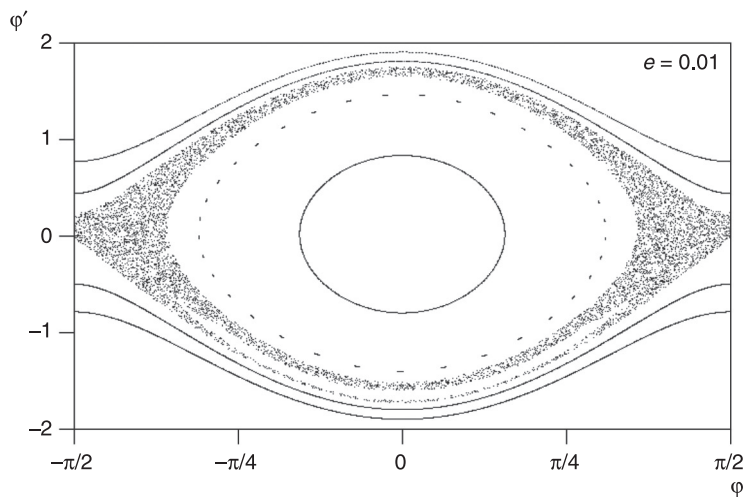
**Figure 5.10** Poincaré section of an unperturbed system [5.9]



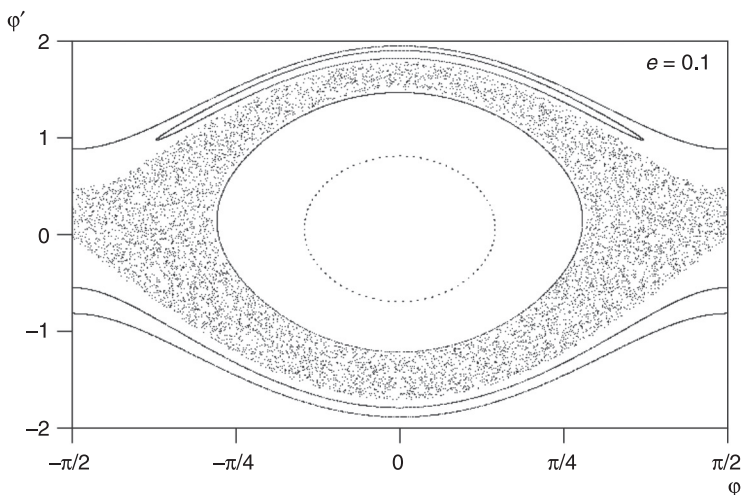
**Figure 5.11** Poincaré section of a perturbed system [5.8] at  $\epsilon = 0.001$



**Figure 5.12** Poincaré section of a perturbed system [5.8] at  $\epsilon = 0.01$

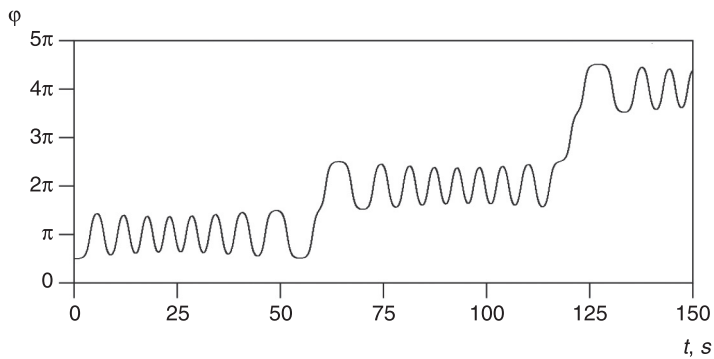
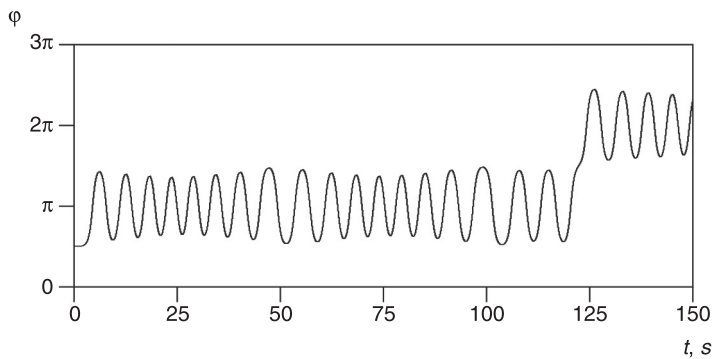
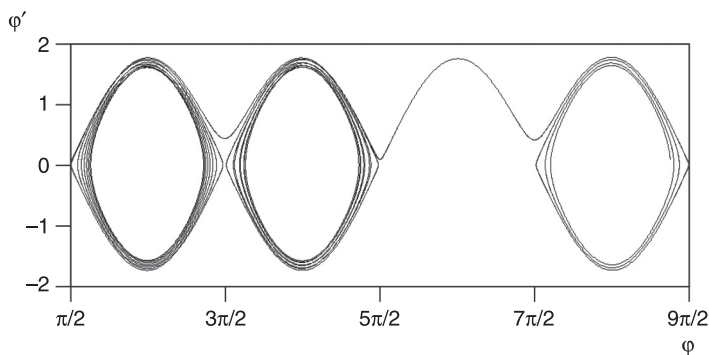


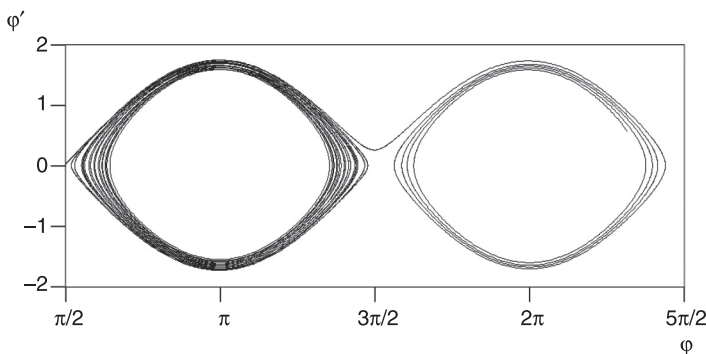
**Figure 5.13** Poincaré section of a perturbed system [5.8] at  $e = 0.1$



From the physical point of view, the presence of a chaotic layer leads to the conclusion that the STS can pass in a random way from an oscillating motion to a rotational and inverse motion. In Figures 5.14–5.17, the oscillations of the STS and the corresponding phase portraits obtained at the numerical integration of system [5.8] at  $e = 0.01$  and close located initial points  $\varphi_0 = \pi/2 - 0.001$ ,  $\dot{\varphi}_0 = 0$  and  $\varphi_0 = \pi/2 - 0.002$ ,  $\dot{\varphi}_0 = 0$  are shown. Even such small deviations lead to an essential modification of the picture of a STS motion.

Besides splitting the separatrix, and the origin of the chaotic layer as a result, on the Poincaré sections there are also new zones of steady oscillations which are exhibited as light spots in a chaotic layer (see Figure 5.12 and Figure 5.13). From Figure 5.11 it is also noticeable that at a distance from the separatrix, the phase trajectories keep a regular shape.

**Figure 5.14** Oscillation of a STS at  $\varphi_0 = \pi/2 - 0.001$ ,  $e = 0.01$ **Figure 5.15** Oscillation of a STS at  $\varphi_0 = \pi/2 - 0.002$ ,  $e = 0.01$ **Figure 5.16** Phase portrait at  $\varphi_0 = \pi/2 - 0.001$ ,  $e = 0.01$ 

**Figure 5.17** Phase portrait at  $\vartheta_0 = \pi/2 - 0.002$ ,  $e = 0.01$ 

Let us calculate the Melnikov function characterising the thickness of a chaotic layer and the presence of chaos in the system. If the Melnikov function  $M(\vartheta_0)$  has simple roots in a point  $\vartheta_0$ , then at small enough  $e$  the stable and unstable manifolds are intersected transversally. If function  $M(\vartheta_0)$  has no simple roots stable and unstable manifolds are not intersected and the chaotic modes caused by the intersection of homoclinic structures do not arise. In other words, the Melnikov function allows us to judge the stability of the areas of a system's motion. In this case, where the Melnikov function has simple roots at the system, there is chaos and a phase trajectory can intersect a separatrix and leave its area.

Let us write a differential equation of the second order [5.8] in the form convenient for use of the Melnikov method.

$$\begin{aligned} \varphi' &= \sigma = f_1 + g_1, \\ \sigma' &= 2e \sin \vartheta(1 + \varphi') + 3e \sin \varphi \cos \varphi \cos \vartheta - 3 \sin \varphi \cos \varphi \\ &= f_2 + g_2, \end{aligned} \quad [5.15]$$

where

$$\begin{aligned} f_1 &= \sigma, g_1 = 0, f_2 = -3 \sin \varphi \cos \varphi, g_2 = 2 \sin \vartheta(1 + \varphi') \\ &+ 3 \sin \varphi \cos \varphi \cos \vartheta. \end{aligned}$$

The Melnikov function for the perturbed system [5.8] takes the form:

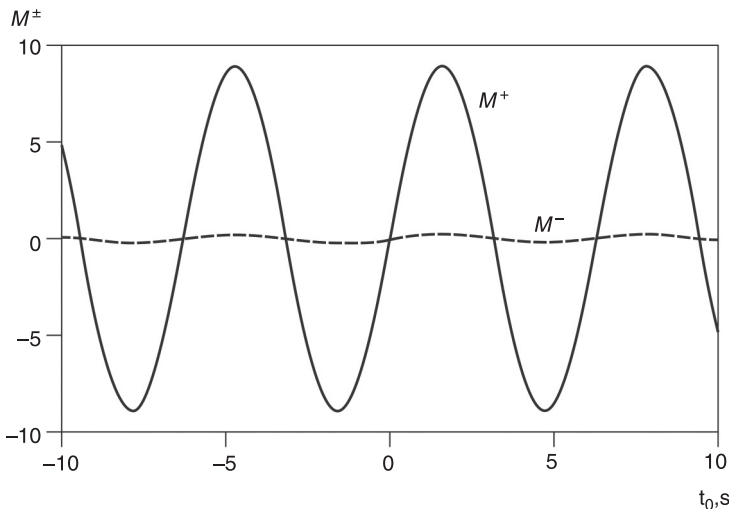
$$\begin{aligned} M(\vartheta_0)^\pm &= \int_{-\infty}^{\infty} (f_1 g_2 - f_2 g_1) d\vartheta = \\ &= \int_{-\infty}^{\infty} (\sigma_\pm(\vartheta) (2 \sin(\vartheta + \vartheta_0) (1 + \sigma_\pm(\vartheta)) \\ &\quad + 3 \sin \varphi_\pm(\vartheta) \cos \varphi_\pm(\vartheta) \cos(\vartheta + \vartheta_0))) d\vartheta, \end{aligned} \quad [5.16]$$

where  $\varphi_\pm(\vartheta)$ ,  $\sigma_\pm(\vartheta)$  – analytical solutions for an unperturbed separatrix [5.13] and [5.14].

From Figure 5.18, it is noticeable that the Melnikov function has roots, therefore it is possible to say that at the system there is chaos.

In modelling, the motion of the simple model has been used. Equation [5.8] does not contain any other parameters, except for an orbit eccentricity. So, irrespective of the length of the tether and its properties, the motion of the STS in an elliptic orbit is subject to chaos which is exhibited if the oscillations happen near a separatrix of the unperturbed

**Figure 5.18** The Melnikov function for a perturbed system at  $e = 0.01$



system. On the other hand, near the point corresponding to a local vertical  $\varphi = 0$ ,  $\varphi' = 0$ , the movement remains regular even at rather large values of eccentricity.

### 5.2.2 Chaotic behaviour of the biharmonic system

Let us consider the periodically perturbed biharmonic dynamic system with a damping:

$$\ddot{\alpha} = a \sin \alpha + b \sin 2\alpha + \varepsilon(c_1 \sin \alpha + c_2 \sin 2\alpha + c_3) \times \cos(\Omega t + \phi_{t0}) - \delta \dot{\alpha}, \quad [5.17]$$

where  $\varepsilon$  and  $\delta$  are assumed to be small positive parameters;  $\Omega > 0$  – the frequency of the external force;  $a$ ,  $b$  and  $c_i$  ( $i = 1, 2, 3$ ) are coefficients; and  $\phi_{t0}$  – the initial phase of the periodic perturbation (we suppose for simplicity that  $\phi_{t0} = 0$ ).

The terms  $\varepsilon$  and  $\delta$  in equation [5.17] can be considered as small perturbations. Equation [5.17] can be used for describing the motion of different mechanical systems, in particular such an equation describes the mathematical pendulum, the spatial motion of a spacecraft in the atmosphere (Aslanov, 2009a), or the motion of a STS. Let us consider equation [5.17] without paying attention to the physical sense of its factors.

Let us show that equation [5.17] is equivalent to the Duffing equation for small values of  $\alpha$ . It is known that:

$$\sin x = x - \frac{x^3}{3!} + \dots$$

Using expansion for  $x = \alpha, 2\alpha$ , the equation [5.17] can be written as

$$\begin{aligned} \ddot{\alpha} - a(\alpha - \frac{\alpha^3}{3!}) - b[2\alpha - \frac{(2\alpha)^3}{3!}] &= \varepsilon\{a(\alpha - \frac{\alpha^3}{3!}) \\ &+ b[2\alpha - \frac{(2\alpha)^3}{3!}] + c_3\} \cos \Omega t - \delta \dot{\alpha} + \dots \end{aligned}$$

If the variable  $\alpha$  is of a small of order  $\varepsilon$ , then we have the Duffing equation:

$$\ddot{\alpha} + \lambda\alpha + \mu\alpha^3 = \varepsilon(c_3 - \lambda\alpha)\cos\Omega t - \delta\dot{\alpha} + O(\varepsilon^4),$$

where  $\lambda = -(a + 2b)$ ; and  $\mu = \frac{a+8b}{3!}$ .

If  $\varepsilon = 0$  and  $\delta = 0$ , then the periodic and the damping force are absent, and we have the conservative system describing the motion of the unperturbed biharmonic oscillator as:

$$\ddot{\alpha} = a\sin\alpha + b\sin 2\alpha. \quad [5.18]$$

The equilibrium positions of the unperturbed system [5.18] are defined as solutions of an equation:

$$\sin\alpha(1 + \gamma\cos\alpha) = 0, \quad [5.19]$$

where  $\gamma = 2b/a$ .

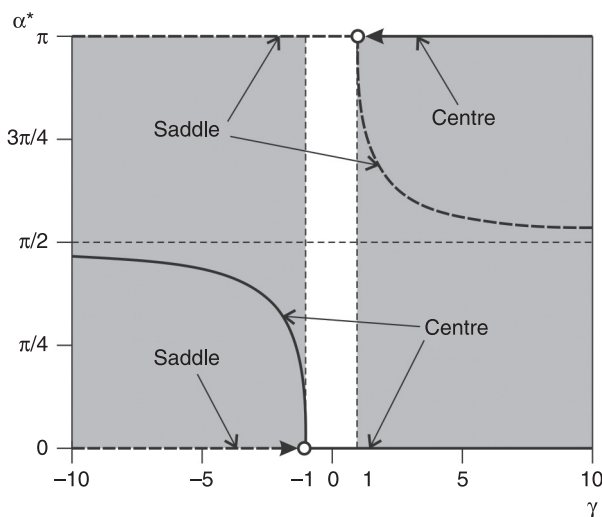
From [5.19], it follows that there are two equilibrium positions  $\alpha_* = 0, \pi$ , and the third position of equilibrium  $\alpha_* \in (0, \pi)$  exists under the condition:

$$|\gamma| > 1. \quad [5.20]$$

If this condition is not satisfied, then on a system's phase portrait only two equilibrium positions are observed. The centre is always in the point  $\alpha_* = 0$ , and a saddle is in the point  $\alpha_* = \pi$ . It is obvious that for  $\gamma < -1$ , points  $\alpha_* = 0, \pi$  are saddles, and an intermediate point:

$$\alpha_* = \pm\arccos(-1/\gamma) \quad [5.21]$$

is the centre (the left branch of the diagram in Figure 5.19). If  $\gamma > 1$ , the inverse picture is observed (the right branch of the diagram in Figure 5.19). We will notice that the bifurcation diagram (see Figure 5.19) for negative angles  $\alpha$  can be obtained by a mirror image around an abscissa axis. Solid lines on the diagram correspond to the centres, and shapes refer to saddles (Aslanov, 2009b).

**Figure 5.19** Bifurcation diagram

For research into the chaotic behaviour of a perturbed system [5.17] in the neighbourhood of separatrixes, we will use the Melnikov method. For its application, it is necessary to receive the analytical expressions for homoclinic and heteroclinic orbits. In other words, it is necessary to find solutions to the equation of an unperturbed motion on separatrixes. The form of the solutions depends on the position of the hyperbolic point on the bifurcation diagram (see Figure 5.19), and on the initial conditions of motion. Let us consider some characteristic cases.

**Case 1.** At:

$$\gamma > 1, \quad [5.22]$$

saddle

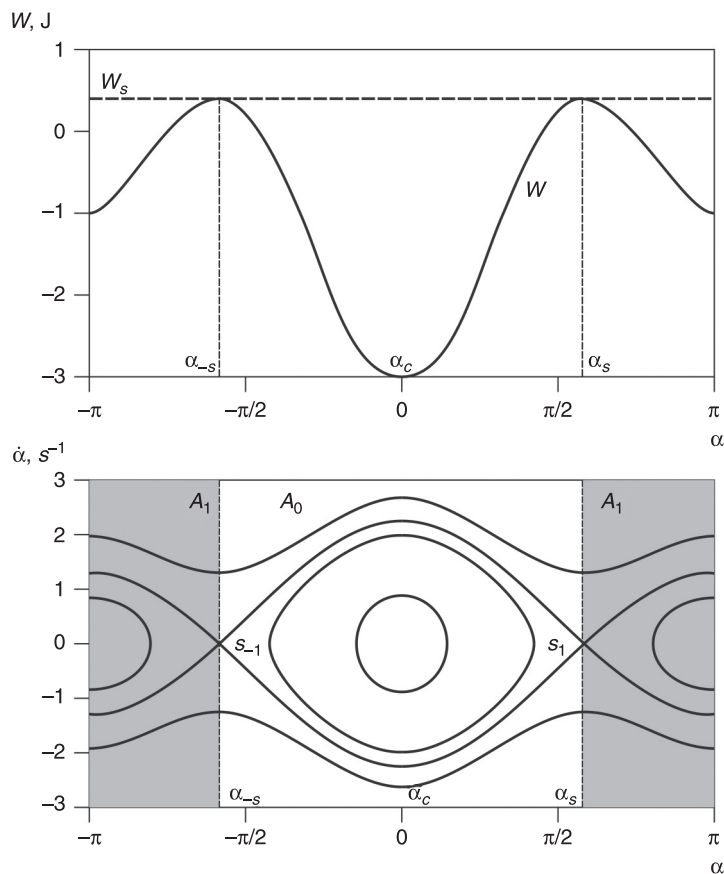
$$\alpha_s = \pm \arccos(-1/\gamma) \quad [5.23]$$

lies between values 0 and  $\pi$ , and in points:

$$\alpha_c = 0, \pm \pi \quad [5.24]$$

there are centres. Let us notice that the centre  $\alpha_C = -\pi$  coincides with the centre  $\alpha_C = \pi$ . At  $\alpha \rightarrow -\pi$  and at  $\alpha \rightarrow \pi$ , velocities  $\dot{\alpha}$  coincide; therefore, it is possible to assert that the phase trajectories are closed on a cylindrical phase space. We will consider the evolution of phase trajectories for all cases on a cylindrical space  $\alpha \in [-\pi, \pi]$ . In the current case, we select two areas  $A_0$  and  $A_1$ , divided by two saddles  $s_1$  and  $s_{-1}$  (see Figure 5.20). It is necessary to notice that the area  $A_1$

**Figure 5.20** Potential energy and a phase portrait of [5.18] for  $\gamma > 1$



is cut on a vertical  $\alpha = \pi, -\pi$ . From [5.23], it follows that the saddle  $s_1$  belongs to an interval  $\alpha_s \in (\pi/2, \pi)$  and  $\alpha_s \rightarrow \pi/2$  at  $\gamma \rightarrow \infty$ .

Equation [5.18] has an energy integral:

$$\frac{\dot{\alpha}^2}{2} + W(\alpha) = h, \quad [5.25]$$

$$W(\alpha) = a \cos \alpha + b \cos^2 \alpha, \quad [5.26]$$

where  $W$  – potential energy; and  $h$  – total energy.

If  $h > W_s$ , where  $W_s = W(\alpha_s)$ , then the system makes a rotation in one of the exterior areas (see Figure 5.20). If  $h < W_s$ , oscillations in one of the interior areas, depending on initial conditions, are observed. At equality  $h = W_s$ , the motion happens on the heteroclinic trajectories which connect the hyperbolic points  $s_1$  and  $s_{-1}$ .

First, let us consider the area  $A_0$  (see Figure 5.20). We will find a solution for equation [5.18] on the separatrixes. Let us divide the variables in an energy integral [5.25]:

$$t = \int_{\alpha_0}^{\alpha} \frac{d\alpha}{\sqrt{2W(\alpha_s) - 2a \cos \alpha - 2b \cos^2 \alpha}}, \quad [5.27]$$

where  $W(\alpha_s) = -a^2/4b$ .

Change of variables:

$$x = \tan(\alpha / 2) \quad [5.28]$$

in integral [5.27] leads to the following solutions (Bateman and Erdelyi, 1954):

$$\begin{aligned} \alpha_{\pm}(t) &= \pm 2 \arctan \left( \tan \frac{\alpha_s}{2} \tanh \frac{\lambda_1 t}{2} \right), \\ \sigma_{\pm}(t) &= (\dot{\alpha})_{\pm} = \pm \frac{\lambda_1 \sin \alpha_s}{\cosh \lambda_1 t + \cos \alpha_s}, \end{aligned} \quad [5.29]$$

where  $\lambda_1 = \sqrt{\frac{a^2 - 4b^2}{2b}}$  – a real number at satisfaction of the condition [5.22].

Similarly, for area  $A_1$  the heteroclinic trajectories take the form:

$$\alpha_{\pm}(t) = \pi \pm 2 \arctan \left( \tan^{-1} \frac{\alpha_s}{2} \tanh \frac{\lambda_1 t}{2} \right), \quad [5.30]$$

$$\sigma_{\pm}(t) = (\dot{\alpha})_{\pm} = \frac{\lambda_1 \sin \alpha_s}{\cosh^{-1} \lambda_1 t - \cos \alpha_s}.$$

**Case 2.** At:

$$\gamma = 1, \quad [5.31]$$

the saddle is in point  $\alpha_s = \pi$  (see Figure 5.19) and the heteroclinic orbits (see Figure 5.21) are defined by the consecutive integration by analogy with equations [5.26]–[5.28] by the following solutions:

$$\alpha_{\pm}(t) = \pm 2 \arctan(\lambda_2 t), \quad \sigma_{\pm}(t) = (\dot{\alpha})_{\pm} = \pm \frac{2\lambda_2}{1 + \lambda_2^2 t^2}, \quad [5.32]$$

where  $\lambda_2 = \sqrt{-a}$ .

**Case 3.** At:

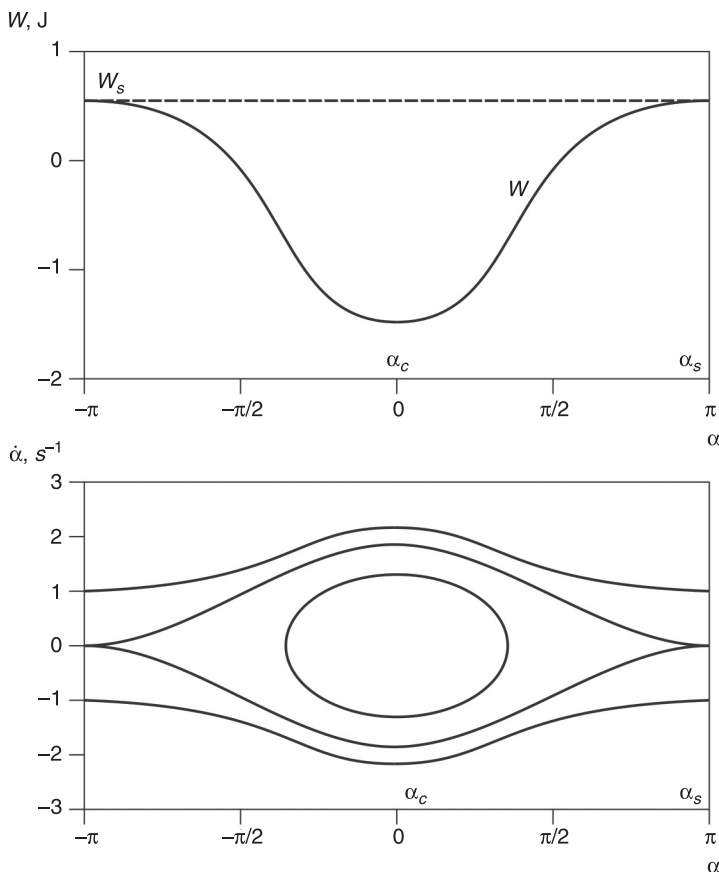
$$\gamma < -1, \quad [5.33]$$

the saddle and the centre are in points  $\alpha_s = 0$  and  $\alpha_c \in (0, \pi)$  accordingly (see Figure 5.19):

$$\alpha_c = \pm \arccos(-1/\gamma). \quad [5.34]$$

In this case, we have two homoclinic trajectories which are symmetrised around a vertical passing through a hyperbolic point  $\alpha_s = 0$  (see Figure 5.22). We will consider only the right

**Figure 5.21** Potential energy and a phase portrait of [5.18] for  $|\gamma| \leq 1$

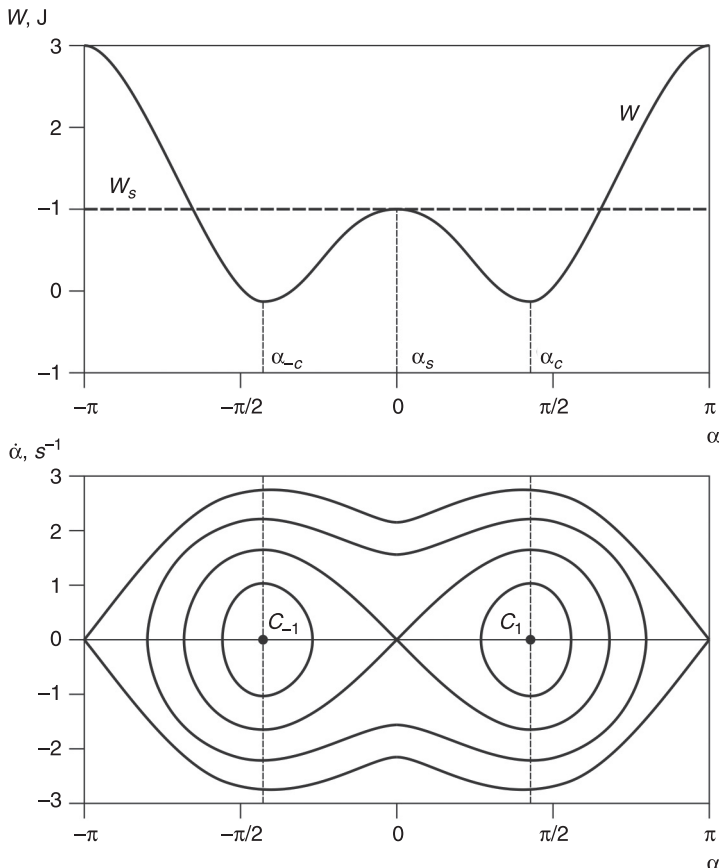


homoclinic trajectory. The change of variables [5.28] allows us to simplify an integral [5.27] and to calculate it:

$$t = \frac{1}{\sqrt{-a}} \int_{x_0}^x \frac{dx}{x \sqrt{x_2^2 - x^2}} = -\frac{1}{\lambda_3^2} \ln \left. \frac{x_3 + \sqrt{x_3^2 - x^2}}{x} \right|_{x_0}^x, \quad [5.35]$$

where  $\lambda_3 = \sqrt{a+2b}$ ,  $x_3 = \sqrt{-(a+2b)/a}$  – real numbers at performance of a condition [5.33].

**Figure 5.22** Potential energy and a phase portrait of [5.18] for  $\gamma < -1$



From [5.35] and [5.28] we obtain the following separatrix solutions:

$$\alpha_{\pm}(t) = \pm 2 \arctan \left( \frac{x_3}{\cosh \lambda_3 t} \right), \quad \dot{\alpha}_{\pm}(t) = (\dot{\alpha})_{\pm} = \mp \frac{2\lambda_3 x_3 \sinh \lambda_3 t}{\cosh^2 \lambda_3 t + x_3^2}. \quad [5.36]$$

In the considered case  $\gamma < -1$ , besides a separatrix [5.36], containing the saddle  $\alpha_s = 0$  there is one more separatrix passing through the saddles in points  $\alpha_s = \pm\pi$  (see Figure 5.19 and Figure 5.22). Making the calculations similar to [5.35], we obtain separatrix solutions for this case:

$$\begin{aligned}\alpha_{\pm}(t) &= \pm 2 \arctan(x_4 \sinh \lambda_4 t), \sigma_{\pm}(t) = (\dot{\alpha})_{\pm} \\ &= \pm \frac{2\lambda_4 x_4 \cosh \lambda_4 t}{1 + x_4^2 \sinh^2 \lambda_4 t},\end{aligned}\quad [5.38]$$

where  $\lambda_4 = \sqrt{2b-a}$ ,  $x_4 = \sqrt{a/(a-2b)}$  – real numbers at the performance of a condition [5.37].

**Case 4.** At:

$$\gamma = -1,$$

the saddle is in point  $\alpha_s=\pi$  (see Figure 5.19) and the heteroclinic orbits (see Figure 5.21) are defined by [5.38], where  $\lambda_4 = \sqrt{-2a}$ ,  $x_4 = \sqrt{2}/2$ .

**Case 5.** At:

$$|\gamma| < 1,$$

the unperturbed system [5.18] has two positions of equilibrium: the centre and the saddle. It is easy to be convinced that the heteroclinic orbits will be described by formulas [5.38].

We use the Melnikov method for analysis of a perturbed system [5.17]. Let us rewrite [5.17] in a more convenient form:

$$\begin{aligned}\dot{\alpha} &= \sigma = f_1 + g_1, \\ \dot{\sigma} &= a \sin \alpha + b \sin 2\alpha + \varepsilon(c_1 \sin \alpha + c_2 \sin 2\alpha + c_3) \\ &\quad \cos \phi - \delta \sigma = f_2 + g_2, \\ \dot{\phi} &= \Omega,\end{aligned}\quad [5.39]$$

where  $f_1 = \sigma$ ,  $g_1 = 0$ ,  $f_2 = a \sin \alpha + b \sin 2\alpha$ , and  $g_2 = \varepsilon(c_1 \sin \alpha + c_2 \sin 2\alpha + c_3) \cos \phi - \delta \sigma$ .

The Melnikov function [5.3] for system [5.39] takes the form:

$$M^{\pm}(t_0, \phi_0) = \int_{-\infty}^{\infty} \{f_1[q_{\pm}^0(t)] g_2[q_{\pm}^0(t), \Omega t + \Omega t_0 + \phi_0]\} dt, \quad [5.40]$$

where  $q_{\pm}^0(t) = [\alpha_{\pm}(t), \sigma_{\pm}(t)]$  – one of the solutions of the undisturbed heteroclinic orbits: [5.29], [5.30], [5.32], [5.36] or [5.38].

### Calculation of the Melnikov function for particular cases

For example, let us consider several particular cases. Let  $c_1 = 0$ ,  $c_2 = 0$ ,  $c_3 = 1$ ,  $\gamma > 1$ , and the system [5.39] in this case takes the form:

$$\begin{aligned}\dot{\alpha} &= \sigma = f_1 + g_1, \\ \dot{\sigma} &= a \sin \alpha + b \sin 2\alpha + \varepsilon \cos \phi - \delta \sigma = f_2 + g_2, \\ \dot{\phi} &= \Omega,\end{aligned}\quad [5.41]$$

where  $f_1 = \sigma$ ,  $g_1 = 0$ ,  $f_2 = a \sin \alpha + b \sin 2\alpha$ ,  $g_2 = \varepsilon \cos \phi - \delta \sigma$ .

Substituting [5.41] into [5.40] gives:

$$\begin{aligned}M^{\pm}(t_0, \phi_0) &= \int_{-\infty}^{\infty} \sigma_{\pm} \{ \varepsilon \cos(\Omega t + \Omega t_0 + \phi_0) - \delta \sigma_{\pm} \} dt \\ &= \varepsilon \int_{-\infty}^{\infty} \sigma_{\pm} \cos(\Omega t + \Omega t_0 + \phi_0) dt - \delta \int_{-\infty}^{\infty} (\sigma_{\pm})^2 dt = M_{\varepsilon} + M_{\delta}\end{aligned}\quad [5.42]$$

where  $M_{\varepsilon}$  and  $M_{\delta}$  are the functions corresponding to both perturbations – the external periodic force ( $\varepsilon \cos \omega t$ ) and the damping force ( $-\delta \dot{\alpha}$ ), respectively. The Melnikov function describes the splitting of the stable and unstable manifolds of the disturbed hyperbolic fixed points as defined on the cross-section. Thus, there are transverse intersections between the stable and unstable trajectories, if  $M^{\pm}(t_0) = 0$ .

First, we consider the functions  $M_{\delta}^{(0)}$  and  $M_{\varepsilon}^{(0)}$  for the area  $A_0$ , including the centre  $\alpha_C = 0$  (see Figure 5.20). Substituting [5.29] into [5.30] gives:

$$M_{\delta}^{(0)} = -\delta \int_{-\infty}^{\infty} (\sigma_{\pm})^2 dt = -\delta \sin^2 \alpha_s \int_{-\infty}^{\infty} \frac{dt}{[\cosh(\lambda_1 t) + \cos \alpha^*]^2}, \quad [5.43]$$

$$\begin{aligned}M_{\varepsilon}^{(0)}(t_0, \phi_0) &= \varepsilon \int_{-\infty}^{\infty} \sigma_{\pm} \cos(\Omega t + \Omega t_0 + \phi_0) dt \\ &= \varepsilon \lambda \sin \alpha_s \int_{-\infty}^{\infty} \frac{\cos(\Omega t + \Omega t_0 + \phi_0)}{\cosh(\lambda_1 t) + \cos \alpha^*} dt.\end{aligned}\quad [5.44]$$

So, using the tabulated integrals (Bateman and Erdelyi, 1954) for the integrals [5.43] and [5.44], we obtain the following expressions:

$$M_{\varepsilon}^{(0)} = -2\delta\lambda_1(1 - \alpha_* \cot \alpha_*), \quad [5.45]$$

$$\begin{aligned} M_{\varepsilon}^{(0)}(t_0, \phi_0) &= 2\varepsilon\pi \frac{\sinh\left(\alpha_* \frac{\omega}{\lambda_1}\right)}{\lambda_1 \sin(\alpha_*) \sinh\left(\pi \frac{\Omega}{\lambda_1}\right)} \cos(\Omega t_0 + \phi_0) \\ &= M_{\varepsilon \max}^{(0)} \cos(\Omega t_0 + \phi_0). \end{aligned} \quad [5.46]$$

Similar expressions can be obtained for the area  $A_1$ , including the centre  $\alpha_C = \pi$  (see Figure 5.20), using the solutions [5.30]:

$$\begin{aligned} M_{\varepsilon}^{(1)} &= -\delta \int_{-\infty}^{\infty} (\sigma_{\pm})^2 dt = -\delta \sin^2 \alpha_* \int_{-\infty}^{\infty} \frac{dt}{[\cosh(\lambda_1 t) - \cos \alpha_*]^2}, \\ M_{\varepsilon}^{(1)}(t_0, \phi_0) &= \varepsilon \int_{-\infty}^{\infty} \sigma_{\pm} \cos(\Omega t + \Omega t_0 + \phi_0) dt \\ &= \varepsilon \lambda \sin \alpha_* \int_{-\infty}^{\infty} \frac{\cos(\Omega t + \Omega t_0 + \phi_0)}{\cosh(\lambda_1 t) - \cos \alpha_*} dt, \end{aligned}$$

or

$$M_{\varepsilon}^{(0)} = -2\delta\lambda_1[1 + (\pi - \alpha_*) \cot \alpha_*], \quad [5.47]$$

$$\begin{aligned} M_{\varepsilon}^{(1)}(t_0, \phi_0) &= 2\varepsilon\pi \frac{\sinh\left[(\pi - \alpha_*) \frac{\Omega}{\lambda_1}\right]}{\lambda_1 \sin(\alpha_*) \sinh\left(\pi \frac{\Omega}{\lambda_1}\right)} \cos(\Omega t_0 + \phi_0) \\ &= M_{\varepsilon \max}^{(1)} \cos(\Omega t_0 + \phi_0), \end{aligned} \quad [5.48]$$

where  $M_{\varepsilon \max}^{(1)}$  and  $M_{\varepsilon \max}^{(2)}$  are measures of the maximum splitting of the stable and unstable manifolds, when the disturbed system [5.17] is only under the action of one perturbation the external periodic force ( $\varepsilon \cos \Omega t$ ) for the regions  $A_0$  and  $A_1$  respectively.

Obviously, at  $\alpha = 0$  the undisturbed biharmonic oscillator [5.18] is transformed to the simpler system:

$$\ddot{\alpha} = \sin 2\alpha.$$

The regions  $A_0$  and  $A_1$  are equal. From [5.21], [5.29] and [5.30] we obtain:

$$\alpha_* = \frac{\pi}{2}, \quad \lambda_1 = \sqrt{-2b}.$$

Following the expressions [5.45]–[5.48], the Melnikov function becomes identical for the regions  $A_0$  and  $A_1$ :

$$\begin{aligned} M^\pm(t_0, \phi_0) &= M_\delta + M_\varepsilon(t_0 \phi_0, ) \\ &= -2\delta\lambda_1 + \varepsilon \frac{\pi}{\lambda_1} \sec h \left( \frac{\pi}{2} \frac{\Omega}{\lambda_1} \right) \cos(\Omega t_0 + \phi_0). \end{aligned} \quad [5.49]$$

From [5.45]–[5.48], it is easy to see that the conditions for the manifolds to intersect in terms of the parameters ( $\delta, \varepsilon$ ) are given by:

$$\delta < \left[ \frac{\pi \sinh \left( \alpha_* \frac{\Omega}{\lambda_1} \right)}{\lambda_1^2 (1 - \alpha_* \cot \alpha_*) \sin(\alpha_*) \sinh \left( \pi \frac{\Omega}{\lambda_1} \right)} \right] \varepsilon \text{ (for the area } A_0), \quad [5.50]$$

and

$$\delta < \left[ \frac{\pi \sinh \left[ (\pi - \alpha_*) \frac{\Omega}{\lambda_1} \right]}{\lambda_1^2 [1 + (\pi - \alpha_*) \cot \alpha_*] \sin(\alpha_*) \sinh \left( \pi \frac{\Omega}{\lambda_1} \right)} \right] \varepsilon \text{ (for the area } A_1). \quad [5.51]$$

Let us define a new parameter of the damping force, divided into the amplitude of the external force:

$$\tilde{\Delta} = \frac{\delta}{\varepsilon}, \quad [5.52]$$

then conditions [5.50] and [5.51] are given by:

$$\tilde{\Delta} < \frac{\pi \sinh\left(\alpha_* \frac{\Omega}{\lambda_1}\right)}{\lambda_1^2 (1 - \alpha_* \cot \alpha_*) \sin(\alpha_*) \sinh\left(\pi \frac{\Omega}{\lambda_1}\right)} \quad [5.53]$$

$= \Delta_0 \quad (\text{for the area } A_0),$

$$\tilde{\Delta} < \frac{\pi \sinh\left[(\pi - \alpha_*) \frac{\Omega}{\lambda_1}\right]}{\lambda_1^2 [1 + (\pi - \alpha_*) \cot \alpha_*] \sin(\alpha_*) \sinh\left(\pi \frac{\Omega}{\lambda_1}\right)} \quad [5.54]$$

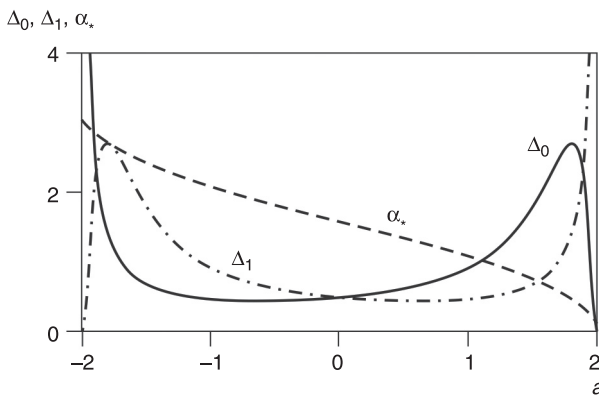
$= \Delta_1 \quad (\text{for the area } A_1).$

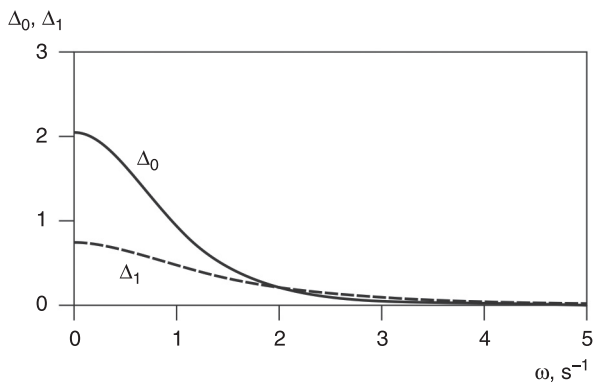
Let us note that  $\alpha_*$  and  $\lambda_1$ , according to [5.21] and [5.29], depend on coefficients  $a$  and  $b$ , therefore criteria [5.53] and [5.54] are functions of the parameters  $a$ ,  $b$  and  $\Omega$ :

$$\Delta_j = \Delta_j(a, b, \Omega) \quad j = 0, 1. \quad [5.55]$$

The criteria [5.55] define the chaotic behaviour of the perturbed system [5.41] in the regions  $A_0$  and  $A_1$ . In Figure 5.23, we chart these criteria and the variable  $\alpha_*$  as

**Figure 5.23** Dependences of  $\Delta_i$  and  $\alpha_*$  on  $a$  for  $b = -1$  and  $\omega = 1$



**Figure 5.24** Dependences of  $\Delta_i$  on frequency  $\omega$ 

functions of the parameter  $a$  for the fixed parameter  $b = -1$  and  $\Omega = 1$ . Figure 5.24 shows the criteria [5.55] as functions of the frequency  $\Omega$ .

Let us consider one more example:  $c_1 \neq 0$ ,  $c_2 \neq 0$ ,  $c_3 = 0$ ,  $\gamma > 1$ . The system [5.39] in this case takes the form:

$$\begin{aligned}\dot{\alpha} &= \sigma = f_1 + g_1, \\ \dot{\sigma} &= a \sin \alpha + b \sin 2\alpha + \varepsilon(c_1 \sin \alpha + c_2 \sin 2\alpha) \\ &\quad \times \cos \phi - \delta \sigma = f_2 + g_2, \\ \dot{\phi} &= \Omega,\end{aligned}\tag{5.56}$$

where  $f_1 = \sigma$ ,  $g_1 = 0$ ,  $f_2 = a \sin \alpha + b \sin 2\alpha$ ,  $g_2 = \varepsilon(c_1 \sin \alpha + c_2 \sin 2\alpha) \cos \phi - \delta \sigma$ . The Melnikov function can be written as:

$$M^\pm(t_0, \phi_0) = \int_{-\infty}^{\infty} \sigma_\pm [\varepsilon(c_1 \sin \alpha_\pm + c_2 \sin 2\alpha_\pm) \times \cos(\Omega t + \Omega t_0 + \phi_0) - \delta \sigma_\pm] dt = M_\varepsilon + M_\delta,$$

Where:

$$\begin{aligned}M_\varepsilon &= \varepsilon \int_{-\infty}^{\infty} \sigma_\pm (c_1 \sin \alpha_\pm + c_2 \sin 2\alpha_\pm) \\ &\quad \times \cos(\Omega t + \Omega t_0 + \phi_0) dt,\end{aligned}\tag{5.57}$$

$$M_\delta = -\delta \int_{-\infty}^{\infty} (\sigma_\pm)^2 dt.\tag{5.58}$$

For the two regions  $A_0$  and  $A_1$ , the functions [5.57] and [5.58] can be represented as:

$$M_{\varepsilon}^{(k)} = -\varepsilon I_{\pm}^{(k)} \sin(\Omega t_0 + \phi_0), \quad [5.59]$$

$$M_{\delta}^{(k)} = -\delta J_{\pm}^{(k)}, k = 0, 1, \quad [5.60]$$

Where:

$$I_{\pm}^{(k)} = \int_{-\infty}^{\infty} \sigma_{\pm}^{(k)} (c_1 \sin \alpha_{\pm}^{(k)} + c_2 \sin 2\alpha_{\pm}^{(k)}) \sin(\Omega t) dt, \quad [5.61]$$

$$J_{\pm}^{(k)} = \int_{-\infty}^{\infty} (\sigma_{\pm}^{(k)})^2 dt. \quad [5.62]$$

It is obvious that by using [5.45] and [5.46], the integrals [5.62] can be written as

$$J_{\pm}^{(0)} = 2\lambda(1 - \alpha_* \cot \alpha_*), J_{\pm}^{(1)} = 2\lambda[1 + (\pi - \alpha_*) \cot \alpha_*]. \quad [5.63]$$

The improper integral [5.61], in view of solutions [5.29] and [5.30], is calculated numerically. For parameter [5.52], the conditions for the manifolds to intersect are given by:

$$\tilde{\Delta} < \frac{I_{\pm}^{(0)}}{J_{\pm}^{(0)}} = \Delta_0 \quad (\text{for the area } A_0), \quad [5.64]$$

$$\tilde{\Delta} < \frac{I_{\pm}^{(1)}}{J_{\pm}^{(1)}} = \Delta_1 \quad (\text{for the area } A_1). \quad [5.65]$$

Criteria [5.64] and [5.65] define the behaviour of the perturbed system [5.56] in a vicinity of the separatrixes.

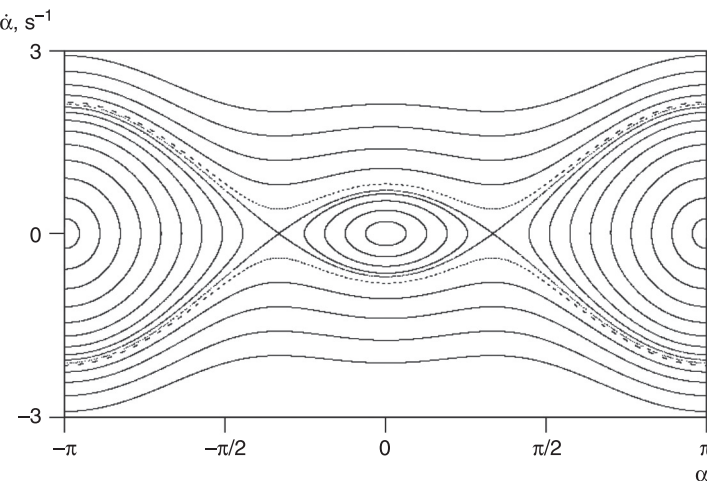
## The numerical analysis

Let us analyse the evolution of the dynamical behaviour of the perturbed system [5.17]. Numerical techniques are based on the numerical integration of the equation of the disturbed motion implementing a fixed-step, fourth-order Runge–Kutta algorithm. For all numerical calculations, the following biharmonic force parameters are used:  $a = 1$ ,  $b = -1$  and the

frequency of the perturbed force is  $\Omega = 1$ . For the numerical analysis of the perturbed system [5.17], we use the Poincaré section method, examining the manifolds with plane sections, perpendicular to the phase axis  $\phi$  in the two-dimensional space  $(\alpha, \dot{\alpha})$ , divided with an interval of  $2\pi$ . It allows us to study the disturbed system using a discrete phase instead of examining the continuous dynamics of the system. At  $\varepsilon = 0, \delta = 0$ , the regular structure of the phase space is observed, the trajectories have no intersections, and the Poincaré sections coincide with the undisturbed phase portrait (see Figure 5.25).

The disturbances ( $\varepsilon \neq 0$ ) lead to complication of the phase space and the occurrence of a chaotic layer near the unperturbed separatrix (see Figure 5.20). Figures 5.26–5.29 show the Poincaré sections for examples considered above. The growth of disturbances leads to an increase in the width of the chaotic layer, and the new oscillatory modes determined by examples of closed curves uncharacteristic for the undisturbed case which are observed. In the presence of

**Figure 5.25** Poincaré section for  $\varepsilon = 0, \delta = 0$



damping, phase trajectories eventually tend to reach steady positions of equilibrium of the undisturbed system (see Figure 5.30 and Figure 5.31).

**Figure 5.26** Poincaré section in the case of  $c_1 = 0$ ,  $c_2 = 0$ ,  $c_3 = 1$  for  $\varepsilon = 0.01$ ,  $\delta = 0$

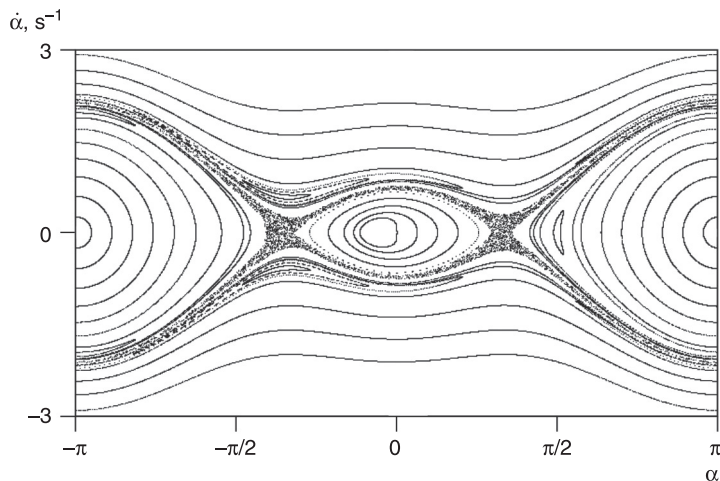


**Figure 5.27** Poincaré section in the case of  $c_1 = 0$ ,  $c_2 = 0$ ,  $c_3 = 1$  for  $\varepsilon = 0.02$ ,  $\delta = 0$

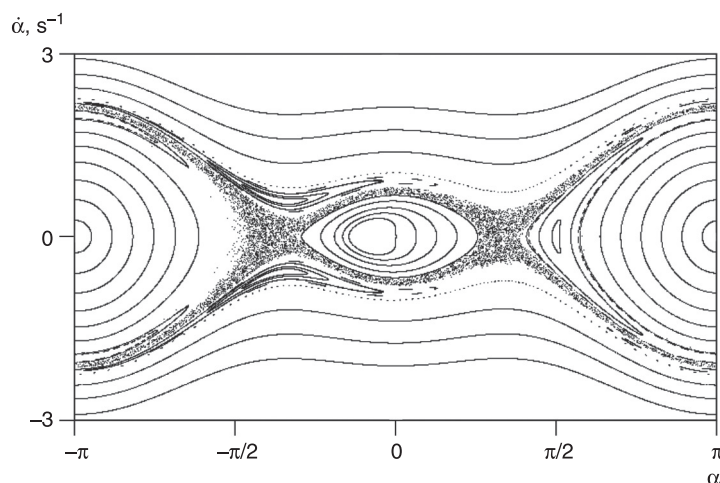


**Figure 5.28** Poincaré section in the case of  $c_1 = 1$ ,  $c_2 = -1$ ,  $c_3 = 0$  for  $\varepsilon = 0.01$ ,  $\delta = 0$

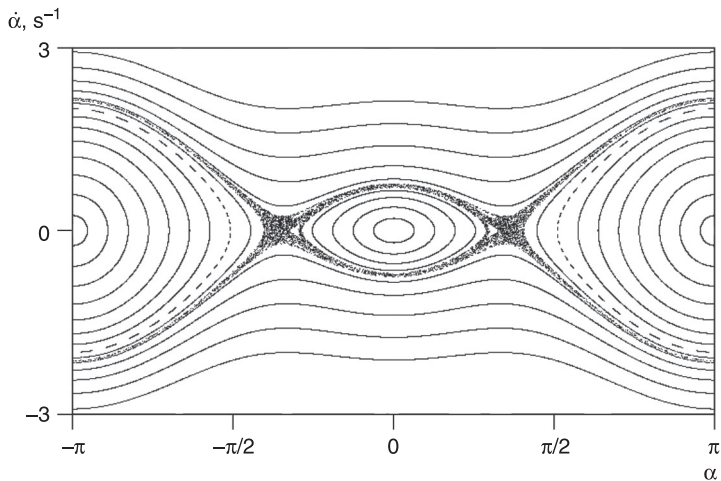


**Figure 5.29** Poincaré section in the case of  $c_1 = 1$ ,  $c_2 = -1$ ,  $c_3 = 0$  for  $\varepsilon = 0.02$ ,  $\delta = 0$

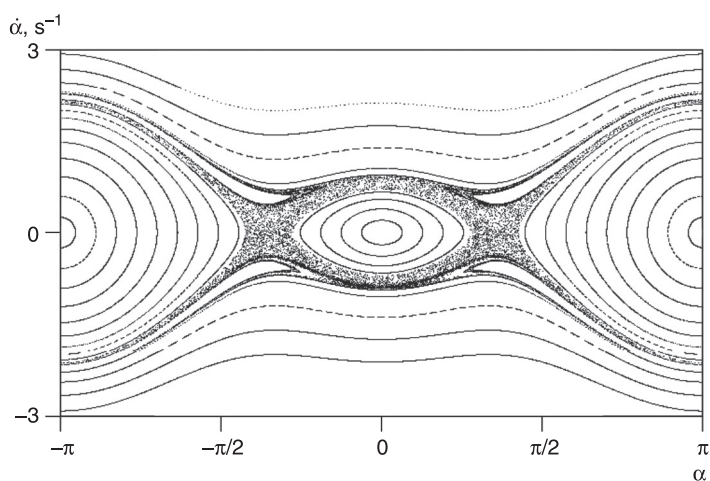


**Figure 5.30** Poincaré section in the case of  $c_1 = 0$ ,  $c_2 = 0$ ,  $c_3 = 1$  for  $\varepsilon = 0.02$ ,  $\delta = 0.0001$

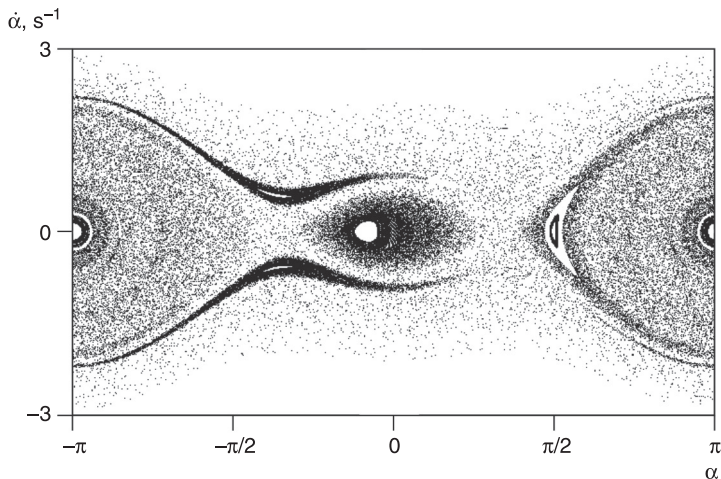
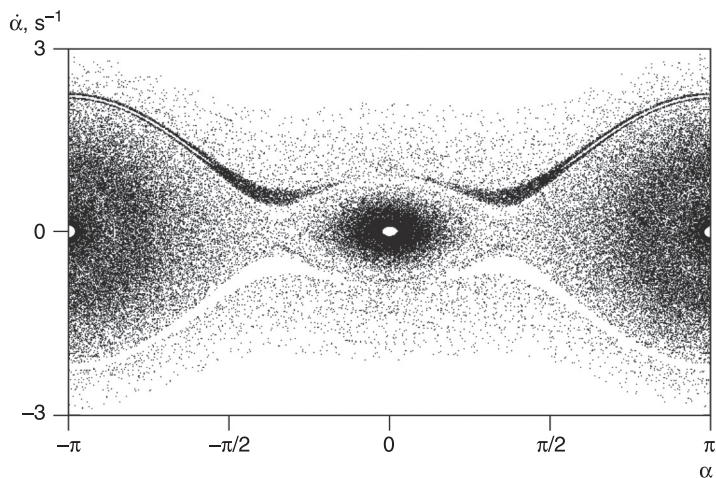


**Figure 5.31** Poincaré section in the case of  $c_1 = 1$ ,  $c_2 = -1$ ,  $c_3 = 0$  for  $\varepsilon = 0.02$ ,  $\delta = 0.0001$



In order to check in a quantitative way the validity of the analytic criteria [5.53] and [5.54], we focus on the evolution of the stable and unstable manifolds associated with the saddle fixed points. Parameters  $a = 1$ ,  $b = -1$  and the frequency

$\Omega = 1$  in expressions [5.53] and [5.54] give a critical value for the regions  $A_0$  and  $A_1$ :

$$\Delta_0 = 0.9115, \Delta_1 = 0.4530$$

or critical values of the coefficients of a damping force for  $\varepsilon = 0.02$ :

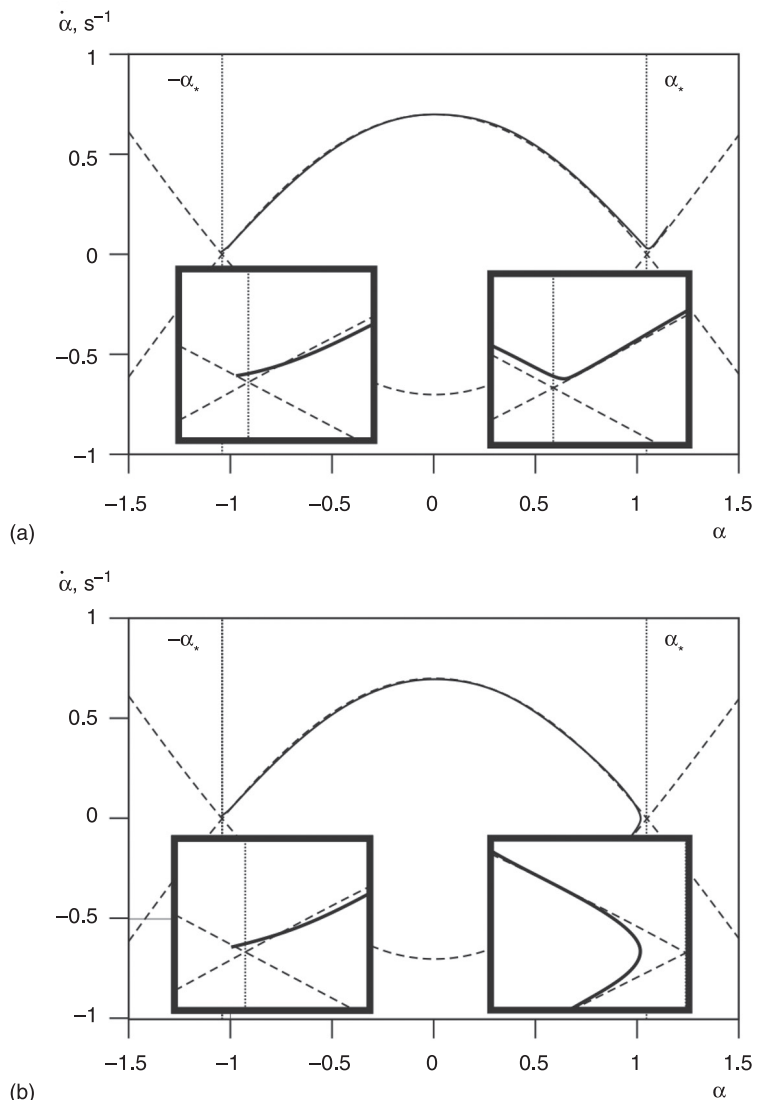
$$\delta_0 = \varepsilon\Delta_0 = 0.01823, \delta_1 = \varepsilon\Delta_1 = 0.00906.$$

Figure 5.32 shows example numerical simulations of the phase space with initial conditions close to the undisturbed separatrix ( $\alpha_0 = -1.0572$ ,  $\dot{\alpha}_0 = 0.001$ ,  $\phi_0 = \pi/10$ ) for the region  $A_0$ . Let us consider the behaviour of an example system at various values of the damping parameter. It can be observed clearly that, for  $\delta < \delta_0$  ( $\delta = 0.018$ ), the stable and unstable manifolds transversally intersect each other (see Figure 5.32(a)). However, when  $\delta > \delta_0$  ( $\delta = 0.020$ ), the invariant manifolds do not intersect (see Figure 5.32(b)). Similar results for region  $A_1$  are shown in Figure 5.33 ( $\delta_1 = 0.00906$ ) for the following initial conditions:  $\alpha_0 = 0.9472$ ,  $\dot{\alpha}_0 = 0.2$ ,  $\phi_0 = \pi$ , and for different values of the damping parameter:  $\delta < \delta_1$  ( $\delta = 0.0090$ ) in Figure 5.33a and  $\delta > \delta_1$  ( $\delta = 0.0113$ ) in Figure 5.33b. Thus, the description, based on numerical simulations for some certain parameter values, makes a good match with the analytic criteria [5.53] and [5.54] provided by the example Melnikov method.

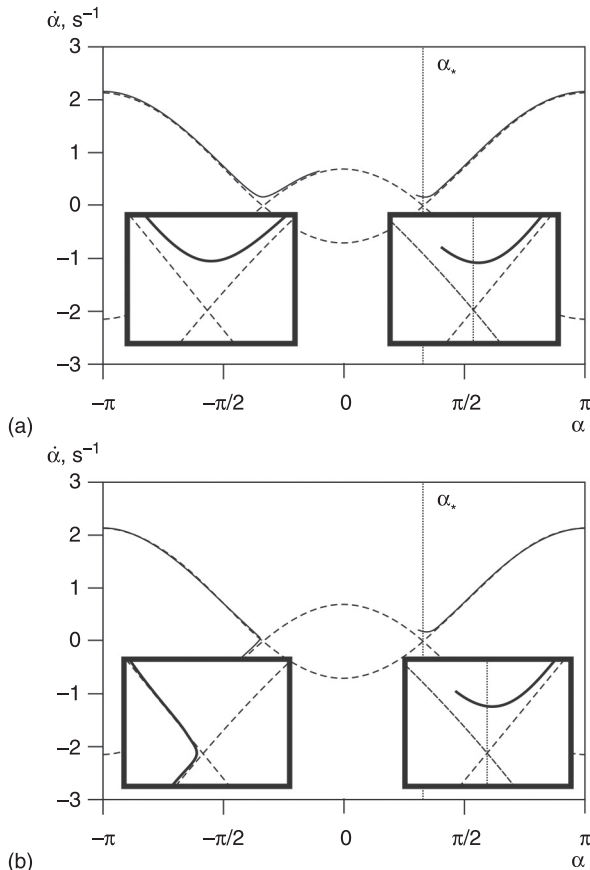
### 5.2.3 Oscillations of the spacecraft with a vertical elastic tether in an orbit

Let us use the methods of chaotic dynamics for an estimate of the influence of an elastic tether on the motion of a base spacecraft with a vertically deployed tether (Aslanov, 2010). Equation [3.84], describing the motion of a base spacecraft

**Figure 5.32** Phase trajectory for  $a = 1$ ,  $b = -1$ ,  $\varepsilon = 0.02$ ,  $\Omega = 1$  and two different values of  $\delta$  close to the critical value  $\delta_0 = 0.01823$ : (a)  $\delta = 0.018$ , (b)  $\delta = 0.020$ , with the following initial conditions:  $\alpha_0 = -1.0572$ ,  $\dot{\alpha}_0 = 0.001$ ,  $\phi_0 = \pi/10$  for the area  $A_0$



**Figure 5.33** Phase trajectory for  $a = 1$ ,  $b = -1$ ,  $\varepsilon = 0.02$ ,  $\Omega = 1$  and two different values of  $\delta$  close to the critical value  $\delta_1 = 0.00906$ : (a)  $\delta = 0.0090$ , (b)  $\delta = 0.0113$ , with the following initial conditions:  $\alpha_0 = 0.9472$ ,  $\dot{\alpha}_0 = 0.2$ ,  $\phi_0 = \pi$  for the area  $A_1$



around its centre of mass is a particular case of the biharmonic oscillator [5.17] at the following values of factors:

$$\begin{aligned} a &= -\frac{\Delta T_0}{I_z}, b = 3\omega^2 \frac{I_x - I_y}{2I_z}, c_1 = -1, c_2 = c_3 = 0, \\ \varepsilon &= \frac{\Delta T_t}{I_z}, \phi_{t0} = -\frac{\pi}{2}, \delta = 0. \end{aligned} \quad [5.66]$$

Owing to [5.66], the factor  $a$  is always negative, and the sign  $b$  depends on a relation of the moments of inertia  $I_x$  and  $I_y$ .

Let us consider the system parameters' influence on the character of the phase portrait. Taking into account [5.66] and that for a circular orbit  $\omega^2 = \mu/r^3$ , we obtain:

$$\gamma = 3\omega^2 \frac{I_y - I_x}{\Delta T_0}.$$

Substituting  $T_0$  from [3.82] into the last equation we obtain:

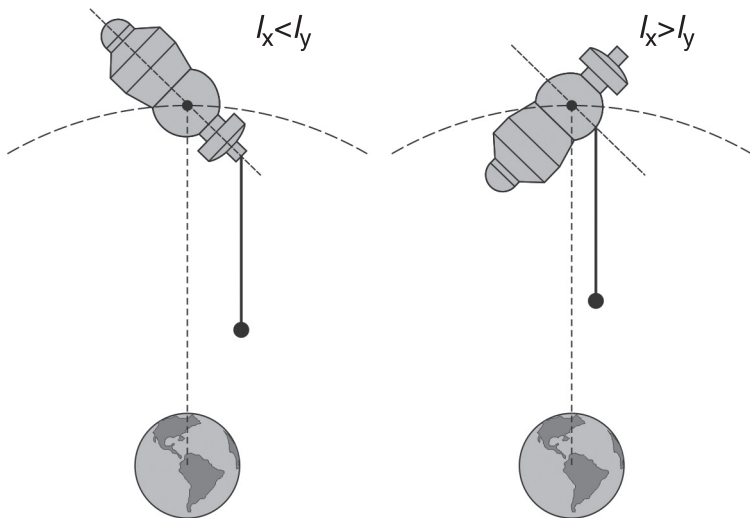
$$\gamma = \frac{I_y - I_x}{\Delta} \cdot \frac{c - 3m_2\omega^2}{m_2 cl_0} = \frac{I_y - I_x}{\Delta} \cdot \left( \frac{1}{m_2 l_0} - \frac{3\omega^2}{cl_0} \right).$$

At the surface of the Earth  $\omega \approx 1.12 \cdot 10^{-3} \text{ s}^{-1}$ , and this magnitude decreases with the increasing of height of an orbit. For modern tethers, the minimum value  $c = ES_T/l_0$  is a magnitude in the order of 0.001 N/m, the mass of the payload does not exceed hundreds of kilograms, and there is a tether length of tens of kilometres. In this case, the second multiplier in [3.41] does not exceed single figures, and the behaviour of the system basically depends on the ratio  $(I_y - I_x)/\Delta$ . The sign of the first multiplier depends on the manner in which the tether is fastened to the spacecraft (see Figure 5.34).

It is possible to achieve the required motion of a system by changing the tether's fixing point and thus influencing the parameter  $\Delta$ . From the point of view of safety, the most acceptable is the case shown in Figure 5.20. In this case, in the vertical position of the spacecraft  $\alpha = 0$  is stable.

Numerical modelling of equation [3.84] has been made in section 3.7. Let us investigate the behaviour of this system with the help of the methods of chaotic dynamics. We will consider the mechanical system having parameters as specified in section 3.7. We will assume that during motion the tether at all time remains parallel to the local vertical passing through the spacecraft's centre of mass.

**Figure 5.34** Dependence of the principal moment of inertia on the manner of tether fastening



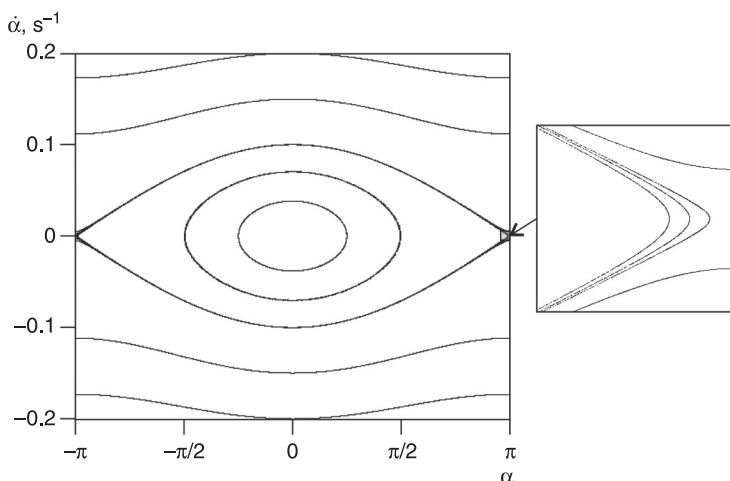
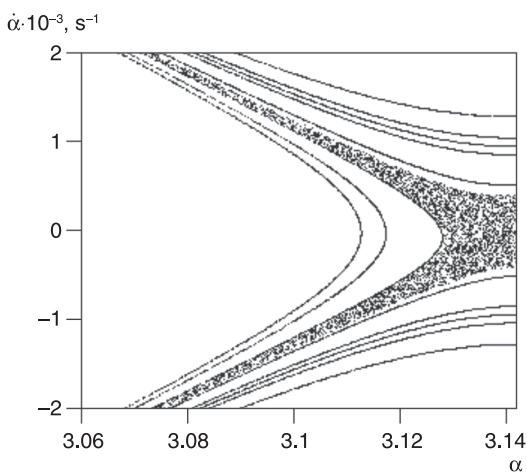
In Figure 5.35, the Poincaré section for the unperturbed system ( $\varepsilon = 0$ ) is shown. According to [5.66], such motion is possible at  $V_0 = 0$ . For  $E = 5$  GPa the factors in equation [5.17] are equal:

$$a = -2.503 \cdot 10^{-3}, \quad b = -1.545 \cdot 10^{-5}, \quad \varepsilon = 0, \quad \Omega = -1.798 \cdot 10^{-2},$$

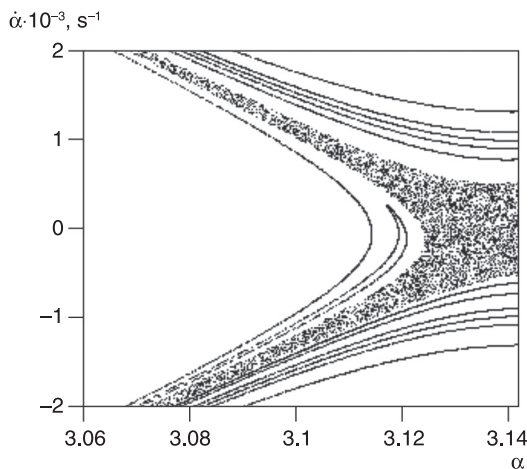
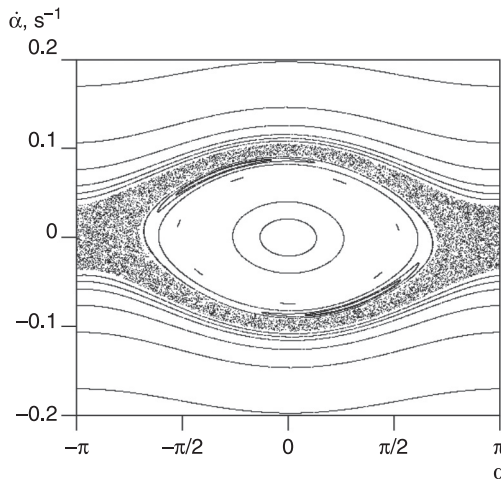
then  $\gamma = 1.234 \cdot 10^{-3}$  and the case shown in Figure 5.21 is realised. With the growth of  $V_0$ , the parameter  $\varepsilon$  increases too. So at  $V_0 = 0.001$  there is  $\varepsilon = 3.641 \cdot 10^{-7}$ . In this case, on the Poincaré section in a separatrix neighbourhood the chaotic layer is observed (see Figure 5.36). At  $V_0 = 0.002$  there is  $\varepsilon = 7.292 \cdot 10^{-7}$ . The thickness of the chaotic layer increases (see Figure 5.37).

Let us consider the behaviour of the system shown in Figure 3.10. In it,  $\varepsilon$  cannot be considered as a small parameter, as

$$a = -2.503 \cdot 10^{-3}, \quad b = -1.545 \cdot 10^{-5}, \quad \varepsilon = -7.282 \cdot 10^{-4}, \\ \Omega = -1.798 \cdot 10^{-2}.$$

**Figure 5.35** Poincaré section of an unperturbed system**Figure 5.36** Poincaré section at  $V_0 = 0.001$ 

The behaviour of the system is essentially nonlinear (see Figure 5.38). It is seen that near the origin of the coordinates there are isolated areas of motion. At a distance from the origin of coordinates, a rather wide chaotic layer is observed,

**Figure 5.37** Poincaré section at  $V_0 = 0.002$ **Figure 5.38** Poincaré section at  $V_0 = 2$ 

in which the system can make both oscillations and rotations (see Figure 3.10). Outside of a random stratum there is a rotation area.

Let us consider in more detail a case where the parameter  $\varepsilon$  is small in comparison with  $a$  and  $b$ . We write a differential

equation of the second order [5.17] in the form convenient for use of the Melnikov method:

$$\begin{aligned}\dot{\alpha} &= \sigma = f_1 + g_1, \\ \dot{\sigma} &= \alpha \sin \alpha + b \sin 2\alpha - \varepsilon \sin \alpha \sin \Omega t = f_2 + g_2,\end{aligned}\quad [5.67]$$

where  $f_1 = \sigma$ ;  $g_1 = 0$ ;  $f_2 = \alpha \sin \alpha + b \sin 2\alpha$ ; and  $g_2 = -\sin \alpha \sin \Omega t$ .

The thickness of the chaotic layer is characterised by the Melnikov function (Melnikov, 1963), which for the perturbed system [5.67] takes the form:

$$\begin{aligned}M^\pm(t_0) &= \int_{-\infty}^{\infty} (f_1 g_2 - f_2 g_1) dt = - \int_{-\infty}^{\infty} \sigma_\pm [\sin \alpha_\pm \sin(\Omega t + \Omega t_0)] dt \\ &= -\cos \Omega t_0 \int_{-\infty}^{\infty} \sigma_\pm \sin \alpha_\pm \sin \Omega t dt,\end{aligned}\quad [5.68]$$

where  $\alpha_\pm(t)$ ,  $\sigma_\pm(t)$  are solutions for homo/heteroclinic orbits [5.29], [5.30], [5.36] or [5.38]. An integral from [5.68]:

$$I = - \int_{-\infty}^{\infty} \sigma_\pm \sin \alpha_\pm \sin \Omega t dt \quad [5.69]$$

defines the thickness of the chaotic layer. We will discover its absolute value over four orbits: three heteroclinic [5.29], [5.30] and [5.38], and one homoclinic [5.36]. Let us substitute the solutions [5.29], [5.30], [5.36] and [5.38] in an integral [5.69] and lead the obtained expressions to a dimensionless time:

$$I_0 = \sin^2 \alpha_s \int_{-\infty}^{\infty} \frac{\sinh \tau_1}{(\cosh \tau_1 + \cos \alpha_s)^2} \sin \Omega_1 \tau_1 d\tau_1, \quad [5.70]$$

$$I_1 = \sin^2 \alpha_s \int_{-\infty}^{\infty} \frac{\sinh \tau_1}{(\cosh \tau_1 + \cos \alpha_s)^2} \sin \Omega_1 \tau_1 d\tau_1, \quad [5.71]$$

$$I_2 = 2d_2^2 \int_{-\infty}^{\infty} \frac{\sinh 2\tau_2}{(\cosh^2 \tau_2 + d_2^2)^2} \sin \Omega_2 \tau_2 d\tau_2, \quad [5.72]$$

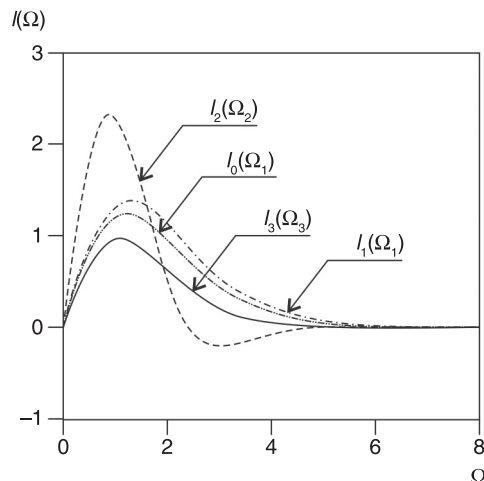
$$I_3 = 2d_3^2 \int_{-\infty}^{\infty} \frac{\sinh 2\tau_3}{(1 + d_3^2 \sinh^2 \tau_3)^2} \sin \Omega_3 \tau_3 d\tau_3, \quad [5.73]$$

where  $T_1 = \lambda_1 t$ ,  $\tau_2 = \lambda_2 t$ ,  $\tau_3 = \lambda_3 t$  – dimensionless time;  $\Omega_1 = \Omega \lambda_1^{-1}$ ,  $\Omega_2 = \Omega \lambda_2^{-1}$ ,  $\Omega_3 = \Omega \lambda_3^{-1}$  – dimensionless frequencies of elastic oscillations of a tether;  $\lambda_1 = \sqrt{\frac{a^2 - 4b^2}{4b}}$ ,  $\lambda_2 = \sqrt{a + 2b}$ ,  $\lambda_3 = \sqrt{2b - a}$  – frequencies of the spacecraft's oscillations; and  $d_2 = \sqrt{-\frac{a+2b}{2}}$ ,  $d_3 = \sqrt{\frac{a}{a-2b}}$ .

Let us note that the frequencies  $\lambda_1$ ,  $\lambda_2$ ,  $\lambda_3$  depend on the parameters of the tether system and the spacecraft's moments of inertia. Dependences of a maximum thickness of a chaotic layer [5.70]–[5.73] for homo/heteroclinic orbits [5.29], [5.30], [5.36] and [5.38] on dimensionless frequencies of the perturbing force are shown in Figure 5.39.

Numerical calculations of integrals [5.70]–[5.73] show that at  $\Omega_i > 6$  thickness of the chaotic layer aspires to zero (see Figure 5.39), and the perturbed system [5.67] makes possible regular motion without homo/heteroclinic

**Figure 5.39** Dependence of integrals [5.70]–[5.73] on the dimensionless frequency



intersections. It means that at  $\Omega_i > 6$  the perturbing force  $\varepsilon \sin \alpha \sin \Omega t$ , connected with an elastic oscillation of a tether, does not influence the behaviour of the spacecraft around the centre of mass.

Assuming the above example corresponds to [5.73], the  $\Omega_3$  is a function of the STS parameters:

$$\Omega_3 = \frac{(ES_T - 3m_2\omega^2 l_0)\sqrt{I_z}}{\omega\sqrt{3m_2l_0}\sqrt{\Delta 3m_2l_0S_T - (I_y - I_x)(S_T - 3m_2\omega^2 l_0)}}.$$

In Figure 5.40, the dependence of the dimensionless frequency  $\Omega_3$  on the rigidity of a tether is shown for the case given in Figure 5.37. It is seen that the elastic oscillations of a tether will influence the STS motion even at very large values of  $E$ . With the growth of the payload's mass and the lengths of the tether, the  $\Omega_3$  decreases (see Figure 5.41 and Figure 5.42). For a reduction of the tether's influence on the

**Figure 5.40** Dependence of the dimensionless frequency  $\Omega_3$  on the elastic modulus of the tether

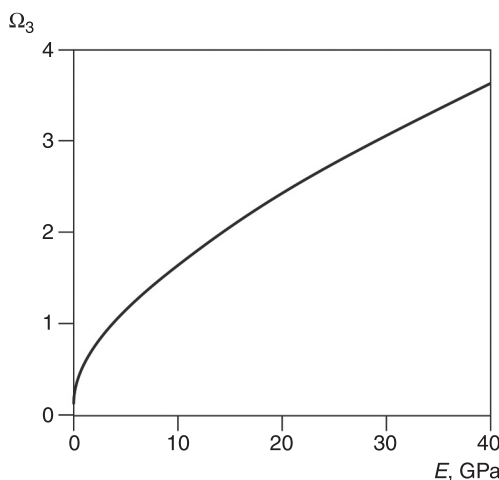


**Figure 5.41** Dependence of the dimensionless frequency  $\Omega_3$  on the payload mass

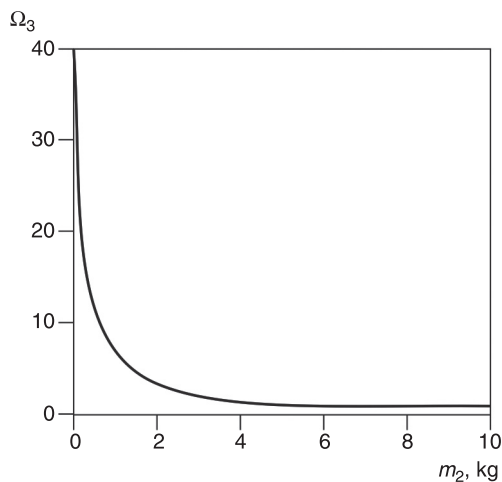
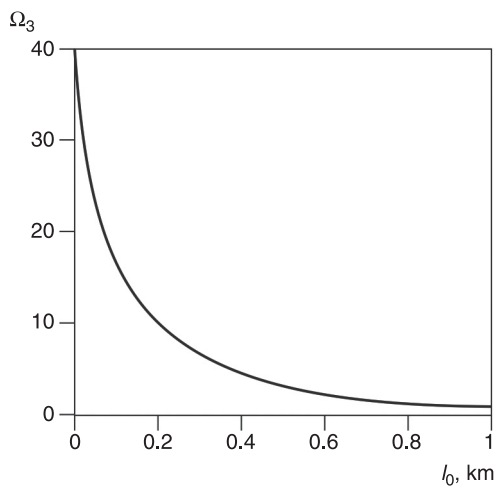


**Figure 5.42** Dependence of the dimensionless frequency  $\Omega_3$  on the tether length



base spacecraft motion, it is possible to recommend using a light payload and a short tether with large enough rigidity.

### ***5.2.4 Selection of the parameters of the thrusters for the prevention of chaotic motions of a spacecraft with a vertical tether***

In the previous sections it has been shown that the oscillations of an elastic vertical tether can lead to chaotisation of the spacecraft's motion. We will assume that the thrusters creating the moment hindering its rotation are mounted on the spacecraft. Let us assume that equation [5.17] becomes:

$$\ddot{\alpha} = a \sin \alpha + b \sin 2\alpha - \varepsilon \sin \alpha \sin \Omega t - \delta \dot{\alpha}. \quad [5.74]$$

Factors of this equation are defined by [5.66], and the last term on the right-hand side is caused by the presence in the system of the moment created by the thrusters.

Instead of equation [5.74], we will use system [5.67] in which  $f_1 = \sigma$ ,  $g_1 = 0$ ,  $f_2 = a \sin \alpha + b \sin 2\alpha$ ,  $g_2 = -\varepsilon \sin \alpha \sin \Omega t - \delta \sigma$ . The Melnikov function for such a perturbed system becomes:

$$M^\pm(t_0) = \int_{-\infty}^{\infty} (f_1 g_2 - f_2 g_1) dt = M_\varepsilon + M_\delta, \quad [5.75]$$

Where:

$$M_\varepsilon = -\varepsilon \int_{-\infty}^{\infty} \sigma_\pm \sin \alpha_\pm \sin \Omega(t + t_0) dt, \quad [5.76]$$

$$M_\delta = -\delta \int_{-\infty}^{\infty} \sigma_\pm^2 dt. \quad [5.77]$$

Functions  $M_\varepsilon$  и  $M_\delta$  correspond to two kinds of small perturbations: to the periodic moment of a tether's tension and to the moment of the thrusters. Also, in section 5.2.2 of the condition of separatrixes intersection, it is possible to write it as:

$$M_\delta < M_\varepsilon. \quad [5.78]$$

Let us write functions [5.76] and [5.77] in the form:

$$M_\varepsilon^{(k)} = -\varepsilon \int_{-\infty}^{\infty} \sigma_\pm^{(k)} \sin \alpha_\pm^{(k)} \sin \Omega(t + t_0) dt, \quad [5.79]$$

$$M_\delta^{(k)} = -\delta \int_{-\infty}^{\infty} (\sigma_\pm^{(k)})^2 dt = \delta J_\pm^{(k)}, \quad [5.80]$$

where the index  $k$  (see Table 5.1) defines the expressions for the homo/heteroclinic trajectory. We simplify an integral [5.51]:

$$\begin{aligned} & \int_{-\infty}^{\infty} \sigma_\pm^{(k)} \sin \alpha_\pm^{(k)} \sin \Omega(t + t_0) dt \\ &= \int_{-\infty}^{\infty} \sigma_\pm^{(k)} \sin \alpha_\pm^{(k)} (\sin(\Omega t) \cos(\Omega t_0) + \cos(\Omega t) \sin(\Omega t_0)) dt \\ &= \int_{-\infty}^{\infty} \sigma_\pm^{(k)} \sin \alpha_\pm^{(k)} (\sin(\Omega t) \cos(\Omega t_0) dt + \int_{-\infty}^{\infty} \sigma_\pm^{(k)} \sin \alpha_\pm^{(k)} \cos(\Omega t) \sin(\Omega t_0) dt) \\ &= \sin(\Omega t_0) \int_{-\infty}^{\infty} \sigma_\pm^{(k)} \sin \alpha_\pm^{(k)} \cos(\Omega t) dt = \sin(\Omega t_0) I_\pm^{(k)}, \end{aligned}$$

Then:

$$M_\varepsilon^{(k)} = -\varepsilon I_\pm^{(k)} \sin(\Omega t_0).$$

Improper integrals:

$$I_\pm^{(k)} = \int_{-\infty}^{\infty} \sigma_\pm^{(k)} \sin \alpha_\pm^{(k)} \cos(\Omega t) dt, \quad J_\pm^{(k)} = \int_{-\infty}^{\infty} (\sigma_\pm^{(k)})^2 dt \quad [5.81]$$

are calculated taking into account solutions [5.29], [5.30], [5.36] and [5.38].

**Table 5.1** Homoclinic and heteroclinic trajectories

$k$	$\gamma$	The equations of trajectories	Phase portrait
1	$\gamma > 1$	(6.29)	Figure 5.20, $A_0$ area
2	$\gamma > 1$	(6.30)	Figure 5.20, $A_1$ area
3	$\gamma < -1$	(6.36)	Figure 5.22
4	$ \gamma  \leq 1$	(6.38)	Figure 5.21

By means of the parameter  $\tilde{\Delta} = \frac{\delta}{\varepsilon}$ , the condition of the existence of chaos in the system [5.74] can be written as:

$$\tilde{\Delta} < \frac{I_{\pm}^{(k)}}{J_{\pm}^{(k)}} = \Delta_k, \quad [5.82]$$

where  $\Delta_k$  depends on the STS parameters:

$$\Delta_k = \Delta_k(I_x, I_y, I_z, \Delta, p, m_2, l_0, E, V_0). \quad [5.83]$$

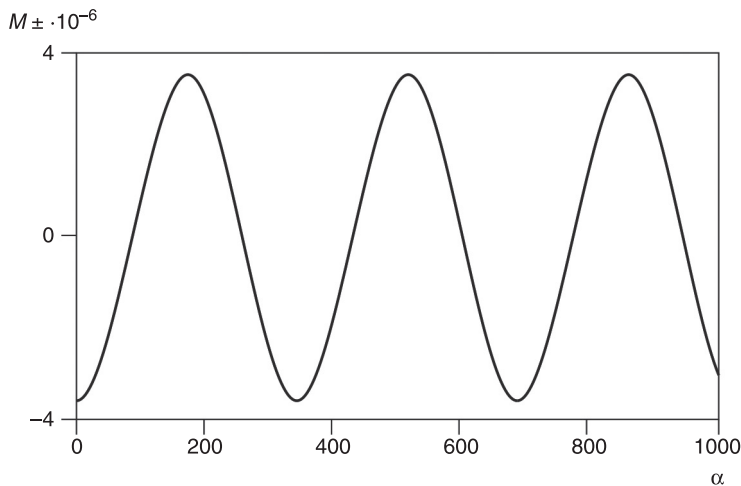
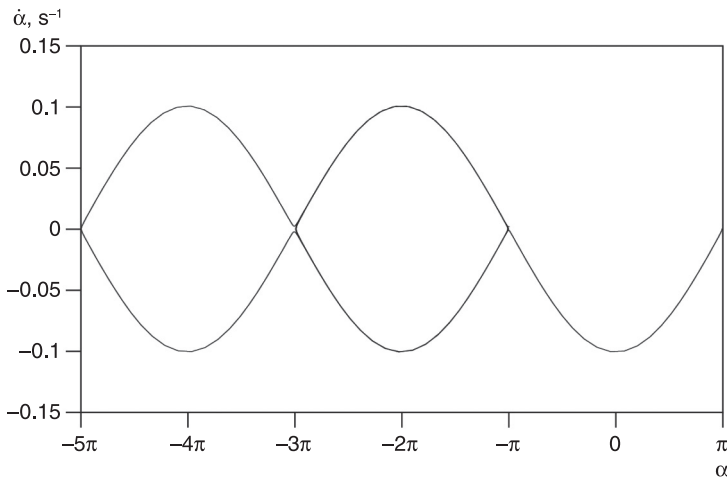
The magnitude of [5.83] defines the behaviour of the perturbed system around the separatrixes.

For a check of the condition in Eq. [5.82], we investigate the behaviour of the perturbed system in a separatrix neighbourhood. Let  $V_0 = 0.01$  m/s. In this case, the factors in Eq. [5.74] are:

$$a = -2.503 \cdot 10^{-3}, \quad b = -1.545 \cdot 10^{-5}, \quad \varepsilon = 3.641 \cdot 10^{-6}, \\ \gamma = 1.261 \cdot 10^{-3}.$$

and the case corresponding to  $k = 4$  (see Table 5.1) is realized. Let us consider the behaviour of a system with acting thrusters. We assume  $\delta = 5 \cdot 10^{-7}$ , then  $\tilde{\Delta} = 0.1373$ ,  $\Delta_4 = 9.698$ . In this case, the condition [5.54] is satisfied and the Melnikov function has simple roots (see Figure 5.43 curves for the upper and lower loop of a heteroclinic trajectory coincide). It means that in the system there is a chaos, and the phase trajectories can intersect a separatrix, passing from the area of oscillative motions into the rotation area and vice versa (see Figure 5.44).

With an increase in the damping factor  $\delta$ , the curve of the Melnikov function is displaced downwards (see Figure 5.45), and the difference between  $\tilde{\Delta}$  and  $\Delta_i$  is reduced. From Figure 5.46, it is seen that at some value of  $\delta = \delta_*$  the curves of the functions  $\tilde{\Delta}$  and  $\Delta_i$  are intersected. In this case, the condition [5.82] is violated, and the chaos in the system is not observed.

**Figure 5.43** The Melnikov function**Figure 5.44** Phase trajectory for  $\alpha_0 = 3.11$ ,  $\dot{\alpha}_0 = 0 \text{ s}^{-1}$ 

From Figure 5.47, it can be seen that  $\delta_*$  has an order which exceeds an order of the factors  $b$  and  $\varepsilon$ . In this case, for application as described above, the necessary approach is to consider the second term in [5.74] as a small perturbation.

**Figure 5.45** The Melnikov function at various values of  $\delta$

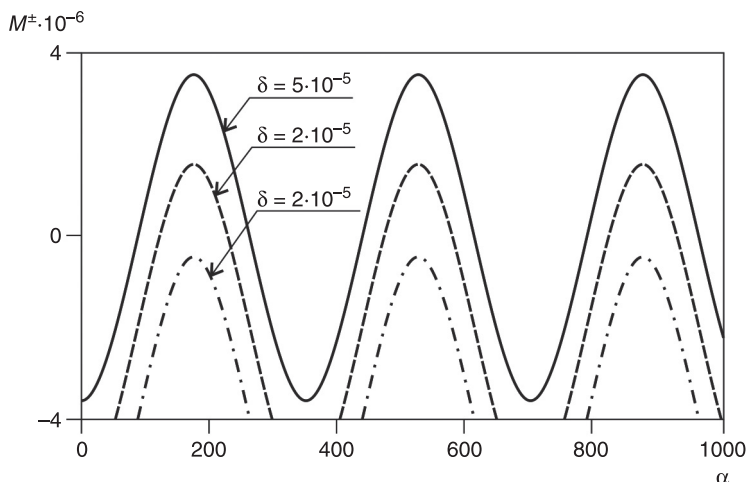
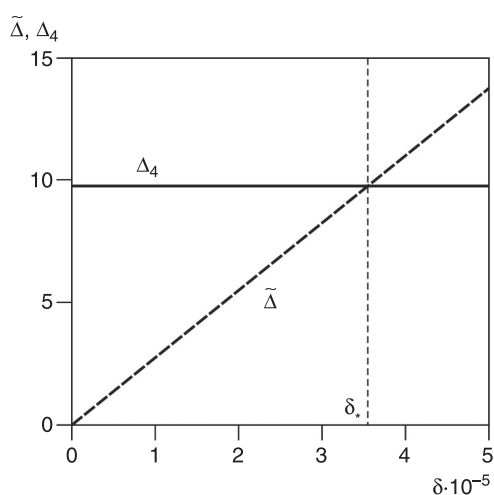


**Figure 5.46** Dependences of  $\tilde{\Delta}$  and  $\Delta_4$  on  $\delta$



We rewrite [5.74] in the form:

$$\dot{\alpha} = \sigma = f_1 + g_1,$$

$$\dot{\sigma} = f_2 + g_2,$$

where  $f_1 = \sigma$ ,  $g_1 = 0$ ;  $f_2 = a \sin \alpha$ ; and  $g_2 = b \sin 2\alpha - \varepsilon \sin \alpha \sin \Omega t - \delta \sigma$ .

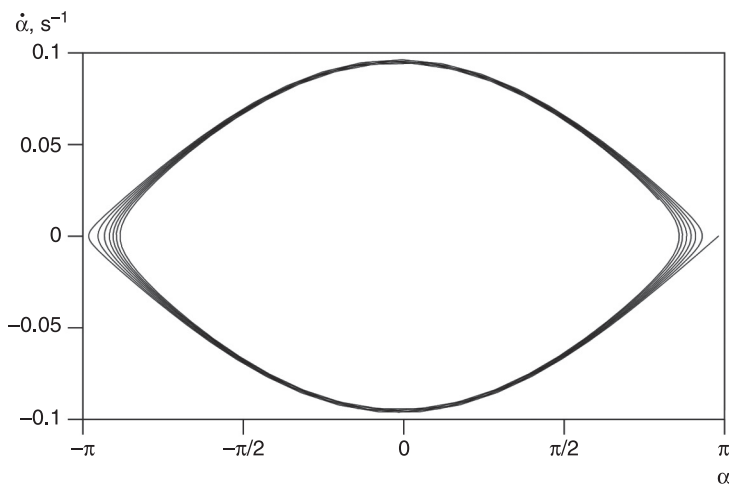
In this case, the expression [5.76] can be written as:

$$\begin{aligned} M_\varepsilon = & -\varepsilon \int_{-\infty}^{\infty} \sigma_\pm \left[ \sin \alpha_\pm \sin \Omega(t+t_0) + \frac{-2b}{\varepsilon} \sin \alpha_\pm \cos \alpha_\pm \right] dt \\ & -\varepsilon \int_{-\infty}^{\infty} \sigma_\pm \sin \alpha_\pm \sin \Omega(t+t_0) dt + 2b \int_{-\infty}^{\infty} \sigma_\pm \sin \alpha_\pm \cos \alpha_\pm dt \\ & -\varepsilon \int_{-\infty}^{\infty} \sigma_\pm \sin \alpha_\pm \sin \Omega(t+t_0) dt. \end{aligned}$$

Adding a new term in  $g_2$  does not influence the Melnikov function, and a condition of the existence of chaos in system [5.81] keeps its form.

In Figure 5.47, the phase portrait of the system is shown at  $\delta = 4 \cdot 10^{-5}$ . In this case:  $\delta > \delta_*$ , and  $\tilde{\Delta} = 10.986$ ,  $\Delta_4 = 9.698$ . As the condition [5.82] is not fulfilled, the Melnikov function

**Figure 5.47** Phase trajectory for  $\alpha_0 = 3.141$ ,  $\dot{\alpha}_0 = 0 \text{ s}^{-1}$



has no simple roots (see Figure 5.45), and the chaos in the system is absent. In Figure 5.47, one phase trajectory for  $\alpha_0 = 3.141$ ,  $\dot{\alpha}_0 = 0$  is shown. It is seen that the trajectory does not intersect a separatrix of the unperturbed system, smoothly coming nearer to the centre  $\alpha_* = 0$ .

Results of numerical modelling are validated based on the Melnikov method of discovery of the condition of chaos existence in equation [5.82].

## 5.3 References

- Aslanov V S (2009a) ‘Chaotic Behavior of the Biharmonic Dynamics System’, *International Journal of Mathematics and Mathematical Sciences*, 1–18, doi:10.1155/2009/319179, Article ID 319179.
- Aslanov V S (2009b) ‘Oscillations of a Spacecraft with a Vertical Tether’, *Proceedings of the World Congress on Engineering*, Vol 2, 1827–31.
- Aslanov V (2010) ‘Oscillations of a Spacecraft with a Vertical Elastic Tether’, *AIP (American Institute of Physics) Conference Proceedings* 1220, *Current Themes in Engineering Science 2009: Selected Presentations at the World Congress on Engineering-2009*. Published February 2010; Vol. 1, 1–16.
- Bateman H and Erdelyi A (1954) *Table of Integrals Transforms* (Vol. 1). New York: McGraw-Hill.
- Beletsky V V and Levin E M (1993) *Dynamics of Space Tether Systems*. SanDiego, CA: American Astronautical Society.
- Birkhoff G D (1927) *Dynamical Systems*. Providence, RI: American Mathematical Society.
- Loskutov A (2007) ‘Dynamical Chaos. Systems of Classical Mechanics’ (in Russian), *Uspekhi Fizicheskikh Nauk*, 177, 9, 989–1015.

- Melnikov V K (1963) ‘On Stability of the Center for Time Periodic Perturbations’, *Transactions of the Moscow Mathematical Association*, 12, 1–57.
- Poincaré H (1912) *Calcul des Probabilité* As. Paris: Gauthier-Villars (in French).
- Simiu E (2009) *Chaotic Transitions in Deterministic and Stochastic Dynamical Systems: Applications of Melnikov Processes in Engineering, Physics, and Neuroscience*. Princeton, NJ: Princeton University Press.



## Conclusion

The mechanics of space tether systems is an extensive area of the modern mechanics of space flight. In this book we have tried to show on the one hand a variety of tasks and areas of research related with space tether systems, and on the other, their practical feasibility based on modern technology, and their ability to solve existing problems.

In one book it is impossible to answer all questions related with dynamics of space cable systems. Therefore, we have tried to focus on problems that may find wide application in the coming decades: the delivery of cargo from an orbit without the cost of rocket fuel, exploring the atmosphere and surface of the Earth by a subsatellite lowered on a tether. The specificity of these problems require us to create new mathematical models that take into account the interaction of the tether with the atmosphere and the movement around the centre of the mass of the spacecraft. Practical implementation cannot be made without assessment of potential emergencies and their consequences. Therefore, we have developed models that take into account various abnormal situations. Presented in the book, models and analytical results were used in the preparation and post-flight analysis of the international experiment YES2.

The study of chaotic behaviour of a mechanical system in space is a relatively new direction of tether system's mechanics. The presence of orbital eccentricity and the phenomenon of elasticity of tethers are the cause of the chaos

in space tether system's motion. Chaos can be a serious obstacle to the successful implementation of the space missions, because it can lead to off-normal operation of the system and to accidents. Using the methods of chaotic dynamics allows us to carry out a selection of space tether system parameters that preclude the possibility of chaos.

Another new trend that is discussed in detail in the book, is the study of dynamics of motion, relative to the centre of mass of the spacecraft with an attached tether. Tether systems have a significant influence on spacecraft dynamics, despite the low weight of the tether and tethered payload in comparison with the mass of the spacecraft. In some cases the spacecraft can be observed swinging with a subsequent transition into the rotation. New analytical solutions describing the plane vibrations of the spacecraft are illustrated in the book. These solutions can be used for quick calculations and qualitative analysis of the spacecraft motion with a tether.

The authors wish to thank the readers for their patience. We hope that the book will not only broaden your horizons, but will also arouse an interest in further study of the dynamics of space tether systems.

# Index

- Abnormal situation, 242  
Adiabatic invariant, 202  
Aerodynamic force, 153  
Analytical solution, 192  
Angle  
    of attack, 171  
    of slip, 171  
Approximate law of the tether's  
    length, 144  
Artificial gravity, 5  
  
Barycentric coordinate system,  
    172  
Bifurcation diagram, 290  
Biharmonic oscillator, 289  
Braking mechanism, 232  
Breakage of tether, 154  
  
Chaotic layer, 277  
Coefficient of  
    aerodynamic lift, 155  
    cross-section force, 155  
    drag, 155  
    hunting moment, 155  
    longitudinal force, 155  
    normal force, 155  
    pitching moment, 155  
    rolling moment, 155  
    side force, 155  
    stiffness, 135  
    tangential force, 155  
  
zonal harmonic, 162, 164  
Conductive tether, 33  
  
Delivery of a payload, 22  
Density, 63  
Deployment  
    dynamic, 23, 227  
    static, 23, 226  
Duffing equation, 289  
Dynamic pressure, 156  
  
Eccentricity of orbit, 108, 121  
Elastic modulus, 63, 108  
Electrodynamic tether, 4  
Elementary work, 186  
Elliptic integral, 194, 195  
Elongation, 124, 152  
Equations of Lagrange, 119  
Experiments:  
    Advanced Tether Experiment  
        (ATEx), 55  
    Cooperative High Altitude  
        Rocket Gun Experiment  
        (CHARGE), 49  
    DAPRA Picosat, 56  
    Gemini missions, 46  
    Observations of Electric-field  
        Distribution in the  
        Ionospheric Plasma, a  
        Unique Strategy  
        (OEDIPUS), 50

- Plasma Motor Generator (PMG), 53
- Propulsive Small Expendable Deployer System (ProSEDS), 59
- Small Expandable Deployer System (SEDS), 52, 54
- Space Tether Experiment (T-REX), 58
- Tether Physics and Survivability (TiPS), 55
- Tether Satellite System (TSS), 51
- Tethered Payload Experiment (TPE), 48
- Young Engineers Satellite 1 (YES1), 59
- Young Engineers Satellite 2 (YES2), 57, 229
- Factor of an interior friction, 152
- FLOYD, 230
- Focal parameter of orbit, 108
- Force of inertia
- Centrifugal, 164
  - Coriolis, 164
- Fotino, 230
- Foton-3M, 230
- General equation of dynamics, 106
- Generalised force, 119
- Gravitational moment, 134
- Gravity stabilisation, 31
- Gravitational constant of Earth, 106, 162
- Gravitational force, 107, 161
- Gravitational potential, 161
- Greenwich coordinate system, 160
- Heavy flexible thread, 104
- Heteroclinic trajectories, 267
- Homoclinic trajectories, 267
- Hooke's law, 124
- Hoytether, 65
- Isothermal atmosphere, 156
- Jacobi amplitude function, 194
- Jamming of tether, 248
- Keplerian orbit, 105
- Kinetic energy, 129
- Koenig theorem, 129
- Laws of tether control
- Exponential, 79
  - Fast, 24, 82
  - Linear, 79
  - Simple, 24, 82
  - Uniform, 79
  - with feedback, 80
- Lagrange equation, 119, 135
- Lagrangian, 119, 135
- Lunavator, 19
- MASS, 230
- Materials:
- Carbon nanotube, 61
  - Dyneema, 63
  - Kevlar, 63
  - Spectra, 63
  - Zylon, 63
- Mathematical model, 68, 103
- Matrix of direction cosines, 168
- Melnikov function, 271

- Microaccelerations, 183, 207  
 Mode of motion:  
     chaotic, 75  
     libration, 72  
     resonance, 74  
     rotation, 73  
 Module of elasticity, 64, 108  
 Moment of momentum, 170,  
     191  
 Multipoint model, 149  
 Newtonian potential, 161  
 Optimum two-impulse  
     transfer, 7  
 Poincaré mapping, 274  
 Potential energy, 134  
 Project  
     Advanced Safety Tether  
         Operation and Reliability  
         (ASTOR), 85  
     Cislunar Tether Transport  
         System, 18  
     Electrodynamic De-Orbiting  
         And Re-entry Device  
         (EDOARD), 38, 64  
     In-Space Propulsion Technology  
         (ISPT), 36  
     Mir Electrodynamic Tether  
         System, 37  
     Momentum eXchange  
         Electrodynamic Reboost  
         (MXER), 35  
 Terminator Tether, 38  
 Terrestrial Planet Finder, 40  
 Tros-1, 26  
 Voshod-2, 46  
 Znamya 2, 41  
 Retrieval of tether, 24  
 Skyhook, 19  
 Space debris, 37, 64  
 Space elevator, 13  
 Space escalator, 12  
 Space harpoon, 42  
 Space mirror, 41  
 Space ring, 39  
 Space tether systems, 3  
     dynamic, 4  
     electrodynamic, 4  
     static, 4  
 Spherical function, 162  
 Spherical hinge, 33  
 Spinup, 84  
 Stability, 76  
 Stable manifolds, 269  
 Tensile strength, 63, 109  
 Tension force, 108, 151  
 Tensor of inertia, 116, 170  
 Theorem of a moment of  
     momentum, 169  
 Unstable manifolds, 269  
 Van der Pol method, 199